Approaches to Developing Occupational Exposure Limits or Bands for Engineered Nanomaterials: User Guide and Technical Report

Disclaimer

Mention of any company or product does not constitute endorsement by the National Institute for Occupational Safety and Health, Centers for Disease Control and Prevention. In addition, citations to websites external to NIOSH do not constitute NIOSH endorsement of the sponsoring organizations or their programs or products. Furthermore, NIOSH is not responsible for the content of these websites. All web addresses referenced in this document were accessible as of the publication date.

June 3, 2021

Description of Contents

This report describes approaches to assess typical microscale airborne particles and various engineered nanomaterials by their possible health impact. These approaches can be used to group engineered nanomaterials into categories based on how much their effects may harm the health of exposed workers. This is a two-part report. Part I is the User Guide, which describes the tools for gathering and assessing information on occupational exposure limits or bands for engineered nanomaterials. The User Guide is for occupational safety and health practitioners who assess risks or decide how to manage risks in the workplace. Part II is the Technical Report, which describes the development of the methods to group engineered nanomaterials. Part II also describes the basis for the categorical occupational exposure limits or bands illustrated in Part I. The Technical Report is for professionals who assess risks or decide how to manage risks in the workplace. These findings give evidence to support enhanced safety and health policies for engineered nanomaterials.

Table of Contents

I. User Guide:

Gathering and Assessing Information for Occupational Exposure Limits or Bands for Engineered Nanomaterials

This page intentionally left blank.

I. User Guide:
Gathering and Assessing Information for Occupational Exposure Limits or Bands for Engineered Nanomaterials

DEPARTMENT OF HEALTH AND HUMAN SERVICES
Centers for Disease Control and Prevention
National Institute for Occupational Safety and Health

Abstract

Federal agencies and safety and health groups set occupational exposure limits (OELs) to protect workers from harmful substances in the workplace. Some OELs apply to engineered nanomaterials, which are purposely created products with at least one dimension between 1 and 100 nanometers. Some types of these materials can harm workers who breathe them in, absorb them through their skin, or swallow them. This report focuses on airborne nanomaterials and potential lung effects in workers.

Most engineered nanomaterials lack enough research data to set an OEL. This report shows how occupational exposure bands can be developed for some engineered nanomaterials without an OEL. Other engineered nanomaterials can be grouped into categories of materials with similar physicochemical properties and potential adverse health effects. This method can give evidence to support safety policies such as engineering controls and other measures.

Engineered nanomaterials are evaluated based on research in rodents and cell systems. Studies in rodents have observed sudden or long-term inflammation of the lungs, which is a biological response to these materials in the lungs. Some rodent studies have reported fibrosis (thickening or scarring of lung tissue) or lung cancer. Statistical research shows how physical and chemical properties of the nanomaterials can help predict potential early lung effects.

The methods described in this report are used to assess typical microscale airborne particles and various engineered nanomaterials by their possible health impact. This process can be used to group engineered nanomaterials into categories based on how much their effects may harm the health of workers.

This report is for occupational safety and health practitioners who assess risks or decide how to manage risks in the workplace. This is Part I of a two-part report. Part I is the User Guide, which describes the tools for gathering and assessing information on occupational exposure limits or bands for engineered nanomaterials. Part II is the Technical Report, which describes the development of the methods to group engineered nanomaterials. Part II also describes the technical basis for the categorical occupational exposure limits or bands illustrated in Part I. The findings give evidence to support enhanced safety and health policies.

Contents

This page intentionally left blank.

Abbreviations

BMD	Benchmark dose
BMDL	95% Lower confidence limit of benchmark dose
CNF	Carbon nanofibers
CNT	Carbon nanotubes
cOEL	Categorical occupational exposure limit
ENM	Engineered nanomaterial
GHS	Globally Harmonized System of Classification and Labeling of Chemicals [UNECE 2015]
LOAEL	Lowest Observed Adverse Effect Level
MWCNT	Multi-walled carbon nanotubes
NIOSH	National Institute for Occupational Safety and Health
NOAEL	No Observed Adverse Effect Level
OSHA	Occupational Safety and Health Administration
OEB	Occupational Exposure Band
OEL	Occupational Exposure Limit
PEL	Permissible Exposure Limit (OSHA)
PNOR	Particles Not Otherwise Regulated (OSHA)
PSHT	Poorly soluble high toxicity
PSLT	Poorly soluble low toxicity
REL	Recommended Exposure Limit (NIOSH)
STOT-RE	Specific Target Organ Toxicity – Repeated Exposure
SWCNT	Single-walled carbon nanotubes
TR	Technical Report
TWA	Time-weighted average (concentration)

Acknowledgments

This draft User Guide was developed by the scientists and staff of the National Institute for Occupational Safety and Health (NIOSH), Division of Science Integration (DSI), Nanotechnology Research Center (NTRC), and Emerging Technologies Branch (ETB). Paul A. Schulte is the director of DSI and co-manager of the NTRC. Charles L. Geraci is the NIOSH associate director for Emerging Technologies and co-manager of the NTRC. Jay Vietas is the branch chief of ETB. Laura Hodson is the coordinator of the NTRC and deputy branch chief of ETB.

This document was authored by Eileen D. Kuempel and Nathan M. Drew, NIOSH/DSI/NTRC and ETB. It is based on the NIOSH Draft Technical Report (Volume II): Approaches to Developing Occupational Exposure Limits or Bands for Engineered Nanomaterials. The following individuals are acknowledged for providing technical review of an earlier draft of this document: Melissa Seaton Edmondson, NIOSH/DSI/SAB; TJ Lentz, NIOSH/DSI/SAB; Eric Glassford, NIOSH/DFSE/HETAB; Aleks Stefaniak, NIOSH/RHD/FSB; Duane R. Hammond, NIOSH/DPSE/EPHB; and Ryan F. Lebouf, NIOSH/RHD/FSB. Paul Schulte, Kathleen MacMahon, DSI, and Gerald Joy, NIOSH Office of the Director, provided scientific and policy reviews of the external review draft document.

The authors acknowledge the editorial input of John Lechliter, NIOSH/DSI/SAB.

1 Introduction

1.1 Target Audience

This user guide is for occupational safety and health practitioners, including industrial hygienists, safety professionals, and risk managers who use scientific information and tools to assess safety and health in the workplace.

1.2 Objectives

This user guide reviews the tools and information available to occupational safety and health practitioners to evaluate the potential occupational health hazards of engineered nanomaterials (ENMs). This information includes references to locate existing occupational exposure limits (OELs) for ENMs, guidance to develop an occupational exposure band (OEB), and examples of OEBs derived from published or other publicly available data. These OEBs or OELs are used along with exposure information in control banding to evaluate the exposure control options. This user guide is a resource for risk management decision-making to protect workers from potential exposures to ENMs.

1.3 Tools in the Toolbox

1.3.1 Occupational Exposure Limits (OELs)

OELs for airborne particles typically are particle mass or number concentrations. OELs are derived from scientific data and provide a quantitative health basis for assessing and adopting risk management practices and tools, including engineering controls. Authoritative OELs are those developed by government, consensus, or peer-reviewed processes [NIOSH 2019]. In the United States, the Occupational Safety and Health Administration (OSHA) Permissible Exposure Limits (PELs) and the National Institute for Occupational Safety and Health (NIOSH) Recommended Exposure Limits (RELs) are examples of authoritative OELs [NIOSH 2007]. OELs may apply to short-term exposures (e.g., 15 minutes or less) or to repeated exposures measured as a time-weighted average (TWA) concentration during an 8- to 10-hour workshift over a 40-hour workweek for up to a 45-year working lifetime [NIOSH 2007, 2011, 2013].

1.3.2 Occupational Exposure Bands (OEBs)

Most chemical substances, including ENMs, do not have OELs. Only about 1% of the tens of thousands of chemicals that are commercially available in the United States have been assigned an authoritative OEL, such as an OSHA PEL or NIOSH REL [NIOSH 2019]. To help fill the gap, NIOSH [2019] has developed guidance on deriving OEBs.

OEBs are bands, rather than single values, that define a range of air concentrations expected to protect worker health [NIOSH 2019]. An OEB does not replace an OEL. Rather, an OEB serves as a starting point to inform risk management decisions when an OEL is not available. Examples of OEBs for ENMs derived using the NIOSH [2019] banding criteria are provided in Section 4 of this guide.

1.3.3 Alternative Methods to Derive an OEL or OEB

Alternative methods have been proposed for chemicals that do not meet the minimum data requirements to derive an OEL or OEB. These methods include utilizing results from quantitative modeling and grouping [Drew et al. 2017], read-across from data on similar chemicals [OECD 2014a,b], or selecting a default most protective option [Schulte and Salamanca-Buentello 2007].

2 Steps in Identifying an Occupational Exposure Limit or Band

A step-by-step process is described for occupational safety and health practitioners to evaluate the information sources for identifying or deriving OELs or OEBs for ENMs. This process is shown in Figure 2-1 and described in the following steps:

2.1 Step 1: Is an OEL available?

OELs have been developed for several ENMs. Section 3 describes these OELs and where to find more information about them. If an authoritative (government, consensus, or peer reviewed) OEL is available, the OEL would be used. An OEB is not meant to replace an OEL; rather, it serves as a starting point to inform risk management decisions when an OEL is not available [NIOSH 2019].

2.2 Step 2: Do you have enough data for an OEB?

NIOSH [2019] hazard banding is a three-tiered approach, which has increasing data requirements from Tiers 1 to 3. Tier 1 is a screening-level process based on the Globally Harmonized System of Classification and Labeling of Chemicals (GHS) [UNECE 2015]. Tier 2 requires additional toxicological data from publicly available sources, which may be used to select a quantitative OEB [NIOSH 2019]. Tier 3 is a critical assessment of all available experimental data and may require a higher level of effort and expertise to develop compared to Tiers 1 or 2.

Examples of Tier 2 OEBs for ENMs derived using the NIOSH [2019] criteria are shown in Section 4. Data used in these OEB derivations are from published toxicology studies of lung effects in rodents exposed to nanoscale or microscale particles. Applying OEBs to occupational control banding is described in Section 6.

2.3 Step 3: Can you use an alternative method?

Several alternative methods have been proposed when not enough data are available to derive an OEL or an OEB, as described in Section 5. In one method, which is described in this report, NIOSH has developed a quantitative model for assigning ENMs to preliminary groups based on hazard potency for acute lung inflammation in rodents. These groups were used in deriving categorical OEL estimates for several ENMs. Other alternative methods include read-across to similar substances, categorical reference values, relative potency comparison, and qualitative hazard banding. If none of the above are possible, defaulting to the most stringent OEB may be an option until more data become available. Selection among these options depends on the data available and the needs of the assessment.

The process shown in Figure 2-1 is based on a hierarchy of data. This process starts with a search for a specific OEL for the individual ENM. If an OEL is not found, then an OEB might be derived [NIOSH 2019]. If deriving an OEB is not feasible using the NIOSH [2019] criteria, then alternative methods to derive an OEB may be considered.

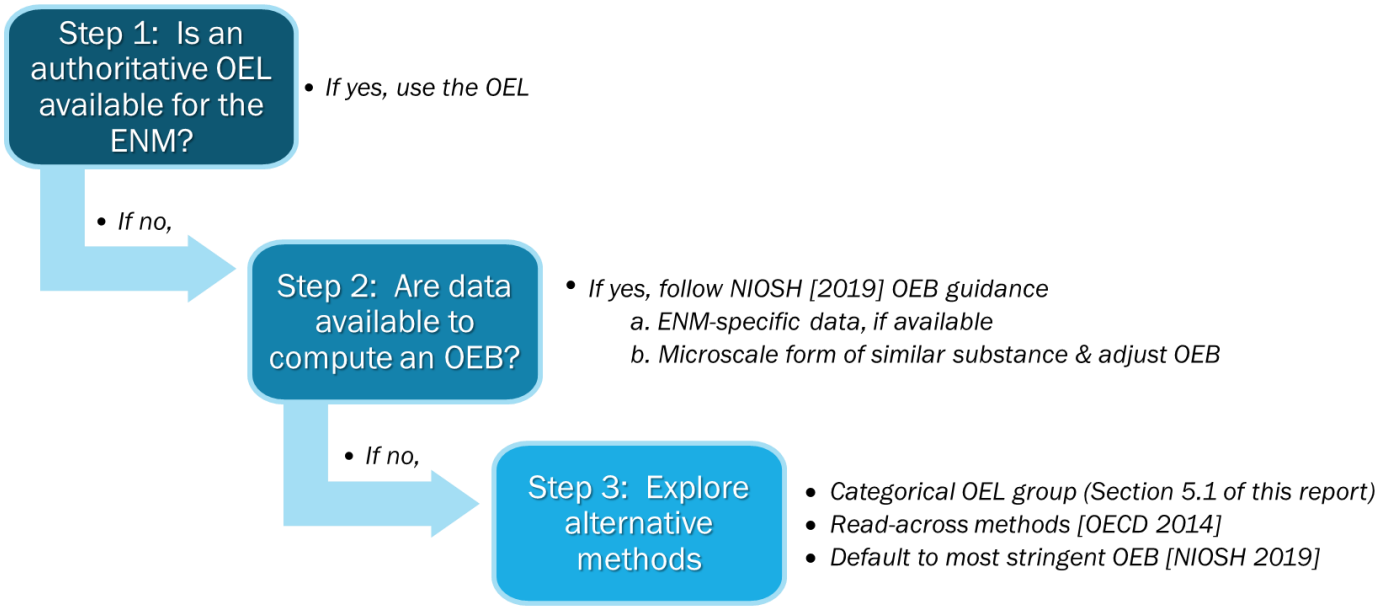

Figure 2-1. Selecting occupational exposure limits or bands (OELs or OEBs) for engineered nanomaterials (ENMs).

3 Occupational Exposure Limits

3.1 Overview

OELs are important tools for prevention of occupational disease from exposure to potentially hazardous substances [Schulte et al. 2010; Gordon et al. 2014]. An OEL (e.g., NIOSH REL or OSHA PEL) is a single value that generally refers to a specific substance, although some OELs apply to broader categories, such as dust or particles not otherwise regulated [NIOSH 2007; ISO 2016]. Relatively few OELs have been derived for ENMs in the United States or other countries [Mihalache et al. 2017; Rodriguez-Ibarra et al. 2020].

Inhalation exposures, a primary concern in the workplace, are the focus of most OELs for ENMs to date, although some values have been developed for dermal or oral exposure routes as well [Mihalache et al. 2017]. Most OELs are time-weighted average airborne concentrations (typically 8 hours) representing a safe level of exposure for most workers over their working lifetime [Gordon et al. 2014; ACGIH 2014].

3.2 Examples of Occupational Exposure Limits for Engineered Nanomaterials

OELs have been developed for a few specific ENMs [Mihalache et al. 2017], including titanium dioxide (TiO_2), carbon nanotubes, and silver [NIOSH 2011; NIOSH 2013; NIOSH 2021]. Development of OELs is typically based on toxicological data and risk assessment methods [NIOSH 2020]. Often, these assessments have used subchronic (13-week) inhalation studies in rodents. The specific methods used in deriving those OELs have varied, resulting in a range of published OELs for a given ENM [ISO 2016; Mihalache et al. 2017] (Table 3-1). The OELs for nanoscale particles are all generally much lower than OELs for microscale particles of the same chemical substance (Table 3-1).

If available, an OEL for the specific material is selected for exposure control decision-making (Section 6). NIOSH [2019] recommends use of authoritative (government, consensus, or peer reviewed) OELs.

Table 3-1. Examples of Occupational Exposure Limits (OELs) for Engineered Nanomaterials and Related Bulk Materials. *(Adapted from Table S-1 in Dunn et al. [2018]).*

Material name (chemical formula)	Published OELs as airborne particle mass concentration (mg/m^3), 8-hr TWA, unless otherwise stated (see footnotes for references)	
	Nanoscale	**Microscale or unspecified**
Silica (SiO_2) *Crystalline* *Amorphous*	 NA 0.3 [a]	 0.05 (resp) [b] 6 (total) [b]
Titanium dioxide (TiO_2)	0.017 [c] 0.1 [d] 0.3 [e,f] 0.61 [g]	2.4 (resp) [h] 15 (total) [i]
Silver (Ag)	0.00033, 0.00067 [j] 0.00019 [k] 0.0009 [l]	 0.01 (total) [m, n] 0.1 (total) [n]
Carbon nanotubes (C) *Multiwalled carbon nanotubes (MWCNT)* *Carbon nanotubes and fibers, including single-walled carbon nanotubes (*SWCNT) *MWCNT* *CNT, including SWCNT* *MWCNT (Baytubes®)*	 0.00067 [o] 0.001 [p] 0.001, 0.002 [q] 0.03 [r] 0.05 [s]	 NA
Graphene (C)	NA	NA
Graphite (C) – chemically-related material *Synthetic* *Natural*	NA	 15 (total) [t] 5 (resp) [t] 2.5 (resp) [u]
Carbon black (C) – chemically-related material	NA	3.5 (resp) [v]
Cellulose	0.01 fibers/ml [w]	15 (total) [x] 10 (total) [y] 5 (resp) [x,y]
Particles not otherwise regulated (PNOR)	NA	5 (resp) [z]

Footnotes to Table 3-1:
Silica: [a] Stockmann-Juvala et al. [2014]; [b] NIOSH [2007] (crystalline SiO_2: potential occupational carcinogen).
Titanium dioxide: [c] Aschberger et al. [2011]; [d] Stockmann-Juvala et al. [2014]; [e] NIOSH [2011] (ultrafine TiO_2: potential occupational carcinogen); [f] JSOH [2013]; [g] Gamo [2011]; Nakanishi [2011]; [h] NIOSH [2011]; [i] OSHA [29 CFR 1910.1000].
Silver: [j] Aschberger et al. [2011], Stone et al. [2009]; [k] Weldon et al. [2016]; [l] NIOSH [2021]; [m] NIOSH [2007], OSHA [29 CFR 1910] (metal dust, fume, and soluble compounds); [n] ACGIH [2001]: 0.01 mg/m^3 (soluble compounds); 0.1 mg/m^3 (metal dust and fume).
Carbon nanotubes: [o] Stone et al. [2009]; [p] NIOSH [2013]; [q] Aschberger et al. [2010, 2011]; [r] Nakanishi [2011]; [s] Pauluhn [2010b].
Graphite: [t] OSHA [29 CFR 1910]; [u] NIOSH [2007].
Carbon black: [v] NIOSH [2007] (not in presence of polycyclic aromatic hydrocarbons); OSHA [29 CFR 1910].
Cellulose: [w] Stockmann-Juvala et al. [2014]; [x] OSHA [29 CFR 1910]; [y] NIOSH [2007].
PNOR: [z] OSHA [29 CFR 1910.1000].
Abbreviations: TWA: time-weighted average concentration; Resp: respirable particle size fraction; Total: total airborne particle mass; NA: not available or not applicable.
Note: OELs reported in this table are those derived for chronic inhalation exposure in workers. OELs for acute inhalation exposure or for dermal or oral exposure have also been developed for some ENMs (e.g., Table 2 of Mihalache et al. [2017]). Other OELs cited in Mihalache et al. [2017] but not reported here are those for which the derivation methods were unclear [Warheit 2013]; available only in a non-English language (Swidwinska-Gajewska and Czerczak 2014, 2015); or quantitative risk estimates rather than OELs [Kuempel et al. 2006]. Ogura et al. [2011] is cited by Mihalache et al. [2017] for a TiO_2 OEL[g]. Weldon et al. [2016] is not cited in Mihalache et al. [2017] but is reported in this table.

4 Occupational Exposure Bands

4.1 Overview

OEBs are bands, rather than single limit values, that define a range of air concentrations exposure to which is expected to be protective of worker health [NIOSH 2019]. The NIOSH OEBs for airborne particle mass concentrations are the following order-of-magnitude ranges (mg/m^3): E ($\leq$0.01), D (>0.01 to 0.1), C (>0.1 to 1), B (>1 to 10), A (>10). As shown in Figure 6-1, these bands are used in the hazard component of control banding (Section 6). Band E, which specifies the lowest exposure range, is reserved for substances with the greatest toxicity potential. Band A indicates the highest exposure range for those substances which are least toxic.

As described in NIOSH [2019], an OEB is not meant to replace an OEL; rather, it serves as a starting point to inform risk management decisions when an OEL is not available. An OEB can also assist with prioritizing chemical substances for which an OEL should be developed. In the absence of an OEL and until one can be established, an OEB can guide users, including enterprises of all sizes, in setting internal ranges for controlling exposures to specific chemical substances. The NIOSH [2019] occupational exposure banding process is one approach or tool for assessing chemical hazards and prioritizing control efforts. Special considerations for banding ENMs are described in Section 3.14 of NIOSH [2019]. The NIOSH [2019] OEB approach to banding nanoscale materials is illustrated in this user guide for several ENMs using published data sources.

The adverse health effects targeted in this report are the NIOSH [2019] OEB Tier 2 endpoints of Specific Target Organ Toxicity-Repeated Exposure (STOT-RE) and cancer based on rodent studies. OEBs were derived for nanoscale and microscale materials with at least the minimum required data. The required data for the OEB Tier 2 endpoint STOT-RE ("Inhalation (dusts/particles)") are from rodent inhalation studies with at least 28 days of exposure (Table 3-12 in NIOSH [2019]). For the OEB Tier 2 endpoint of cancer, the criteria for carcinogenicity toxicity (quantitative analysis) are shown in Table 3-7 of NIOSH [2019]. If a material were classified into more than one band because of having multiple potency estimates from the rodent data, the most stringent of those bands (i.e., lowest exposure range) was chosen (Table 4-1). For more information on these methods, please see Section 4 in TR Vol. II.

4.2 Examples of Occupational Exposure Bands for Engineered Nanomaterials

NIOSH derived examples of OEBs for ENMs (Table 4-1), based on rodent studies of lung effects from exposure to nanoscale or microscale particle data, and using the NIOSH [2019] hazard banding criteria. Most of the microscale particles have nanoscale applications (Table 2-6 of TR Vol. II). These OEBs were based on points of departure – either BMDLs (benchmark dose lower 95% confidence limit estimates), NOAELs (No Observed Adverse Effect Levels), or LOAELs (Lowest Observed Adverse Effect Levels) with uncertainty factor adjustments—from databases by the National Toxicology Program (NTP) or Organization for Economic Cooperation and Development (OECD), and systematic literature searches. These data met the NIOSH [2019]

criteria for deriving a Tier 2 OEB. In Table 4-1, the OEB estimates for microscale materials are *not* adjusted to the nanoscale form. According to the NIOSH [2019] banding criteria, the microscale OEBs would be divided by a factor of 10 – resulting in the next more stringent band – if the microscale data are used to derive an OEB for the nanoscale form of the material.

None of the particles evaluated in these analyses were assigned to the NIOSH band A, which indicates that the ENMs evaluated have toxic effects at lower concentrations. However, most ENMs and many microscale materials were assigned to band E, several of which could be assigned to a hypothetical new band F (discussed further in Section 5). With a new band F, the NIOSH OEBs for airborne particles would be the following airborne concentrations (mg/m^3): F ($\leq$0.001), E (>0.001 to 0.01), D (>0.01 to 0.1), C (>0.1 to 1), B (>1 to 10), A (>10), as shown in Table 6-2.

The OEBs shown in Table 4-1 are examples to consider along with other relevant data and information in selecting initial values of OEBs for ENMs with the same or similar chemical composition and other physicochemical properties. The materials in Table 4-1 are grouped according to four broad particle categories based on physicochemical properties and biological mode of action: Fibrous, Poorly Soluble High Toxicity (PSHT), Poorly Soluble Low Toxicity (PSLT), or Soluble. These categories are similar to those reported previously [BSI 2007; SER 2012] (Section 5.3). Hazard potency is represented by the OEBs: Band E represents the most potent materials and band A represents the least potent materials. These nanoscale and microscale materials display a wide range of hazard potencies.

Table 4-1 provides some information on how the physicochemical properties, including particle size, may relate to the band assignments. Within the PSLT group, the OEBs for the nanoscale materials tend to be more stringent than the OEBs for the microscale materials. The data within the other physicochemical groups are generally too sparse to see any patterns based on particle size. Some of the variability in the OEB estimates is likely attributable to the different types of lung endpoints evaluated (inflammation, fibrosis, cancer) and the different points of departure (BMDL or NOAEL) that were used in the derivation of these OEB estimates.

Differences in potency within the four mode-of-action groups are to be expected, as potency is a quantitative measure of toxicity, while these four groups represent qualitative descriptors of biological mechanisms associated with certain types of materials. For example, within the PSLT category, nanoscale TiO_2 has been shown in a number of studies to have greater toxicity on a mass basis compared with microscale TiO_2 [NIOSH 2011]. The mechanism is considered to be related to the total particle surface area or volume dose, which are greater for a given mass dose of nanoscale TiO_2 than for microscale TiO_2.

Figure 4-1 shows the range of individual OEB estimates for a given material, based on all of the data used in these analyses (Table E-5 of TR Vol. II). In the case of multiple OEB estimates for one material, a general practice is to select the most stringent band (lowest exposure range) [NIOSH 2019], as shown in Table 4-1.

Table 4-1‡. Most Stringent Occupational Exposure Bands in Workers and Material Assignments Across Lung Endpoints in Rodents, using NOAELs, LOAELs or BMDLs.

Physico-chemical Group (Fig 4-1)*	Nanoscale or microscale with nanoscale uses	Material	Most Stringent Band***	Health Endpoint(s)
Fiber	Nano	Multiwalled carbon nanotube	E	Lung Inflammation
Fiber	Nano	Single walled carbon nanotube	D	Lung Inflammation
Fiber	Micro	Wollastonite calcium silicates	C	Lung Fibrosis
PSHT	Micro	Cobalt	E†	Lung Inflammation
PSHT	Micro	Gallium arsenide	E†	Lung Inflammation
PSHT	Micro	Indium phosphide	E†	Lung Neoplasia; Fibrosis; Inflammation
PSHT	Micro	Nickel (II) oxide	E†	Lung Inflammation
PSHT	Micro	Nickel subsulfide	E†	Lung Inflammation; Fibrosis
PSHT	Micro	Antimony trioxide	E	Lung Fibrosis
PSHT	Micro	Vanadium pentoxide	D	Lung Neoplasia
PSHT	Micro	Sand blasting agents**	C	Lung Fibrosis
PSLT	Nano	(Au) Gold	E†	Lung Inflammation
PSLT	Nano	Carbon black	E	Lung Inflammation
PSLT	Nano	Ferrous carbonate ($FeCO_3$)	E	Lung Inflammation
PSLT	Nano	Iron oxide (Fe_3O_4)	E	Lung Inflammation
PSLT	Nano	Cerium oxide	D	Lung Inflammation
PSLT	Nano	Fullerene (C60)	D	Lung Inflammation
PSLT	Nano	Titanium dioxide (Nano)	C	Lung Inflammation
PSLT	Nano	Silicon dioxide, amorphous (Nano)	C	Lung Inflammation
PSLT	Micro	Talc	D	Lung Neoplasia
PSLT	Micro	Titanium dioxide (Micro)	C	Lung Neoplasia
PSLT	Micro	Calcium chromate	B	Lung Inflammation; Fibrosis
PSLT	Micro	Molybdenum trioxide	B	Lung Inflammation
Soluble	Nano	(Ag) Silver	E	Lung Inflammation
Soluble	Nano	Zinc oxide	C	Lung Inflammation
Soluble	Micro	Cobalt sulfate heptahydrate	E†	Lung Inflammation; Fibrosis
Soluble	Micro	Nickel sulfate hexahydrate	D	Lung Inflammation; Fibrosis
Soluble	Micro	Chromium, hexavalent	C	Lung Inflammation
Soluble	Micro	Ferrocene	B	Lung Inflammation

Footnotes on next page.

Footnotes to Table 4-1:

Abbreviations: NOAEL: No observed adverse effect level; LOAELs: Lowest observed adverse effect level; BMDL: Benchmark dose, 95% lower confidence limit. Nano: nanoscale; Micro: microscale particle. PSHT: Poorly soluble high toxicity; PSLT: Poorly soluble low toxicity.

* Solubility groups include medium or high solubility, as defined in Table 2-7 of TR Vol. II. Toxicity groups are based on definitions by Guest [1998] and as used in Brouwer [2012]. High toxicity is assigned here for poorly soluble materials with an OEL <1 mg/m^3 for the same or similar material including OELs for the non-nanoscale (bulk) materials.

** No nanoscale commercial form found for most of the sand blasting agents (Table 2-6 in TR Vol. II). High toxicity assumption is based on analogy to crystalline silica.

*** No microscale-to-nanoscale adjustment [NIOSH 2019] was made to the OEBs for the microscale materials.

† Adjusted points of departure below 0.001 mg/m3, suggesting a lower band F.

Notes: Table 4-1 is revised from Table 5-6 in TR Vol. II. The two particulate pesticides are omitted here.
Colors show differences in materials by physicochemical group (Column 1), also shown in Figure 4-1. Nanoscale materials (Column 2) are shown in a lighter shade of a given color in Table 4-1.

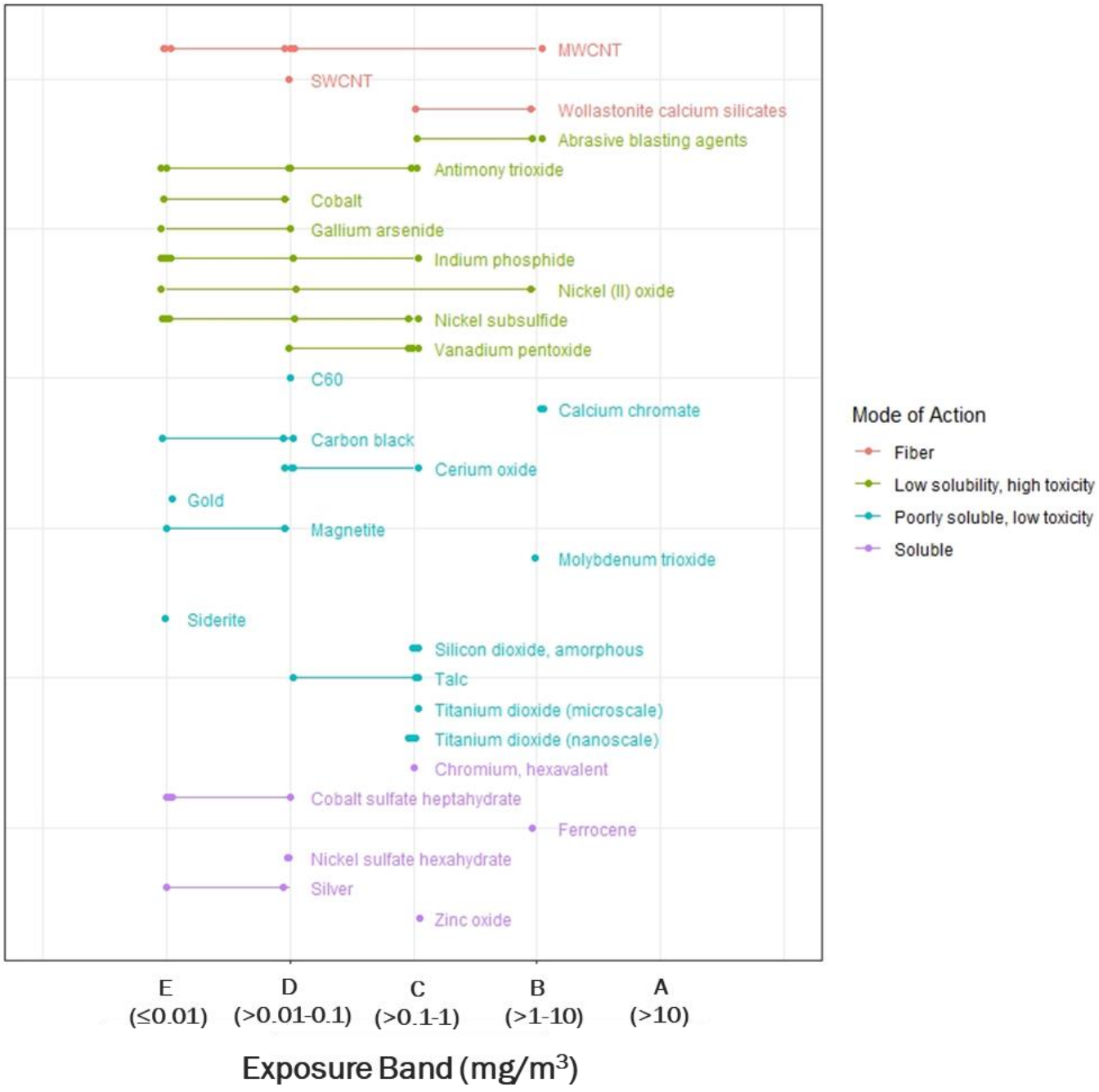

Figure 4-1: Occupational Exposure Band Estimates for Various Materials across Data Sources.
Revised from Figure 5-1 in TR Vol. II (two particulate pesticides are omitted here). Data are derived from Tables 5-2 through 5-5 in TR Vol. II. Horizontal lines indicate estimates span more than one band.

5 Alternative Methods to Derive Occupational Exposure Limits or Bands

5.1 Categorical OELs

Categorical OELs (cOELs) are group-based OELs. In this example, NIOSH estimated cOELs for ENMs based on hazard potency groups (Table 5-1). These groups were derived from statistical modeling and hierarchical clustering of rodent dose-response data of acute lung inflammation (detailed description provided in TR Vol. II, Sections 2 and 3). cOEL estimates were derived from two datasets: individual experimental data, reported in Drew et al. [2017], and a more comprehensive dataset with the addition of literature-based summary data, reported in Boots et al. [submitted]. Acute lung inflammation was used an endpoint because it is commonly reported in toxicology studies and provides information about the relative potency of ENMs. It does not meet the NIOSH [2019] criteria for a Tier 2 OEB. Further research is needed to determine if acute inflammation responses may be predictive of adverse lung effects from repeated exposures.

Particle lung dose associated with acute lung inflammation in rodents (measured as an added 4% polymorphonuclear leukocytes (PMNs) in bronchoalveolar lavage fluid) is the effect level that was used to derive an acute cOEL estimate. The BMD associated with lung inflammation was estimated from modeling the rodent dose-response data. A BMD is a dose estimate that provides an indication of hazard potency. The lower the BMD estimate, the greater the estimated potency of the material. The BMDL is the lower confidence limit on the BMD estimate and is typically used as a point of departure in quantitative risk assessment to account for uncertainty in the BMD estimate [NIOSH 2020]. Among the ENMs in each group, the 5th percentile of the distribution of BMDLs was used as the rodent effect level from which to estimate the human-equivalent concentration and to derive an acute cOEL estimate (8-hr TWA airborne mass concentration) (Table 5-1). The 5th percentile BMDL was selected to be precautionary if predicting the hazard potency group of a new material from modeling using the physicochemical properties (Section 2.1 of TR Vol. II).

These cOEL estimates reflect differences in the potency of the grouped ENMs for this endpoint in rodents. Overall, the cOEL estimates are similar whether derived from the initial experimental dataset or from the more comprehensive data set that includes literature-based data. For groups 2, 3, and 4, these cOEL estimates for the more comprehensive dataset are similar to but smaller than those from the initial dataset (reported in Drew et al. [2017]). For group 1, the cOEL estimate was much lower in the more comprehensive dataset (from Drew et al. [2017] and Boots et al. [submitted]). These differences could be due to the addition of more potent materials in the more comprehensive dataset, most of which were assigned to group 1, and/or more uncertain BMD estimates based on those data.

The materials in the least hazardous group 4 elicited a relatively low acute inflammation response, resulting in a relatively high dose estimate in the rodents and in humans at an estimated equivalent single day (8-hr) TWA airborne exposure concentration. It is important to note that these cOEL estimates for a single day 8-hr exposure

would not be considered protective for repeated exposures. For example, microscale (fine) TiO_2 is one of the materials in group 4, and the NIOSH REL for fine TiO_2 is 2.4 mg/m^3 as a TWA concentration for up to 10 hr/day during a 40-hour work week over working lifetime [NIOSH 2011].

Additional cOEL estimates based on other data and endpoints are shown in Tables 3-39 through 3-31 in TR Vol. II. Those data are from the NTP rodent chronic bioassays of (primarily) microscale particles, most of which have nanoscale applications (Table 2-6 in TR Vol. II). Endpoints evaluated in the NTP data include pulmonary inflammation, fibrosis, and cancer based on histopathology. These cOEL estimates tend to be lower than those shown in Table 5-1, which is consistent with longer exposures being associated with greater sensitivity of effects.

Table 5-1*. Categorical OEL Estimates for Acute Inflammation in Rats and Mice (4% PMNs above Background, 0–3 Days Post-Exposure); Nanoscale and Microscale Particle Lung Dose

Hazard Potency Group [a]	Rodent Estimated Effect Level [b] (µg/g lung)	Human-Equivalent Lung Dose (mg) [c]	Human-Equivalent Concentration, 8-hr TWA (mg/m^3) [d]	Categorical OEL Estimate for an 8-hr TWA exposure (mg/m^3) [e]	Associated OEB and exposure range (mg/m^3)
Initial dataset (NIOSH/ENPRA/CIIT)					
1	0.23	0.059	0.0309	0.0021	E (>0.001 to 0.01)
2	84.7	21.6	11.2	0.75	C (>0.1 to 1)
3	365	93.1	48.4	3.2	B (>1 to 10)
4	2,366	603	314	21	A (>10)
More comprehensive dataset—initial plus literature-based dataset					
1	**0.0032**	0.00082	0.00043	0.000029	F (<0.001)
2	**34.6**	8.83	4.6	0.31	C (>0.1 to 1)
3	**207**	52.9	27.5	1.8	B (>1 to 10)
4	**2,289**	584	304	20	A (>10)

* Same as Table 3-27 in TR Vol. II.

[a] Potency group created using complete linkage in initial dataset and using Ward's linkage in more comprehensive dataset.

[b] 5th percentile of the distribution of the BMDLs; boldface indicates the estimates shown in Table 4-2.

[c] Estimated by assuming rat lung weight of 1 g, then extrapolating the rat particle mass lung dose to humans by normalizing on the lung surface area in humans/rats of (102/0.4) (m^2/m^2).

[d] Estimated as: Human-equivalent Lung Dose (mg) / Worker reference air intake per day (9.6 m^3 [ICRP 1994]) x Alveolar deposition fraction estimate (estimate of 0.2 across respirable particle sizes).

[e] After application of total uncertainty factor of 15 to the human-equivalent concentration based on lung surface area dose normalization.

Abbreviations: PMNs: Polymorphonuclear leukocyte cells, measured in bronchioalveolar lavage fluid; BMDL: Benchmark dose, 95% lower confidence limit estimate; TWA: time-weighted average.

The materials that are included in these hazard potency groups are listed in Table 5-2. Table 5-2 provides information about the most likely group for a particular material. It also provides information on the number of studies on that material in the experimental and literature-derived database that NIOSH compiled and used in these analyses. Materials include both nanoscale and microscale forms of some materials (TiO_2 and silica).

Carbon nanotubes, TiO_2, and ZnO are the three most highly represented materials in this database. Among the carbon nanotubes, most are in group 1 (most potent) (73%) and the remainder are in group 2 (27%). TiO_2 is more broadly distributed among groups 1–4, which include 44% for group 1, 25% for group 2, 28% for group 3, and 3% for group 4. All ZnO materials are in group 1. Overall, 70% of materials are in group 1, 21% in group 2, 8% in group 3, and only 1% in group 4 (Table 5-2).

Table 5-2. Material Counts within Hazard Potency Group.

		Group*			
		1 (Most hazard)	2	3	4 (Least hazard)
Material	Total Count	Count within Group			
Carbon	5	3	1	0	1
CeO_2	8	8	0	0	0
CNT	33	24	9	0	0
MWCNT	32	23	9	0	0
SWCNT	1	1	0	0	0
Fe_3O_4	1	1	0	0	0
Graphene	6	4	2	0	0
In_2O_3	1	0	1	0	0
M5 (organic polymer)	1	1	0	0	0
Silica	6	3	3	0	0
crystalline	5	2	3	0	0
amorphous	1	1	0	0	0
TiO_2	32	14	8	9	1
ZnO	18	18	0	0	0
Total	**115**	**80**	**24**	**9**	**2**

* Hierarchical clustering based on Ward's method (Table 3-5 in TR II).

Additional information about the physicochemical properties within these hazard groups is shown in Table 5-3. Smaller median particle diameter is associated with greater hazard (assignment to group 1). Likewise, larger

median particle specific surface area is associated with assignment to group 1. Data are more limited for the other physicochemical properties shown in Table 5-3 and no clear trends are seen for those properties and group assignment.

Table 5-3. Physicochemical Properties within Hazard Potency Groups.

Physicochemical Property	Group*			
	1 (Most hazard) n=80	2 n=24	3 n=9	4 (Least hazard) n=2
	Median (Range) [Number included]			
Diameter (nm)	26	30	78	184
	(6–5,000)	(2–2,700)	(21–135)	(68–300)
	[68]	[22]	[2]	[2]
Specific surface area (m^2/g)	53	40	27	6
	(2–513)	(5–747)	(6–50)	(6)**
	[68]	[20]	[8]	[1]
Length (nm)	7,250	7,000	–	–
	(800–20,000)	(670 – 20,000)	–	–
	[30]	[10]	[0]	[0]
Density (g/mL)	5.6	2.11	3.9	4.25
	(0.01–7.22)	(0.10—7.16)	(3.9)**	(4.25)**
	[22]	[4]	[1]	[1]
Zeta Potential (mV)	-14.45	-30.3	–	–
	(-48.4– -9.35)	(-48.4– -11.8)	–	–
	[18]	[7]	[0]	[0]
Primary Particle Size (nm)	111	3,846	1,530	–
	(19–20,000)	(2,692–5,000)	(25–2,891)	–
	[17]	[2]	[7]	[0]

* Hierarchical clustering based on Ward's method.
** Only 1 value used in calculation.

In summary, the role of physicochemical properties suggested in these data analyses (see also Sections 3.1 and 3.3 in TR Vol. II) includes the following observations:

- Nanoscale materials tend to be assigned to more hazardous groups than microscale materials.

- Soluble metal oxides such as ZnO tend to be among the most hazardous materials for acute lung inflammation.
- Smaller diameter and larger particle surface area are associated with more hazardous groups.
- The structural form of the material is related to group assignment.
- Fiber-like materials are assigned to more hazardous groups.
- Material type or chemical composition is a strong predictor of hazard group.

The findings in Section 5.1 are intended to provide an overview of the hazard grouping based on the available data used in this report. The model for predicting group assignments of new materials was built using the combined data on all of the available physicochemical properties for a given material. Thus, these findings should not be used in read-across of a new material to assign a hazard group for a new material based on only some subset of these properties.

The ENM data available for the dose-response modeling and grouping analyses in this report tended to be for a small set of materials, such as TiO_2 and CNTs. A fully validated grouping framework will require a data with wider coverage to include more ENM types to further evaluate and validate the model. A more complete dataset on a core set of physicochemical properties is needed to further investigate the contribution of various physicochemical properties on the toxicity and grouping of ENMs. Additional assay and endpoint data, including acute to chronic in vivo assays and associated in vitro assays are needed to fully evaluate the potential health hazards of ENMs. Several datasets have been created or identified with the goal of meeting these requirements (e.g., NanoInformaTIX, https://www.nanoinformatix.eu/; see also Appendix F in TR Vol. II).

5.2 Read-across to Similar Materials

Read-across is a technique for predicting missing information for a substance of interest using data from a similar substance for the same endpoint [OECD 2014a,b; ECHA 2017]. Similarity is typically based on the structure, physicochemical properties, and biological activities. A weight-of-evidence approach is used to determine if the data being used are applicable to the target chemical. Read-across may involve qualitative evaluations and/or quantitative assessments including modeling structure-activity relationships (QSAR). Read-across may be used for different purposes, such as in screening, classification/labelling, or risk assessment. The steps in read-across include developing a read-across hypothesis, gathering data, and assessing the adequacy of the data to fill data gaps within the group of substances [ECHA 2019].

5.3 Categorical Reference Values

Early efforts in grouping of ENMs focused on four categories of ENMs based on broad physicochemical and toxicological properties. This pragmatic approach was proposed since the state of the science was too limited to derive health-based OELs for nanomaterials. Two such categorical approaches are shown in Table 5-4, which

includes the British Standards Institute [BSI 2007] benchmark exposure levels and the Dutch Social and Economic Council [SER 2012] provisional nano reference values. While efforts are underway to develop health-based OELs for ENM categories, preliminary groups such as those in Table 5-4 could serve as a starting point.

Table 5-4. Summary of previous European efforts to develop preliminary categories and reference values for occupational airborne nanomaterials.

Source	Name of categorical exposure limit	Categories and Exposure Limits			
British Standards Institute [BSI 2007]	Benchmark exposure levels	Fibrous 0.01 fibers/ml by scanning or transmission electron microscopy	CMAR* 0.1 × material workplace exposure limit (WEL)	Insoluble 0.066 × WEL (mass concentration) or 20 000 particles/ml	Soluble 0.066 × WEL
Dutch Social and Economic Council [SER 2012]	Provisional nano reference values	Nanofibers, rigid biopersistent 0.01 fibers/cm^3 (=10,000 fibers/m^3)	Granular biopersistent, density >6,000 kg/m^3 20,000 particles/cm^3	Granular biopersistent, density <6,000 kg/m^3 40,000 particles/cm^3	Non-biopersistent granular Applicable occupational exposure limit

Note: ml = cm^3

* Carcinogenic, mutagenic, asthmagenic or a reproductive toxin in larger particle form

5.4 Nanoscale vs. Microscale Potency Factor

Studies of poorly soluble particles of relatively low toxicity such as TiO_2 and carbon black have shown that nanoscale particles may elicit a greater pulmonary inflammation response in rats and mice than an equivalent mass dose of microscale particles [NIOSH 2011; Elder et al. 2006]. The toxicity relates to the greater particle surface area per unit mass of nanoscale than microscale particles. Limited evidence is available to estimate a microscale-to-nanoscale potency adjustment factor and is primarily focused on PSLT materials. In rats, the lung cancer incidence after chronic inhalation exposure to TiO_2 was estimated to be approximately eight times greater for nanoscale than microscale TiO_2 at an equivalent mass dose. That factor of eight reflects the difference in the specific surface area of those materials. In other analyses of PSLT materials based on rodent lung tumors or inflammation response, a factor of two to four has been proposed to adjust the microscale OELs to nanoscale OELs [Gebel 2012; Gebel et al. 2014; BAuA 2015].

PSLT is the most highly represented category in the data analyzed for OEBs in this report (Table 4-1). Among the PSLT particles, the nanoscale materials were generally assigned to more stringent bands than were the microscale particles (Table 4-1). For example, a post-hoc analysis in which the bands were assigned numerical values from 1 to 5 (for order-of-magnitude Bands A to E, respectively) resulted in average numeric scores of 4.25 and 2.75 for nanoscale and microscale particles, respectively (representing bands D-E for nanoscale vs. bands B-C for microscale particles). In other words, nanoscale materials were assigned to an exposure band that is one to two orders of magnitude lower than the exposure bands to which the microscale materials were assigned. This finding lends support to the NIOSH [2019] recommendation to reduce the OEB based on a microscale material to the next more stringent band (an order of magnitude lower exposure) for a nanoscale material of similar chemical composition. Representation of particles in the other categories was more limited, although the higher toxicity materials tended to be assigned to the more stringent bands regardless of particle size (Table 4-1).

5.5 Qualitative Hazard Bands

The Globally Harmonized System (GHS) hazard banding tool is a qualitative banding method based on the nature and severity of toxicity [WHO 2017]. The GHS criteria are also used in the NIOSH [2019] Occupational Exposure Banding tool. WHO [2017] applied the GHS criteria to the data available for a list of ENMs included in a study dossier of the OECD (Table 5-5). GHS category 1 implies serious and/or irreversible damage. Category 2 implies milder or reversible damage. Within a category, the designation "A" implies more serious effects, and "B" implies milder effects.

Table 5-5. Classification of hazardous properties of manufactured nanomaterials (MNMs) that have an Organization for Economic Cooperation and Development (OECD) Dossier [adapted from Table 2 in WHO 2017].

MNM	Acute toxicity	Skin corrosion/ irritation	Serious eye damage/eye irritation	Respiratory or skin sensitization	Germ cell mutagenicity	Carcinogenicity	Reproductive toxicity	Specific target organ toxicity (single exposure)	Specific target organ toxicity (repeated exposure)	Specific target organ toxicity (repeated exposure)
Fullerene (C_{60})	No[1]	No	No	No	No	No data[2]	No data	No data	No data	No
SWCNT	No	No	Cat 2A (H)[7]	No	Cat 2B[3] (L)[4]	No data IARC[5] 3	No data	No data	No data	Cat 1 (L)
MWCNT	No	No	No	No	Cat 2 (H)	MWCNT–7: Cat 2 (M)[6], IARC 2B Other MWCNTs: IARC 3	No	No data	No data	Cat 1 (M)
AgNP	No	No	No data	Cat 1B (M)	No	No data	No	No data	No data	Cat 1 inhalation (H) Cat 2 oral (H)
AuNP	No data	No data	No	No data	No data	No data	No data	No data	No data	Cat 1 inhalation (H)
SiO_2	No	No	No	No	No	No data	No	No data	No data	Cat 2 inhalation (H)
TiO_2	No	No	No data	No	No	No data; IARC 2B	Cat 2 (L)	No data	No data	Cat 1 inhalation (H)
CeO_2	No	No data	No data	No data	No data	No data	No data	No data	No data	Cat 1 inhalation (M)
Dendrimer	No data	No data	No data	No data	No data	No data	No data	No data	No data	No data

Footnotes on next page.

Footnotes to Table 5-5:

AgNP: silver nanoparticles; AuNP: gold nanoparticles; CeO_2: cerium dioxide; MWCNT: multi-walled carbon nanotubes; SiO_2: silicon dioxide; SWCNT: single-walled carbon nanotubes; TiO_2: titanium dioxide; ZnO: zinc oxide.

1 No: no hazard class assigned based on data.

2 No data: no studies available in OECD dossier.

3 GHS categories: Cat 1 usually implies serious and/or irreversible damage; Cat 2 milder or reversible damage. Within a category A implies more serious and B milder damage.

4 L: low level of evidence.

5 IARC refers to the International Agency for Research on Cancer categories of confidence in carcinogenicity: IARC Cat 2B = possibly carcinogenic; IARC Cat 3 = not enough evidence to draw conclusion.

6 M: moderate level of evidence.

7 H: high level of evidence.

5.6 Precautionary Approach

For new ENMs lacking data, initial decisions may need to be made regarding the potential occupational health hazard of exposure to the material. Guidelines on the use of a precautionary matrix for ENMs have been proposed [Höck et al. 2013]. If no relevant data are identified to derive an OEL, OEB, cOEL, or hazard band for the specific material, then the material should be assigned to the most protective hazard band. For ENMs, results from this analysis suggest the need for a more stringent OEB band F of <0.001 mg/m^3 (discussed further in Section 6.1).

Testing strategies to obtain the data needed for hazard assessment of ENMs have been proposed [Stone et al. 2014]. Coordination among various research consortia is underway to develop a more comprehensive database of ENMs for further analyses (Appendix F of TR Vol. II).

6 Application of Available Methods to Control Banding

6.1 Hazard Banding

Hazard banding is a systematic process that uses toxicology data to assign substances to hazard categories. Some hazard banding systems are qualitative only and others include quantitative exposure ranges. For example, the United Nations Globally Harmonized System of Classification and Labelling of Chemicals [UNECE 2015] is based on qualitative hazard bands that use information from established databases. The NIOSH [2019] Occupational Exposure Banding Process for Chemical Risk Management is a three-tiered system (depending on the data available and the purpose of the assessment) for banding substances by hazard and deriving quantitative OEBs.

OEBs are order-of-magnitude exposure concentrations designated by bands A through E. Substances with the lowest toxicity are assigned to Band A, and substances with the highest toxicity are assigned to Band E. The lower the concentration associated with the toxic effects, the more potent the substance. Hazard bands are used in conjunction with exposure banding (its own process) to derive appropriate control options in control banding frameworks (Figure 6-1).

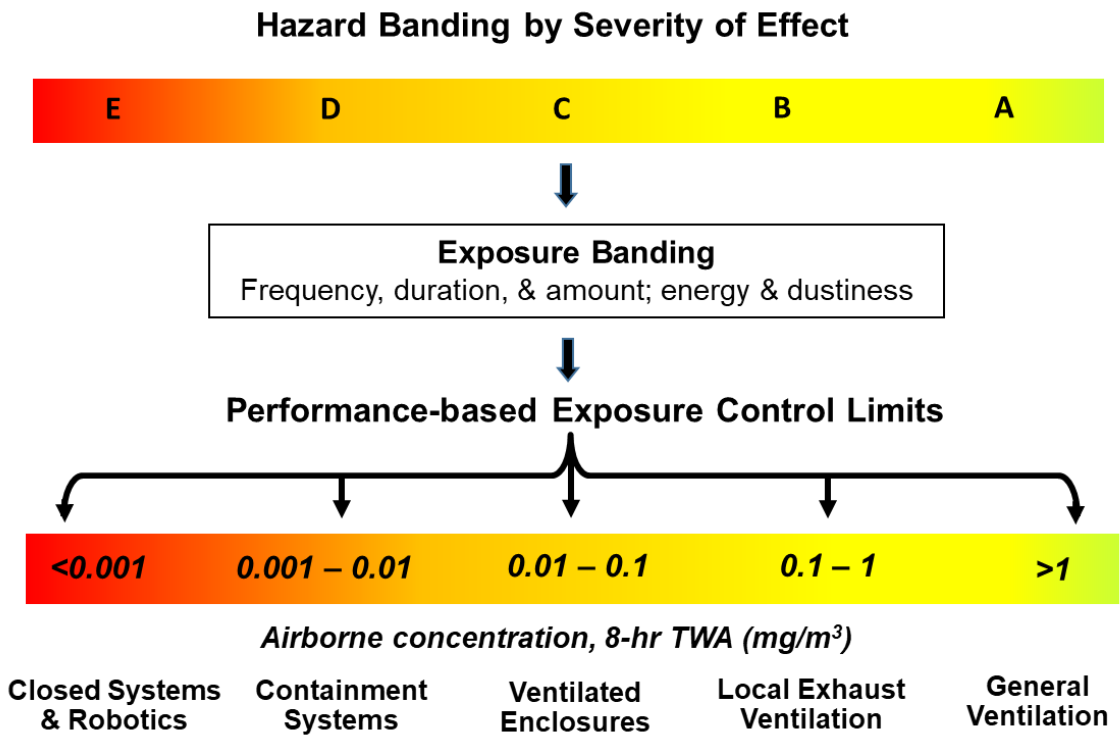

Figure 6-1. Example of a Control Banding Approach for Engineered Nanomaterials.

Adapted from Dunn et al. [2018]; ISO [2014a]; ANSES [2010]; HSE [2009]; Zalk and Nelson [2008]; Ader et al. [2005]; Brooke [1998]; Naumann et al. [1996]. The airborne concentrations shown here most closely align with those in Brooke [1998], HSE [2009], ANSES [2010], and ISO [2014a]. Colors indicate hazard, from red: most hazardous and most stringent exposure control options, to green: least hazardous and least stringent controls.

OEBs are defined differently in various approaches. The NIOSH [2019] OEBs are shifted towards higher exposures for a given band compared to those of several other hazard banding approaches (Table 6-1). This information needs to be considered when using these OEBs in control banding (Figure 6-1). Although the lowest exposure concentration is <0.01 mg/m^3 in each of these approaches, that concentration is aligned with band E in the NIOSH [2019] approach and with band D in the other approaches (Table 6-1).

Results from the derivation of OEBs for nanoscale and microscale particles (Section 4.2 of TR Vol II) suggest that in addition to the NIOSH [2019] OEBs, a more stringent band "F" (<0.001 mg/m^3) might be warranted to reflect the greater hazard potency estimates (lower OEBs) for some ENMs. A new band F in the NIOSH [2019] approach (Table 6-2) would align with band E in other banding tools (Table 6-1). Examples of exposure controls to achieve these and other airborne concentration bands are shown in Figure 6-1. In addition to the Hazard Band, an Exposure Band (determined separately) [NIOSH 2009] contributes to the determination of a Control Band.

Table 6-1. Comparison of Occupational Exposure Band (OEB) Definitions.

Reference	OEB (mg/m^3)				
	E	D	C	B	A
NIOSH [2019], Table 1-1	≤0.01	>0.01 to 0.1	>0.1 to 1	>1 to 10	>10
ISO [2014a]; ANSES [2010]; HSE [2009]; Brooke [1998]	Seek specialist advice	<0.01	0.01 to 0.1	0.1 to 1	1 to 10

Table 6-2. Suggested Extension of the NIOSH Occupational Exposure Bands (OEBs) for Application to Engineered Nanomaterials (ENMs).

Reference	OEB (mg/m^3)					
	F	E	D	C	B	A
NIOSH [2019], Table 1-1	NA	≤0.01	>0.01 to 0.1	>0.1 to 1	>1 to 10	>10
Recommended bands for ENMs*	≤0.001	>0.001 to 0.01	>0.01 to 0.1	>0.1 to 1	>1 to 10	NA

NA: Not applicable

* Based on analyses in TR Vol. II (Section 4.2), revision to NIOSH [2019] Table 1-1, "Airborne target range for dust or particle concentration (mg/m^3)," as applied to ENMs.

6.2 Example of Highly Produced Engineered Nanomaterials

ENMs of particular interest are those with the highest commercial production volume. Workers potentially can be exposed to these materials during their production or use, and also during maintenance and repair of equipment or systems. Figure 6-2 shows the hazard bands for the ENMs with the highest commercial volume [WHO 2017]. These materials are a subset of the materials in Figure 4-1, for which OEBs were estimated using the NIOSH [2019] Tier 2 criteria "STOT-RE" or "Carcinogenicity toxicity" endpoints. The minimum data requirement to estimate a Tier 2 OEB under these criteria is a 28-day inhalation exposure study in rats or mice. NIOSH recommends using the most stringent OEB in the event of multiple OEB estimates for a specific substance [NIOSH 2019].

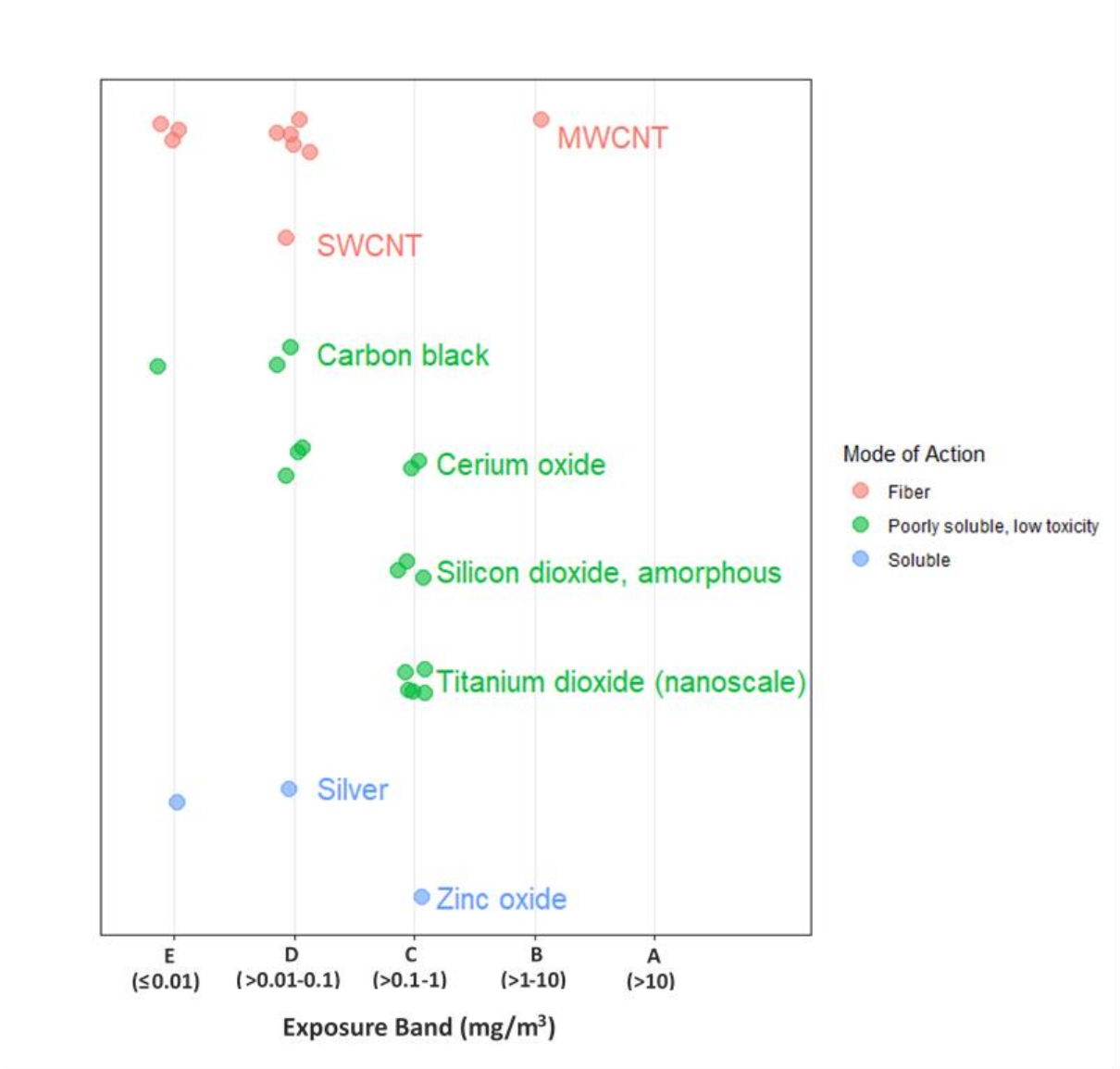

Figure 6-2: Occupational Exposure Band for Engineered Nanomaterials with Highest Commercial Volume [WHO 2017]. Adapted from Figure 5-2 of TR Vol. II. OEB results are jittered (scattered) around the band to show multiple estimates within the same band.

OEBs for the most highly produced ENMs [WHO 2017] are compared with the NIOSH REL [NIOSH 2007] for the same material in Table 6-3. The NIOSH REL shown is either nanoscale or unspecified particle size, as indicated. Of the six materials that each have a REL, the OEB for one material (TiO_2) contains the exposure concentration for the REL for nanoscale TiO_2. This is shown by the vertical alignment of the REL and OEB for TiO_2 in Table 6-3. The OEBS for three materials (carbon black, amorphous silica, and ZnO) were more stringent than their RELs, none of which was specific to the nanoscale form. In those cases, the OEB for the nanoscale form of the material was more stringent than the REL for the same material that was not specific to particle size. For the two ENMs with nanoscale RELs (CNT/CNF, silver), the OEBs were less stringent and also quite varied (Table 6-3). These results illustrate the importance of using the ENM REL, if available.

Table 6-3. Comparison of Occupational Exposure Bands (OEBs) – derived using NIOSH [2019] criteria – and NIOSH Recommended Exposure Limits (RELs) for the highest commercially produced engineered nanomaterials.

Occupational Exposure Band					
F[a]	E	D	C	B	A
Airborne Exposure concentration (mg/m^3)					
≤0.001	>0.001 to 0.01	>0.01 to 0.1	>0.1 to 1	>1 to 10	>10
Silver nano REL: 0.9 µg/m³	Silver OEB				
	Carbon black OEB			Carbon black REL[b,c]: 3.5 mg/m³	
		Cerium oxide OEB			
CNT & CNF REL: 0.9 µg/m³	MWCNT OEB				
		SWCNT OEB			
			Silica OEB	Silica amorph REL[c]: 5 mg/m³	
			TiO_2 nano OEB		
			TiO_2 nano REL: 0.3 mg/m³		
			ZnO OEB	ZnO REL[c]	

[a] Suggested extension of NIOSH [2019] band E, which is currently ≤0.01 mg/m^3 and thus includes exposures in band F.

[b] NIOSH REL includes carcinogen (Ca) designation; time-weighted average concentration of polycyclic aromatic

hydrocarbons (PAHs): 0.1 mg PAHs/m^3.

[c] Particle size not specified [NIOSH 2007].

Abbreviations: CNT: carbon nanotubes; CNF: carbon nanofibers: MWCNT: multi-walled CNT; SWCNT: single-walled CNT; nano: nanoscale; amorph: amorphous; TiO_2; titanium dioxide; ZnO: zinc oxide.

Notes: Commercial production information from WHO [2017]. OEB estimated range are shown in light blue and correspond to the individual OEB estimates shown in Fig. 6-2. RELs falling within exposure range of an OEB are shown in darker blue. Cerium oxide does not have a NIOSH REL. SWCNT is included in the NIOSH REL for CNTs and CNFs.

The differences in the OELs and OEBs may also reflect differences in the data and methods used to derive these values. Even among OELs, the values may cover a range of values (e.g., as shown in Table 3-1). This evaluation illustrates the current state of the health effects information for these commercially produced ENMs and identifies potential data gaps and research needs.

6.3 Summary of Steps

The first choice of an exposure limit for controlling workplace exposures is an authoritative OEL for a specific ENM (for examples, see Table 3-1). If an OEL is not available, the occupational health practitioner then evaluates the available hazard information for input into control banding (Section 6.1). Targeted literature searches should also be performed to identify any additional data sources that could be used to derive an OEB for the ENM of interest. One option may be to derive an OEB based on specific toxicity data for the nanoscale or microscale form of the material [NIOSH 2019]. Some examples of OEBs for ENMs derived using the NIOSH [2019] criteria are shown in this report (Table 4-1 and Figures 4-1 and 6-2). These examples show that the OEBs vary within material types or physicochemical groups. This variability may be attributable to differences in material properties as well as experimental design, duration of exposure, and lung response endpoint. In the absence of substance-specific data, NIOSH recommends selecting the most stringent band (lowest exposure range) derived from multiple data sources for a given ENM.

If an authoritative OEL is not available for the ENM, then NIOSH recommends evaluating the feasible options depending on the data available. It may be possible to derive an OEB or use one that was developed in these examples. Other approaches include categorical OEL grouping (Section 5.1), read-across to similar materials (Section 5.2), other categorical approaches Sections 5.3–5.5), or defaulting to the most stringent (most health protective) band until more information becomes available (Section 5.6).

The selected OEL, OEB, or cOEL is used in assessing the hazard of occupational exposures and making decisions about application of the hierarchy of controls and other risk management measures. Ultimately the selection of a specific tool depends on the purpose of the evaluation (e.g., prioritizing risks or evaluating exposure controls) and the availability of the input information [Dunn et al. 2018].

NIOSH recommends the following steps to occupational health practitioners assessing health hazards of ENMs:

- Use a level of evidence-based approach to select an OEL or OEBs for ENMs (Figure 2-1);

- Do a literature search for current information for use in hazard banding [NIOSH 2019];
- Use the updated OEBs for banding ENMs (Table 6-2); and
- Apply a validated control banding tool that meets the needs of the evaluation (e.g., Dunn et al. [2018]; see also Bibliography).

7 Conclusions

This user guide describes current scientific approaches for developing OELs or OEBs for ENMs that lack authoritative OELs. In the absence of a substance-specific OEL, NIOSH [2019] recommends occupational exposure banding to derive an OEB. If enough data are not available to derive an OEB, NIOSH recommends evaluating alternative methods, including categorical OEL grouping (described here), read-across to similar materials [OECD 2014a,b], or defaulting to the most stringent (most health protective) band until more information becomes available.

Such hazard information is used to inform workplace exposure controls and practices. Examples of OELs, OEBs, and cOELs for ENMs are provided in this report to assist the occupational health practitioner in hazard assessment and risk management decision-making.

Bibliography

For More Information on Occupational Exposure Limits, Hazard Banding, and Risk Management:

Gordon SC, Butala JH, Carter JM, Elder A, Gordon T, Gray G, Sayre PG, Schulte PA, Tsai CS, West J [2014]. Workshop report: strategies for setting occupational exposure limits for engineered nanomaterials. Regul Toxicol Pharmacol *68*(3):305–311. https://doi.org/10.1016/j.yrtph.2014.01.005

ISO [2016]. Nanotechnologies — Overview of available frameworks for the development of occupational exposure limits and bands for nano-objects and their aggregates and agglomerates (NOAAs). International Organization for Standardization (ISO) Technical Report ISO/TR 18637. Geneva, Switzerland: ISO. https://www.iso.org/standard/63096.html

Mihalache R, Verbeek J, Graczyk H, Murashov V, van Broekhuizen P [2017]. Occupational exposure limits for manufactured nanomaterials, a systematic review. Nanotoxicology *9*:1–13. https://doi.org/10.1080/17435390.2016.1262920

NIOSH [2007]. NIOSH pocket guide to chemical hazards. Cincinnati, OH: U.S. Department of Health and Human Services, Centers for Disease Control and Prevention, National Institute for Occupational Safety and Health, DHHS (NIOSH) Publication No. 2005–149. https://www.cdc.gov/niosh/npg

NIOSH [2009a]. Approaches to safe nanotechnology: managing the health and safety concerns associated with engineered nanomaterials. Cincinnati, OH: U.S. Department of Health and Human Services, Centers for Disease Control and Prevention, National Institute for Occupational Safety and Health, DHHS (NIOSH). Publication No. 2009–125. https://www.cdc.gov/niosh/docs/2009-125/pdfs/2009-125.pdf

NIOSH [2012]. General safe practices for working with engineered nanomaterials in research laboratories. Cincinnati, OH: U.S. Department of Health and Human Services, Centers for Disease Control and Prevention, National Institute for Occupational Safety and Health, DHHS (NIOSH). Publication No. 2012–147. https://www.cdc.gov/niosh/docs/2012-147/pdfs/2012-147.pdf?id=10.26616/NIOSHPUB2012147

NIOSH [2019]. Technical report: The NIOSH occupational exposure banding process for chemical risk management. By Lentz TJ, Seaton M, Rane P, Gilbert SJ, McKernan LT, Whittaker C. Cincinnati, OH: U.S. Department of Health and Human Services, Centers for Disease Control and Prevention, National Institute for Occupational Safety and Health, DHHS (NIOSH) Publication No. 2019-132. https://doi.org/10.26616/NIOSHPUB2019132

Schulte PA, Salamanca-Buentello F [2007]. Ethical and scientific issues of nanotechnology in the workplace. Environ Health Perspect 115(1):5–12. [also published in: Cien Saude Colet *12*:1319–1332]. https://dx.doi.org/10.1590/s1413-81232007000500030

Schulte P, Geraci C, Zumwalde, Hoover M, Kuempel E [2008]. Occupational risk management of engineered nanoparticles. J Occup Environ Hyg *5*:239–249. https://dx.doi.org/10.1080/15459620801907840

Schulte PA, Murashov V, Zumwalde R, Kuempel ED, Geraci CL [2010]. Occupational exposure limits for nanomaterials: State of the art. J Nanopart Res *12*(6):1971–1987. https://doi.org/10.1007/s11051-010-0008-1

Stone V, Pozzi-Mucelli S, Tran L, Aschberger K, Sabella S, Vogel U, Poland C, Balharry D, Fernandes T, Gottardo S, Hankin S, Hartl MG, Hartmann N, Hristozov D, Hund-Rinke K, Johnston H, Marcomini A, Panzer O, Roncato D, Saber AT, Wallin H, Scott-Fordsmand JJ [2014]. ITS-NANO—prioritising nanosafety research to develop a stakeholder driven intelligent testing strategy. Part Fibre Toxicol. *11*:9. https://dx.doi.org/10.1186/1743-8977-11-9

UNECE [2015]. Globally harmonized system of classification and labelling of chemicals (GHS). New York and Geneva: United Nations Economic Commission for Europe (UNECE). https://www.unece.org/fileadmin/DAM/trans/danger/publi/ghs/ghs_rev06/English/ST-SG-AC10-30-Rev6e.pdf

For More Information on Engineering Controls and Control Banding:

AIHA [2007]. Guidance for conducting control banding analyses. Fairfax, VA: American Industrial Hygiene Association. https://online-ams.aiha.org/amsssa/ecssashop.show_product_detail?p_mode=detail&p_product_serno=879

ANSES [2010]. Development of a specific control banding tool for nanomaterials. Maisons-Alfort Cedex, France: Agence nationale de sécurité sanitaire. [French Agency for Food, Environmental and Occupational Health & Safety. Request no. 2008-SA-0407. https://www.anses.fr/en/system/files/AP2008sa0407RaEN.pdf

Brouwer DH [2012]. Control banding approaches for nanomaterials. Ann Occup Hyg *56*(5):506–514. https://dx.doi.org/10.1093/annhyg/mes039

Dunn KH, Eastlake AC, Story M, Kuempel ED [2018]. Control Banding Tools for Engineered Nanoparticles: What the Practitioner Needs to Know. Annals of Work Exposures and Health *62*(3):362–388. https://dx.doi.org/10.1093/annweh/wxy002

Duuren-Stuurman B, Vink SR, Verbist KJ, Heussen HG, Brouwer DH, Kroese DE, Van Niftrik MF, Tielemans E, Fransman W [2012]. Stoffenmanager Nano version 1.0: a web-based tool for risk prioritization of airborne manufactured nano objects. Ann Occup Hyg *56*:525–541. https://dx.doi.org/10.1093/annhyg/mer113

Eastlake A, Zumwalde R, Geraci C [2016]. Can control banding be useful for the safe handling of nanomaterials? A systematic review. J Nanopart Res *18*:1–24. https://dx.doi.org/10.1007/s11051-016-3476-0

HSE UK [2013]. Control of substances hazardous to health: Approved code of practice and guidance 2002. 6th ed. Sudbury, UK: HSE Books. https://books.hse.gov.uk/?DI=649406

ISO [2014a]. Nanotechnologies—occupational risk management applied to engineered nanomaterials. Part 2: Use of the control banding approach. ISO/TS 12901-2. Geneva, Switzerland: International Organization for Standardization. https://www.iso.org/standard/53375.html

Liguori B, Hansen SF, Baun A, Jensen KA [2016]. Control banding tools for occupational exposure assessment of nanomaterials—ready for use in a regulatory context? NanoImpact *2*:1–17. https://doi.org/10.1016/j.impact.2016.04.002

NIOSH [2009b]. Qualitative risk characterization and management of occupational hazards: control banding (CB): a literature review and critical analysis. Cincinnati, OH: U.S. Department of Health and Human Services, Centers for Disease Control and Prevention, National Institute for Occupational Safety and Health, DHHS (NIOSH) Publication No. 2009-152. https://www.cdc.gov/niosh/docs/2009-152/

NIOSH [2013b]. Current strategies for engineering controls in nanomaterial production and downstream handling processes. Cincinnati, OH: U.S. Department of Health and Human Services, Centers for Disease Control and Prevention, National Institute for Occupational Safety and Health, DHHS (NIOSH). Publication No. 2014–102. https://www.cdc.gov/niosh/docs/2014-102/pdfs/2014-102.pdf

Sánchez Jiménez A, Varet J, Poland C, Fern GJ, Hankin SM, van Tongeren M [2016]. A comparison of control banding tools for nanomaterials. J Occup Environ Hyg *13*(12):936–949. https://dx.doi.org/10.1080/15459624.2016.1200191

Zalk DM, Nelson DI [2008]. History and evolution of control banding: a review. J Occup Environ Hyg 5(5):330–346. DOI: 10.1080/15459620801997916

Zalk DM, Paik SY, Swuste P [2009]. Evaluating the control banding nanotool: a qualitative risk assessment method for controlling nanoparticle exposures. J Nanopart Res 11:1685–1704. https://doi.org/10.1007/s11051-009-9678-y

Zalk DM, Kamerzell R, Paik S, Kapp J, Harrington D, Swuste P [2010]. Risk level based management system: a control banding model for occupational health and safety risk management in a highly regulated environment. Indust Health 48(1):18–28. https://dx.doi.org/10.2486/indhealth.48.18

Zalk DM, Paik SY, Chase WD [2019]. A quantitative validation of the Control Banding Nanotool. Ann Work Expo Health 63(8):898-917. https://dx.doi.org/10.1093/annweh/wxz057

References Cited

Please see References in Technical Report Volume II for a complete list of references cited in this User Guide.

II. Technical Report:

Approaches to Developing Occupational Exposure Limits or Bands for Engineered Nanomaterials

Centers for Disease Control and Prevention
National Institute for Occupational Safety and Health

Page intentionally left blank

II. Technical Report:
Approaches to Developing Occupational Exposure Limits or Bands for Engineered Nanomaterials

DEPARTMENT OF HEALTH AND HUMAN SERVICES
Centers for Disease Control and Prevention
National Institute for Occupational Safety and Health

Abstract

Federal agencies and safety and health groups set occupational exposure limits (OELs) to protect workers from harmful substances in the workplace. Some OELs apply to engineered nanomaterials, which are purposely created products with at least one dimension between 1 and 100 nanometers. Some types of these materials can harm workers who breathe them in, absorb them through their skin, or swallow them. This report focuses on airborne nanomaterials and potential lung effects in workers.

Most engineered nanomaterials lack enough research data to set an OEL. This report shows how occupational exposure bands can be developed for some engineered nanomaterials without an OEL. Other engineered nanomaterials can be grouped into categories of materials with similar properties and potential adverse health effects. This method can give evidence to support safety policies such as engineering controls and other measures.

Engineered nanomaterials are evaluated based on research in rodents. Studies in rodents have observed sudden or long-term inflammation of the lungs, which is a biological response to these materials in the lungs. Some rodent studies have reported fibrosis (thickening or scarring of lung tissue) or lung cancer. Statistical research shows how physical and chemical properties of the nanomaterials can help predict potential early lung effects.

The described methods assess typical microscale airborne particles and various engineered nanomaterials by their possible health impact. This process can be used to group engineered nanomaterials into categories based on how much their effects may harm the health of exposed workers.

This report is for professionals who assess risks or decide how to manage risks in the workplace. This is Part II of a two-part report. Part I is the User Guide, which describes the tools for gathering and assessing information on occupational exposure limits or bands for engineered nanomaterials. Part II is the Technical Report, which describes the development of the methods to group engineered nanomaterials. Part II also describes the basis for the categorical occupational exposure limits or bands illustrated in Part I. These findings give evidence to support enhanced safety and health policies for engineered nanomaterials.

Executive Summary

The objectives of this Technical Report (TR) are to describe state-of-the-science approaches for developing categorical occupational exposure limits (cOELs) or occupational exposure bands (OEBs) for engineered nanomaterials (ENMs) that lack sufficient experimental data to develop substance-specific occupational exposure limits (OELs). This information is intended for occupational safety and health professionals and researchers assessing the data and methods available to estimate the potential occupational health risks of exposure to airborne ENMs.

A common goal in the health and safety research community is to develop evidence-based approaches to deriving occupational exposure limits or bands for ENMs [ISO 2016]. Individual OELs have been developed for some ENMs [Mihalache et al. 2017; Rodriguez-Ibarra et al. 2020], including titanium dioxide, carbon nanotubes, and silver [NIOSH 2011, 2013, 2021]. Typically, these assessments have used a common set of studies for a given ENM (in part because of the relatively few studies of ENMs that are sufficient for quantitative risk assessment), although the specific methods and assumptions have varied, resulting in a wide range of proposed OELs for a given ENM [ISO 2016; Mihalache et al. 2017]. Earlier, cOELs were proposed for groups of ENMs that reflect broad physicochemical and toxicological characteristics, such as poorly soluble (biopersistent) low-toxicity (PSLT) particles, versus higher-toxicity fiber-shaped or soluble materials [BSI 2007; SER 2012].

Because of the large and growing number of ENMs, methods are needed that use available scientific information to characterize their potential occupational health risks. Testing all new materials individually is typically not feasible because of time and economic factors, and grouping strategies are being developed to provide a timely solution. Traditionally, a two-year bioassay including hundreds of rodents would be used to generate data to assess the health hazard of a single material. These bioassays are very expensive, and when this expense is considered jointly with the rapid rate at which new ENMs are entering production processes, the need for novel hazard assessment methodologies arises.

This report has two parts. Part I of this report is the User Guide, which describes the tools for gathering and assessing information on OELs or OEBs for ENMs. This document is Part II, which describes the development of the methods to group ENMs by hazard potency and to predict the hazard potency group based only on the physicochemical information. Part II also describes the technical basis for deriving the cOELs or OEBs illustrated in Part I. This information is provided for occupational safety and health professionals and researchers who use scientific information and analytical methods to assess safety and health risks in the workplace.

The information on a new material will likely include only limited (if any) experimental data but may include physicochemical descriptors. In this report, statistical learning methods are described that can be used to explore the predictive potential of various physicochemical properties to classify the material into a hazard group. This framework is explored across several toxicological assay types and health endpoints with use of currently available data from *in vivo* (rodent) and *in vitro* (cellular) studies.

The animal and cellular data were evaluated with quantitative risk assessment methods to examine the relationships between exposure to nanoscale or microscale materials and biological responses relevant to workers' health. Biological responses and adverse outcomes examined include pulmonary inflammation in rodents 1 to 3 days post-exposure, cytokine release in THP-1 cells (human monocytic cell line), mortality after 24 hours in zebrafish embryos, and persistent pulmonary inflammation, fibrosis, and lung cell neoplasia in rodents following sub-chronic and chronic inhalation exposures. The relative rankings of material hazard estimates (based on potency of response) were compared across different experimental conditions, and data sources available for further analysis were summarized.

Comparison of the hazard potency groupings and relative ranking results for nanoscale and microscale materials showed similar findings in rodent and cellular studies. Nanoscale materials tended to be more potent on a mass basis than microscale materials. The total particle surface area dose is greater for nanoscale materials than for microscale particles because of the greater number of particles in a given mass of nanomaterials. Within a given particle size category (nanoscale or microscale), other physicochemical factors that contributed to ENM potency include shape and surface modification. These results are consistent with previous findings, which suggest that material chemical composition is not sufficient to predict the toxicity across various types of materials. The relative rankings of hazard potency across the materials studied were similar between the rodent *in vivo* and the rodent or human cell *in vitro* assays for inflammation. These results are consistent with previous findings suggesting that *in vitro* assays may be useful in predicting acute pulmonary inflammation of ENMs [Monteiller et al. 2007; Donaldson et al. 2008; Rushton et al. 2010; Zhang et al. 2012]. Various experimental factors were also found to contribute to reported hazard potency, including differences in assay type, laboratory, material type, species/strain/sex, route/duration of exposure, and specific endpoints studied. These results indicate that, in addition to differences in physicochemical properties of the materials, these various experimental factors need to be considered in any evaluation of relative potency across materials.

The large amount of varied data allows for numerous exploratory insights; however, several common data limitations became apparent and additional research questions were identified. The set of materials analyzed in the document may not be representative of the universe of materials to which workers are exposed, resulting in uncertainty regarding the potential hazard of unstudied materials. Many factors contribute to the estimation of a material's hazard, including experimental design (route and duration of exposure, exposed organism, biological endpoint) and intrinsic material properties (size, modification). It was rare to have relevant data for a given material across all of the different assays and endpoints explored here, leading to uncertainty in the effects of these factors on material hazard. Because of the available data, health hazards were estimated on a particle mass basis, whereas other metrics such as surface area may be better suited for hazard identification across a range of particle sizes and types. Physicochemical properties were considered to be the information most likely to be available for new ENMs yet exploring the utility of these properties was hampered by inconsistent reporting of the properties themselves or inconsistent methods of measurement.

OELs and OEBs are important tools for prevention of occupational disease from exposure to potentially hazardous substances [Schulte et al. 2010; NIOSH 2019]. An OEL is a single value that generally refers to a specific substance, although some OELs apply to broader categories, such as dust or particles not otherwise regulated [NIOSH 2007; ISO 2016]. Most OELs are time-weighted average airborne concentrations (typically over 8 hours) representing a safe level of exposure for most workers over their working lifetime [Gordon et al. 2014; ACGIH 2014]. OEBs are bands, rather than single values, that define a range of air concentrations expected to protect worker health [NIOSH 2019]. OEBs are derived from standardized criteria when data are too limited to develop substance-specific OELs, as is the case for many ENMs [Kuempel et al. 2012; ISO 2016; Dunn et al. 2018; NIOSH 2019]. OELs and OEBs are used in assessing and controlling workplace exposures and for triggering the use of personal protective equipment (PPE) and other risk management measures [NIOSH 2009; Schulte et al. 2010].

Traditionally, OELs are derived for individual materials with quantitative risk assessment methods using subchronic or chronic data on humans or rodents [NIOSH 2020]. Thus, uncertainty arises when estimating the working lifetime health risk for humans with use of data from acute or short-term *in vivo* or *in vitro* experiments. To help address this uncertainty, we developed hazard potency estimates for representative (benchmark) materials (primarily microscale) and a variety of ENMs. These hazard potency estimates provide a basis for comparative toxicity of the ENMs and for estimating cOELs for groups of similar materials with regard to specific health endpoints. These hazard potency estimates are also used to evaluate the OEB process for nanoscale and microscale airborne particles. For ENMs, data are often lacking to estimate an OEL, but an OEB may be derived from adjustments to data for microscale forms of the materials [NIOSH 2019]. This information supports occupational health decision-making, such as for evaluation of engineering controls and other occupational risk management measures.

In addition to evaluating the available data to develop OEBs for ENMs in this report, the toxicology data available for specific ENMs were analyzed for their utility in developing a predictive model for grouping ENMs on the basis of hazard potency. This proof-of-concept model uses ENM-specific data that have the potential to replace the default adjustments currently used for ENMs in the OEB framework. Currently, the data are too heterogeneous to fully develop and validate a predictive model for hazard potency based on ENM physicochemical properties. However, it was feasible to derive hazard potency groups for ENMs with sufficient data and to use those findings to estimate cOELs for materials of similar hazard potency for specific endpoints. This document provides an overview of the type of data available and shows what methods can be applied to those data for estimating and grouping ENMs according to risk of occupational respiratory effects.

The analysis framework described in this document was developed on the basis of currently available data, sourced from within NIOSH, external collaborators, or publicly available repositories, and the framework can be used to analyze new data as they become available. Several efforts are underway at NIOSH and with collaborators to build more comprehensive databases including more robust data for quantitative analyses. As these databases grow, new analyses will build onto this framework. The picture will begin to fill out across a full

range of materials and experimental designs. Additional linkages across assays and endpoints could facilitate comparative potency analyses and development of a predictive model based on physicochemical properties and/or short-term *in vivo* or *in vitro* assays.

With additional data and analyses, the currently limited and preliminary estimates of cOELs or OEBs can be expanded and uncertainties reduced. Confidence in the estimates would increase with additional data and evaluation. A strength of this methodology is that the biologically relevant metric of hazard potency is estimated with use of standard quantitative analyses across a range of materials, including benchmark materials, which are relatively well studied and with more complete data. Ultimately, a goal of predicting the material-specific differences in hazard potency is to provide an opportunity for prevention through design of nanoscale and other emerging materials, that is, to fine-tune the material to reduce its hazard while retaining its functionality for the intended purpose. In addition, a predictive model will be informative on the minimum set of toxicity assays needed for input into the predictive models to assess hazard potency. Finally, the cOEL and OEB estimates provide an example of the evidence basis needed to support evaluation of workplace exposure controls, including the use of control banding procedures.

Contents

Abbreviations

AIC	Akaike information criterion
BMD	Benchmark dose
BMDL	95% Lower confidence limit of benchmark dose
BMR	Benchmark response
cOEL	Categorical occupational exposure limit
DAF	Dosimetric adjustment factor
EPA	U.S. Environmental Protection Agency
ENM	Engineered nanomaterial
GHS	Globally Harmonized System of Classification and Labelling of Chemicals
HEC	Human equivalent concentration
ISO	International Standards Organization
LOAEL	Lowest observed adverse effect level
μg/g lung	Microgram per gram of lung
mg/m^3	Milligram per cubic meter
NIOSH	National Institute for Occupational Safety and Health
NOAEL	No observed adverse effect level
OEB	Occupational exposure band
OEL	Occupational exposure limit
PB-ECL	Performance-based exposure control limit
PoD	Point of departure
QRA	Quantitative risk assessment
QSAR	Quantitative structure-activity relationship
STOT-RE	Specific target organ toxicity – repeated exposure
STOT-SE	Specific target organ toxicity — single exposure
TR	Technical report
UF	Uncertainty factor

Glossary

Acute toxicity: Adverse effects that occur following oral or dermal administration of a single dose of a substance, multiple doses given within 24 hours, or inhalation exposure of 4 hours

Benchmark dose (BMD): A dose that produces a predetermined change in the response rate of an adverse effect relative to the background response rate of this effect. The dose may be as administered or as measured in biological tissues or fluids.

Benchmark response (BMR): A predetermined change in the response rate of an adverse effect relative to the background response rate of this effect. A BMR is typically in the low-dose region of the data (e.g., 10% increase over background response).

Categorical occupational exposure limit (cOEL): An OEL for a category of substances with similar potency with respect to adverse health endpoints.

Carcinogenicity: The ability of a chemical substance or a mixture of chemical substances to induce tumors, increase tumor incidence and/or malignancy, or shorten the time to tumor occurrence.

Dose: The total amount of an agent administered to, taken up by, or absorbed by an organism, system, or (sub)population.

Dose-response: The relationship between the amount of an agent administered to, taken up by, or absorbed by an organism, system, or population and the change developed in that organism, system, or population in reaction to the agent.

Dosimetric adjustment factor (DAF): A multiplicative factor used to adjust observed animal or epidemiological data to estimate a human equivalent concentration (HEC) for an exposure scenario of interest. For inhaled particles, DAFs include factors to account for interspecies differences in ventilation rate, particle deposition fraction, and surface area of the respiratory tract region(s) of interest [adapted from U.S. EPA 1994].

Exposure: Contact between an agent and a target. Contact takes place at an exposure surface over an exposure period.

Hazard: The inherent property of an agent (or situation) having the potential to cause an adverse effect when an organism, system, or population is exposed to that agent.

Lowest observed adverse effect level (LOAEL): The lowest dose or concentration at which there are statistically significant increases in the frequency or severity of biologically significant adverse effects between the exposed population and its appropriate control group [adapted from U.S. EPA 1994].

No observed adverse effect level (NOAEL): The highest dose or concentration at which there are no statistically significant increases in the frequency or severity of biologically significant adverse effects between the exposed

population and its appropriate control group; some effects may be produced at this dose level, but they are not considered adverse or precursors of adverse effects observed [adapted from U.S. EPA 1994].

Occupational exposure band (OEB): The range of air-concentration levels expected to be protective of worker health. The bands range from A (highest range of exposure concentrations) to E (lowest range) [NIOSH 2019].

Occupational exposure limit (OEL): An upper limit on the acceptable concentration of hazardous substance in workplace air for a particular material or class of materials. OELs may apply to ceiling short-term exposure limits (STELs) or time-weighted average (TWA) limits.

Point of departure (PoD): A point on the dose-response curve from experimental or observational data, which is a dose associated with a level of no or low effect, and which is estimated without significant extrapolation beyond the data. A PoD is often a NOAEL, LOAEL, or BMD estimate from an animal study.

Potency: The inverse of dose of a substance eliciting a specified biological response (that is, the smaller the dose, the greater the potency).

Specific target organ toxicity—repeated exposure: All significant health effects, not otherwise specifically included in the Globally Harmonized System of Classification and Labeling of Chemicals, that can impair function after repeated exposure to a substance. The effects can be reversible, irreversible, immediate, and/or delayed.

Acknowledgments

This draft Technical Report (TR) was developed by the scientists and staff of the National Institute for Occupational Safety and Health (NIOSH), Division of Science Integration (DSI), Nanotechnology Research Center (NTRC) and Emerging Technologies Branch (ETB). Paul A. Schulte is the Director of DSI and Co-Manager of the NTRC. Charles L. Geraci is the NIOSH Associate Director for Emerging Technologies and Co-Manager of the NTRC. Jay Vietas is the Branch Chief of ETB. Laura Hodson is the Coordinator of the NTRC and Deputy Branch Chief of ETB.

This document was authored by Nathan M. Drew and Eileen D. Kuempel, NIOSH/DSI/NTRC and ETB, and by Theresa E. Boots, NIOSH/Health Effects Laboratory Division/BioAnalytics Branch, formerly an Oak Ridge Associated Universities (ORAU) Fellow at NIOSH/NTRC.

The authors appreciate the technical contributions of the following individuals: Alyssa Kogel, formerly an ORAU Fellow at NIOSH/NTRC, and Sarah E. Davidson, an ORAU Fellow at NIOSH/NTRC, who assisted with the data curation and benchmark dose modeling; Randall J. Smith, NIOSH/DSI/Risk Evaluation Branch, who provided input on some of the statistical methods used in these analyses; and Ann F. Hubbs, NIOSH/Health Effects Laboratory Division/Pathology and Physiology Research Branch, who provided input on the histopathological diagnostic terms for pulmonary inflammation, fibrosis, and neoplasia in the National Toxicology Program (NTP) histopathology database.

The following individuals are acknowledged for providing comments on earlier drafts of the document: Laura Hodson, NIOSH/DSI/ETB; Aleks Stefaniak, NIOSH/RHD/FSB; Jenny Roberts, NIOSH/HELD/ACIB; Kevin L. Dunn, NIOSH/DFSE/HETAB; Melissa Seaton, NIOSH/DSI/SAB; T.J. Lentz, NIOSH/DSI/SAB; Dana Rottach, NIOSH/NPPTL/RB; Christopher Coffey, NIOSH/NPPTL; and William King, NIOSH/NPPTL/RB.

The authors thank research colleagues from NIOSH and other institutes for providing experimental data from toxicology studies that were used in these analyses.

The NIOSH NTRC acknowledges the contributions of Vanessa Williams for desktop publishing and graphic design and Seleen Collins for editing.

1 Introduction

1.1 Background and Objectives

The objectives of this Technical Report (TR) are to describe state-of-the-science approaches for developing categorical occupational exposure limits (cOELs) or occupational exposure bands (OEBs) for engineered nanomaterials (ENMs) for which the experimental data are insufficient for development of substance-specific OELs. OEBs are based on easily accessible qualitative and quantitative hazard information used in a tiered methodology to identify the appropriate category for guiding risk management, with information being GHS codes, points of departure, and more detailed data. Categorical OELs are based on benchmark dose estimates, with categories consisting of chemicals with similar hazard identified via statistical learning methods. Examples of categorical OELs (Section 3.5) and OEBs (Section 4.1) for ENMs are provided on the basis of evaluation of available dose-response data for nanoscale and microscale particles.

Nanomaterials represent a subset of particulate materials that can be dispersed in the air and can represent health risks via inhalation, ingestion, or dermal exposures. Nanomaterials include spheres, fibers, or other structures with one, two, or three external dimensions in the nanoscale (from approximately 1 nm to 100 nm for primary structures). Nanomaterials can consist of individual primary structures or aggregated or agglomerated structures (including >100 nm). An aggregate comprises strongly bonded or fused particles (structures). An agglomerate is a collection of weakly bound particles (structures) [ISO 2007; ISO 2014a,b]. Broad terms for nanomaterials proposed by the International Standards Organization (ISO) are Nano-Objects and their Aggregates and Agglomerates (NOAAs) [ISO 2007; ISO 2014a,b]. The commonly used term *ENMs* refers to intentionally produced or manufactured nanomaterials for commercial use.

In this report, published data on nanoscale and microscale particulate materials from experimental data on animal and cell systems are compiled and analyzed to compare hazard potency for pulmonary endpoints. The application of these analyses is to evaluate the occupational health risks of existing and new ENMs. Another term for ENMs is manufactured nanomaterials, and both terms distinguish the intentionally produced nanomaterials from incidental (e.g., combustion-derived) nanomaterials, which is beyond the scope of this document.

Workers have the potential for exposure during the production, use, recycling, and disposal of ENMs. Workers may also be exposed to other hazardous substances in the workplace. Inhalation is a primary route of exposure to airborne nanomaterials and to other airborne substances (e.g., respirable particulate matter including a nanoscale fraction, such as from combustion sources).

OELs and OEBs are important tools used in the assessment and control of exposures to prevent occupational illness. OELs have a long history in industrial hygiene and are based on observations in workers or studies in laboratory animals [Schulte et al. 2010; Gordon et al. 2014]. An OEL is generally substance-specific (though sometimes generically expressed, such as dust). Relatively few ENMs have individual OELs. Some OELs have been developed for ENMs by government agencies, nongovernmental organizations, companies, and academic researchers [NIOSH 2011, 2013; Gordon et al. 2014; ISO 2016; Mihalache et al. 2017]. No regulatory OELs have been developed to date for ENMs in the United States or other countries.

The OELs that have been developed for individual ENM particles include primarily metals or metal oxides (ultrafine titanium dioxide, silver) and carbonaceous nanoparticles (carbon nanotubes, fullerenes) [NIOSH 2011, 2013; Weldon et al. 2016; Mihalache et al. 2017; Schulte et al. 2018; NIOSH 2021]. The specific methods used to develop these OELs have varied, resulting in a range of published OELs for a given ENM [ISO 2016; Mihalache et al. 2017] (also see Table 3-1 in TR Vol. I). Despite these differences, the OELs for ENMs are generally much lower than the OELs for microscale particles of the same chemical substance (as shown in Table 3-1 in TR Vol. I). In addition to OELs for individual ENMs, OELs have been proposed for some broad categories of ENMs, including poorly soluble low-toxicity particles, soluble particles, and fibers [BSI 2007; ISO 2016]. Inhalation exposures, a primary concern in the workplace, are the focus of most OELs for ENMs to date, although some values have been developed for dermal or oral exposure routes as well [Mihalache et al. 2017].

When adequate data are not available to develop an OEL, it may be feasible to derive an OEB. OEBs are exposure bands used in hazard communication and exposure control decisions for substances without OELs. Control banding consists of hazard banding and exposure banding, and it has been used for many years to identify appropriate control options [Henry and Schaper 1990; Naumann et al. 1996; HSE 2009]. Control banding tools specific to ENMs have been reviewed in several articles [Brouwer 2012; Eastlake et al. 2016; Liguori et al. 2016; Sánchez Jiménez et al. 2016; Dunn et al. 2018]. The terms OEB and hazard band are sometimes used interchangeably, but in general OEB refers to a quantitative exposure range, while hazard bands may be limited to qualitative categories. Examples of quantitative, order-of-magnitude exposure bands include: <0.001 mg/m^3; 0.001 mg/m^3 to <0.01 mg/m^3; 0.01 mg/m^3 to <0.1 mg/m^3; 0.1 mg/m^3 to <1 mg/m^3; and ≥ 1 mg/m^3 (Table 1-1; Figure 1-5). Both OELs and OEBs provide occupational safety and health professionals with a health basis for assessing the effectiveness of exposure controls and other risk management practices [Dunn et al. 2018; NIOSH 2019].

The data available for hazard assessments vary across materials and are often limited for emerging materials such as ENMs. Substances are assigned to a hazard band on the basis of toxicity data, usually from animal studies. The GHS hazard codes [UNECE 2015] are useful for a qualitative assessment of hazard. An estimate of hazard potency (e.g., a low or no observed adverse effect level) is typically used to develop an OEB. The more complete dose-response data from well-designed experimental studies in rodents are preferred and typically used in quantitative risk assessment (QRA) and development of an OEL (Figure 1-1). The three tiers of assessment shown in Figure 1-1 are consistent with those described in the NIOSH occupational banding framework [NIOSH 2019]. Tier 2 OEBs were estimated for ENMs in this report by using the NIOSH [2019] recommendations for two health endpoints in rodent studies: Specific Target Organ Toxicity-Repeated Exposure (STOT-RE) and cancer. Hazard potency groups of ENMs based on pulmonary inflammation in rodents are also provided as a frequently reported endpoint in animal studies.

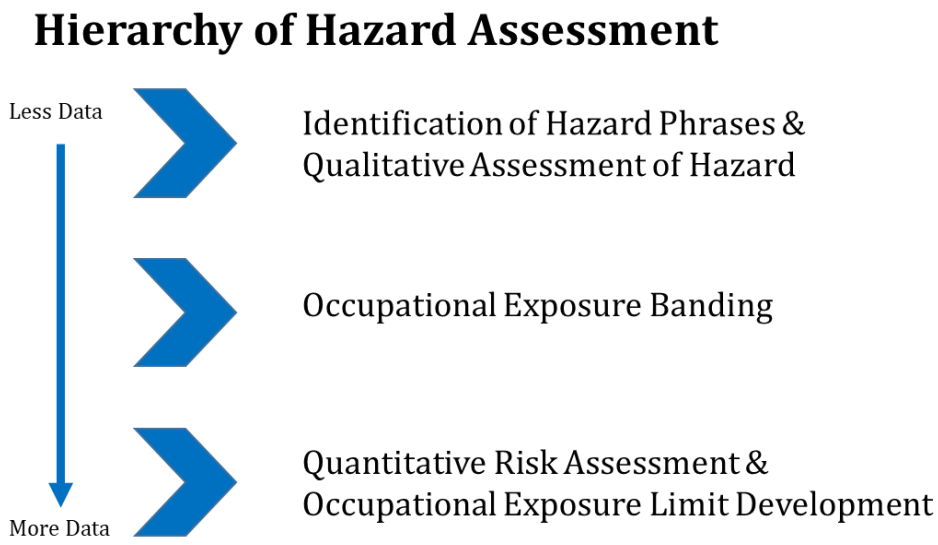

Figure 1-1. Hierarchy of data needed to assess the health hazard or risk of chemicals and the development of OEBs or OELs.

For QRA, the types of data that potentially could be used are shown in Figure 1-2. Human data are preferred, when available, to estimate potential health risks in workers, although animal data are more likely to be available. In addition, for emerging materials with limited data, alternative approaches (e.g., grouping, read-across, high-throughput assays) have been proposed to fill these gaps [U.S. EPA 2014; OECD 2014a,b; OECD 2016; NAS

2017]. The degree of uncertainty in the data is illustrated in Figure 1-2 by the surface area shown; and the position illustrates the relative importance and utility of data for risk assessment and estimation of OELs. In general, the available data on humans are insufficient for estimating dose-response relationships for occupational hazards. Rodent models are the most prominent in standard toxicology studies, and these models have known applications to quantitative risk assessment. Alternative testing strategies are being explored in earnest to reduce the use of animal models and to improve the efficiency of toxicology testing [NAS 2017]. However, data limitations remain in the validation of alternative testing strategies, and limited data were available in the current analyses to examine these models. Nonetheless, the hazard potency rankings for adverse pulmonary effects are estimated across a range of *in vivo* and *in vitro* assays and endpoints in these analyses.

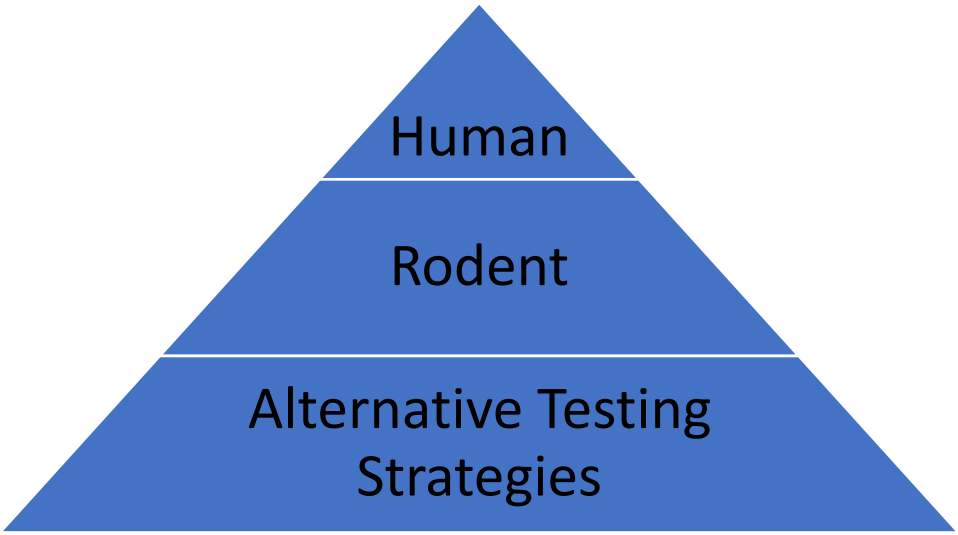

Figure 1-2. Hierarchy of data for quantitative risk assessment and estimation of occupational exposure limits.

1.2 Data and Methods

The methods for developing OELs or OEBs depend on the available data. As shown in Figure 1-3, if adequate dose-response data are available for a chemical substance (a.k.a. material), an individual OEL can be developed with use of QRA. Such materials can serve as benchmarks for comparison to materials with limited data and to provide a reference point for interpreting experimental results for new materials [Oberdörster et al. 2005; Kuempel et al. 2006, 2012; Nel et al. 2013]. Rodent bioassay data are often used in QRA because human dose-response data are typically not available. Standard risk assessment methods are applied to rodent data, including

hazard assessment, dose-response modeling, interspecies dosimetry adjustments, risk characterization, and uncertainty evaluation [NAS 1983, 2009; U.S. EPA 1994; NIOSH 2021]. However, rodent data may not be available for QRA of new materials, and global efforts to reduce animal testing and improve the efficiency of hazard and risk assessments also support the need for alternative methods. For example, Drew et al. [2017] describe a proof-of-concept quantitative framework with potential application to the derivation of OELs for new ENMs for which physicochemical property information but insufficient dose-response data are available. This methodology is consistent with the 21st-century toxicology and risk assessment goals to increase the efficiency and utility of risk assessment for human health risk decision-making [NAS 2007, 2017].

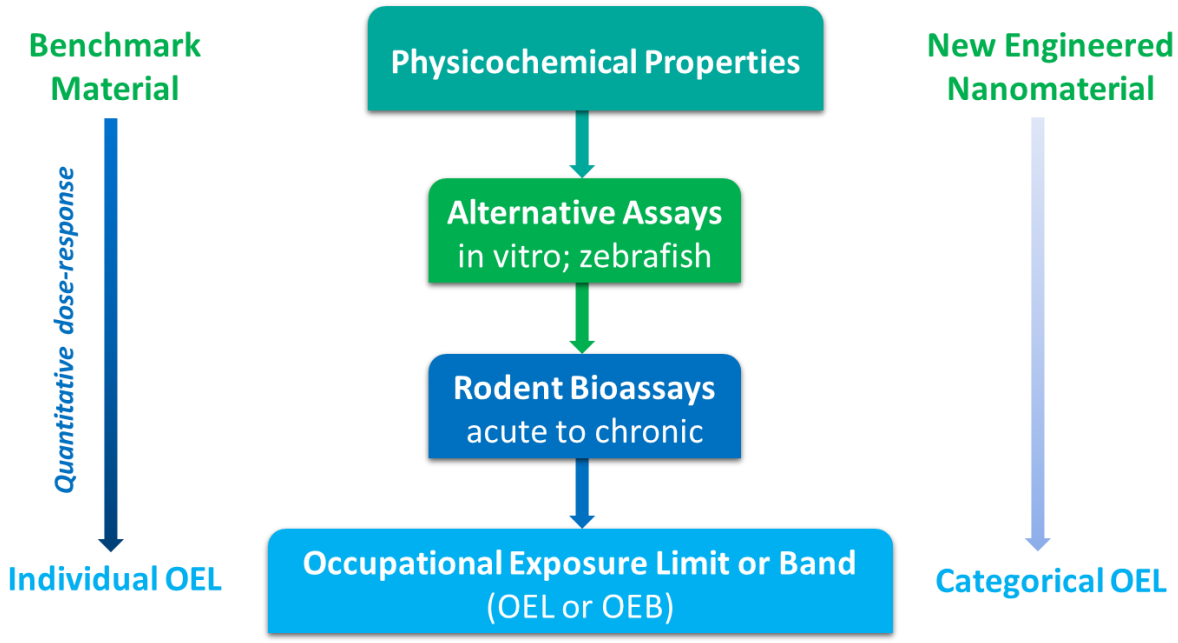

Figure 1-3. Overall Framework for Developing Occupational Exposure Limits or Bands.

Experimental data from other toxicology testing systems (e.g., *in vitro* assays using animal or human cells, zebra fish assays) have also been proposed for use in human health risk assessment, although validation of these systems, including for dose-response analysis, is still needed [Crump et al. 2010; Gangwal et al. 2011; Maier 2011; Cote et al. 2012; Nel et al. 2013]. Data on physicochemical properties of ENMs are still too limited to validate predictive models based on those properties alone, although information is emerging on the important properties associated with toxicological responses [Gernand and Casman 2014; Gernand and Casman 2016; Drew et al. 2017; Dekkers et al. 2018; Yanamala et al. 2019; Ramchandran and Gernand 2019, 2020]. These analyses

have shown that various experimental factors as well as physicochemical properties can have a large influence on the toxicological responses within and across materials [Bonner et al. 2013; Xia et al. 2013; Dekkers et al. 2018; Drew and Kuempel 2018].

A number of hazard and risk assessment frameworks for ENMs have been developed. In general, these frameworks apply standard risk assessment principles and practices to ENMs [OECD 2012]. These frameworks have proposed grouping ENMs according to hazard and exposure potential [Arts et al. 2015, 2016; Bos et al. 2015; Braakhuis et al. 2016; Cohen et al. 2013; Gebel et al. 2014; Godwin et al. 2015; Landsiedel et al. 2017; Oomen et al. 2015; Oosterwijk et al. 2016; Stone et al. 2014; Walser and Studer 2015], although many of them have not been tested with quantitative data. Case study data have been used with some of these frameworks [Arts et al. 2016; Gkika et al. 2016; Grieger et al. 2015]. Exposure scenarios along the ENM "lifecycle" (production to disposal) are included in some of the conceptual frameworks [Arts et al. 2015; Environmental Defense–DuPont Nano Partnership 2007; Shatkin 2013]. Weight of evidence and decision analysis methods have been proposed in other analysis frameworks [Hristozov et al. 2014; Zuin et al. 2011]. Other methods include evaluating the similarity among nanomaterials for read-across, although data gaps in "quantitative, unambiguous, and measurable parameters describing NM properties" [Park et al. 2018] limit the utility of that approach currently.

Several quantitative structure-activity relationship (QSAR) models have been developed, which describe the important factors influencing the toxicity [Munro et al. 1996; Burello and Worth 2011a; Gernand and Casman 2014; Yanamala et al. 2019; Ramchandran and Gernand 2020] and allow for hazard grouping and ranking [Liu et al. 2011, 2013a,b; Oh et al. 2016; Zhang et al. 2012; Scott-Fordsmand et al. 2018; Sheehan et al. 2018]; however, these models have not been used in human health risk assessment. Another quantitative framework proposes a human health risk prioritization based on a margin-of-exposure method (i.e., estimating the ratio between animal effect level and human exposure) [Hristozov et al. 2016]. Still lacking in these frameworks is an integrated methodology to use quantitative dose-response data to group ENMs by hazard potency, using biological responses and dose metrics that allow for the estimation of human-equivalent concentration (HEC) and development of cOELs for ENMs. The current analysis in this TR provides progress toward filling this gap in available methods for cOEL derivation of a large set of diverse materials.

Categorical methods of data analysis for hazard and risk assessment can provide more efficient use of data and support comparative potency, read-across, and other alternative methods [OECD 2007, 2012, 2014b, 2016; U.S. EPA 2014; NAS 2017; ECHA 2017, 2019]. In the absence of sufficient evidence to develop individual OELs for

specific ENMs, cOELs or OEBs could be developed to inform exposure control decision-making in the workplace [Kuempel et al. 2012; ISO 2016; Schulte et al. 2018; NIOSH 2019].

The goal and sub-goals of achieving a predictive model for evidence-based hazard categorization across a wide variety of ENMs, specifically a new ENM, are illustrated in Figure 1-3. To show how this document explores these goals, the following information identifies the corresponding sections:

- Section 3.1: Developing and evaluating a predictive model for hazard classification using physicochemical properties.
- Section 3.2: Ranking of *in vitro* rodent lung inflammation hazard potencies.
- Section 3.3: Analyzing histopathological data on rodent lung inflammation, fibrosis, and neoplasia for varying assay durations (acute to chronic).
- Section 3.4: Exploring the commonalities and differences in hazard rankings across assay type.
- Section 3.5: Deriving cOELs from the acute *in vivo* rodent lung inflammation grouping results and standard risk assessment methods.
- Section 4: Applying the NIOSH OEB framework and standard risk assessment methods to estimate OEBs.
- Section 5.5: Discussing uses for these findings for evaluating the risk management options to control exposures and protect workers' health during the manufacture, application, and end-of-life processing of ENMs.
- Appendices C and D: Analyzing alternative assays (cytotoxicity and zebrafish mortality) to rank materials by their hazard potency.

The decision logic or process for estimating an OEL or OEB for ENMs and other emerging materials, as described in this document, is shown in Figure 1-4.

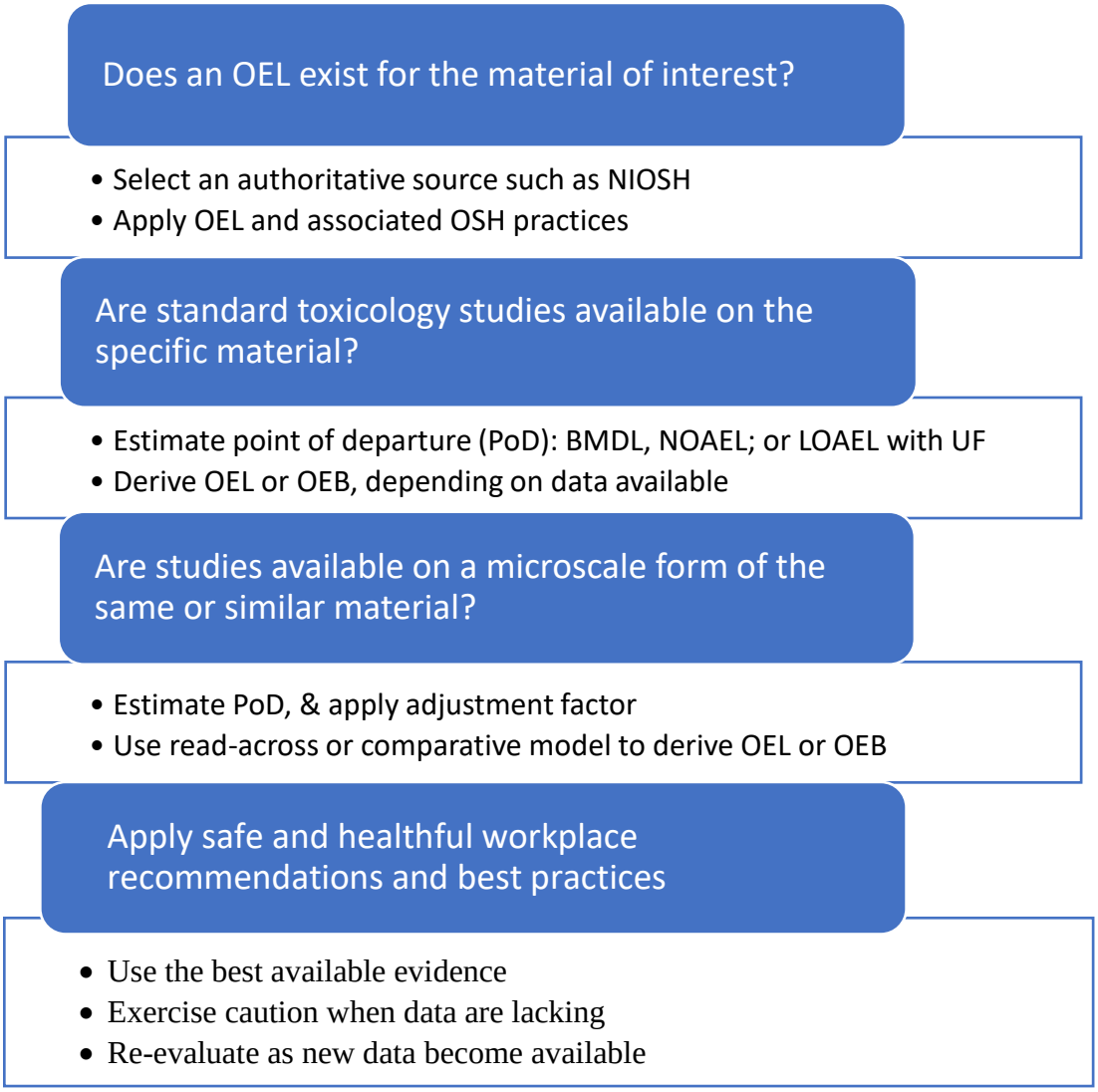

Figure 1-4. Decision Logic in Estimating an Occupational Exposure Limit or Band (OEL or OEB) for engineered nanomaterials and other emerging materials.

Abbreviations: BMDL: benchmark dose lower 95% confidence interval estimate; NOAEL: no observed adverse effect level; LOAEL: lowest observed adverse effect level; UF: uncertainty factor.

OELs or OEBs are criteria used to evaluate the effectiveness of exposure controls in controlling airborne exposure concentrations to those levels or bands. Control banding frameworks include both hazard banding and exposure banding components (Figure 1-5). Some hazard banding strategies have quantitative ranges of airborne

concentrations associated with the bands (also called categories) [Naumann et al. 1996; Brooke 1998; Guest 1998; HSE 2009; ANSES 2010; ISO 2014a; NIOSH 2019] (Table 1-1). In Table 1-1 it can be seen that the NIOSH [2019] quantitative ranges (OEBs) associated with the hazard band categories (A-E) are shifted toward higher airborne exposure concentrations by one order of magnitude. That is, the NIOSH [2019] band A is >10 mg/m^3, whereas in several other hazard banding frameworks [Brook 1998; HSE 2009; ANSES 2010; ISO 2014a], band A is lower by an order of magnitude (1-10 mg/m^3). Likewise, the NIOSH [2019] band E is <0.01 mg/m^3, which is band D in those other hazard banding frameworks [Brook 1998; HSE 2009; ANSES 2010; ISO 2014a]. In Naumann et al. [1996], the "typical exposure limits" within performance-based exposure-control limit (PB-ECL) bands 1 and 2 are similar to the airborne concentrations for bands A and B, respectively, of those latter four hazard banding frameworks; however, PB-ECL 3 in Naumann et al. [1996] includes a broader range of values than do the other frameworks (Table 1-1). The lower the airborne exposure concentration, the higher the potency; thus, the potency of materials within these exposure bands increases from band A to band E.

In this report, cOELs for ENMs are estimated from statistical analyses to derive hazard potency groups of ENMs and microscale particles based on toxicology data on adverse lung effects in animals. In addition, OEBs are derived for those materials that meet the minimum data requirements according to NIOSH [2019]. These findings are discussed with respect to assigning exposure limits or bands to ENMs for the purpose of evaluating and selecting engineering control options in workplaces producing or using ENMs.

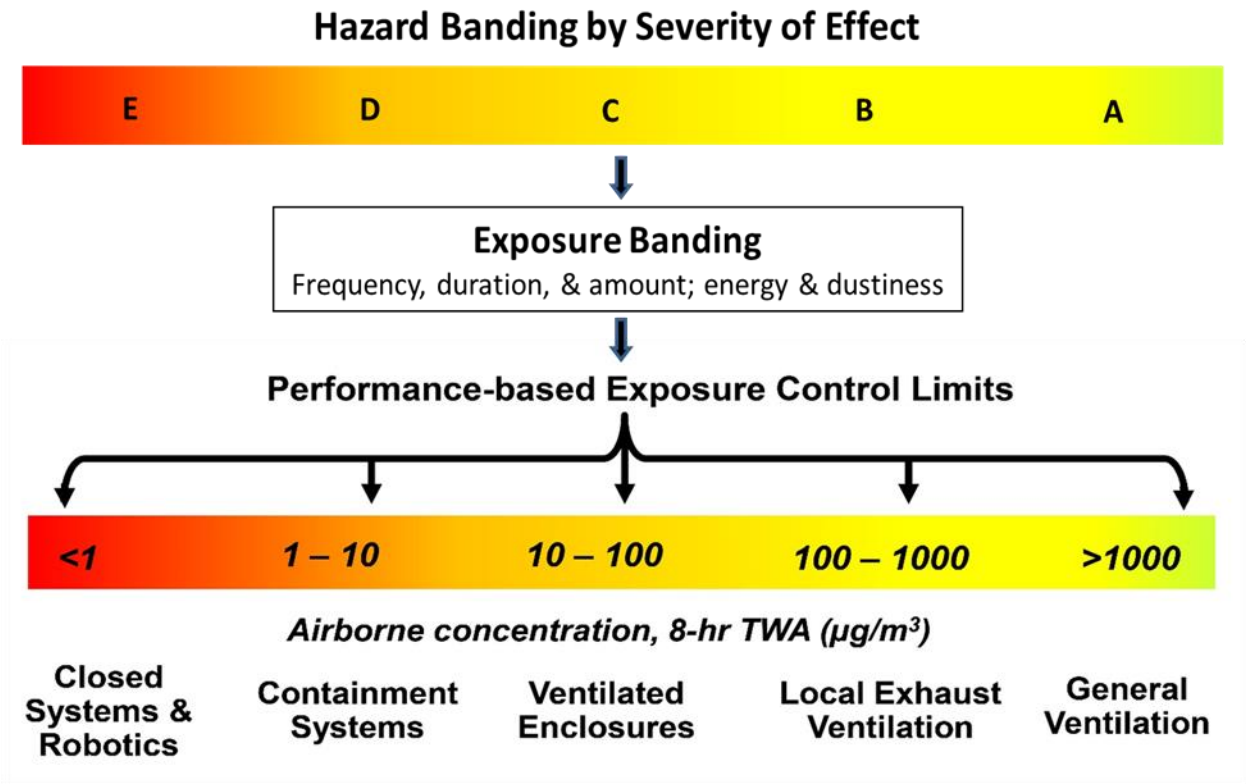

Figure 1-5. Control Banding Approaches for Nanomaterials. [Adapted from Dunn et al. [2018]; ISO [2014a]; ANSES [2010]; HSE [2009]; Zalk and Nelson [2008]; Ader et al. [2005]; Brooke [1998]; Naumann et al. [1996]. The airborne concentrations shown here most closely align to those in Brooke [1998], HSE [2009], ANSES [2010], and ISO [2014a]. The airborne concentration of <1 µg/m^3 is an extension of the order-of-magnitude bands A-D.

Table 1-1: Hazard and occupational exposure band (OEB) frameworks for inhaled dusts, fumes, or mists: Acute and chronic effects (selected) [Adapted from ISO 2016]*

Reference	Hazard bands and OEBs				
NIOSH [2019], Table 1-1 & Section 1-4: OEBs	**A**	**B**	**C**	**D**	**E**
Airborne target range for dust or particle concentration (8 h TWA) (mg/m^3)	>10	>1 to 10	>0.1 to 1	>0.01 to 0.1	≤0.01
NIOSH Tier 2 banding criteria for Specific Target Organ Toxicity, repeated dose (STOT_RE) in rats or other animals (NOAEL/BMDL/BMCL): Inhalation (dust/ particles) (mg/m^3) (NIOSH [2019], Table 3-12) (converted from $\mu g/m^3$)	>30	>3 to ≤30	>0.3 ≤3	>0.03 to ≤0.3	≤0.03
NIOSH Tier 2 banding criteria for Carcinogenicity: TC_{05} (mg/m^3) (NIOSH [2019], Table 3-7) (converted from $\mu g/m^3$)			>16.7	>0.005 to ≤16.7	≤0.005
ISO [2014a], Table 1; ANSES [2010], Annex 2	**Category A** No significant risk to health	**Category B** Slight hazard - Slightly toxic	**Category C** Moderate hazard	**Category D** Serious hazard	**Category E** Severe hazard
OEL (8 h TWA) (mg/m^3)	1 to 10	0.1 to 1	0.01 to 0.1	<0.01	Seek specialist advice [a]
Acute toxicity: Rat LC50 inhalation 4 h (mg/m^3) (converted from mg/l). Aerosols/particles.	>5,000	1,000 to 5,000	250 to 1,000	<250	—
Likelihood of chronic effects (e.g. systemic)	Unlikely	Unlikely	Possible STOT RE 2	Probable STOT RE 2	

Adverse effects by inhalation, 90 d, 6 h/d (mg/m^3) (converted from mg/l). Aerosols/particles. [a]			<200	<20	

Table 1-1: ***Continued***

GHS [UNECE 2015]; OSHA [2012] [b]	**Category 5**	**Category 4**	**Category 3** ! - Warning	**Category 2** Health hazard - Warning	**Category 1** Health hazard - Danger
Acute toxicity: Rat LC50 inhalation 4 h (mg/m^3) (converted from mg/l). Dusts and mists.	[c] Warning: May be harmful if inhaled	5,000 Warning: Harmful if inhaled	1,000 Danger: Toxic if inhaled	500 Danger: Fatal if inhaled	50 Danger: Fatal if inhaled
STOT-SE: Rat inhalation 4 h single exposure (mg/m^3) (converted from mg/l). Dust, mist, fume.				1,000 < STOT-SE < 5,000	<1,000
STOT-RE Rat inhalation 6 h/d repeated exposure (mg/m^3) (converted from mg/l). Dust, mist, fume.				20 to 200 Warning: May cause damage to organs through prolonged or repeated exposure	<20 Danger: Causes damage to organs through prolonged or repeated exposure
HSE [2009] COSHH Essentials, Table 3	**Hazard Group A**	**Hazard Group B**	**Hazard Group C**	**Hazard Group D**	**Hazard Group E**
Concentration range (mg/m^3) [d]	1 to 10	0.1 to 1	0.01 to 0.1	<0.01	—
Brooke [1998], Table 1	**Hazard Band A**	**Hazard Band B**	**Hazard Band C**	**Hazard Band D**	**Hazard Band E**
Target airborne concentration range (mg/m^3)	>1 to 10	>0.1 to 1	>0.01 to 0.1	<0.01	Seek specialist advice
Key R-phrase [e]			Harmful: R48/20	Toxic: R48/23	
Repeated exposure: Rat inhalation 6 h/d for at least 90 d (mg/m^3) (converted from mg/l)			25 to 250	<25	

Table 1-1: ***Continued***

Guest [1998], Table 1	**OEB C**	**OEB B**	**OEB A**	**Category X**	
Occupational exposure band	1 – 10	0.1 – 1	<0.1	Special considerations	
Naumann et al. [1996], incl. Table 1 [f]	**PB-ECL 1**	**PB-ECL 2**	**PB-ECL 3**	**PB-ECL 4**	**PB-ECL 5**
"Typical exposure limits" within PB-ECLs Categories (8 h TWA) (mg/m^3)	1 to 5	0.1 to 1	0.001 to 0.1	<0.001	
Acute effects potency (mg/m^3) (converted from mg/d, assuming humans and occupational air intake of 10 m^3/d)	>10	>1 to 10	>0.01 to 1	<0.01	<0.01
Severity of acute effects	Low	Low/Moderate	Moderate	Moderate/High	High
Severity of chronic effects	None	None	Slight	Moderate	Severe
Henry and Schaper [1990] Tables I & XI [g]	**Hazard 0** Minimal	**Hazard 1** Slight	**Hazard 2** Moderate	**Hazard 3** Serious	**Hazard 4** Severe
Acute health hazard criteria: Rat LC50 inhalation 1 h (mg/m^3) (converted from mg/l). Dusts, fumes, mists.	>200,000	>20,000 to <200,000	>2,000 to <20,000	>200 to <2,000	>0 to <200

Footnotes on next page.

Footnotes to Table 1-1.

[a] Listed in ANSES [2020], not ISO [2014a].

[b] GHS [UNECE 2015] information is from Tables 3.1.1 and 3.1.3 (acute toxicity); Figure 3.8.1, Table 3.8.1, and Table 3.8.3 (STOT-SE); Figure 3.9.1, Table 3.9.1, 3.9.2, and 3.9.3 (STOT-RE). OSHA [2012] criteria are essentially the same, except that only Categories 1 through 4 are used; see Table A.1.1 (acute toxicity); Table A.8.1 (single dose); Tables A.9.1 and A.9.2 (90-day study) [OSHA 2012].

NOTE GHS [UNECE 2015] and OSHA [2012] do not include OEBs. Comparison of the animal exposure concentrations across schemes suggests that Categories 2 and 1 of GHS [UNECE 2015] and OSHA [2012] would align, respectively, with Categories C and D of ISO/TS 12901-2, HSE [2009] and Brooke [1998].

[c] GHS [UNECE 2015] includes a Category 5 for substances with relatively low acute toxicity; LD50 in range of 2,000 mg/kg to 5,000 mg/kg BW or equivalent for inhalation.

[d] See Table 3 of HSE [2009] for specific R-phrases and H-statements that are used to assign hazard group; allocation based on Brooke [1998]. Hazard group E with "—" indicates that no airborne concentration can be found to provide adequate control [HSE 2009].

[e] The EU CLP Regulation [Regulation (EC) No 1272/2008] phases in the use of H phrases instead of R-phrases, in most cases. The deadline for transition from R to H was 1 June 2015.

[f] PB-ECL: performance-based exposure control limit.

[g] Safety and Health Index System (SHIS).

*Adapted from ISO [2016], Table 6, originally developed by E Kuempel, NIOSH, coauthor on ISO [2016]; used by permission from ©ISO. This material is excerpted from ISO/TR 18637:2016 with permission of the American National Standards Institute (ANSI) on behalf of the International Organization for Standardization. All rights reserved.

Page intentionally left blank

2 Categorical OEL Methods

2.1 Framework Summary

Categorizing ENMs with regard to potential occupational health hazards would be highly useful information for assessing risk of exposures and evaluating engineering controls and other occupational risk management measures. To establish groups of ENMs of similar hazard, a general analysis process was used in each of the current analyses (Figure 2-1). Data from animal and cellular studies were derived from several sources, including individual datasets (as described in a previous analysis [Drew et al. 2017]) and systematic reviews of the literature with extraction of the sufficient summary statistical data needed for quantitative analyses [Boots et al. 2021]. These data were used to derive benchmark dose estimates (a.k.a. points of departure [NIOSH 2019]), which provide a standard measure of the dose associated with specific lung responses (inflammation, fibrosis, cancer). For each response endpoint, these nanoscale and microscale materials were clustered (grouped) on the basis of estimates of their potency.

The factors associated with these response endpoints and with these potency groups were explored by random forest methods, which provided predictor-variable importance measures but may not clearly show the direction of the associations. Factors evaluated include both the physicochemical properties of the materials and experimental factors. The estimated potency groups provide an evidence-basis to derive cOELs for ENMs from the available data. These analyses also provide further information toward the verification of a predictive model to estimate the potency group of a new ENM using only its physicochemical properties (described in Drew et al. [2017]).

The several steps in the data analysis follow:

1. Search and review the available data from either individual experiments or summary data from systematic searches of the literature to obtain the dose-response information needed for quantitative analysis.

Studies involving at least three doses (including a control dose) are desired, with at least two subjects per dose, although more subjects are preferable to reduce variability; however, data from studies of two-dose groups can also be used. The subjects must be randomly assigned to a dose group. Data reported by individual animal are preferred, but sufficient summary data can also be used (mean response, variability in response, number of animals per dose group). Adequate dose-response data allow for a point of departure (PoD) to be estimated, such as a no observed adverse effect level (NOAEL), lowest observed adverse effect level (LOAEL), or benchmark dose (BMD). For BMD estimation, additional data requirements apply [U.S. EPA 2012]. The dose-response trend must be statistically significant. Preferably, at least one dose group must be in the low dose region (near the selected benchmark response level) to give a better estimate of the BMD; if the data are too sparse in this region,

it may not be feasible to estimate a BMD. The exploratory data analysis stage reveals the subset of the data that are eligible for the next phases of analysis, including statistical modeling.

2. Estimate the PoDs.

Statistically, the BMD is preferred for several reasons: the BMD is not constrained to be one of the experimental dose groups, unlike a NOAEL or LOAEL; the BMD is not as sensitive as a NOAEL or LOAEL to changes in sample sizes; and the BMD makes better use of all of the experimental data. To estimate a BMD, the EPA Benchmark Dose Software (BMDS) was used for both dichotomous and continuous responses. In one analysis, stochastic kriging (SK) (Wang et al., 2014) was used to estimate BMDs for a continuous response. A BMD is the dose associated with a pre-specified response level called the benchmark response (BMR), which can either be a default value or be biologically relevant. For lung inflammation responses measured by PMNs, a BMR of 4% above background was used because of its biological basis [NIOSH 2011, Section 3.5.2.2], whereas a default BMR of a 10% added risk [U.S. EPA 2012] was used as the point of departure for linear extrapolation of rodent lung tumor response. The EPA BMD guidance was used to identify the best-fitting model, and the BMD and benchmark dose lower 95% confidence limit (BMDL) from that model were used to represent a given material's potency.

3. Identify which materials have similar potency estimates.

We employed agglomerative hierarchical clustering [Sneath and Sokal 1973] using complete linkage [Sorensen 1948] or Ward's minimum variance criterion [Ward 1963] to identify materials with similar potency estimates, and the a priori decision was to have four groups of materials, reflective of the four mode-of-action categories (Poorly Soluble Low Toxicity; Poorly Soluble High Toxicity; Soluble; Fibers). Hierarchical clustering is a data-driven algorithm, which makes it flexible, but results can change as the amount of data changes. Clusters are created by measuring the Euclidean distance between potency estimates and gradually combining the nearest potency estimates (determined by the linkage method) until every estimate belongs to one of four groups. We also explored clusters based on order-of-magnitude bands. The four clusters of potency estimates are a sample representation of the categories of similar materials that would be used for categorical OEL creation.

At this point in the analysis, the perspective changes to that of a new material, whose potency group is unknown, and the potency is not estimable because dose-response data are likely not available. The new material is assumed to have some information, such as physicochemical property data, that can be leveraged for potency group classification.

4. Identify the factors other than the potency estimates that could be used to assign new materials to a potency cluster.

We explored experimental design and physicochemical information of the grouped materials by using random forests [Breiman 2001]. This method identified and ranked factors based on how important they are for

predicting the potency cluster. This phase remains exploratory, as the available physicochemical property data are often quite sparse, making it challenging to accurately test and validate the predictive ability of the random forest models.

The currently available experimental data used in this document provided insights into understanding how the calculated material potency changes are associated with physicochemical properties and experimental design decisions. The data also added to the understanding of how to identify materials with similar potencies. However, these data are not sufficient for creating nor validating categories to which new materials can be compared. Table 2-1 illustrates examples of potential types of data and what could be done with those data. Note that many combinations of the scenarios below are possible, but these were chosen to highlight the primary sources of uncertainty: interspecies extrapolation, exposure duration, health endpoint, and experimental design/data.

Table 2-1. Example of potential types of data and their utility in quantitative risk assessment.

Potential Data	Potential Utility
Long-term observational (epidemiological) data in humans on materials currently in production processes, with sufficient physicochemical descriptions	An OEL could be derived for each material with minimal uncertainty, groups of materials with similar OELs could be identified, and a model to predict an OEL for a new material given physicochemical properties could be built and validated
Chronic (or sub-chronic) experimental rodent data on all materials, with sufficient physicochemical descriptions	The same process as above could be completed, with additional uncertainty added for the species extrapolation or exposure duration
Chronic (or shorter term) observational (epidemiological) data in humans on a representative sample of materials currently in production processes, with less sufficient physicochemical descriptions	Additional uncertainties are added because of the exposure duration, and inferences are required as the potency information for all materials is estimated from the sample of materials. Predictive model creation and validation become more difficult with incomplete physicochemical information, adding uncertainty to the classification of a new material.
Chronic (or sub-chronic) experimental rodent data on a representative sample of all materials currently in production processes, with less sufficient physicochemical descriptions	Additional uncertainties added to those stated in the above case because of the requirements for inter-species extrapolation.
Chronic (or sub-chronic) experimental rodent data or alternative rodent assays (acute *in vivo* or *in vitro*) for varied toxicological endpoints on a non-representative sample of all materials currently in production processes, with insufficient physicochemical descriptions	The data type described on the left is approximately the status of the current data. The uncertainties above are magnified because of the small number of materials, increased variability in potency due to differences in experimental design, and difficulties building and validating predictive models given the sparse predictor information. Questions about the relevance of a given endpoint and utility of alternative assays to

	long-term human health also add difficulty to interpreting and applying results.

2.2 Acute Inflammation

2.2.1 Initial Database and Methods

- A database of nanoscale and microscale particulate materials was constructed to describe the dose-response relationships for pulmonary inflammation in rodents and the physicochemical properties of those materials. Inflammation potency was estimated with benchmark dose modeling, and materials were grouped with hierarchical clustering. Potency is defined in this analysis as the reciprocal of the mass deposited lung dose associated with a specific inflammatory response in the lungs. The specific lung inflammation responses evaluated included 4% or 10% higher levels of polymorphonuclear leukocytes (PMNs) in the bronchioalveolar lavage fluid (BALF) than with the control (unexposed) mean response in rats or mice. These responses are considered biologically significant and relevant to workers because these levels of PMNs in BALF were associated with the early stages of overloading of lung clearance in rats and with chronic lung disease in humans (described in Section 3.5.2.2 of NIOSH [2011]).

- A classification random forest model was developed to identify the physicochemical properties that were predictive of the hazard potency group [Drew et al. 2017]. The model was then tested on a separate dataset of new materials, using only the physicochemical information to predict the hazard potency group, and evaluating the predictions against potency estimates derived from the dose-response data.

- Individual rodent study data on nanoscale and microscale particles from a variety of material types were obtained from studies identified through research collaborations and from the published literature. Files for 25 *in vivo* rodent studies comprising data for 1,899 unique animals (from 1,929 records) were provided by researchers from NIOSH (Porter et al., 2001, 2004, 2013; Roberts et al., 2013; Sager et al., 2013; Xia et al., 2011); CIIT (renamed Hamner Institute) (Bermudez et al., 2002, 2004); and the European Framework 7 Programme on Engineered NanoParticle Risk Assessment (ENPRA), to which NIOSH was a research partner (ENPRA 2013). Exposure-

response information was available for the individual rodents, and experimental design properties (e.g., post-exposure duration, method of exposure) were included. Information on the experimental design and physicochemical properties of these materials is shown in Figure 2-2. In general, the experimental design information was available, but the physicochemical property information varied widely by material and was missing for many of the properties.

Figure 2-2. Summary of Physicochemical Properties and other Factors Available in the NIOSH/ENPRA/CIIT Dataset.

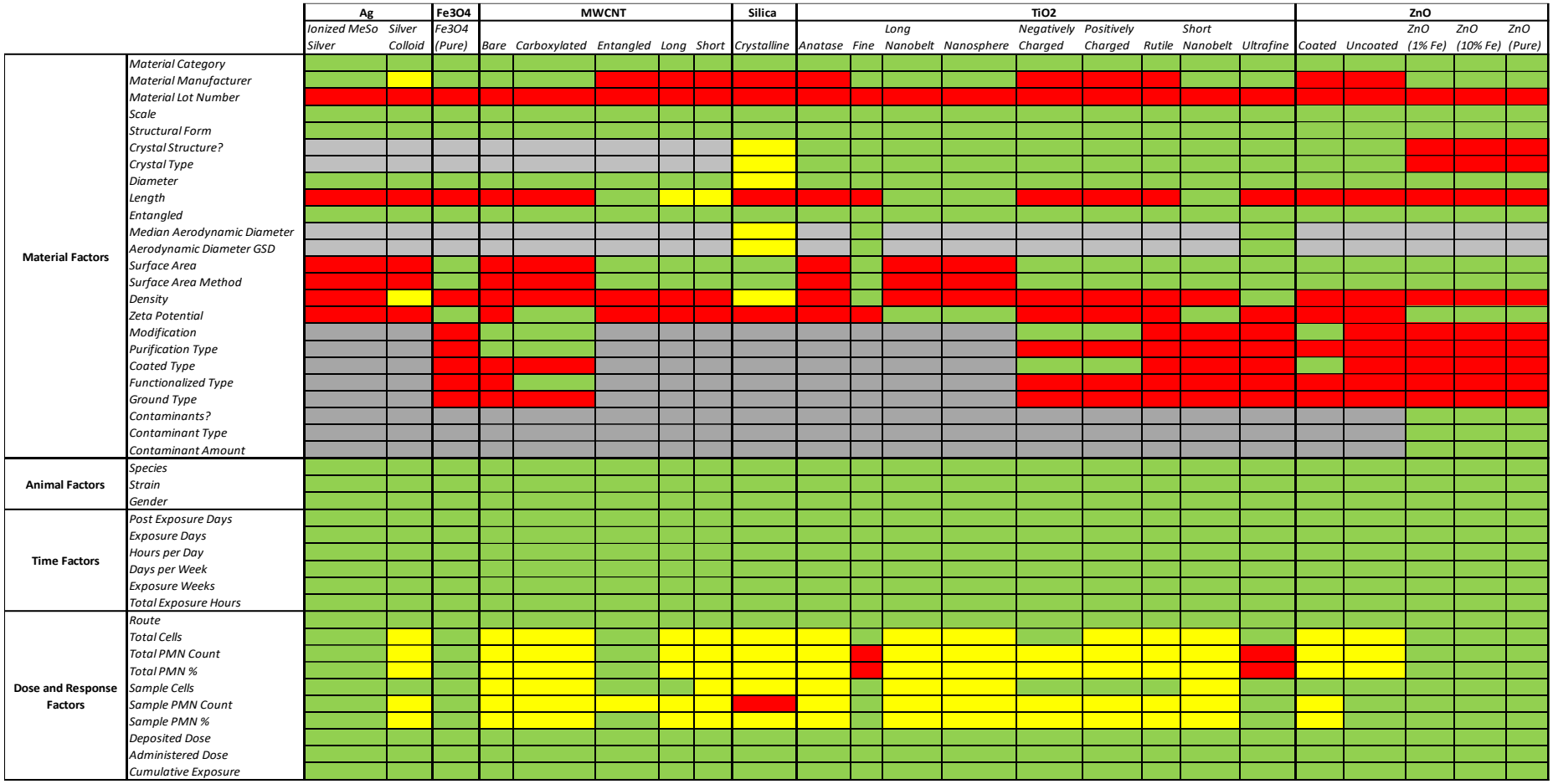

Color Key: Red = Missing; Yellow = Partially Missing; Green = Not Missing; Grey = Not Applicable

Properties Considered but Missing Values for All Materials: Volume, Solubility, Solubility Measurement Method, Surface Charge, Rigidity, Material Lot Number, Measure of Agglomeration

The duration of exposure varied across materials in this analysis, from single bolus administration (intratracheal instillation [IT] or pharyngeal aspiration [PA]) to subchronic inhalation (up to 116 days) (Table 2-2). The estimated total deposited mass dose of particles in the lungs provides a normalized dose metric over time. For inhalation studies, the total deposited dose was calculated as follows:

$$Deposited\ lung\ dose\ (mg) = exposure\ concentration\ \left(\frac{mg}{m^3}\right) * duration\ of\ exposure\left(\frac{hr}{d} * \frac{d}{wk} * wk\right) * minute\ ventilation\ \left(\frac{L}{\min}\right) * pulmonary\ deposition\ fraction * units\ conversion\ (0.001\frac{m^3}{L} * 60\frac{min}{hr})$$

[Equation 2-1]

where exposure concentration and duration are as reported in the animal study. Minute ventilation was calculated as shown in Equation 2-2. The pulmonary deposition fractions were estimated in the Multiple-Path Particle Dosimetry (MPPD) model, v. 2.90.1 (an interim version run in MPPD v. 2.1 platform) [ARA 2011]. MPPD model software is freely available at www.ara.com/products/mppd.htm; and beginning with MPPD v. 3, models for other animal species, including mice, have been added [Asgharian et al. 2014]. Model input values for particle size distribution (e.g., mass median aerodynamic diameter and geometric standard deviation) are those reported in the studies. The respiratory parameters are based on the rodent species/strain and body weight.

Minute ventilation (L/min) in the rats was estimated from the average body weight, as shown in the following allometric equation]:

$$\ln(V_E) = b_0 + b_1 \ln(BW) \qquad \text{[Equation 2-2]}$$

where V_E is the minute ventilation (L/min); BW is body weight (kg); and $b_0 + b_1$ are the species-specific parameters. These parameters for rat are -0.578 (b_0) and 0.821 (b_1); and for mice, they are 0.326 (b_0) and 1.05 (b_1) [as shown in Equation 4-4 and Table 4-6 of U.S. EPA 1994].

Thus, V_E is calculated as

$$V_E\ (L/min) = Exp(b_0) * BW\text{^}b_1 \qquad \text{[Equation 2-3]}$$

where the parameter values are as described in Equation 2-3. For a rat with BW of 0.3 kg, V_E is calculated as 0.21 L/min (Equation 2-3). This value is used in Equation 2-1 to estimate the rat deposited lung dose, and also in Equation 2-7 as part of the dosimetric adjustment to estimate the human-equivalent deposited lung dose [Equation

2-4]. For mice, V_E estimates were calculated in the same way (Equation 2-3), by using the mouse parameter values; V_E estimates of 0.027 or 0.037 L/min (based on BW of 0.024 or 0.032 kg, respectively) were used to estimate the mouse deposited lung doses. The mouse BW values used are from one of the studies in this analysis (Ryman-Rasmussen et al [2009], 0.024 kg, for C57BL6 adult male mice age 6-8 weeks) and from U.S. EPA [1994], Table 4-5, for male B6C3F1 mice subchronic. The V_E of 0.037 was also used in NIOSH [2013, p. 100].

Total deposited dose is a type of cumulative dose metric, which is similar in concept to "Haber's rule." Haber's rule assumes that a specific adverse effect would be associated with exposure by a constant factor (K) that is the linear product of concentration (C) and time (T), such that C x T = K. These dose metrics do not account for particle clearance from the lungs. Normal clearance of poorly soluble low-toxicity particles, such as titanium dioxide (TiO_2), from the lungs is relatively slow (e.g., clearance half-time of 60–90 days in rats) [Pauluhn 2014]. Pulmonary clearance of poorly soluble, high-toxicity particles such as crystalline silica (SiO_2) is even slower, and these particles are more likely to be sequestered in the lung interstitial region and lymph nodes [Tran et al. 2002]. The subchronic data in this analysis includes TiO_2 and crystalline silica. In the acute studies, clearance would be minimal at 0 to 1-day post-exposure. The total dose metric does not account for possible nonlinearity in the relationship of effect of duration of exposure to the biologically effective dose.

The pulmonary region of the respiratory tract is the biological site of the adverse responses evaluated, and doses were proportional to the deposited mass dose of particles in the pulmonary region for the data analysis. Estimating hazard potency across numerous nanoscale and microscale particles involved pooling data across many studies, which included a range of experimental designs and routes of exposure. In order to utilize as much of the data as possible for the comparative potency and grouping analyses, we needed to normalize the doses to the same units for the dose-response modeling and benchmark dose estimation. Dose was expressed as the total deposited mass dose per gram of wet lung tissue. Dose normalization would not account for possible differences in sensitivity of response by strain/species/sex.

Table 2-2. Description of NIOSH/CIIT/ENPRA Experimental Designs

Reference^	Route** & Frequency	Sex and Species	Strain	Material	Material Type	Number of Animals	Exposure Groups
Porter et al. 2013	PA Single	Male Mouse	C57BL/6J	TiO_2	Short Nanobelt	115	7.5, 15, 30 (µg)
					Long Nanobelt	140	1.875, 7.5, 15, 30 (µg)
					Nanosphere	92	7.5, 15, 30 (µg)
					Control	54	Dispersion Medium
Xia et al. 2011	IT Single	Male Rat	Sprague-Dawley	Fe_3O_4	Fe_3O_4 pure	41	0.0375, 0.075, 0.15, 0.3 (mg/rat)
					ZnO 1% Fe	38	0.0375, 0.075, 0.15, (0.3 mg/rat)
					ZnO 10% Fe	42	0.0375, 0.075, 0.15, 0.3 (mg/rat)
					ZnO pure	36	0.0375, 0.075, 0.15, 0.3 (mg/rat)
					Control	21	Dispersion Medium
Roberts et al. 2013	Inh 5 hours	Male Rat	Sprague-Dawley	Ag	Ionized	12	100 µg/m^3
					Colloidal	12	1000 µg/m^3
					Control	24	Control Aerosol
Sager et al. 2013	PA Single	Male Mouse	C57BL/6J	MWCNT	Bare	80	2.5, 10, 40 (µg)
					Carboxylated	82	2.5, 10, 40 (µg)
					Control	61	Dispersion Medium
Porter et al. 2001	Inh 6h/d, 5d/wk, 116d	Male Rat	F344	Silica	Crystalline	120	15 (mg/m^3)
					Control	120	Filtered Air
Porter et al. 2004	Inh 6h/d, 5d/wk, 20d or 40d or 60d	Male Rat	F344	Silica	Crystalline	66	15 (mg/m^3)
					Control	66	Filtered Air
ENPRA-RIVM	IT Single	Female Mouse	C57BL/6N	Ag	Colloidal	21	1, 4, 8, 16, 32, 64, 128 (µg/mouse)
					Control	3	Dispersion Medium
ENPRA-NRCWE	IT Single	Female Mouse	C57BL/6N	MWCNT	Long	24	32, 128 (µg/mouse)
					Control	12	Dispersion Medium
ENPRA-NRCWE‡	IT Single	Female Mouse	C57BL/6-Apoetm1	MWCNT	Long	26	32, 128 (µg/mouse)
					Control	16	Dispersion Medium
ENPRA-NRCWE‡	IT Single	Female Mouse	C57BL/6-Apoetm1	MWCNT	Short	26	32, 128 (µg/mouse)
					Control	16	Dispersion Medium
ENPRA-NRCWE	IT Single	Female Mouse	C57BL/6N	MWCNT	Short	24	32, 128 (µg/mouse)
					Control	12	Dispersion Medium
ENPRA-RIVM	IT Single	Female Mouse	C57BL/6N	MWCNT	Long	21	1, 4, 8, 16, 32, 64, 128 (µg/mouse)
					Control	3	Dispersion Medium
ENPRA-RIVM	IT Single	Female Mouse	C57BL/6N	MWCNT	Short	21	1, 4, 8, 16, 32, 64, 128 (µg/mouse)

					Control	3	Dispersion Medium
ENPRA-UC†*	IT Single	Female Mouse	C57BL/6N	Silica	Crystalline	8	2500 (µg/mouse)
				MWCNT	Entangled	20	12.5, 25, 50, 100 (µg/mouse)
					Control	7	Dispersion Medium
ENPRA-UC†*	IT Single	Female Mouse	C57BL/6N	Silica	Crystalline	8	2500 (µg/mouse)
				MWCNT	Entangled	20	12.5, 25, 50, 100 (µg/mouse)
					Control	7	Dispersion Medium
ENPRA-RIVM	IT Single	Female Mouse	C57BL/6N	ZnO	Coated	21	1, 4, 8, 16, 32, 64, 128 (µg/mouse)
					Control	3	Dispersion Medium
ENPRA-RIVM	IT Single	Female Mouse	C57BL/6N	ZnO	Uncoated	21	1, 4, 8, 16, 32, 64, 128 (µg/mouse)
					Control	3	Dispersion Medium
ENPRA-UC†	IT Single	Female Mouse	C57BL/6N	Silica	Crystalline	8	2500 (µg/mouse)
				ZnO	Coated	10	12.5, 25, 50, 100 (µg/mouse)
					Control	5	Dispersion Medium
ENPRA-RIVM	IT Single	Female Mouse	C57BL/6N	TiO_2	Negatively Charged	21	1, 4, 8, 16, 32, 64, 128 (µg/mouse)
					Control	3	Dispersion Medium
ENPRA-RIVM	IT Single	Female Mouse	C57BL/6N	TiO_2	Positively Charged	21	1, 4, 8, 16, 32, 64, 128 (µg/mouse)
					Control	3	Dispersion Medium
ENPRA-RIVM	IT Single	Female Mouse	C57BL/6N	TiO_2	Anatase	39	1, 4, 8, 16, 32, 64, 128 (µg/mouse)
					Control	3	Dispersion Medium
ENPRA-RIVM	IT Single	Female Mouse	C57BL/6N	TiO_2	Rutile	21	1, 4, 8, 16, 32, 64, 128 (µg/mouse)
					Control	3	Dispersion Medium
ENPRA-RIVM	IT Single	Female Mouse	C57BL/6N	TiO_2	Rutile	21	1, 4, 8, 16, 32, 64, 128 (µg/mouse)
					Control	3	Dispersion Medium
Bermudez et al. 2002	Inh 6h/d, 5d/wk, 13 wk	Female Rat	F344	TiO_2	Fine	75	10, 50, 250 (mg/m^3)
					Control	25	Filtered Air
Bermudez et al. 2004	Inh 6h/d, 5d/wk, 13 wk	Female Rat	F344	TiO_2	Ultrafine	75	0.5, 2, 10 (mg/m^3)
					Control	25	Filtered Air
					Total Observations	1,929	

- † The same group of 8 positive control animals (Silica) are used across the 3 studies.
  * The same group of 7 negative control animals (MWCNT) are used across the 2 studies.
- ‡ An identical set of 7 negative control animals appear in both studies.
- ** Inh = Inhalation; IT = Intratracheal Instillation; PA = Pharyngeal Aspiration

- ^ Not all studies were used in this analysis (Section 3.2)
- All materials are nanoscale except: Porter et al. 2001; Porter et al. 2004; Bermudez et al. 2002.

Some physicochemical property information about the materials was provided in the files, but most of this information was gleaned from the resulting publications of the researchers. Six chemicals of various forms were studied: iron oxide (Fe_3O_4, solution) (nano-scale), silver (Ag, solution) (nano-scale), multi-walled carbon nanotubes (MWCNT, solution), crystalline silica (powder and solution) (micro-scale), titanium dioxide (TiO_2, powder and solution) (nano- and micro-scale), and zinc oxide (ZnO, solution) (nano-scale). The chemicals listed as solutions were as administered for the route of exposure. The experimental designs of these studies varied by exposure route, rodent species and strain, and exposure and post-exposure duration. A majority of the studies used intratracheal instillation (IT) as the exposure route, whereas the remainder used inhalation (Inh) or pharyngeal aspiration (PA). Various strains and both sexes of rats (male Sprague-Dawley, male and female F344) and mice (Female C57BL/6N, Male C57BL/6J, Female C57BL/6-Apoetm1) were used across the studies. The ApoE mouse strain is used primarily to investigate atherosclerosis and cardiovascular disease following respiratory exposures to particles (strain information, for example, available at: https://www.labome.com/method/Laboratory-Mice-and-Rats.html). Acute pulmonary response data (0–1 d post-exposure) were available for most studies, whereas some studies reported pulmonary response at the end of repeated inhalation exposure (also 0–1 d post-exposure). A summary of these experimental characteristics for the various types of the materials is shown in Table 2-2. This database (henceforth NIOSH/CIIT/ENPRA) was used for training the predictive models.

A separate database of *in vivo* rodent studies of similar experimental design was constructed from the U.S. National Institute for Environmental Health Studies (NIEHS) NanoGo Consortium [Bonner et al. 2013]. This inter-laboratory research program studied three forms each of nanoscale TiO_2 and MWCNT in 258 unique rats (male Sprague-Dawley, male F344) and 177 mice (male C57BL/6), for a total of 435 unique rodents. Physicochemical property information for these materials was provided in Xia et al. [2013], which included *in vitro* studies of the same nanomaterials studied *in vivo* [Bonner et al. 2013]. This database (henceforth NanoGo) was used for validating the predictive framework, as these data were received after the NIOSH/CIIT/ENPRA database had been created. A deposited dose metric was created for these data also in order to be commensurate with the NIOSH/CIIT/ENPRA database. A description of the experimental design characteristics of the NanoGo studies is provided in the Appendix (Table A-6).

The response of interest was the proportion of PMNs (a.k.a. neutrophils), which is a common measure of pulmonary inflammation. This response is often reported in particle toxicology studies of the lungs; other endpoints include lactate dehydrogenase (LDH) and fibrosis severity scores. If the proportion of PMNs was not reported in the file, it was calculated from the primary data (ratio of PMN count to total cell count). Toxicology studies often report the PMN percentage, which is simply the proportion x 100. PMN percentage has also been used to compare results between studies, because differences in the methods used for BALF and cell counting may result in different total cell counts (Bonner et al., 2013). In order to compare the lung doses across the various routes of exposure, a deposited dose (in micrograms) metric was created. The administered particle mass lung doses were used for IT or PA studies, and the deposited mass dose was assumed to be equivalent to the administered mass dose. For inhalation studies, the total deposited mass dose was estimated as described above (Equations 2-1 through 2-3).

Because both mice and rats were used in the toxicology studies, species adjustments were required. To account for the differences in size of the animals, the deposited lung doses were normalized by the wet lung weight of the species. It was assumed that a typical control lung weight was 0.9 g for F344 rats and 1.3 g for Sprague-Dawley rats; for mice, a typical control lung weight was 0.15 g. These values were based on data from the compiled database, where available, and also from the literature for rodents of the same species, strain, sex, and age [Kobayashi et al. 2009; NIOSH 2013; Porter et al. 2001]. The normalized dose metric was the ratio of the particle mass in the lungs to the control lung weight expressed as micrograms per gram of wet lung tissue. Normalizing particle dose per gram of lung has been used in other analyses of rodent data [NIOSH 2011; Schmid and Stoeger 2016].

During the exploratory data analysis stage to learn about factors that may need to be considered when estimating potency, a random forest regression model was used to identify which experimental factors were most predictive of the PMN proportion across all studies. These factors included the dose, post-exposure duration, exposure duration, route of exposure, and the species, sex, and strain of the rodents. Exposure duration values in hours per day, days per week, and number of weeks were used to allow for any unit conversions or potential dosimetric adjustments.

Physicochemical property data were evaluated later, after the dose-response modeling and grouping of materials according to their hazard potency (associated with PMN response). The purpose of those analyses was to evaluate the feasibility of using the most important physicochemical properties to predict the hazard potency group of a new ENM.

The variable importance of a particular factor is estimated by measuring the change in mean squared error (MSE), a measure of predictive accuracy, when the values of that factor are re-assigned based on random permutations. Thus, if permuting the values of a factor produces a large increase of the MSE and poorer predictive accuracy, it is an important predictor and receives a high variable importance score.

Initial efforts to model the post-exposure dose-response surfaces via multiple SK regression were unfavorable because of both the heterogeneity in experimental designs (e.g., dose spacings) and large variability in the responses both within and across studies. As a result, the NIOSH/CIIT/ENPRA database was stratified by post-exposure duration: 0 to 3 days; 7 to 14 days; 28 to 60 days; and 91 days to 1 year. These strata reflect typical toxicology study designs. A majority of the data and studies were contained in the stratum of 0 to 3 days, which is the focus of this analysis (Table 2-3).

Table 2-3. Distribution of Post-Exposure Durations in the NIOSH/CIIT/ENPRA Database

		Post Exposure Days												
Reference	Material	0	1	3	7	14	28	30	36	60	91	112	182	364
Porter et al. 2013	TiO_2		■	■	■		■					■		
Xia et al. 2011	Fe_3O_4, ZnO		■			■		■						
Roberts et al. 2013	Ag		■		■									
Sager et al. 2013	MWCNT		■		■									
Porter et al. 2001	Silica	■												
Porter at al. 2004	Silica	■							■					
ENPRA - RIVM	Ag		■											
ENPRA - NRCWE	MWCNT		■				■							
ENPRA - NRCWE	MWCNT		■				■							
ENPRA - NRCWE	MWCNT		■				■							
ENPRA - NRCWE	MWCNT		■				■							
ENPRA - RIVM	MWCNT		■											
ENPRA – RIVM	MWCNT		■											
ENPRA – UC	MWCNT, Silica									■				
ENPRA – UC	MWCNT, Silica									■				
ENPRA – RIVM	ZnO		■											
ENPRA – RIVM	ZnO		■											
ENPRA – UC	ZnO, Silica									■				
ENPRA – RIVM	TiO_2		■											
ENPRA – RIVM	TiO_2		■											
ENPRA – RIVM	TiO_2		■											
ENPRA – RIVM	TiO_2		■											
ENPRA – RIVM	TiO_2		■											
Bermudez et al. 2002	TiO_2	■					■				■		■	■
Bermudez et al. 2004	TiO_2	■					■				■		■	■

Dose-response modeling was used to quantify the potency of a given material, where potency is inversely proportional to the BMD for a specified increase of the response (BMR) [Crump 1984, 2002]; that is, when doses are in comparable units, a larger value for the BMD indicates lower potency for the specified BMR. The total deposited lung dose (normalized as particle mass per gram wet lung), as discussed above, is the dose metric used

in these analyses. An increase of neutrophilic pulmonary inflammation quantified by the proportion of PMNs in BALF over the controls is the BMR used in these analyses. The specific BMRs evaluated were either an additional 4% PMNs over background (i.e., in the unexposed control animals) or a total of 10% PMNs in BALF, based on biological evidence described below. Because potency is defined here as the reciprocal of the mass deposited lung dose per gram of wet lung tissue associated with pulmonary inflammation, the lower that dose (i.e., BMD), the greater the potency of the material.

These BMRs were selected as being biologically relevant responses in both rodents and humans [as discussed in NIOSH 2011]. In rats, a response of approximately 4% PMNs in BALF has been associated with particle lung doses at or near overloading of lung clearance in rats exposed to poorly soluble particles [Muhle et al. 1991; Tran et al. 1999; Pauluhn 2012]. Overloading results in a dose-dependent increase in the particle retention in the lungs [Morrow 1988; Elder et al. 2005; Pauluhn 2011] and the development of persistent pulmonary inflammation, fibrosis, and lung cancer in rats [Muhle et al. 1991; ILSI 2000; IARC 2010]. Dose metrics that are most predictive of overloading across microscale and nanoscale particle sizes include particle volume [Pauluhn 2011, 2014] and particle surface area [Oberdörster et al. 1994; Tran et al. 2000; Morfeld et al. 2015].

The background percentage of PMNs in control rats in long-term studies is generally low (<1%), whereas in the acute studies, higher background percentages of PMNs were observed in animals treated with vehicle control [e.g., Bonner et al. 2013]. In humans, a value of approximately 4% PMNs in BALF was associated with respiratory impairment in workers in dusty jobs [Rom 1991; NIOSH 2011]; and 10% PMNs in BALF is considered to be clinically abnormal [Crystal et al. 1981; Martin et al. 1985]. The selection of biologically significant BMRs is relevant for risk assessment [U.S. EPA 2012]. The specific BMR used (i.e., an additional 4% PMNs or a total of 10% PMNs) influenced the number of rodent studies with sufficient dose-response data for BMD estimation in this analysis (as explained further in Results).

BMD estimation for each of the dose-response relationships was performed individually with SK, which is a flexible modeling method suited for handling the non-linear, heteroscedastic dose-response relationships often seen in toxicology studies [Wang et al. 2014]. A wide range of continuous dose-response relationships can be modeled with SK, and the capability to automate the modeling process facilitated the estimation of BMDs from multiple studies, although it still requires a specification of the covariance function. The popular Gaussian covariance function was first used, which should suffice for all of the two-dimensional dose-response shapes and generally creates a smooth curve. However, the model curve fit to the data was not restricted to biologically relevant shapes and included shapes such as sinusoidal or non-monotonic. If the visual fit was inadequate, the

General Exponential covariance function was used, which generally creates a non-smooth curve (e.g., piecewise linear). See Rasmussen and Christopher [2006] for additional information on covariance functions and the mechanisms underlying SK. Only dose-response relationships with statistically significant differences in mean response across dose groups were modeled, and this characteristic was investigated via ANOVA (results not shown). Decisions on the presence of a trend were made at the 5% level of significance. Modeling with SK was completed in MATLAB [MATLAB 2016].

Dose-response modeling was initially completed with the U.S. EPA Benchmark Dose Software (BMDS), version 2.6 [U.S. EPA 2015], which offers the choice of several parametric model forms to fit to a single relationship. BMD estimates from BMDS were similar to those from SK [Wang et al. 2014]; however, modeling many relationships is more time-consuming with BMDS (Table A-3). Variability in the dose-response data in an experiment can result in uncertainty in the estimated potencies; thus, the 95% one-sided lower confidence limit estimate of the BMD (i.e., BMDL) is calculated in the U.S. EPA BMDS and the SK modeling to provide an estimate of that uncertainty. Under the model, the BMDL estimate provides 95% confidence that the true BMD is not lower than the BMDL. The BMDL estimates from SK tended to be higher than those from BMDS, indicating higher accuracy for a given confidence level if nominal coverage is achieved. As a result, BMDs from SK modeling were chosen to represent the potency of the nanoscale or microscale particles in this first analysis only. Other published software that allow for the fitting of several BMD model forms to numerous dose-response relationships in succession [Wignall et al. 2014; Shao and Shapiro 2016] may be useful considerations for future investigations.

Once potency estimates are obtained for each of the dose-response relationships in the stratum of 0 to 3 days, similarly behaving materials are identified by comparing those potency estimates. Materials with similar potency estimates are assumed to behave similarly with respect to pulmonary inflammation. Hierarchical clustering with complete linkage was used to create four groups of materials with similar potency estimates. Four groups were chosen to potentially reflect the four broad categories that have been proposed for ENMs, based on the biological mode of action and physicochemical properties (e.g., poorly soluble low toxicity, high toxicity, soluble, high aspect ratio) [BSI 2007; Kuempel et al. 2012; BAuA 2013; Arts et al. 2016].

The grouping process involves agglomerative clustering in which each potency estimate first begins as its own cluster. The Euclidean distances (differences) between potency estimates are calculated, and potency estimates (or clusters) nearest to one another are then combined into a set of new clusters. This process repeats until all potency estimates are represented by one of four mutually exclusive clusters such that the potencies within each

cluster are comparatively more similar and the potencies from different clusters are dissimilar. The terms *cluster* and *group* are used interchangeably. This process creates groups with descriptively different potency estimates as opposed to statistically different. The BMDs are the best estimates of potency and thus were used when creating the groups of materials with similar potencies. Variability in the experimental dose-response data was not considered in creating the groups; however, variability will be considered later by evaluating the distribution of the BMDL estimates within the final groups. BMDL estimates are used as the PoD in risk assessment to estimate a safe dose in humans [U.S. EPA, 2012].

In order to classify a new material into a potency cluster on the basis of that new material's physicochemical properties, a classification random forest model was developed. Note that this is not the same random forest model used in the exploratory data analysis stage, which was a regression model for identifying experimental design factors that are important in predicting PMN proportion. The classification random forest described next seeks to predict the potency group (1, 2, 3, or 4) of a material by using only the available physicochemical property information as predictors. Because of the limited number of materials with a potency cluster label and numerous but sparse physicochemical property data, traditional modeling schemes are not well suited to describe the physicochemical property-cluster space. A non-parametric solution is a classification tree [Breiman et al. 1984]; however, a single tree can tend to over-fit the data and have a large amount of variability in its predictions.

A classification random forest is a collection of many classification trees that has improved predictive accuracy [Breiman 2001]. The "random" namesake is due to two characteristics: a tree is constructed from a random bootstrap sample of the data, and a random subset of all predictor variables is considered for every branch in the tree. This process is repeated many times, creating many trees, hence a forest. The result is a collection of many de-correlated trees, each of which can provide different information about the relationship of interest. For a given new material, each tree in the forest casts a vote for a potency group, with the final group prediction being the potency group that received a plurality of the votes.

Default options were used when constructing the random forest: 500 trees were created, and the number of predictors, p, considered at each branch in the tree was $\sqrt{p}$, rounded down to the nearest integer. Because many physicochemical properties have missing values, distinct values (-99 if quantitative; "N/A" if qualitative) were used to indicate missingness. Physicochemical properties with missing values for all materials were excluded from the modeling process (Figure A-1). An examination of pairwise correlation estimates was used to ensure that few, if any, highly correlated physicochemical properties were included in the model, as this can lead to a

preference of correlated predictors when the classification trees are created [Strobl et al. 2008]. Hierarchical clustering and random forest modeling were completed using R [R Core Team 2014].

The six material forms in the NanoGo database, five of which were not used in the model development (anatase/rutile nanospheres are the same type of material used in Bermudez et al. [2004]), were considered to be "new materials" and were used to evaluate the random forest models. On the basis of the physicochemical properties of these new materials, a potency cluster was predicted by the random forest model. Pulmonary inflammation potencies were estimated with SK from the individual dose-response data by laboratory and material. The median potency estimate for each material was used to identify the nearest potency cluster to which the material would be assigned and was then used as a comparison to the predicted cluster.

2.2.2 Updates to the Database and Methods

Because of the limited number of materials used in the framework development (Section 2.2.1), a series of four literature searches were conducted in order to add dose-response and physicochemical information for more materials to the database [Boots et al. submitted]. Three of the searches used online databases (PubMed, Scopus, Toxline, and Web of Science), and one used NIOSHTIC-2 (Figure 2-3). These searches sought out nanomaterial toxicity studies in which the endpoint was pulmonary inflammation. The resulting studies were filtered on the basis of minimum data criteria: experimental designs amenable to benchmark dose estimation; post-exposure duration of no more than 3 days; and sufficient summary statistics (e.g., sample size, sample mean, and sample standard deviation or sample standard error). Any available physicochemical information was gleaned from the publications, although such information remained sparse.

Figure 2-3: Study selection process for the updated literature searches (Swiss-VCI/NIOSHTIC/ATL) [Boots et al. submitted].

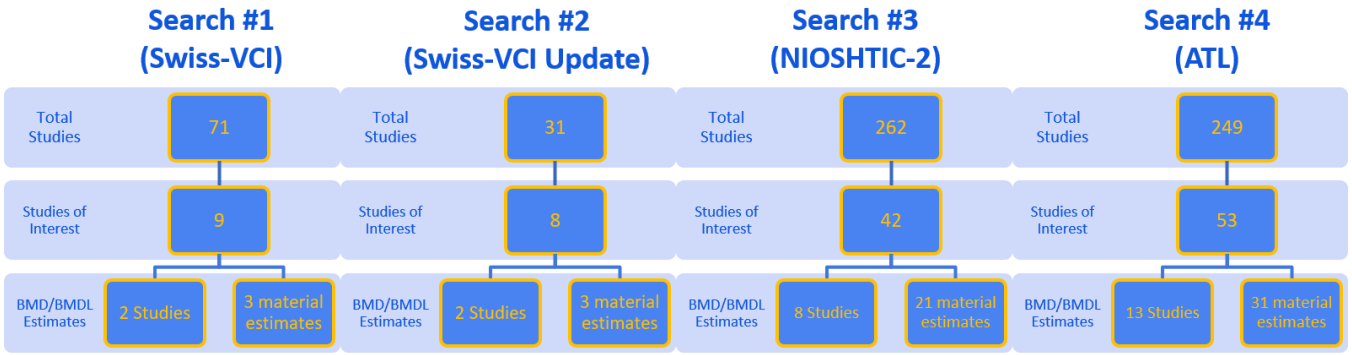

Ultimately, the unit of analysis is a dose-response relationship from which a benchmark dose is estimated. A subset of search results provided enough information to summarize the relationship, and yet another subset were found to be amenable for dose-response modeling based on characteristics such as these: at least two exposure groups and one negative control; more than one subject per dose group; and a statistically significant trend at the 5% level of significance.

Benchmark doses were estimated with use of the continuous model suite in EPA BMDS 2.7. All models were fit to a given dose-response relationship, and the best-fitting model was identified by (1) passing the four diagnostic tests available within BMDS and (2) having the lowest AIC. In some instances, a complex model may appear to have the lowest AIC but one of its parameter estimates reached a predefined boundary. In these cases, the

software treats those parameters as being known, with their value equal to the boundary, and they are not included in the penalty portion of the AIC. Thus, for every boundary estimate, the AIC value is increased by 2.

The previous framework analysis [Drew et al. 2017] proposed identifying clusters of materials with similar potencies by using hierarchical clustering, where clusters are formed with complete linkage, creating clusters that can be very close to others. When clusters are close together, it may occur that the endpoints of two clusters are closer together than those endpoints to members of their own cluster. As was illustrated, 78% of materials (14 of 18) were assigned to the most potent cluster, which may be practically effective (i.e., assigning a new material to the most potent group can lead to very protective recommendations) but not biologically representative (i.e., broadly classifying all new materials as very potent can ignore mechanistic information and place too much weight on the representativeness of the data used to identify the clusters).

Other linkage methods are available, such as single linkage and Ward's Minimum Variance method [Ward 1963]. Single linkage may be seen as an opposite to complete linkage, in that clusters can be spread out and not compact. Ward's method seeks to minimize the within-cluster variance, leading to clusters that can be compact and more evenly sized. The linkage method was further evaluated here by comparing the previous proposal of complete linkage to Ward's method. No other linkage methods (e.g., single) were evaluated for use.

Other clustering methods are available in addition to hierarchical clustering, such as k-means. That process, however, requires the user to specify the true number of clusters, which is assumed to be known. In this framework the true number of clusters is unknown but is hypothesized to be four to align with mode-of-action categories. To further evaluate the decision to use four clusters, an exploratory k-means approach was used to measure the total within-clusters sum of squares for values of k from 1 to 10. Lastly, the potency estimates may be grouped by orders of magnitude (e.g., less than 0.01 μg/g lung, 0.01 to 0.1 μg/g lung).

The potency cluster of a material is considered a label, and the statistical model is used to predict the label, given physicochemical properties. The premise is that a new ENM will likely have physicochemical descriptors but not dose-response information. Because the form of the association between numerous physicochemical properties and cluster labels is assumed to be complicated and non-linear, a random forest model is used to estimate that association. A random forest is an ensemble of decision trees, where each tree is constructed on a bootstrap sample of the data; at each branch in a given tree, a random sample of physicochemical properties are considered. The result is a set of short trees, each learning about different portions of the data space. For each tree, the input is the physicochemical properties of a material, and the output is a vote for a cluster. The output of the random forest is then a tally of votes, where the predicted cluster of the material is that which received the most votes.

The advantage of the random forest model is that it is able to handle complex associations, with the disadvantage that it can be difficult to interpret the components of the model. See Breiman [2001] for additional information.

The set of potency clusters (by order of magnitude or via complete linkage and Ward's method for hierarchical clustering) and physicochemical properties were split into a training and test subsets using 2/3 and 1/3 of the estimates, respectively. A random forest model was built with the training set, and classification accuracy was evaluated with the test set.

Thus, the general process remains mostly the same as that described earlier in this section, except that data from literature searches have been added to the database, potency clusters were additionally formed by orders of magnitude or by hierarchically using Ward's method, and a random forest model was trained and tested to classify a material into a potency cluster for the order-of-magnitude labels and each linkage method.

2.3 In Vitro Inflammation

The ENPRA and NanoGo data were used in the *in vivo* analysis, and data are available from these groups *in vitro*. A similar endpoint is of interest, so IL-1 beta was chosen because it is a marker for inflammation. Other cytokines indicative of inflammation could be used, such as TNF-alpha, IL-6, MIP-1, or MIP-2, but these other markers either were not available or were measured for a non-respiratory cell line. An exploration of the data found that there are 12 ENPRA dose-response assays with the IL-1 beta endpoint (six using cell line LA-4 and six using cell line MH-S); there are 42 NanoGo dose-response assays with the IL-1 beta endpoint using the THP-1 cell line. The LA-4 cells are from the mouse lung, MH-S cells are mouse lung alveolar macrophages, and THP-1 cells are human monocytes.

The sparsity of the ENPRA data makes it unsuitable for use as a training dataset for the framework. Furthermore, no cell lines were in common across ENPRA and NanoGo, which may affect comparisons of potency estimates. Thus, the NanoGo data were chosen for analysis; potency estimates will be derived via SK, and a ranking of material potencies will be compared to those *in vivo*.

The NanoGo *in vitro* IL-1 beta database was created from the base file received from the researchers. The 42 dose-response relationships consist of seven laboratories, each testing six materials: zinc oxide (ZnO), original multi-walled carbon nanotubes (MW-O), purified multi-walled carbon nanotubes (MW-P), functionalized multi-walled carbon nanotubes (MW-F), titanium dioxide nanobelts (TNB), and crystalline silica (SiO_2). Each laboratory followed the same protocol (Phase II), using three replicates at five exposure groups: 0, 10, 25, 50, and

100 μg/mL. The response, IL-1 beta, was measured in pg/mL. Measurements were taken 24 hours after exposure.

BMD modeling via SK is used to estimate the potency (a BMD and BMDL) of a material for each of the 42 dose-response relationships. The BMD is the dose associated with some specified level of response, known as the BMR. Two BMRs were of interest: a response of 5% above background (γ+5%) and a response of 1.1 standard deviations above background (γ+1.1 SD). The BMR of γ+5% is a default option when any prior information is lacking on biologically significant levels of response (similar to the additional 4% PMNs associated with inflammation in rats and humans [Section 3.5.2.2 of NIOSH 2011]). The BMR of γ+1.1 SD for these continuous data is approximate to a BMR of 10% for quantal endpoints where the probability that an unexposed subject will have an abnormal response is 1% (see Crump [1995] for additional details).

Before using SK, we used ANOVA to determine if a difference in mean response across dose groups could be detected. If no association was found, that relationship will not be modeled. Decisions were made at the 5% level of significance.

Of the 42 dose-response relationships, 31 were found to have a statistically significant difference in mean response across the dose groups (11 relationships did not). SK was used to model the dose-response association, from which a BMD and BMDL could be estimated from the model for a given BMR. The Gaussian covariance function was used first, as it generally provides a smooth fit. If the resulting model fit was not monotonic, then the General Exponential covariance function was used. The best-fitting model was chosen visually, and if neither model fit the data adequately, then no estimates of potency were derived.

It was assumed that as the dose increases, the level of IL-1 beta measured would increase. However, for the seven ZnO associations, a significant negative relationship was observed. As a result, no potency estimates could be derived for the two chosen BMRs. However, data on cytotoxicity (percentage of viable cells relative to control) were available, which revealed that the ZnO material was highly toxic even at the lowest dose group used in the NanoGo experimental design. Therefore, because cells were rapidly dying, IL-1 beta could not be produced. This means that even though a BMD estimate could not be determined for ZnO, it was assumed to be lower than the other BMD estimates for the other five materials. This assumption is used when presenting the BMD results, where the BMD estimates for ZnO are reported to be less than TiO_2 nanobelts.

The relative ranking of the potency estimates for these materials can be compared to those from the acute inflammation analysis, as the same laboratories and materials were used. Comparisons were made qualitatively and were based on ranking comparisons. No further analysis of the potency estimates has been completed, such as clustering or random forest predictive models.

2.4 NTP Inflammation, Fibrosis, and Lung Cell Neoplasia

The CEBS (Chemical Effects in Biological Systems) is a compilation of data from the National Toxicology Program (NTP) that contains all of the individual or summary data from the completed carcinogenicity and toxicity studies for a variety of substances, including particles (https://manticore.niehs.nih.gov/cebssearch). The route of exposure in these studies was inhalation, and the animal species were rats and mice. Most of the particles included in the NTP database appear to be microscale (on the basis of the particle size data that was reported, Table 2-7), although many of these NTP materials have also been produced in nanoscale form (Table 2-6). This database is a valuable source of benchmark materials, as the experimental data are very high quality and the most relevant for OEL creation, as chronic (2 year) and sub-chronic rodent bioassay data are available. Within CEBS, the NTP histopathology database was chosen for further analysis because this is where the lung inflammation, lung fibrosis, and lung cell neoplasia response data are stored. The histopathology database is massive, containing over 5 million rows of data for over 1,100 materials. A subset of 23 materials were chosen for analysis, as they were administered via inhalation and were found to be a solid particle (Table 2-4). The physical form was found by using a combination of two internet databases, ChemIDLite and HSDB, if such information was not available within the corresponding technical report.

Table 2-4: NTP Materials

Material	CAS Number
Cobalt sulfate heptahydrate	10026-24-1
Nickel sulfate hexahydrate	10101-97-0
Ferrocene	102-54-5
Nickel subsulfide	12035-72-2
Gallium arsenide	1303-00-0
Antimony trioxide	1309-64-4
Molybdenum trioxide	1313-27-5
Nickel (II) oxide	1313-99-1
Vanadium pentoxide	1314-62-1
Calcium chromate	13765-19-0
Wollastonite calcium silicates	13983-17-0
Talc	14807-96-6
Indium phosphide	22398-80-7
o-Chlorobenzalmalononitrile (CS)	2698-41-1
ortho-Phthalaldehyde	643-79-8
Chromium	7440-47-3
Cobalt	7440-48-4
Abrasive Blasting Agents: Blasting Sand	BLASTINGSAND
Abrasive blasting agents (coal slag)	COALSLAG
Abrasive blasting agents (crushed glass)	CRUSHEDGLASS
Abrasive blasting agents (garnet)	GARNET
Abrasive Blasting Agents: Specular Hematite	HEMATITESPEC
1020 Long Multiwalled Carbon Nanotube	L-MWNT-1020

The NTP histopathology database in CEBS contains responses from many different organs, tissues, or body systems, so the analyses focused on the lung responses of relevance to workers. Histopathological diagnoses were identified that indicated pulmonary inflammation, pulmonary fibrosis, and primary pulmonary neoplasia (Table 2-5). Neoplasia originating in extrapulmonary tissues that metastasized to the lung were excluded from the analysis.

Table 2-5: Endpoints and Associated Diagnoses of interest from the NTP histopathology data

Inflammation Response		***Fibrosis Response***		***Lung Cell Neoplasia***
Inflammation		Fibrosis		Carcinoma
Inflammation, Acute Focal		Fibrosis, Diffuse		Sarcoma
Inflammation, Chronic Focal		Fibrosis, Focal		Neoplasm, NOS
Inflammation, Granulomatous Focal		Fibrosis, Multifocal		Teratoma Malignant
Inflammation, NOS				Schwannoma Malignant
Inflammation, With Fibrosis				Carcinosarcoma
Inflammation, Chronic				Leiomyosarcoma
Inflammation, Focal				Neoplasm, Malignant, Nos
Inflammation, Interstitial				Alveolar/Bronchiolar Carcinoma
Inflammation, Obliterative				Alveolar/Bronchiolar Adenoma
Inflammation, Granulomatous				Squamous Cell Carcinoma
Inflammation, Necrotizing				Cystic Keratinizing Epithelioma
Inflammation, Suppurative				Adenocarcinoma
				Fibrosarcoma
				Hemangioma
				Adenoma
				Fibroma

The structure of the database is such that one row corresponds to one histopathological diagnosis for one animal from one study, so the data were summarized first to the animal-level, where an indicator was created for each endpoint:

- Did the animal ever have any type of lung inflammation? (yes or no)
- Did the animal ever have any type of lung fibrosis? (yes or no)
- Did the animal ever have any type of lung cell neoplasia? (yes or no)

Lastly, the data were summarized to the study-duration-material-species-sex level, where the number of animals examined and number of animals with a response were summed.

The dichotomous model suite in the EPA BMDS was used to estimate the BMD and BMDL for each relationship. For lung inflammation, lung fibrosis, and lung cell neoplasia, the BMR corresponded to an added risk of 10%.

The Cochran-Armitage Trend Test identified the subset of relationships eligible for modeling at the 5% level of significance. The best model was chosen with EPA BMD guidance, where there must be adequate goodness-of-fit and, among the fitting models, the one with the lowest Akaike Information Criterion (AIC) is chosen. NOAELs and LOAELs were also estimated for each relationship with pairwise Fisher's Exact Tests.

After BMD modeling, the potency estimates were grouped with Hierarchical Clustering by complete linkage, with grouping determined by the relationships within the data. Hierarchical clusters created by Ward's method were not explored. Potency estimates were also placed into order-of-magnitude bands to correspond to hazard/occupational exposure bands (as discussed in the next section).

Because of the experimental design of the NTP studies, a material typically had histopathological data at earlier time points in addition to the 2-year results. This provided an opportunity to explore how potency estimates change over time through the creation of potency factors. These empirical data were also useful for comparison to the standard uncertainty factors (UFs) that are used in QRA when chronic data are not available and PoDs are estimated from shorter-term data. In cases where 13-week and 2-year potency estimates (BMDL or NOAEL) are available for a given material-species-sex, the relative difference between them is calculated.

The CEBS database did not seem to contain physicochemical information, so the technical reports and material manufacturer websites were consulted for any available data. Other sources (Future Markets report and Nanowerk website) were also consulted for information on the current availability and use of nanomaterials of the same or similar chemical composition as the particulate materials in the NTP studies (Table 2-6). Most of the NTP materials are assumed to have been microscale, primarily on the basis of the mass median aerodynamic diameter (MMAD) information that was reported. However, the primary particle size of these NTP materials remains uncertain because nanoscale particles typically agglomerate and form microscale aerodynamic diameters (e.g., ultrafine TiO_2 and carbon nanotubes and nanofibers [NIOSH 2011; NIOSH 2013]).

The physicochemical information available for the materials in the NTP database was found to vary by material and also tended to be quite sparse (Table 2-7). However, it was possible to use these limited available data in exploratory analyses. Random forest models were constructed to identify the importance of the reported experimental design and physicochemical properties for predicting the potency clusters.

Table 2-6: Nanoscale Production Information for the Analyzed NTP and Additional PSLT Materials

Material	Specific material as nano-product? (Nanowerk; Future Markets)	Nanoproduct in Chemical Class? (Base/primary chemical)	Other Nanoscale Applications (NTP Material + "nano"
Cobalt sulfate heptahydrate	No	See cobalt	Used to synthesize nano cobalt powder
Nickel sulfate hexahydrate	No	Many nickel products	
Ferrocene	No	Iron, Iron oxide, Iron (II) oxide, Iron (III) oxide, Iron Carbon-coated nanoparticles; nanopowders; nanorings; nanotubes	Ferrocene-containing nanomaterials; used in the synthesis of CNTs; nanoelectronics
Nickel subsulfide	No	Many nickel products	
Gallium arsenide	Yes	Gallium Antimonide	Nanowires and nanocrystal formation for optoelectronics; solar cells
Antimony trioxide	No	Antimony oxide nanoparticles; Antimony Tin Oxide nanoparticles; Nano-D Antimony Tin Oxide dispersion	Flame retardant nanopowder; conductive, antistatic, electrochromic, electro-optic, and magnetic applications
Molybdenum trioxide	No	Molybdenum nanoparticles; Molybdenum disulfide nanoparticles; Molybdenum oxide nanopowder; Molybdenum oxide nanowires	Potential cancer therapy utility
Nickel (II) oxide	Yes	Many nickel products	Magnetic applications
Vanadium pentoxide	No	Vanadium Carbide nanopowder & nanoparticle; Vanadium oxide nanowires	Catalyst; optical applications; alloy and ceramic manufacturing

Calcium chromate	No	Calcium carbonate; Calcium zirconate; Lanthanum calcium manganese oxide	
Wollastonite calcium silicates	No		Fire retardant applications
Talc	No		Polymeric nanocomposite filler
Indium phosphide	No	Indium oxide; Indium tin oxide; Indium zinc oxide	Semiconductor and optical applications
o-Chlorobenzalmalononitrile (CS)	No		
ortho-Phthalaldehyde	No		
Chromium	Yes		Refractory applications; steel and automobile manufacturing
Cobalt	Yes		Biomedicines and medical sensors; MRI contrasting agent; cell phone manufacturing; metal ceramics; diamond tools; hominess alloy; magnetic toner; magnetic ink; ferrofluids
Abrasive Blasting Agents: Blasting Sand	No		
Abrasive blasting agents (coal slag)	No		
Abrasive blasting agents (crushed glass)	No		
Abrasive blasting agents (garnet)	No	Yttrium iron garnet	
Abrasive Blasting Agents: Specular Hematite	No		
1020 Long Multiwalled Carbon Nanotube	Yes	Single wall; Short CNT	Conductive applications; sporting goods; high-strength/low weight composites
Titanium Dioxide*	Yes		Sunscreen; housing and construction via additive to paint; UV absorption; photocatalytic sterilizing

Carbon Black*	No		Cosmetics; electronics; plastics; coatings; inks
Toner*	No		

*Chronic inhalation rodent bioassay data obtained from publications [Lee et al. 1985; Heinrich et al. 1995; Nikula et al. 1995; Muhle et al. 1991].

Table 2-7: Physicochemical information gathered on the NTP materials.

Material	CAS Number	Technical Report No.	Shape	Primary Particle Mean Diameter (um)	Diameter Std. Dev.	Mean MMAD (um)	Mean GSD	Molecular Weight (g/mol)	Mean Density (g/cm^3)	Crystal Structure & Type	Solubility	Solubility Unit	Relative Solubility*	Impurities
1020 Long Multiwalled Carbon Nanotube	L-MWNT-1020		fiber	0.015	0.005									
Abrasive blasting agents (coal slag)	COALSLAG			1.11	0.2									SiO_2 (47.2%), AlO (21.39%), FeO (19.23%), CaO (6.8%), KO(1.6%), MgO (1.47%), TiO_2 (1.01%)
Abrasive blasting agents (crushed glass)	CRUSHEDGLASS													SiO_2 (73%), NaO (14%), CaO (10%), MgO (1%), AlO (1%), SO_3 (1%)
Abrasive blasting agents (garnet)	GARNET			0.99	0.21									SiO_2 (36.79%), FeO (32.7%), AlO (25.51%), MgO (3.08%), CaO (1.15%), MnO (1.01%)
Abrasive Blasting Agents: Blasting Sand	BLASTINGSAND			0.92	0.23									Quartz (49%), Aluminum, Barium, Calcium, Chromium, Copper, Iron, Magnesium, Manganese, Phosphorus, Sodium, Titanium, Vanadium, Yttrium, Zinc, Zirconium
Abrasive Blasting Agents: Specular Hematite	HEMATITESPEC			0.99	0.19									Fe_2O_3 (98-99%), SiO_2 (0.1%)
Antimony trioxide	1309-64-4	590	polymorphic			1.22	1.92	291.52	5.3	crystalline powder				Arsenic (0.019%), Lead (0.016%)
Calcium chromate	13765-19-0		rhombic					156.07	2.89	crystal	0.1	mg/mL (at 72F)	V. Low	
Chromium	7440-47-3		cubic					51.996	7.14		0	mg/mL water	Poorly soluble /nonsoluble	
Cobalt	7440-48-4	581	hexagonal/ cubic			1.73	1.73	58.933	8.92	powder	1	mg/mL water (at 66F)	Low	Chromium (84 ppm)
Cobalt sulfate heptahydrate	10026-24-1	471				1.5	2.15	281.094	1.95	crystalline solid	100	mg/mL water (at 64F)	High	Nickel (140 ppm), Other (<175 ppm)
Ferrocene	102-54-5							186.035	1.107	crystalline solid	19	g/100 g benzene (at 25C)	Med	
Gallium arsenide	1303-00-0	492	cubic			0.88	1.85	144.645	5.3176	powder	1	mg/mL water (at 68F)	Low	Aluminum (52 ppm), Silicon (33 ppm),

														Calcium (14 ppm)
Indium phosphide	22398-80-7	499	cubic			1.23	1.72	145.792	4.81	polycrystalline solid	0	mg/mL water	Poorly soluble /nonsoluble	Arsenic (0.01%), Selenium (0.01%), Iron (0.01%), Antimony (0.01%)
Molybdenum trioxide	1313-27-5	462	rhombic			1.87	1.83	143.947	4.69	powder	1.066	g/L water (18C)	Low	Cadmium (100 ppm), Potassium (2400 ppm), Silicon (180 ppm), Sodium (50 ppm)
Nickel (II) oxide	1313-99-1	451	cubic			2.22	1.88	74.692	6.72	powder	0.11	mg/100 mL (20C)	V. Low	Cobalt (2200 ppm), Iron (670 ppm), Sulfur (200 ppm)
Nickel subsulfide	12035-72-2	453	hexagonal			2.1	2.15	240.2	5.87	powder	1	mg/mL water (at 70.7F)	Low	Silicon (1200 ppm), Iron (470 ppm), Phosphorus (335 ppm), Chromium (300 ppm)
Nickel sulfate hexahydrate	10101-97-0	454				2.33	2.23	262.839	2.07	crystalline powder	100	mg/mL (at 68F)	High	Cobalt (1500 ppm), Silicon (470 ppm), Magnesium (120 ppm)
o-Chlorobenzalmalononitrile (CS)	2698-41-1	377						188.614	1.296	microcrystalline powder	5	mg/mL water (at 61F)	Low	Silica (5%)
ortho-Phthalaldehyde	643-79-8							134.134	1.189					
Talc	14807-96-6	421	plate	10		2.98	1.93	379.259	2.7	Mono/triclinic tabular	1	mg/mL (at 70F)	Low	
Vanadium pentoxide	1314-62-1	507		<1		1.24	1.89	181.878	3.654	orthothrombic crystalline solid	0.07	g/100 g water (25C)	V. Low	Barium (170 ppm), Iron (110 ppm), Calcium (440 ppm), Potassium (550 ppm), Sulfur (270 ppm), Silicon (260 ppm), Sodium (1100 ppm), Aluminum (260 ppm), Magnesium (340 ppm)
Wollastonite calcium silicates	13983-17-0							116.16	2.92	monoclinistic crystals	1	mg/mL (at 70F)	Low	

Notes for Table 2-7:

Material-specific information:

Antimony trioxide: Particle sizes varied depending on "tint grade."

Chromium: Information depended on the form of Chromium.

Vanadium pentoxide: 90% of individual particles were reported to have diameter <1 µm; and "individual particles formed aggregates ranging from 40 to 300 µm in diameter, with an average diameter of 170 µm" [NTP TR 507].

1020 L-MWCNT – Mean length: 10 µm; Specific surface area: 170 m^2/g.

Density values were reported to be measured at 20 degrees centigrade for some materials; others did not specify.

Data sources (by variable):
Shape: primarily NTP documentation, confirmed with HSBD
Primary Particle Dimensions: NTP documentation (L-MWCNT-1020 only)
MMAD and GSD: NTP documentation
Density: primarily NTP documentation, confirmed and a few additions from HSBD
Crystal Structure and type: primarily NTP documentation, confirmed with HSBD
Solubility: NTP documentation and HSBD.
Specific Surface Area: NTP documentation (L-MWCNT-1020 only)
Impurities: NTP documentation

Data sources (Abrasive Blasting Agents), which are part of the NTP database:
Blasting sand, coal slag, garnet, Specular Hematite: Hubbs et al. [2001]. Crushed glass: Porter et al. [2002].

***Relative solubility (mg/mL water)** [Arbitrary]: Poorly soluble/nonsoluble: 0; Very Low: <1; Low: 1 - <10; Medium: 10 - <100; High: ≥100.

2.5 Categorical Occupational Exposure Limit Estimation

2.5.1 Grouping

The use of BMD estimates of hazard potency to group materials in this analysis provides a direct linkage to standard quantitative risk assessment methods [NAS 2009; U.S. EPA 2012]. The BMDLs estimated from modeling the dose-response data from rodent studies are typically used in QRA as PoDs to estimate the human-equivalent concentrations (HECs) and to derive OELs. In this case, the nanoscale or microscale materials were first grouped by their hazard potency, based on either pulmonary inflammation or lung neoplasia response. Group assignments were based on hierarchical clustering of materials within a common experimental design (as described in Methods).

2.5.2 Point of Departure

BMD modeling was used to estimate the PoDs in the animal data for extrapolation to humans. The BMR for acute pulmonary inflammation was defined as an additional 4% of PMNs cells in the BALF above the background level of PMNs in unexposed control rats [Drew et al. 2017]. In the subchronic or chronic studies evaluated in this document, the BMR for pulmonary inflammation was defined as an additional 10% in the proportion of rodents (rats or mice), with that response as identified by histopathological evaluation of lung tissue. In the chronic studies evaluated here, the BMR for lung neoplasia was defined as an additional 10% in the proportion of rats or mice, with that response based on histopathological evaluation.

After the materials are grouped according to their hazard potency in the rodent studies, PoDs are selected as the BMDL estimate associated with the BMD at the 5th percentile of the distribution of BMD estimates within each group. When an observed value is not available, the 5th percentile is determined via linear interpolation.

2.5.3 Human-Equivalent Concentration

The HEC to the rodent PoD was estimated with a dosimetric adjustment factor (DAF) approach [U.S. EPA 1994]. The human-equivalent PoDs by potency group were then used to estimate a categorical OEL after application of UFs based on the available data (as discussed in the next section).

2.6 Acute Lung Inflammation

In the acute pulmonary inflammation data on rodents, the BMD and BMDL estimates are based on dose-response modeling as a function of lung dose, expressed as particle mass dose per gram wet lung tissue. Thus, to estimate a human-equivalent dose, an interspecies adjustment is needed to account for the lung size differences. For

example, an interspecies dose adjustment could be made by adjusting by the lung weight. However, pulmonary surface area is considered a relevant metric for interspecies dose normalization for respirable particles that deposit on the pulmonary surface and elicit adverse responses such as persistent inflammation [U.S. EPA 1994; NIOSH 2011]. The particle dose per total alveolar macrophage cell volume, which has been associated with overloading of lung clearance in rats, has also been used for interspecies adjustment of particle lung doses [Pauluhn 2010a]. In the current analysis, pulmonary surface area was used for interspecies dose normalization because of the relationship with pulmonary inflammation (as reviewed in NIOSH [2011] for PSLT). The normalization of dose across species based on pulmonary surface area adjustment results in a lower human-equivalent dose compared to that estimated by using either the lung mass or total alveolar macrophage cell volume (by a factor of ~4.6) (Table 2-8). Thus, in addition to better reflecting the state of the science regarding biological mode of action for pulmonary inflammation, the use of pulmonary surface area to extrapolate the rodent (e.g., rat) lung dose to a human-equivalent dose also provides a lower (more health protective) estimate of a PoD for QRA. The derivation of an OEL from the PoD requires consideration of other factors (e.g., UFs for noncarcinogens and or estimation of lower levels of risk for carcinogens) [NIOSH 2021; NAS 2009; U.S. EPA 1994, 2002, 2005].

Table 2-8. Interspecies Dose Normalization for Respirable Particles.

Interspecies Dose Normalization Factor	Human	Rat	Ratio (Human/Rat)	References
Pulmonary surface area (m^2)	102	0.4	255	Stone et al. [1992]; Mercer et al. [1994]
Alveolar macrophage total cell volume (μm^3)	3.49×10^{13}	3.03×10^{10}	1,152	Pauluhn [2010b]
Lung mass (wet tissue) (g)	1200	1	1,200	ICRP [2002]

For the acute inflammation data reported in Drew et al. [2017], the human-equivalent lung dose was estimated by first adjusting the rodent effect level (µg ENM per g lung in rat or mouse) to the total dose in rats by assuming a rat lung weight of 1 g. The human-equivalent mass doses in the lungs were then estimated by adjusting for the pulmonary surface area in humans and rats (Table 2-8). The human-equivalent 8-hour time-weighted average (TWA) airborne concentration ($\mu g/m^3$) was estimated by assuming the reference worker air intake of 9.6 m^3/8-hour day [i.e., airborne concentration ($\mu g/m^3$) = human-equivalent lung dose (µg)/9.6 m^3]. This air intake corresponds to 5.5 hours of light exercise and 2.5 hours of sedentary activity per workday [ICRP 1994].

The estimation of the 8-hour TWA concentrations includes the assumption that the rodent deposited lung dose, if administered by an intratracheal instillation or pharyngeal aspiration route of exposure, is equivalent to the particle dose deposited by inhalation during an 8-hour day. This assumption was also used in the Hristozov et al. [2016] framework in their estimation of the human-equivalent "margin of exposure" to the rodent effect level.

In the current analysis, UFs were applied to the HEC_PoD to account for uncertainty in animal-to-human toxicodynamics (UF of 3) and worker inter-individual variability (UF of 5) [Dankovic et al. 2015; NIOSH 2021]. Because the deposited lung dose was estimated in humans by accounting for ventilation rate and pulmonary deposition fraction, no UF was used for animal-to-human toxicokinetics. Because BMDLs or NOAELs were used in these analyses, the UF for LOAEL to NOAEL was not applicable. These OEL estimates are intended for a single-day exposure, and thus the UF to adjust from subchronic to chronic exposure duration was not applicable. Thus, the total UF applied was 3 x 5 = 15.

2.7 Short-term to Chronic Lung Inflammation

The experimental inhalation data (primarily from NTP) included exposure durations from 2 weeks to 2 years, but most of the data for which BMDs could be estimated were from subchronic (90-day) or chronic inhalation (2-year) exposure studies. The airborne exposure mass concentrations (mg/m^3) to which rats or mice were exposed were extrapolated to humans by accounting for the morphological and physiological factors that influence the deposited particle dose in the pulmonary region of the respiratory tract in animals or humans [U.S. EPA 1994].

All durations of exposure (including exposures from 2 weeks to 2 years) reported in the NTP studies were included in the lung inflammation grouping. This grouping does not take into account the effect of exposure duration on the BMD estimates, which was shown in these analyses to be an important factor for explaining variability in the BMD estimates. In addition, data from both rats and mice were included in these grouping analyses. However, because the dosimetric adjustment of the single-day deposited lung dose of microscale airborne particles was shown above to be ~1 from rats to humans (Equation 2-8), it was considered reasonable to assume that the dosimetric adjustment of these airborne particle exposures between rats and mice would also be ~1. Thus, the pooling of the rat and mouse data may have not had much effect on the grouping of potency estimates for these airborne particles. The potency estimates (BMDs and BMDLs for lung inflammation) in the NTP data were too sparse for grouping when stratified by rodent species and exposure duration. Data for both sexes of rodent species were also pooled, which appeared to be reasonable on the basis of similar potency estimates for a given material in both sexes in rodents.

These NTP data are assumed to be primarily microscale particles (although the primary particle size is not reported for most materials). MWCNT is the only ENM in the NTP data, and this material has been shown to agglomerate in air, resulting in microscale aerosols (which influences the deposited fractional dose in the respiratory tract).

The human-equivalent concentration (HEC_PoD) is estimated by adjusting the animal PoD by the DAF as follows:

$$HEC\_PoD = PoD_{animal} / DAF \quad \text{[Equation 2-4]}$$

where PoD_{animal} is the estimate of the airborne exposure concentration associated with the selected animal effect level; and DAF is the dosimetric adjustment factor estimated, as shown below:

$$DAF = \left(\frac{VE_H}{VE_A}\right) * \left(\frac{DF_H}{DF_A}\right) * \left(\frac{NF_A}{NF_H}\right) \quad \text{[Equation 2-5]}$$

where VE is the ventilation rate (as the total volume of air inhaled per exposure day, m^3/d) in humans (H) or animals (A); DF is the deposition fraction in the pulmonary region of the respiratory tract region; and NF is the interspecies dose normalization factor (as pulmonary surface area) [NIOSH 2013, 2018].

The ventilation rate per exposure day in humans (VE_H) was assumed to be 9.6 m^3/8-hour workday, which is the reference worker air intake [ICRP 2015].

The ventilation volume per exposure day in animals (VE_A) (m^3) was calculated as follows, based on a 6-hour exposure day in the rat studies:

$$VE_A = V_E * 6\ hr \quad \text{[Equation 2-6]}$$

where V_E (L/min) is the minute ventilation rate.

As shown in Equation 2-3, for a rat with BW of 0.3 kg, V_E is 0.21 L/min.

Thus, VE_A is calculated as follows:

$$0.076\ m^3 = 0.21\ (L/min) \times 360\ min \times (1\ m^3/1{,}000\ L) \quad \text{[Equation 2-7]}$$

The particle deposition fraction in the pulmonary region was estimated in animals and humans by using the Multiple-Path Particle Dosimetry (MPPD) model v. 3.04 [ARA 2015]. DF_H was estimated at 0.3 for nanoparticles

(50-100 nm diameter) or 0.12 for microscale particles; DF_A was estimated at 0.2 for nanoparticles (50–100 nm diameter) or 0.06 for microscale particles.

Interspecies dose normalization (NF_A/NF_H) was based on the pulmonary surface area in rats (0.4 m^2) or humans (102.4 m^2).

Thus, the DAF used to estimate an HEC from the rat PoD (for microscale particles) is

$$0.99 = [9.6\ (m^3/d)/0.076\ (m^3/d)] \times (0.12/0.06)\ x\ (0.4\ m^2/102\ m^2) \qquad \text{[Equation 2-8]}$$

Note that the deposited dose of inhaled microscale particles in the pulmonary region of the respiratory tract in rats and humans is estimated in this example to be approximately equivalent (i.e., the DAF is ~1). For nanoscale particles (with DF_H and DF_A estimates of 0.3 and 0.2, respectively), the DAF estimate is 0.74. Both estimates would default to a DAF of 1, assuming that the HEC would not be greater than airborne exposure concentration in animals. These estimates do not take into account the differences in humans and animals in the long-term clearance or retention of particles that deposit in the lungs, whether the clearance is by alveolar macrophage-mediated clearance or by dissolution of particles in the lungs and clearance through systemic routes.

For mice, a DAF of 1 was also used to estimate an HEC when the PoD is from a mouse study in the NTP data. This assumption is supported in part by an estimate of ~1 when substituting into Equation 2-8 the mouse values of 0.00983 m^3/d and 0.5 m^2, respectively, for ventilation rate per exposure data and pulmonary surface area, and assuming the same DF_A of 0.06. The mouse ventilation rate of 0.00983 m^3/d is calculated by substituting in Equation 2-7 a V_E of 0.0273 L/min for mice of BW 0.024 kg (Equation 2-3). The mouse pulmonary surface area value is from Table 4-4 in U.S. EPA [1994]. A BW of 0.024 kg is that of the B6C3F1/N female mice in the NTP [2019] report of subchronic exposure to MWCNT. The DAF estimate of 1 in mice also assumes an equivalent DF_A to that in rats. Estimates in MPPD suggest that the pulmonary DF in mice may be lower than that in rats, although without specific particle size information in many of the NTP studies, estimates of the DF in rats, mice, or humans are uncertain. If the DF_A is lower than shown in Equation 2-8, then the DAF would be greater than 1.

Another DAF component used in some analyses (e.g., Pauluhn [2011]) is to include RT_H/RT_A to account for the differing retention half-time of particles inhaled and deposited in the respiratory tract. RT_H was estimated to be a 10x greater first-order retention half-time of poorly soluble particles in the lungs compared to the RT_A (rats) [Snipes 1989; Pauluhn 2011]. Studies in humans have shown that the long-term retention of poorly soluble particles would be underestimated by a first-order clearance model [Kuempel et al. 2001, 2015; Gregoratto et al. 2010; NIOSH 2011; ICRP 2015]. Information on the solubility of the various types of particles is not available, and thus clearance is addressed by using UFs in the current analyses.

The PoD_{RAT} (BMDL) from each experiment is divided by the DAF to estimate the HEC_PoD. Once an HEC_PoD is estimated, UFs are applied to the HEC_PoD to derive an OEL estimate that takes into account the uncertainty in applying the animal effect level estimates to predict equivalent dose-response in humans.

UFs used in these categorical OEL estimates include the following:

- Animal-to-human extrapolation: 3 (to account for possible difference in the toxicodynamics across species and potentially greater sensitivity in humans); note that a UF of 1 is used for the toxicokinetic component because of the accounting for the deposited lung dose across species [U.S. EPA 1994; Dankovic et al. 2015].

- Worker inter-individual variability: 5 [ECHA 2012; NIOSH 2021]

- Sub-chronic to chronic: 3–10 (to account for possible temporal effects that may result in a more severe effect or a higher response proportion after chronic exposure, compared to sub-chronic exposure) [Dankovic et al. 2015; NIOSH 2020].

No UF (i.e., UF of 1) was applicable for the LOAEL to NOAEL UF [Dankovic et al. 2015] because the BMDL or NOAEL estimates were used as the PoDs. No database adjustment factor was used, because these data are the NTP high quality standard bioassay data.

Thus, the total UF factor applied was 3 x 5 x 3 = 45 for the STOT-RE effects of pulmonary inflammation. Another UF considered, which may also be reasonable, is 3 x 5 x 10 = 150 (as described above).

2.8 Chronic Lung Neoplasia

The chronic (2-yr) inhalation exposure data were used to estimate the airborne exposure concentration associated with a 10% excess (additional) risk of lung cancer in comparison with control (unexposed) rodents. Both rat and mice data were included. Because the interspecies dosimetric adjustment to extrapolate the rodent 2-year inhalation exposure concentration to humans to estimate the equivalent daily concentration was ~1 (Equation 2-8), it is reasonable to assume the same would be true for the dose adjustment between rats and mice. Note that this adjustment does not account for possible (or likely) differences in the long-term clearance and retention of particles across species, particularly from rodent to human. Accounting for long-term clearance or retention is a large source of uncertainty in these analyses.

The estimation of the cancer-based OEL is made by first applying the DAF, as discussed for the short-term to sub-chronic inhalation studies (i.e., assuming equivalent effects for equivalent daily deposited mass dose of particles per unit surface area in the lungs of humans and rodents). The cancer-based PoD associated with the BMR of 10% excess risk of lung neoplasia in rodents is extrapolated to the lower levels of excess risk of 0.1% or 0.01% (according to the NIOSH carcinogen policy [NIOSH 2017]). Results are shown in the next section.

Page intentionally left blank

3 Categorical OEL Results

3.1 Summary of Results

In total, dose-response data for 234 materials across the various assays and endpoints were analyzed (Table 3-1), although the majority of these were in the zebrafish assay. A complete listing of materials, assays, and endpoints may be found in the Appendix (Table B-1).

Table 3-1: Number of materials analyzed by Assay.

Assay	Number of Materials
Acute inflammation	102
In vitro inflammation and cytotoxicity*	8
Zebrafish mortality†	169
NTP lung inflammation, fibrosis, and lung cell neoplasia	28

*Appendix C
†Appendix D

In each assay analysis, the final subset of data from which conclusions were drawn was typically much smaller than the initial dataset. The reduction in size was due to BMD modeling requirements (number of dose groups, sufficient data, presence of a statistically significant trend, and identification of an adequately fitting dose-response model) and experimental design restrictions (specific route of exposure, specific post-exposure durations).

3.2 Acute Inflammation

The most important factors predicting lung response as PMN proportion in BALF were post-exposure duration (reflecting differences in recovery after exposure ended), the deposited dose (normalized as µg/g lung) (reflecting the dose-response relationship), the material form (e.g., shape), material (e.g., TiO_2), and exposure duration (also reflecting the dose-response relationship) (Figure 3-0). Additional factors that were less important in predicting PMN response included animal strain, gender, and species, and exposure route. These findings suggest that the deposited dose metric is compensating for experimental design differences (e.g., species/strain/sex and route of exposure) by normalizing the administered dose as the total particle mass dose per gram of wet lung tissue.

Figure 3-0: Importance of predictors of a random forest regression analysis of data on PMN proportions from NIOSH/ENPRA/CIIT data.

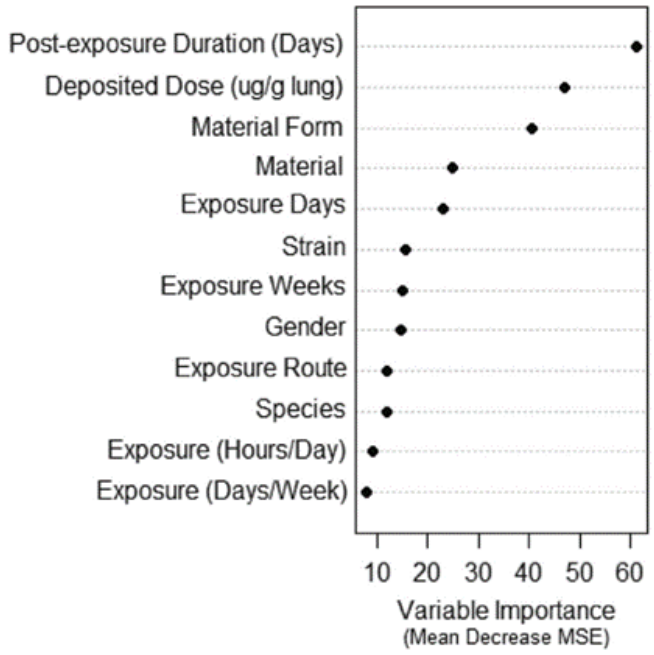

From the initial 1,899 unique rodents, 844 distinct rodents with a measured response were analyzed across 32 dose-response relationships (a combination of material form and post-exposure duration within each study) from the 22 studies with post-exposure durations between 0 and 3 days:

- 1,929 observations for 1,899 unique animals
- 1,557 unique animals with a measured PMN response
- 844 unique animals, each with one measured PMN response 0–3 days post-exposure

The results of hierarchical clustering of the point estimates of the BMDs to create four separate groups of materials with similar potencies are shown in Figure 3-1; each segment begins at its BMDL and ends at its BMD point estimate. A majority of materials belonged to the first and most potent group. The microscale TiO_2 was the sole member of the fourth and least potent group. Of the 32 relationships, 18 were found to have a statistically significant difference in mean response across the dose groups, and SK was able to estimate a BMD and BMDL

for each of those 18 relationships. The BMD potency estimates for the 18 materials ranged from 2.1 µg/g lung to 2,500 µg/g lung for 10% Fe ZnO to Fine TiO_2, respectively, and the corresponding BMDLs ranged from 0.22 µg/g lung to 2,400 µg/g lung (Figure 3-1). The 14 relationships that were not estimable (e.g., no statistically significant difference in mean response) included the TiO_2 nanospheres [Porter et al. 2013], all nano-scale silver [Roberts et al. 2013; ENPRA 2013], and various forms of MWCNT, TiO_2, and ZnO (ENPRA 2013). For the absolute 10% PMN response, BMDs were not estimable in an additional six cases, because extrapolation would be required due to either a high background response or a low response at the highest dose.

Figure 3-1: Visualization of hierarchical clusters of benchmark dose estimates into four potency groups using complete linkage for PMN data from NIOSH/ENPRA/CIIT observed within 3 days after exposure. *

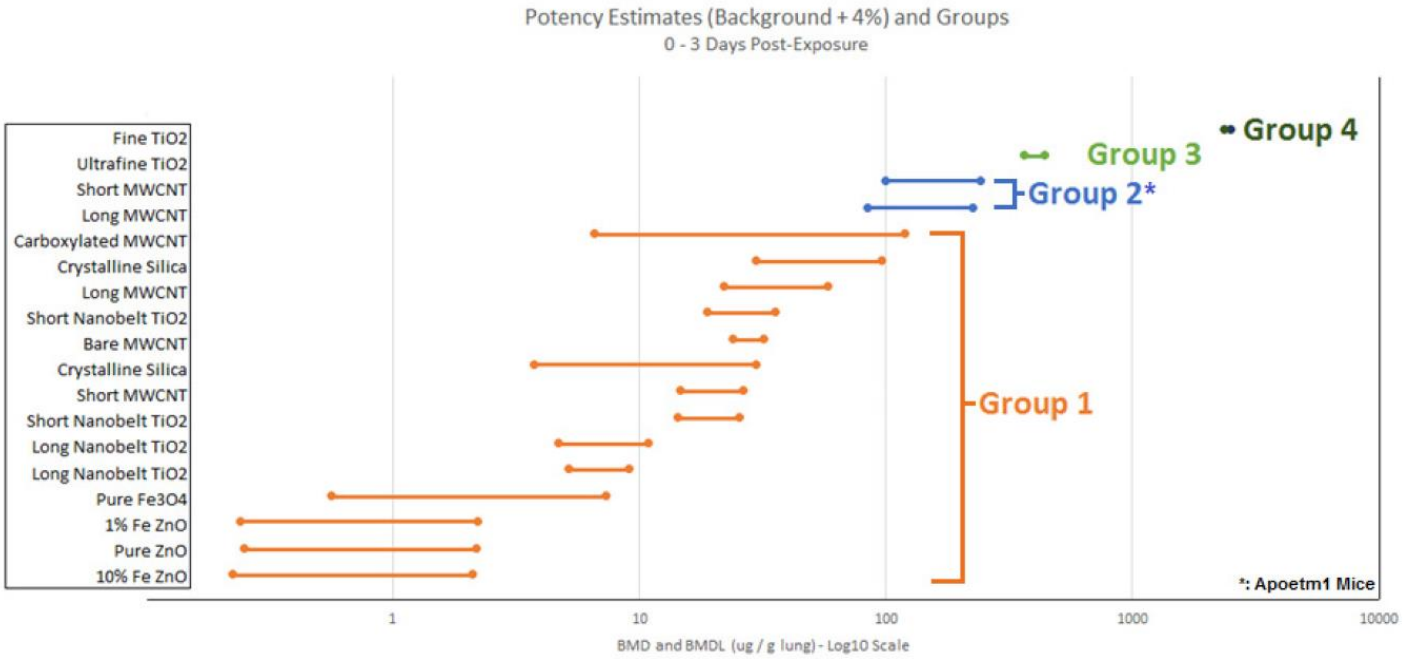

* Each segment begins at the BMDL estimate and ends at the BMD estimate for the corresponding material.

Table 3-2 provides additional information on the potency estimates within each group, including the minimum, median, and maximum BMD values; uncertainty from sampling variations of the BMD estimates are summarized by the minimum and the 5th percentile BMDL estimates within each group (Table 3-2). Based on the BMD estimates, the potency estimates of materials within the first group vary by a factor of about 60; the BMD estimates of the Group 2 materials are about nine times less potent than those in Group 1; the Group 3 material estimate is roughly half as potent as the estimates in Group 2; and the Group 4 material estimate is about six times less potent than that of Group 3 (Table 3-2). The study with ApoE mice exposed to MWCNT appeared in potency Group 2 for inflammation. Micro-size TiO_2 was the only material that grouped into Group 4, and

ultrafine (nanoscale) TiO_2 was the single material in Group 3 in this relatively small database of 18 materials. Most of the ENMs were in the most potent group, Group 1.

Most of the studies shown in Figure 3-1 were the IT route of exposure (Table 2-1). In those studies, the bolus dose of particles could elicit a greater response than would occur for an equivalent mass dose delivered by pharyngeal aspiration or inhalation. Thus, it could be difficult to discern if the %PMN response in an IT study at day 0 or 1 was due to the specific particle or to a general particle effect. This could lead to overestimation of the acute toxicity of those materials and contribute to the large number of particles in group 1.

Table 3-2: Summary of materials and benchmark dose estimates derived from stochastic kriging (SK) modeling of data on PMN proportion of by potency group in NIOSH/CIIT/ENPRA Data.

Group	BMDs Min/Median/Max	BMDLs Min/5th Percentile	Material Types	
1	2.1 / 25.8 / 119.2	0.22 / 0.23	Fe_3O_4 MWCNT Silica TiO_2 ZnO	Pure Bare, Carboxylated, Long, Short Crystalline (2)† Long Nanobelt (2), Short Nanobelt (2) Pure, 1% Fe_3O_4, 10% Fe_3O_4
2*	225.9 / 233.5 / 241.1	83.9 / 84.7	MWCNT	Long, Short
3	440.3	365.3	TiO_2	Ultrafine
4	2489.6	2366.1	TiO_2	Fine†

*C57BL/6-Apoetm1 mice
†Micro-sized materials

Within one material type, TiO_2 potency depended on particle size and shape (Figure 3-1). Among the spherical TiO_2 materials, the microscale (fine) TiO_2 was the least potent in eliciting pulmonary inflammation (Group 4), and nanoscale (ultrafine) TiO_2 was about six times more potent (Group 3). TiO_2 nanobelts were in the most potent group (Group 1) although the short nanobelts were less potent than the long nanobelts. Three types of ZnO were the most potent materials within Group 1 (Figure 3-1). The various types of MWCNTs had varied potencies within Groups 1 and 2. Carboxylated or bare MWCNTs in C57BL/6J mice were in Group 1. The potency of short and long MWCNTs seemed to depend more on the mouse strain than on the shape; that is, the C57BL/6-Apoetm1 mice appeared less sensitive to either short or long MWCNTs (Group 2) than were the C57BL/6N mice for the same MWCNT types (Group 1). However, the Group 2 BMDs for the C57BL/6-Apoetm1 mice were

based on response data measured for controls and one exposed group. As a result, the BMD estimates for the C57BL/6-Apoetm1 mice were based on a linear model assumption.

In C57BL/6N mice, for which more exposure group data were available, nonlinear dose-response relationships were observed, and the steepest part of the nonlinear curve reached the BMR at an earlier dose than that of the linear model. If the dose-responses based on the C57BL/6-Apoetm1 mice behave similarly (i.e., nonlinear, concave) then a bias may be present in those Group 2 BMDs toward underestimating their potency (suggesting these could be in Group 1). On the other hand, if the true dose-response relationship were convex, then the potential bias would be toward overestimating the potency. Microscale crystalline silica (Min-U-Sil®) was in the highest potency group (Group 1).

3.2.1 Predicting Potency

In this framework, a new material is predicted to belong to one of the four groups. In order to derive a potency estimate for that new material, a BMDL from the other materials within that group is used as an estimate for the effect level of the new material. One option is to use the minimum BMDL, but this may be affected by an unusually potent material within a given group, or a material with a high degree of variability in the experimental data; so an alternative is to use the 5th percentile of BMDLs within a given potency group. A table of the individual potency estimates is provided in the Appendix (Table A-1).

A classification random forest model was trained by using the potency group labels and physicochemical properties of these 18 materials. Seventeen physicochemical properties were used during the development of the classification random forest model. In general, these properties are intended to independently describe a given material. The variable material category identifies the material as a metal, metal oxide, or carbonaceous material; the variable scale identifies whether a material is nanoscale or not. Metrics related to particle size—such as density, surface area, and diameter—appeared to be most predictive of the potency group, whereas properties such as presence of impurities or modification types were less predictive (Figure 3-2). These estimates of variable importance should be interpreted with caution because of the small number of materials used to build the model, as well as the paucity of information contained within the 17 physicochemical properties. If more information were available, or if other properties were considered, these estimates of importance would likely change. The material (i.e., TiO_2, MWCNT, ZnO, Silica, Fe_3O_4) is a somewhat important variable. If a new material is a type that was not present in the training data, then this covariate could not be used. Thus, a training dataset should cover as many materials as possible for a reliable and predictive model.

Figure 3-2: Importance of physicochemical properties as predictors of potency group based on a classification random forest analysis of the PMN data in NIOSH/CIIT/ENPRA data.

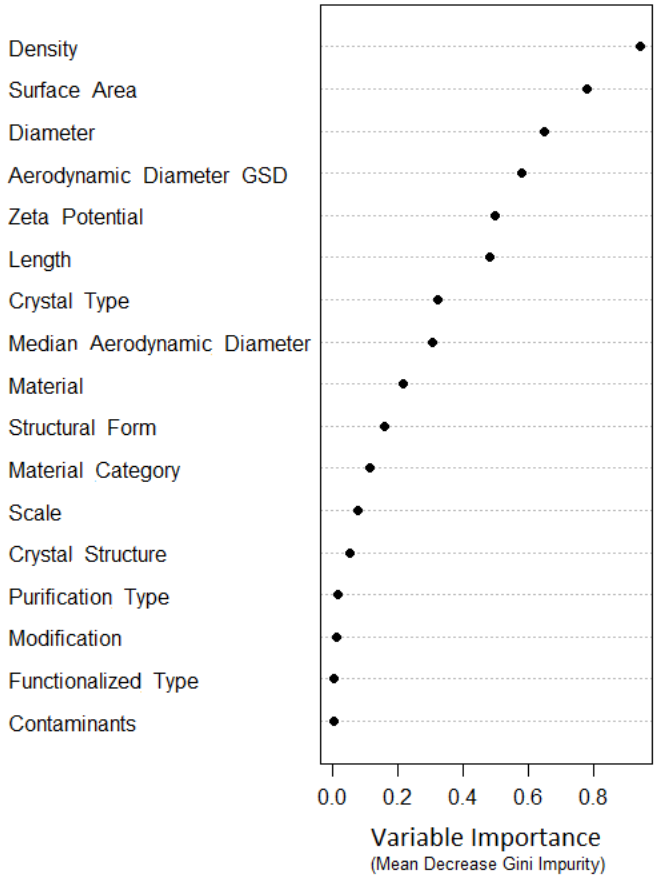

The fitted random forest model was used to classify the NanoGo data (Table A-6). Each of the NanoGo materials was predicted to belong to Group 1, the most potent cluster, by the random forest model on the basis of their physicochemical properties (Table 3-3). Chen et al. [2004] have investigated the behavior of random forests when groups are unbalanced, particularly that the largest class tends to receive the most votes, and they provide alternatives to improve the predictive accuracy for the minority classes. However, these methods were not implemented here, because the minority class is represented by materials with low hazard, and in the case of a misclassification it would be preferable to predict a material as being more hazardous (i.e., belonging to the majority class) than it actually is. With use of SK, a typical potency estimate was found for each of the NanoGo materials by taking the median of the potency estimates across laboratories, where there were up to six potency estimates per material. This median potency estimate was then compared to the four potency groups described in Table 3-2, and the material was assigned to the nearest potency group. The median potency estimate and nearest potency group (Actual Group) are shown in Table 3-3.

For five of the six materials, the group assignment using the dose-response information matched the predicted group assignment using only the physicochemical properties. An exception was the anatase TiO_2 nanosphere material, which was predicted to belong to a more potent cluster (Group 1) than the potency cluster identified by the dose-response information (Group 2). However, this may be explained by the anatase nanosphere material having only one potency estimate out of the six laboratories, whereas each of the other materials had at least three estimates of potency, and those estimates tended to vary widely. A summary of the NanoGo potency estimates can be found in the Appendix (Table A-4).

Misclassification of a new material as belonging to a lower potency group could result in unsafe exposures. The current method appears to be health protective in that it predicted either the correct or higher potency group for a small set of new ENMs (NanoGo data) that were not used in developing the model (Table 3-3). However, more comprehensive data are needed for further evaluation and validation of the model.

Table 3-3: Summary and Evaluation of Random Forest Potency Group Predictions based on Physicochemical Properties and the median of BMD estimates from stochastic kriging (SK) of the NanoGo database.

Material	Distribution of Group Votes in the Forest				Predicted Potency Group	Median BMD	Assigned Potency Group
	1	2	3	4			
Anatase Nanospheres	409 (82%)	70 (14%)	10 (2%)	11 (2%)	1	204.7	2
Anatase Nanobelt	436 (87%)	44 (9%)	2 (0%)	18 (4%)	1	51.5	1
Anatase/Rutile Nanospheres	421 (84%)	56 (11%)	12 (2%)	11 (2%)	1	37.2	1
Original MWCNT	387 (77%)	102 (20%)	0 (0%)	11 (2%)	1	27.6	1
Purified MWCNT	328 (66%)	162 (32%)	0 (0%)	10 (2%)	1	62.3	1
Functionalized MWCNT	413 (83%)	74 (15%)	2 (0%)	11 (2%)	1	52.6	1

3.2.2 Updated Database Results

Table 3-4: Distribution of Materials across Clusters by Linkage Method for acute rodent pulmonary inflammation data from NIOSH/CIIT/ENPRA/NanoGo and Swiss-VCI/NIOSHTIC/ATL

Linkage Method	# Materials in Cluster 1	# Materials in Cluster 2	# Materials in Cluster 3	# Materials in Cluster 4
Complete	104 (90%)	5 (4%)	4 (3%)	2 (2%)
Ward's Method	80 (70%)	24 (21%)	9 (8%)	2 (2%)

Similar to results in Drew et al. [2017], the complete linkage method puts a large majority of materials into the most potent cluster, Cluster 1 (Table 3-4). Ward's method does move toward more evenly distributed clusters; however, a majority of materials still are placed into Cluster 1. In both cases, the least potent Cluster 4 contains the same two materials: Fine TiO_2 and C60. Cluster 3 is made up entirely of various forms of TiO_2 in both linkages, with Ward's method capturing an additional five TiO_2 materials from the Cluster 2 of complete linkage. Clusters identified by Ward's method appear to better account for the variability of the BMDs, particularly in comparing clusters 2 and 3 using complete linkage (Figure 3-3) to Cluster 3 using Ward's method (Figure 3-4), as the intervals (from the BMDL to BMD) within each cluster overlap much less than the complete linkage clusters.

Figure 3-3: Visualization of Benchmark Dose Estimates for acute rodent pulmonary inflammation data from NIOSH/ENPRA/CIIT/NanoGo and Swiss-VCI/NIOSHTIC/ATL with Hierarchical Clustering based on Complete Linkage into Four Potency Groups.

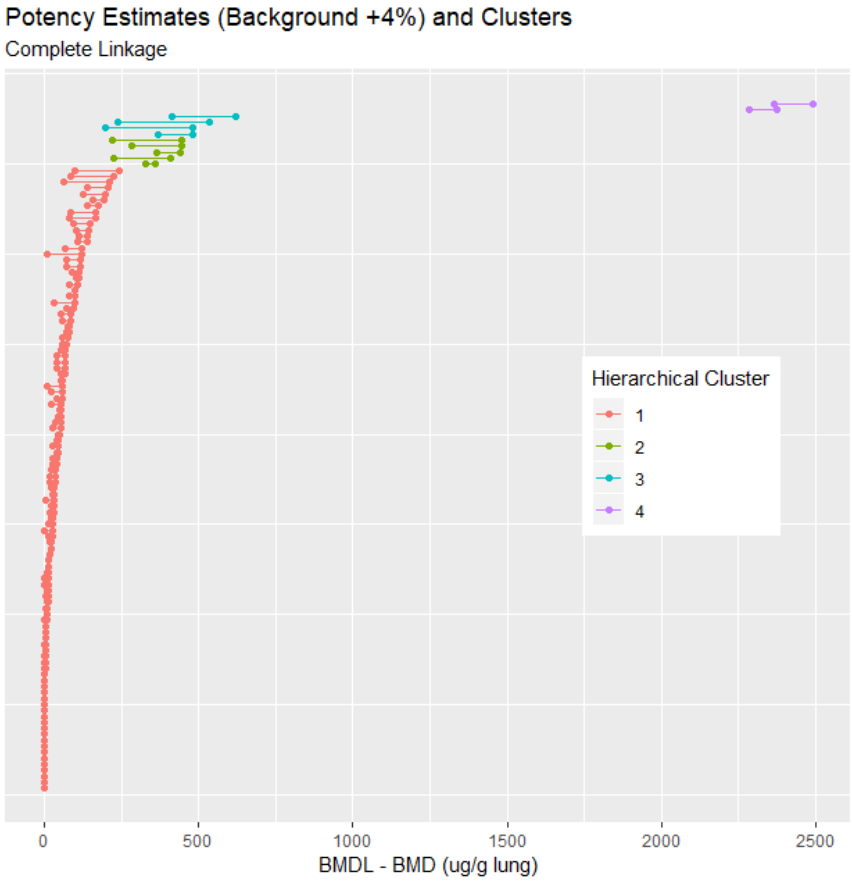

Figure 3-4: Visualization of Benchmark Dose Estimates for acute rodent pulmonary inflammation data from NIOSH/ENPRA/CIIT/NanoGo and Swiss-VCI/NIOSHTIC/ATL with Hierarchical Clustering based on Ward's Method Linkage into Four Potency Groups

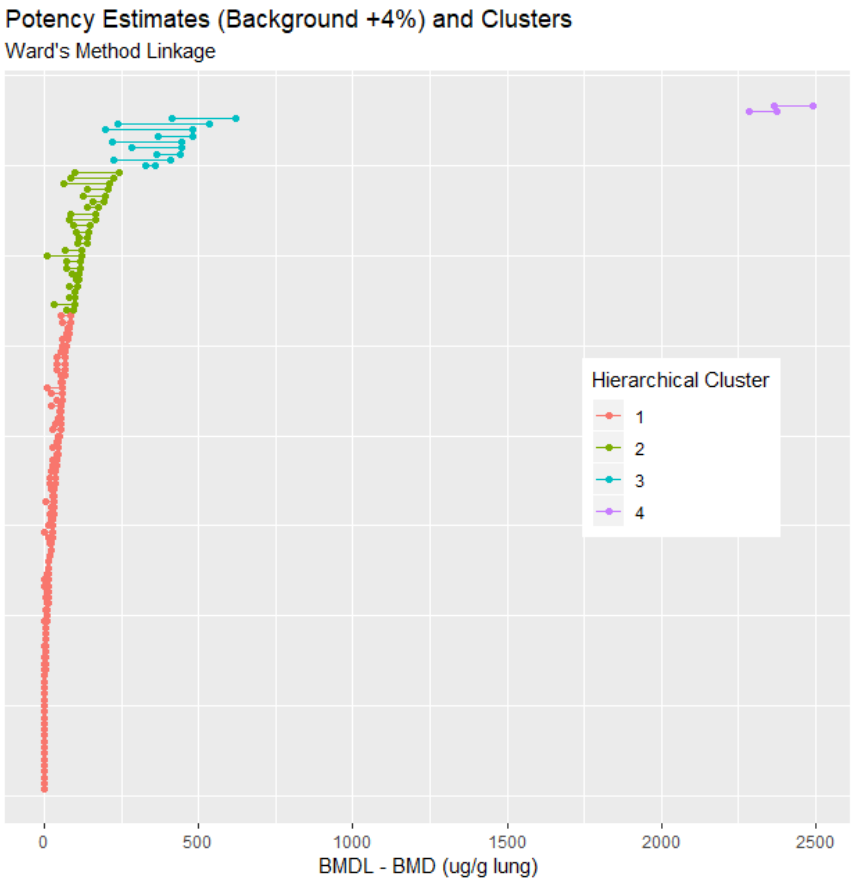

The make-up of clusters 1 and 2 is more difficult to tease out. Many materials were present in the analysis with very few forms; most of the analyzed materials were TiO_2, MWCNT, and ZnO (Table 3-5). For both methods, all 18 ZnO materials were placed into Cluster 1, which agrees with the findings in Drew et al. [2017] that for pulmonary inflammation, ZnO was quite potent. For the most prevalent material, TiO_2 forms were spread across the four clusters, again agreeing with findings from Drew et al. [2017], where it appears that other factors such as size (nano or microscale) and form (particle, belt) contribute to the variability in potency estimates. Most MWCNT/CNT materials were placed in Cluster 1 (all in the case of complete linkage), with some being placed in Cluster 2. In both methods, all eight CeO_2 materials were placed into Cluster 1, which may be related to the

reason ZnO is always classified into Cluster 1. However, it is not as simple as being a metal oxide, as illustrated by the variability of TiO_2 (Table 3-5).

Table 3-5: Frequency of Material Type by Cluster across Linkage Methods for acute rodent pulmonary inflammation data from NIOSH/ENPRA/CIIT/NanoGo and Swiss-VCI/NIOSHTIC/ATL

		Complete Linkage				Ward's Method			
Material	**Frequency**	**1**	**2**	**3**	**4**	**1**	**2**	**3**	**4**
Aluminum	1	1	0	0	0	1	0	0	0
Brass	1	1	0	0	0	1	0	0	0
Carbon	5	4	0	0	1	3	1	0	1
CeO_2	8	8	0	0	0	8	0	0	0
CNF	2	2	0	0	0	2	0	0	0
CNT	12	12	0	0	0	9	3	0	0
MWCNT	32	32	0	0	0	23	9	0	0
SWCNT	1	1	0	0	0	1	0	0	0
Fe_3O_4	1	1	0	0	0	1	0	0	0
Graphene	6	6	0	0	0	4	2	0	0
In_2O_3	1	1	0	0	0	0	1	0	0
M5 (organic polymer)	1	1	0	0	0	1	0	0	0
Silica	6	6	0	0	0	3	3	0	0
Amorphous	1	1	0	0	0	2	3	0	0
Crystalline	5	5	0	0	0	1	0	0	0
TiO_2	32	22	5	4	1	14	8	9	1
ZnO	18	18	0	0	0	18	0	0	0

Table 3-6: Summary of BMDs and BMDLs by Hierarchical Cluster and Linkage Method for acute rodent pulmonary inflammation data from NIOSH/ENPRA/CIIT/NanoGo and Swiss-VCI/NIOSHTIC/ATL

Complete Linkage		
Cluster	BMDs (μg/g lung)	BMDLs (μg/g lung)
	Min/Median/Max	Min/5th Percentile
1	0.003 / 34.4 / 241.1	0.00002 / 0.004
2	361.1 / 440.3 / 443.6	221.5 / 222.3
3	479.2 / 506.1 / 620.7	197.9 / 203.6
4	2375.8 / 2432.7 / 2489.6	2284.8 / 2288.8

Ward's Method		
Cluster	BMDs (μg/g lung)	BMDLs (μg/g lung)
	Min/Median/Max	Min/5th Percentile
1	0.003 / 20 / 84.9	0.00002 / 0.003
2	93.1 / 140.3 / 241.1	6.5 / 34.6
3	361.1 / 443.6 / 620.7	197.9 / 207.3
4	2375.8 / 2432.7 / 2489.6	2284.8 / 2288.8

In order to learn about the relationships between the physicochemical properties and the cluster assignments, statistical summaries were created of material, material category, scale, structural form, surface area, and diameter across the Ward's method clusters (Tables 3-7 to 3-10), as these are the six most complete physicochemical properties (Figure 3-5). Table 3-5 summarizes the materials and material categories (carbon, metal, metal oxide, or other). Additional physicochemical summaries are available in the Appendix (Tables A-10 through A-14).

Table 3-7: Summary of scale across clusters assigned using hierarchical clustering with Ward's method for acute rodent pulmonary inflammation data from NIOSH/ENPRA/CIIT/NanoGo and Swiss-VCI/NIOSHTIC/ATL

Cluster	Scale	N
1	Micro	1
1	Nano	78
1	Sub-micron	1
2	Micro	2
2	Micron	1
2	Nano	19
2	Sub-micron	2
3	Micron	4
3	Nano	3
3	Sub-micron	2
4	Micro	1
4	Nano	1

Table 3-8: Summary of structural forms across clusters assigned using hierarchical clustering with Ward's method for acute rodent pulmonary inflammation data from NIOSH/ENPRA/CIIT/NanoGo and Swiss-VCI/NIOSHTIC/ATL

	Cluster			
	1 (Most hazard)	**2**	**3**	**4 (Least hazard)**
Flake	2	0	0	0
Hexagonal	8	0	0	0
Irregular	1	0	0	0
Microparticle	0	1	0	0
NA (Missing)	11	0	0	1
Nanobelt	7	3	0	0
Nanofiber	2	0	0	0
Nanoparticles	2	0	0	0
Nanoplates	3	2	0	0
Nanorod	2	0	0	0
Nanotube	24	9	0	0
Particle	12	6	8	1
Spherical Particle	6	3	0	0
Ultrafine Particle	0	0	1	0
Total	80	24	9	2

As seen previously, most materials and therefore most structural forms were assigned to Cluster 1, so insights may be found by looking for structural forms not in Cluster 1. For example, materials labeled as ultrafine particles or microparticles were assigned to lower hazard groups (clusters 3 and 2, respectively). Materials that are nanobelt, nanotube, rod, nanofiber, or tube were assigned to the higher hazard groups, with most being assigned to Cluster 1.

Table 3-9: Summary of surface areas across clusters assigned using hierarchical clustering with Ward's method for acute rodent pulmonary inflammation data from NIOSH/ENPRA/CIIT/NanoGo and Swiss-VCI/NIOSHTIC/ATL

		Cluster			
		1 (Most hazard)	**2**	**3**	**4 (Least hazard)**
Surface Area (m^2/g)	*Minimum*	2	4.57	5.8	6
	First Quartile	13.38	18	9	6
	Median	53	39.5	26.95	6
	Mean	123.80	137.76	27.91	6

	Third Quartile	180	170.3	48.2	6
	Maximum	513	747.1	50	6
	n	80	24	9	2
	n missing	12	4	1	1

There is an association between surface area and the assigned hazard cluster, where larger surface area measures tend to be assigned to the more hazardous clusters, as seen when comparing the median, mean, and maximum surface areas across clusters.

Table 3-10: Summary of diameters across clusters assigned using hierarchical clustering with Ward's method for acute rodent pulmonary inflammation data from NIOSH/ENPRA/CIIT/NanoGo and Swiss-VCI/NIOSHTIC/ATL

		Cluster			
		1 (Most hazard)	**2**	**3**	**4 (Least hazard)**
Diameter (nm)	*Minimum*	5.56	1.96	21	68.4
	First Quartile	25	25	49.5	126.3
	Median	26	30	78	184.2
	Mean	632.93	537.31	78	184.2
	Third Quartile	200	300	106.5	242.1
	Maximum	5000	2700	135	300
	n	80	24	9	2
	n missing	12	2	7	0

There are order-of-magnitude differences in diameter across materials within clusters 1 and 2 (minimum to maximum diameter), as well as across all clusters (comparing maximum diameters). There may be a weak association where smaller diameters are assigned to more hazardous clusters (comparing median diameters across clusters), and this may be associated with surface area.

Although these univariate summaries are useful for learning how the physicochemical properties vary across hierarchical clusters, these should not be used one at a time to classify a new material into a cluster while using a read-across type method. Foremost, these physicochemical properties are not always completely available, so any summary of association may change if fewer materials were missing the given property. Cluster assignment must be done at this time by the random forest model, as it accounts for the relationships between all physicochemical properties concurrently, not one at a time. Additionally, the models should be considered exploratory at this time. The model predictions may change if the underlying data are changed, specifically toward a more representative set of materials.

3.3 Predictive Accuracy of Random Forests

To build and evaluate the predictive model, the 115 materials from NIOSH, CIIT, and ENPRA and the updates from ATL, NIOSHTIC, and Nano-AOP were randomly split into a training dataset (74 materials) and a test dataset (41 materials); approximately two-thirds of materials were used for training and the remaining third used for testing the model. Other test and train procedures (e.g., leave one out) could be used and evaluated by cross-validation, but this is an area of future research. Each random forest model was trained on the same 74 materials and tested on the same 41 materials.

Twenty-one physicochemical properties were used as factors for predicting a test material's potency cluster. Initially 25 properties were available, but because of low levels of completeness or interpretability concerns, four were omitted from use in models (Figure 3-5). Descriptions of the variables are in Table A-9.

Figure 3-5. Availability of physicochemical properties across materials for acute rodent pulmonary inflammation data from NIOSH/ENPRA/CIIT/NanoGo and Swiss-VCI/NIOSHTIC/ATL

Physicochemical Property	% Completeness			
Surface Reactivity*	0%			
Surface Modifications*	1%			
Surface Charge*	2%			
Median Aerodynamic Diameter	3%			
Aerodynamic Diameter GSD*	3%			
Modification	15%			
Purification Type	15%			
Impurity Type	15%			
Impurity Amount	15%			
Agglomeration Indicator	16%			
Functionalized Type	16%			
Solubility	21%			
Primary Particle Size (nm)	23%			
Density	24%			
Zeta Potential	30%			
Crystal Type†	32%		If applicable, % complete: 54%	Not applicable: 41%
Length‡	35%		If applicable, % complete: 74%	Not applicable: 53%
Crystal Structure†	37%	See "Crystal Type"		
Impurity Indicator	37%			
Diameter	82%			
Surface Area	84%			
Structural Form	90%			
Scale	100%			
Material	100%			
Material Category	100%			

*: Not included in models

†: Not applicable to materials where Material Category is Carbon (n=47)

‡: Not applicable to materials where Structural Form is not Nanotube, Nanorod, Nanofiber, Nanobelt, Nanoplate, or Flake (n=61)

3.3.1 Complete Linkage

Since 90% of materials were placed into Cluster 1, it is expected that the random forest model will be more likely to classify a test material as belonging to Cluster 1.

Forty-one materials were used to test the model, with 37 being correctly classified (i.e., the predicted cluster using only physicochemical properties matches the cluster assigned from hierarchical clustering with complete linkage). The classifications of the remaining four materials disagreed with the assigned clusters, with all four predicted to belong to cluster 1 when the observed BMDs are assigned to Cluster 2 (for two materials), Cluster 3 (for one material), and Cluster 4 (for one material). Thus, the random forest model predictions and the observed BMDs agreed 90% of the time; however, nearly all of these were from predicting a material as belonging to Cluster 1—which is expected 90% of the time. There were no disagreements wherein the random forest–predicted cluster was less potent than the assigned cluster. It must be noted that cluster assignments were based only on the BMD estimate; thus, the assigned cluster can also be viewed as an estimate. Therefore, with additional dose-response data, the BMD (and hence the cluster) estimate could change, leading to differences in model assessment.

Figure 3-6: Classification Matrix of the 41 Test Materials for Predictive Agreement of the Random Forest and clusters created by complete linkage of observed BMDs for acute rodent pulmonary inflammation data from NIOSH/ENPRA/CIIT/NanoGo and Swiss-VCI/NIOSHTIC/ATL

		Predicted Potency Cluster			
		1	2	3	4
Assigned Potency Cluster	1	36	0	0	0
	2	2	0	0	0
	3	1	0	1	0
	4	1	0	0	0

Various metrics can be used to assess the predictive performance of the classification random forest, such as these:

- Accuracy: Total number of predictions where the predicted cluster matches the assigned cluster divided by the total number of predictions, or equivalently the sum of the diagonal of the classification matrix divided by the grand total
- Recall for Cluster X ($Recall_X$): Number of materials correctly predicted as belonging to Cluster X divided by the total number of materials that were assigned to Cluster X, or equivalently the cell at (X,X) divided by the total of row X

- Precision for Cluster X ($Precision_X$): Number of materials that were assigned to Cluster X divided by the total number of materials predicted to belong to Cluster X, or equivalently the cell at (X,X) divided by the total of column X

As an example, referring to Figure 3-6, the accuracy is equal to $\frac{36+0+1+0}{41} = 90.2\%$. $Recall_1$ is equal to $\frac{36}{36+0+0+0} = 100\%$. $Precision_1$ is equal to $\frac{36}{36+2+1+1} = 90\%$.

For minority classes like Cluster 4, it is possible to have a recall or precision that is undefined (i.e., division by zero) in which case the metric is set as Not Available (N/A).

Table 3-11: Performance Metrics for the Classification Random Forest Model and Complete Linkage for acute rodent pulmonary inflammation data from NIOSH/ENPRA/CIIT/NanoGo and Swiss-VCI/NIOSHTIC/ATL

Accuracy	90.2%
$Recall_1$	100.0%
$Recall_2$	0.0%
$Recall_3$	50.0%
$Recall_4$	0.0%
$Precision_1$	90.0%
$Precision_2$	N/A
$Precision_3$	100.0%
$Precision_4$	N/A

Thus, the random forest model (complete linkage) classified 9.8% of materials (4/41) into groups that disagreed with the observed BMDs, with all four being false positives (predicted to belong to a more potent class than the class of the observed BMD). For this model, primary particle characteristics were the most important for classification (Table 3-12). These factors were also among those less likely to be missing for most materials. Crystal type was primarily available for TiO_2 materials, which were the most common material type in this dataset. Some properties, such as diameter and primary particle size, are correlated but provide different information. The presence of correlated predictors is not of high concern when using a random forest model, as described in Section 2.1; each tree in the forest (500 trees by default) uses a random subset of physicochemical properties, so correlated variables do not always appear in the same tree.

As described in Table A-9, diameter is an as-reported value derived from various types of measurements in the literature-derived data [Boots et al. submitted]. Primary particle size was recorded only if it was specifically

reported in the journal article or dataset. Other data systematically collected from the literature for particulate materials include chemical composition, size, shape, specific surface area, solubility, crystallinity, density, and other properties [Boots et al. submitted]. These physicochemical properties are among those considered to be important in describing the toxicity of ENMs [OECD 2014a, Rasmussen et al. 2018].

Table 3-12: Random Forest Variable Importance – Complete Linkage for acute rodent pulmonary inflammation data from NIOSH/ENPRA/CIIT/NanoGo and Swiss-VCI/NIOSHTIC/ATL

Physicochemical Property	Mean Decrease of Gini Impurity
Crystal Type	1.95
Scale	1.55
Primary Particle Size (nm)	1.44
Surface Area	0.91
Diameter	0.84
Structural Form	0.63
Median Aerodynamic Diameter	0.63
Material	0.59
Density	0.58
Agglomeration Indicator	0.10
Crystal Structure Indicator	0.10
Impurity Type	0.08
Impurity Indicator	0.08
Purification Type	0.06
Modification	0.06
Zeta Potential	0.05
Functionalized Type	0.05
Material Category	0.05
Length	0.03
Solubility	0.02
Impurity Amount	0.00

3.3.2 Ward's Method

This model made classifications in agreement 73% of the time and tended to classify a new material into Cluster 1. This model did misclassify two materials that were placed into Cluster 1 as belonging to Cluster 2, meaning that the potency of these two materials would be underestimated (Figure 3-7).

Figure 3-7: Classification Matrix of the 41 Test Materials for Predictive Agreement of the Random Forest and clusters created by Ward's Method Linkage of Observed BMDs for acute rodent pulmonary inflammation data from NIOSH/ENPRA/CIIT/NanoGo and Swiss-VCI/NIOSHTIC/ATL

		Predicted Potency Cluster			
		1	2	3	4
Assigned Potency Cluster	1	26	2	0	0
	2	6	2	0	0
	3	1	1	2	0
	4	1	0	0	0

Table 3-13: Performance Metrics for the Classification Random Forest Model and Ward's Method Linkage for acute rodent pulmonary inflammation data from NIOSH/ENPRA/CIIT/NanoGo and Swiss-VCI/NIOSHTIC/ATL

Accuracy	73%
$Recall_1$	93%
$Recall_2$	25%
$Recall_3$	50%
$Recall_4$	0%
$Precision_1$	76%
$Precision_2$	40%
$Precision_3$	100%
$Precision_4$	N/A

Classifications disagreed for 27% of materials (11/41) with this model, with a false positive rate of 22% (9/41) and a false negative rate of 5% (2/41) (Table 3-13).

For this model, structural form (e.g., particle, fiber) was the most important factor for classification, followed again by primary particle size properties (Table 3-14).

Table 3-14: Random Forest Variable Importance – Ward's Method Linkage for acute rodent pulmonary inflammation data from NIOSH/ENPRA/CIIT/NanoGo and Swiss-VCI/NIOSHTIC/ATL

Physicochemical Property	Mean Decrease of Gini Impurity
Structural Form	4.16
Crystal Type	3.41
Material	2.81
Surface Area	2.33
Diameter	2.25
Scale	2.13
Primary Particle Size (nm)	1.86
Functionalized Type	1.51
Density	1.00
Median Aerodynamic Diameter	0.88
Length	0.85
Zeta Potential	0.57
Modification	0.45
Impurity Indicator	0.36
Purification Type	0.32
Impurity Type	0.30
Material Category	0.30
Crystal Structure Indicator	0.25
Agglomeration Indicator	0.19
Impurity Amount	0.12
Solubility	0.09

3.3.3 Order-of-Magnitude Groupings

In contrast to the hierarchical clusters, the potency estimates can be assigned to *a priori* groupings rather than assignments based on an algorithm (Figure 3-8). The 115 materials were assigned to order-of-magnitude groups based on the BMDLs, resulting in seven groups (Table 3-15). Assignment was based on the BMDL to reflect the assignment process of occupational exposure banding.

Figure 3-8: Visualization of Benchmark Dose Estimates for acute rodent pulmonary inflammation data from NIOSH/ENPRA/CIIT/NanoGo and Swiss-VCI/NIOSHTIC/ATL with grouping based on orders of magnitude into seven Potency Groups.

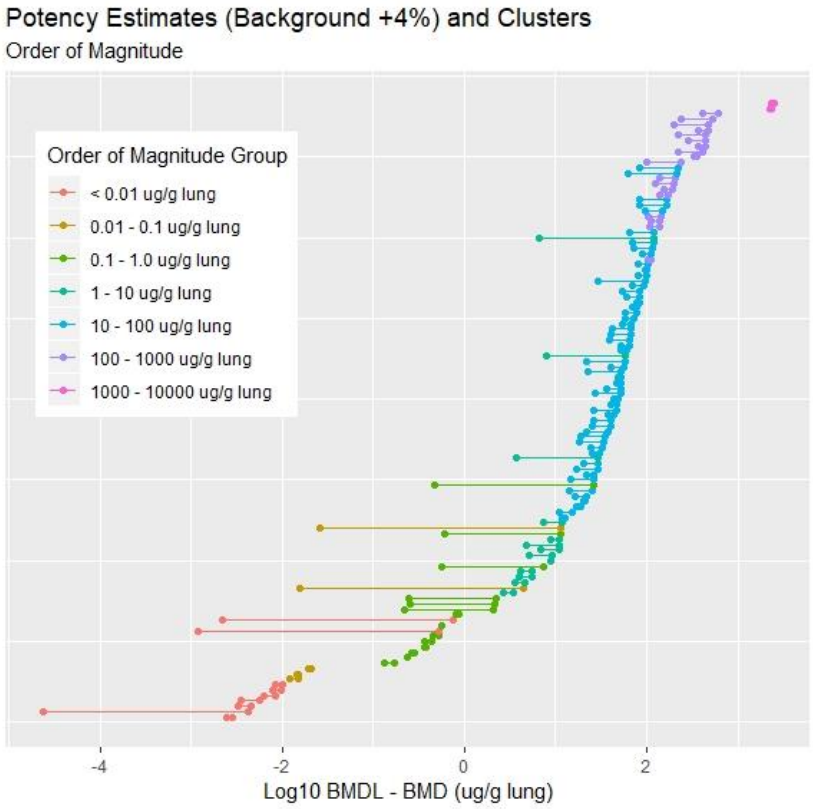

Table 3-15: Frequencies of materials by order-of-magnitude groups for acute rodent pulmonary inflammation data from NIOSH/ENPRA/CIIT/NanoGo and Swiss-VCI/NIOSHTIC/ATL.

Order-of-magnitude Group	Number of materials in the group
< 0.01 μg/g lung	6
0.01 - 0.1 μg/g lung	4
0.1 - 1.0 μg/g lung	10
1 - 10 μg/g lung	11
10 - 100 μg/g lung	53
100 - 1000 μg/g lung	29
1000 - 10000 μg/g lung	2

A plurality of materials were assigned to the 10–100 µg/g lung group, which includes nearly all of the carbon nanotube and graphene materials and also a large portion of the TiO_2 materials (Table 3-16). The plurality of TiO_2 materials were assigned to the 100–1000 µg/g lung group. A majority of the ZnO materials were assigned to the groups less than 1 µg/g lung.

Table 3-16 Frequency of Material by Order-of-magnitude Group for acute rodent pulmonary inflammation data from NIOSH/ENPRA/CIIT/NanoGo and Swiss-VCI/NIOSHTIC/ATL.

	Order-of-magnitude Group						
Material	< 0.01 µg/g lung	0.01 - 0.1 µg /g lung	0.1 - 1.0 µg /g lung	1 - 10 µg /g lung	10 - 100 µg /g lung	100 - 1000 µg /g lung	1000 - 10000 µg /g lung
Aluminum	0	0	0	1	0	0	0
Brass	0	1	0	0	0	0	0
Carbon	0	0	0	0	3	1	1
CeO_2	0	1	4	2	1	0	0
CNF	0	0	0	0	2	0	0
CNT	0	1	1	3	27	1	0
MWCNT	0	1	1	3	26	1	0
SWCNT	0	0	0	0	1	0	0
Fe_3O_4	0	0	1	0	0	0	0
Graphene	0	0	0	0	5	1	0
In_2O_3	0	0	0	0	0	1	0
M5 (organic polymer)	0	0	0	1	0	0	0
Silica	1	0	0	2	3	0	0
Amorphous	1	0	0	0	0	0	0
Crystalline	0	0	0	2	3	0	0
TiO_2	2	0	1	2	12	14	1
ZnO	6	2	7	2	1	0	0
Total	9	5	14	13	54	18	2

Following the previously described analysis workflow, a random forest model was trained on the same subset of 74 materials and evaluated with the same test set of 41 materials, where the order-of-magnitude group label was predicted with the 21 physicochemical properties. For this model, the structural form (e.g., particle, fiber) and the material (e.g., TiO2, MWCNT) were the most important for classifying the test materials into an order-of-magnitude group, followed by descriptors of size (diameter and surface area) (Figure 3-9).

Figure 3-9: Variable importance for classifying materials into order-of-magnitude groups using a random forest model for acute rodent pulmonary inflammation data from NIOSH/ENPRA/CIIT/NanoGo and Swiss-VCI/NIOSHTIC/ATL.

Physicochemical Property	Mean Decrease of Gini Impurity
Structural Form	7.95
Material	6.76
Diameter	3.65
Surface Area	3.15
Crystal Type	3.06
Primary Particle Size (nm)	2.42
Material Category	2.34
Density	2.32
Scale	1.99
Length	1.74
Functionalized Type	1.19
Zeta Potential	0.89
Crystal Structure Indicator	0.59
Median Aerodynamic Diameter	0.52
Modification	0.50
Impurity Type	0.49
Impurity Indicator	0.46
Purification Type	0.36
Impurity Amount	0.30
Solubility	0.23
Agglomeration Indicator	0.22

All seven order-of-magnitude groups were represented in the test set; however, the random forest model did not classify any of the materials into the lowest potency group (1000–10000 μg/g lung). Overall, the random forest model correctly classified test materials 59% of the time, which is better than a naïve classifier assigning all materials to the 10–100 μg/g lung band (which contained a plurality of materials) that would be expected to be accurate 46% of the time (53/115) (Table 3-17). Materials classifications disagreed 41% of the time, almost evenly split between false positives (the predicted group was more potent than the actual group for nine materials) and false negatives (the predicted group was less potent than the actual group for eight materials).

Table 3-17: Classification Matrix of the 41 Test Materials for Predictive Agreement of the Random Forest and order-of-magnitude groups of Observed BMDLs for acute rodent pulmonary inflammation data from NIOSH/ENPRA/CIIT/NanoGo and Swiss-VCI/NIOSHTIC/ATL.

		Predicted Order-of-magnitude Group						
		< 0.01 µg/g lung	**0.01 - 0.1 µg/g lung**	**0.1 - 1.0 µg/g lung**	**1 - 10 µg/g lung**	**10 - 100 µg/g lung**	**100 - 1000 µg/g lung**	**1000 - 10000 µg/g lung**
Actual Order of Magnitude Group	**< 0.01 µg/g lung**	3	1	0	0	0	0	0
	0.01 - 0.1 µg/g lung	0	0	1	0	0	1	0
	0.1 - 1.0 µg/g lung	0	0	3	0	1	0	0
	1 - 10 µg/g lung	0	0	2	0	4	0	0
	10 - 100 µg/g lung	0	0	1	1	14	0	0
	100 - 1000 µg/g lung	0	0	1	0	3	4	0
	1000 - 10000 µg/g lung	0	0	0	0	1	0	0

Table 3-18: Performance Metrics for the Classification Random Forest Model and Order-of-magnitude groups for acute rodent pulmonary inflammation data from NIOSH/ENPRA/CIIT/NanoGo and Swiss-VCI/NIOSHTIC/ATL

Accuracy	58.5%
$Recall_{<0.01\ \mu g/g\ lung}$	75.0%
$Recall_{0.01 – 0.1\ \mu g/g\ lung}$	0.0%
$Recall_{0.1 – 1.0\ \mu g/g\ lung}$	75.0%
$Recall_{1.0 – 10\ \mu g/g\ lung}$	0.0%
$Recall_{10 – 100\ \mu g/g\ lung}$	87.5%
$Recall_{100 – 1000\ \mu g/g\ lung}$	50.0%
$Recall_{1000 – 10000\ \mu g/g\ lung}$	0.0%
$Precision_{<0.01\ \mu g/g\ lung}$	100.0%
$Precision_{0.01 – 0.1\ \mu g/g\ lung}$	0.0%
$Precision_{0.1 – 1.0\ \mu g/g\ lung}$	37.5%
$Precision_{1.0 – 10\ \mu g/g\ lung}$	0.0%
$Precision_{10 – 100\ \mu g/g\ lung}$	60.9%
$Precision_{100 – 1000\ \mu g/g\ lung}$	80.0%
$Precision_{1000 – 10000\ \mu g/g\ lung}$	N/A

3.3.4 Summary of the classification model performances across the three material grouping methods

In comparing the three models, it appears that the model based on clusters formed by complete linkage performs better, but multiple factors should be evaluated when determining the better linkage method. Considering a naïve classifier that always predicts that a material would belong to Cluster 1, the most potent cluster, this classifier would be accurate 90% of time for the complete linkage set—matching the accuracy of the random forest model. The naïve classifier would be accurate 70% of the time for the Ward's method set, which is slightly lower than the 73% accuracy of the random forest model. Lastly, the naïve classifier would be accurate 46% of the time for the order-of-magnitude groupings, which is lower than the 59% accuracy of the random forest model. Thus, the order-of-magnitude classifier performs the best in comparison to the naïve classifier and has the benefit of not assigning most materials to the most potent group.

Because both linkage methods place most materials into Cluster 1, it is expected that the performance metrics for Cluster 1 will be high and similar between the two hierarchical cluster classifiers; model one (classifying into clusters assigned by hierarchical clustering with complete linkage) has higher precision and recall but also has 24

more materials in Cluster 1. For Cluster 2, the second model (classifying into clusters assigned by hierarchical clustering using Ward's method) has higher recall and precision; both models perform equally for clusters 3 and 4. The second model did have a non-zero false negative rate, meaning that in a practical application a categorical OEL could be set too high and not be as protective as needed. Hence, the two linkage methods lead to models that perform similarly by common performance metrics.

For this classification task, it may be desired to minimize the false negative rate, which would prevent a material from being misclassified into a lower potency group. In that case, the first model had the lowest false negative rate. The various performance metrics, and hence their comparisons, must be interpreted cautiously, as uncertainty is present: the various grouping methods used a single value (BMD or BMDL); one iteration of test/train was conducted and may not be representative because of sampling variability. From a practical standpoint, complete linkage is appealing because it may be protective to classify a new material into the most potent cluster until sufficient data are provided to justify a less potent cluster, but this may not be economically viable. Constructing clusters by Ward's method is appealing because it can lead to more evenly sized clusters, thereby providing more opportunities to detect differences in physicochemical properties that explain the cluster compositions. The order-of-magnitude groupings are advantageous in that there is a straightforward interpretation of potency, unlike the hierarchical clusters—a potency group of "1–10 μg/g lung" is clearer than "Cluster 2", for example.

There are additional opportunities for tuning these random forest models. Default settings were used for the number of trees in the forest (500) and the number of physicochemical properties considered at each node in tree construction ($\sqrt{p} = \sqrt{21} = 4$), and adding more trees or increasing the number of considered properties may improve performance. Iterative variable selection or variable selection by other algorithms could also be implemented by successively dropping the physicochemical property with the lowest importance until performance is negatively impacted (Fox et al. 2017; Degenhardt et al. 2019).

3.3.5 Choice of the number of clusters to be assigned by hierarchical clustering

In these analyses, four hierarchical clusters were used to reflect the existing qualitative classification of materials into the four mode of action groups. To further evaluate whether four clusters may be sufficient for grouping the materials, an exploratory k-means analysis was conducted. The 115 acute rodent pulmonary inflammation potency estimates (BMDs) were assigned into varying numbers of clusters (k) from 1 to 10. For each iteration, the total within cluster sum of squares (WSS) was measured, which is a measure of cluster compactness, and this is used to find where the WSS is minimized. The WSS rapidly declines and levels off around four clusters, with

minimal improvement to WSS for larger numbers of clusters (Figure 3-10). An analysis of similar data [Boots et al., submitted] also found that using four clusters adequately separated the materials into similar groups.

Figure 3-10: Total within cluster sum of squares for clusters derived using k-means with 1 to 10 clusters for acute rodent pulmonary inflammation data from NIOSH/ENPRA/CIIT/NanoGo and Swiss-VCI/NIOSHTIC/ATL.

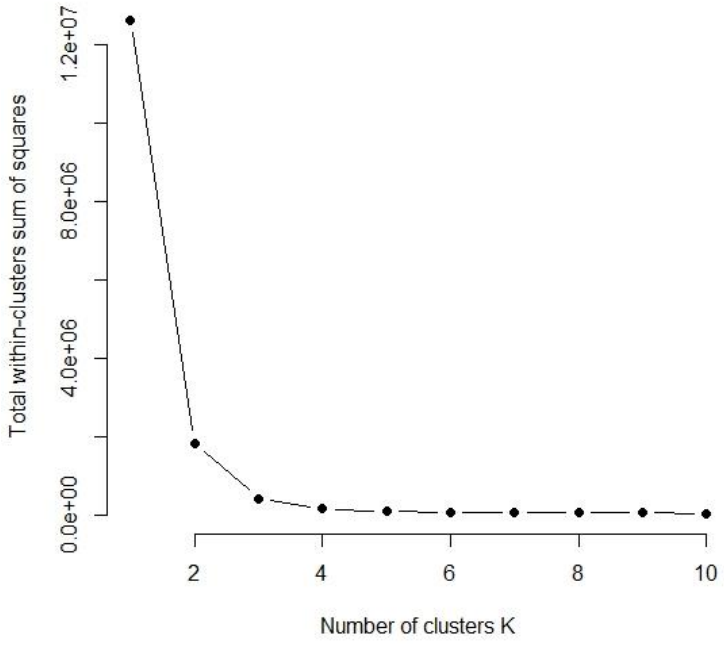

3.4 In Vitro Inflammation

During the exploratory data analysis stage, plots of the dose-response associations for the NanoGo *in vitro* THP-1 cell line showed a decreasing trend for ZnO and increasing trends for the other materials (TiO_2 nanobelts, MWCNT original & purified & functionalized, silica). An increasing trend was expected, so the ZnO finding required further investigation. The trends in the cytotoxicity response were examined because if the material is very toxic, the cells will be killed, thereby causing a decrease in the IL-1 beta cytokine response.

The scatterplot below combines all dose-cytotoxicity data for ZnO from the seven NanoGo laboratories, and the potency of ZnO is readily visible (Figure 3-11).

Figure 3-11: Dose-Cytotoxicity Response of Zinc Oxide for all NanoGo Labs in the THP-1 cell line.

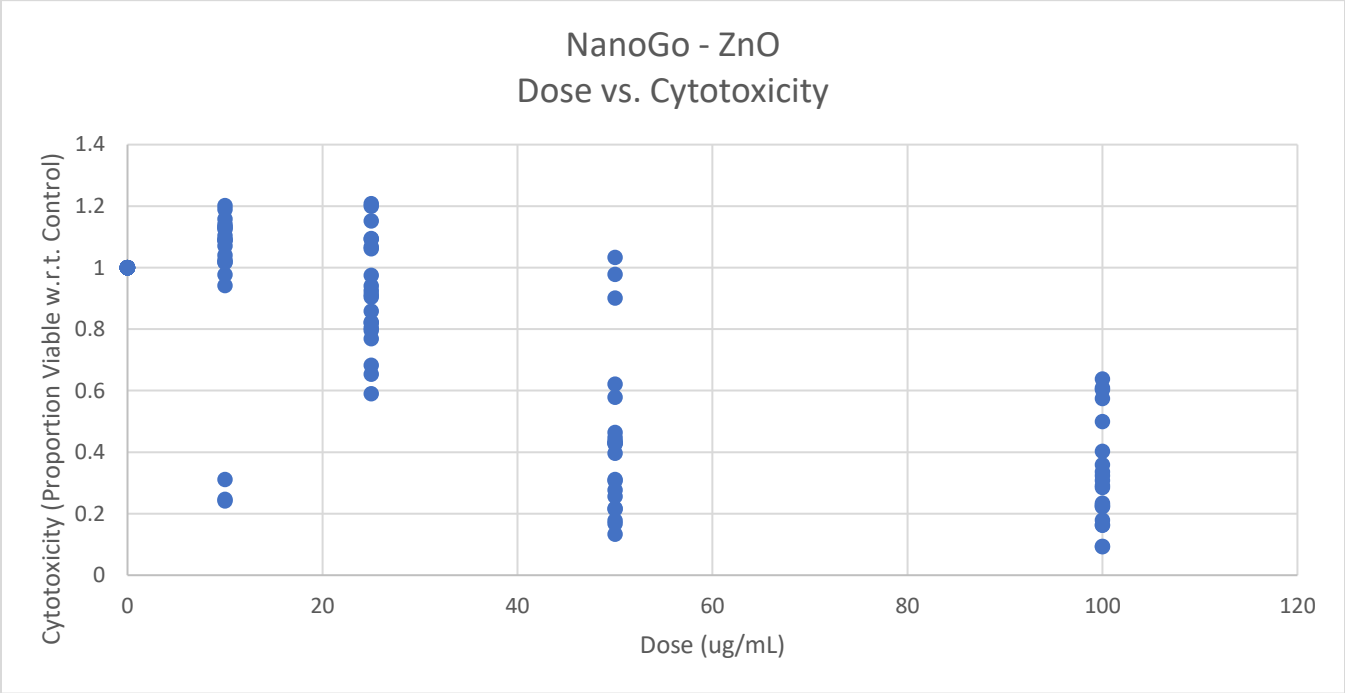

The scatterplot below shows the relationship between the dose of ZnO and the IL-1 beta cytokine response, which decreases as dose increases. These data are from the seven laboratories in the NanoGo consortium. One laboratory reported an unusually high response at control and the first two exposure groups (Figure 3-12).

Figure 3-12: Dose-Inflammation Response of Zinc Oxide for all NanoGo Labs in the THP-1 cell line.

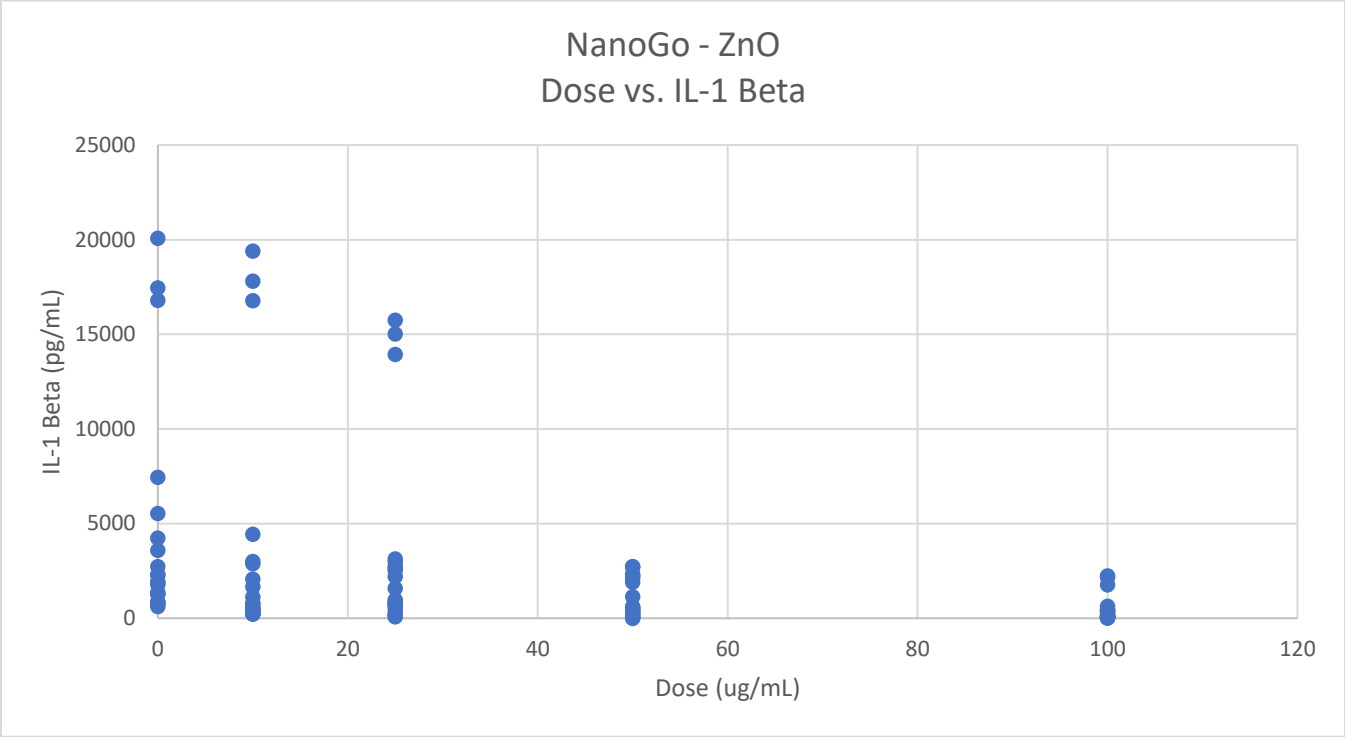

The scatterplot below of the IL-1beta vs. cytotoxicity association for ZnO (from all seven laboratories) shows the sudden drop-off for the IL-1 beta response as soon as cells begin dying (i.e., cytotoxicity less than 1) (Figure 3-13).

Figure 3-13: Association between Cytotoxicity and Inflammation of Zinc Oxide for all NanoGo Labs in the THP-1 cell line.

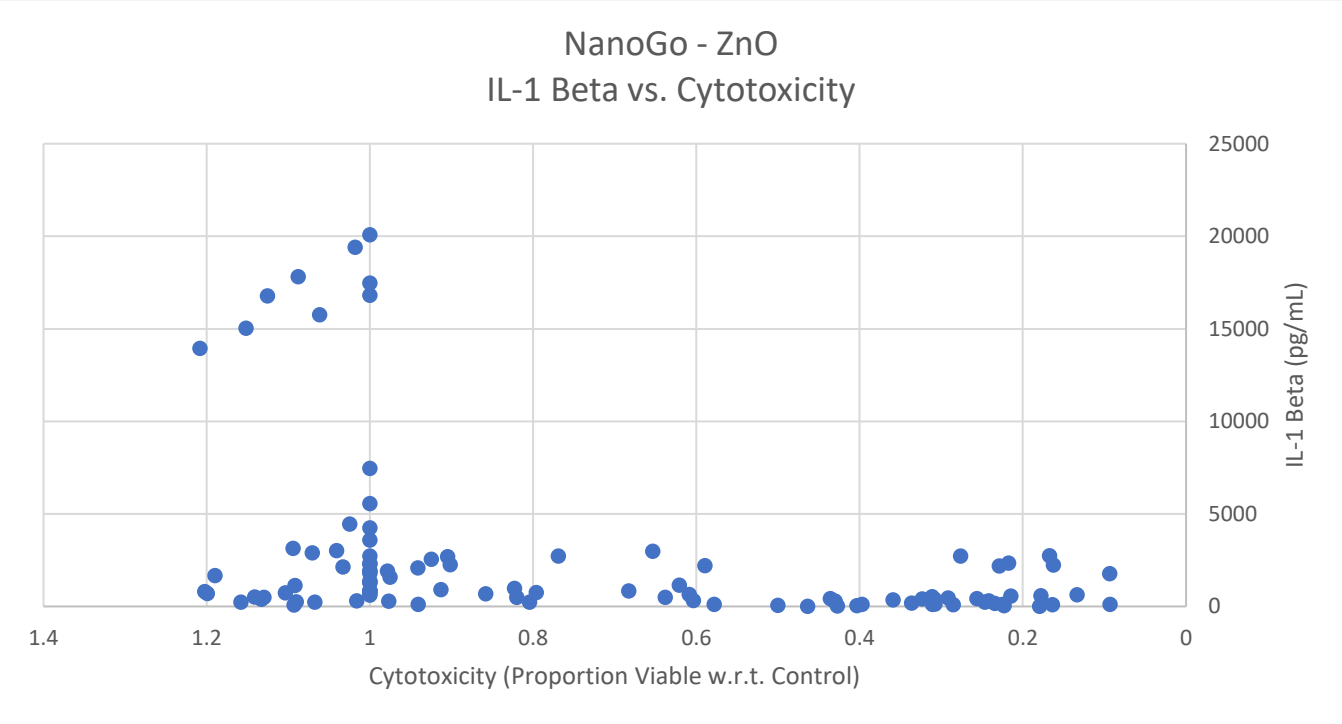

The other materials showed no relationship between dose and cytotoxicity; ZnO and TiO_2 nanobelts were the most potent. As a comparison to ZnO, the relationship between cytotoxicity and IL-1 beta is shown for MWCNT. The association is less clear, with a high amount of IL-1 beta and viable cells even at the highest doses (Figure 3-14).

Figure 3-14: Association between Cytotoxicity and Inflammation of Multiwall Carbon Nanotubes for all NanoGo Labs in the THP-1 cell line.

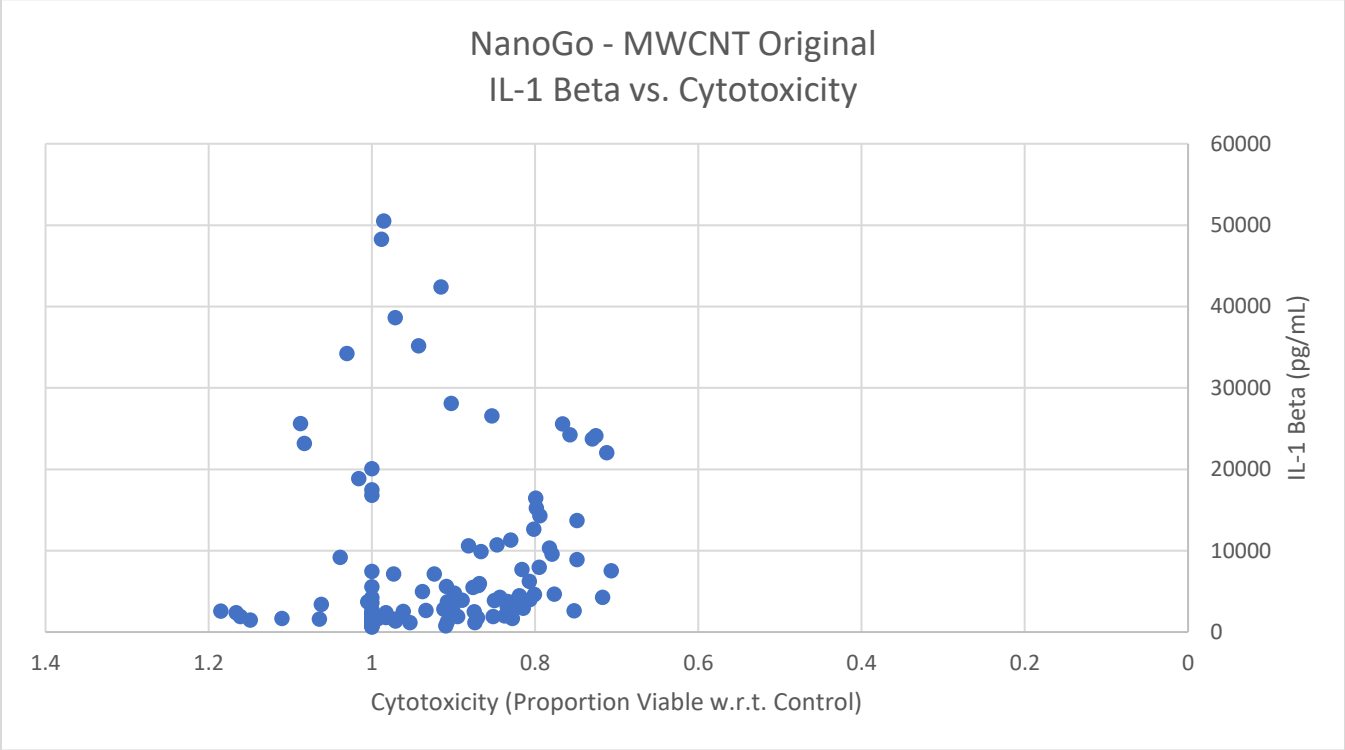

Thus, the ZnO material appears highly potent, killing off the cells and thereby prohibiting the creation of the cytokine even at low doses. The dose-response data for ZnO were not modeled because of the decreasing trend.

3.4.1 Results based on a 5% increase above background of the mean IL-1 beta (BMR = γ+5%)

Initially, 42 relationships were available for modeling. After testing for statistically significant trends, 11 relationships were omitted from further analysis because no trend was detected. BMD and BMDL estimates could be found with SK for 20 of the remaining 31 relationships. Of the 11 for which a potency estimate could not be derived, no model fit adequately to eight; the remaining three were ZnO, for which a model fit the relationship, but the negative trend made BMD estimation from a simple dose-response model unreasonable, given the BMR. BMD estimates of "N/A" indicate that no model adequately fit the data, and "Not Estimable" indicates that a model fit but a BMD estimate was not derived (Appendix Table C-1).

Only ZnO relationships were not estimated because of the negative association while looking for a response above background. Because ZnO was identified to be highly potent, leading to high levels of cytotoxicity at low doses and therefore stopping IL-1 beta production, its potency is assumed to be greater than that of the TiO_2

nanobelts. Thus, the BMD estimates for ZnO are stated as being less than those of TiO_2 nanobelts. Rankings are by BMD; BMDLs are included for completeness but are not used for ranking purposes at this time because the BMD is considered the best estimate of a material's hazard. When considering all of the potency estimates, the minimum BMD per material is used for ranking because it represents the maximum estimate of potency for that material (i.e., the most health-protective estimate of hazard potency). A 5th percentile value was not used because the grouping was based on the best estimate of the dose associated with the BMD. After grouping, BMDLs could be used for the purpose of deriving categorical OELs, following adequate model validation.

Thus, ZnO was assumed to be the most potent material, followed by TiO_2 nanobelts. Original MWCNTs and SiO_2 were observed to have similar potency, more potent than the purified and functionalized MWCNTs (Table 3-19). There may be a relationship between potency rank and the number of missing potency estimates, as the materials with the fewest estimates (e.g., MW-F) tend to be ranked as less potent. Rankings are unchanged when using the median instead of the minimum, but MW-P and SiO_2 swap places if the mean BMD is used for ranking, and MW-P is placed third rather than fifth if the maximum BMD is used for ranking.

Table 3-19: Descriptive Statistics for BMD and BMDL estimates for NanoGo THP-1 IL-1 beta dose-response relationships using stochastic kriging (SK), BMR = γ+5%.

Material	Min BMD BMDL	Mean BMD BMDL	Median BMD BMDL	Max BMD BMDL	Number Missing (out of N=7)
ZnO	BMDs for ZnO assumed to be less than those for TNB				7
	BMDLs for ZnO assumed to be less than those for TNB				5
TNB	0.10	0.23	0.22	0.44	1
	0.002	0.03	0.01	0.09	1
MW-O	0.59	1.81	1.21	4.03	2
	0.01	0.10	0.04	0.36	2
SiO_2	0.78	4.96	1.43	16.19	3
	0.02	1.01	0.09	4.45	3
MW-P	2.12	2.68	2.74	3.17	4
	0.05	0.49	0.49	0.93	4
MW-F	11.14	17.89	17.89	24.64	5
	2.14	3.01	3.01	3.87	5

3.4.2 Results based on a 1.1 standard deviation increase above background of the mean IL-1 beta (BMR = γ+1.1 SD)

BMD and BMDL estimates could be found for 20 of the 31 relationships. Of the 11 for which a potency estimate could not be derived, no model fit adequately to eight; the remaining three were ZnO, for which a model fit the relationship, but the negative trend made BMD estimation impossible, given the BMR. BMD estimates of "N/A" indicate that no model fit the data, and "Not Estimable" indicates that a model fit but a BMD estimate could not be derived (Appendix Table C-2). Only ZnO relationships were not estimable because of the negative association while looking for a response above background.

The ranking of material potencies is not greatly affected by the BMR choice here. The model is unchanged, and a different point on the curve is selected. Variations by laboratory are present, but ZnO was again the most potent material, followed by TiO_2 nanobelts, where the potency estimates for ZnO are assumed to be less than those for TiO_2 nanobelts. The three types of MWCNTs and the SiO_2 material are comparable in potency (Table 3-20). There may be a relationship between potency rank and the number of missing potency estimates, as the materials with the fewest estimates (e.g., MW-F) tend to be ranked as less potent. Rankings are unchanged when using the mean or maximum BMD instead of the minimum, but MW-O and SiO_2 switch order if the median BMD is used for ranking.

Table 3-20: Descriptive Statistics for BMD and BMDL estimates for NanoGo THP-1 IL-1 beta dose-response relationships using stochastic kriging (SK), BMR = γ+1.1 standard deviations.

Material	Min BMD BMDL	Mean BMD BMDL	Median BMD BMDL	Max BMD BMDL	Number Missing (out of N=7)
ZnO	BMDs for ZnO assumed to be less than those for TNB				7
	BMDLs for ZnO assumed to be less than those for TNB				7
TNB	0.16	1.12	0.77	3.87	1
	0.04	0.26	0.22	0.80	1
MW-O	1.12	4.30	2.69	12.06	2
	0.30	1.54	0.75	5.14	2
SiO_2	1.53	9.37	2.31	31.33	3
	0.39	6.33	0.69	23.56	3
MW-P	2.59	7.68	6.72	13.74	4
	0.77	2.91	2.18	5.77	4
MW-F	10.61	21.58	21.58	32.55	5
	1.84	13.48	13.48	25.13	5

3.5 NTP Lung Inflammation, Fibrosis, and Neoplasia

The response data from the NTP dataset are based on microscopic histopathologic evaluations, and the BMR for each endpoint is an additional 10% response (above the control/unexposed group) for lung inflammation, fibrosis, or neoplasia, as recorded by the pathologist. BMD modeling was used to estimate a given material's potency for some combination of material, species, strain, sex, and exposure duration. The response variables are indicators of having observed the endpoint; thus, dichotomous models were fit to the data. The Cochran-Armitage trend test was used to identify whether there was a statistically significant trend prior to model fitting. The best-fitting model was chosen by evaluating goodness-of-fit and AIC. Additionally, NOAELs and LOAELs were determined by Fisher's exact test.

By response endpoint, hierarchical clustering was used to identify the potency estimates (BMDs) that were most similar, and four clusters were used (Table 3-21). A total of 80 potency estimates were found from the 104 dose-response relationships with the inflammation endpoint (additional 4% PMNs in BALF); 94 had a significant trend and 10 did not. Of the 94 with a trend, 14 were not adequately fit by any of the BMDS models (goodness-of-fit *P* value was less than 0.1). For lung fibrosis, 28 potency estimates were found for the initial set of 93 dose-response relationships. No fibrosis response was observed at any dose for 43 of the relationships, leaving 50 for benchmark dose modeling. Thirty-seven had a statistically significant trend, but for nine relationships no BMD could be found because of inadequate model fits. For lung cell neoplasia, 20 potency estimates were found for 100 relationships; 29 had a significant trend, and nine of those dose-response relationships were not adequately fit by the BMDS models.

PSLT studies were added to the lung cell neoplasia data. Some additional inflammation relationships were taken from the technical reports, as shorter-term inflammation results were sometimes reported. A tabulation of all of the modeling results is reported in the Appendix (Tables E-1, E-2, and E-3). The purpose of these analyses was to determine how these materials grouped with regard to potency. A similar pattern is observed for each of these three histopathology endpoints from chronic inhalation studies, as was seen in the grouping based on acute neutrophilic pulmonary inflammation; that is, most of the materials are grouped in the most potent group, with decreasing numbers represented in less potent groups. The hierarchical clustering uses the information in the data to estimate similar groups. As such, this grouping is conducive to predictive modeling, in concept, whereby factors influencing the grouping could be used to predict the group of a new material.

Table 3-21: Hierarchical Cluster Frequencies of BMDs from NTP Chronic Inhalation Rodent Data.

Hierarchical Cluster	Inflammation	Fibrosis	Lung Cell Neoplasia
1 (Most Potent)	66	17	14
2	7	8	4
3	5	2	1
4 (Least Potent)	2	1	1

Order-of-magnitude bands were assigned on the basis of BMDLs as a comparison to the hierarchical clusters, for which Cluster 1 dominates the assignments (Table 3-22). BMDLs were used to allow for conversions to human equivalent concentrations. Although group assignments are not as skewed as the hierarchical cluster assignments, there are still disparities. Furthermore, study size is not explicitly considered when grouping these PoD estimates, with larger studies tending to have less variability in the BMD estimates than smaller studies. Order-of-magnitude grouping imposes a structure consistent with occupational hazard banding and does not reflect the nature of the data as hierarchical clustering does. As such, order-of-magnitude grouping may not be as useful for predictive modeling. Further evaluation of this question is explored for acute pulmonary inflammation in rodents in Section 3.2. The purpose of providing the order-of-magnitude groups is for comparison with the results based on the hierarchical clustering method.

Table 3-22: BMDL Order-of-Magnitude Band Frequencies of BMDLs from NTP Chronic Inhalation Rodent Data.

Order-of-magnitude	Inflammation	Fibrosis	Lung Cell Neoplasia
<0.01 mg/m^3	26	10	1
0.01 – 0.1 mg/m^3	5	0	2
0.1 – 1.0 mg/m^3	26	10	7
1.0 – 10 mg/m^3	19	8	5
>10 mg/m^3	4	0	5

Tables 3-23 and 3-24 summarize the distribution of BMDLs by hierarchical cluster and by the order-of-magnitude bands, respectively.

Table 3-23: Summary of BMDLs from NTP Inhalation Rodent Data – by Hierarchical Cluster and Endpoint.

		Rodent BMDL (mg/m^3)			
Endpoint	Cluster	Minimum	5^{th} Percentile	Maximum	n
Inflammation	1	3.1E-09	4.7E-06	2.3	66
Inflammation	2	2.3	2.5	4.8	7
Inflammation	3	8.0	8.3	13.2	5
Inflammation	4	14.0	14.1	14.5	2
Fibrosis	1	0	4.05E-06	0.0008	17
Fibrosis	2	0.74	0.79	1.96	8
Fibrosis	3	3.06	3.15	4.87	2
Fibrosis	4	9.34	9.34	9.34	1
Lung Cell Neoplasia	1	7.6E-03	3.4E-02	2.7	14
Lung Cell Neoplasia	2	9.3	9.5	22.7	4
Lung Cell Neoplasia	3	153.7	153.7	153.7	1
Lung Cell Neoplasia	4	159.4	159.4	159.4	1

Table 3-24: Summary of BMDLs from NTP Chronic Inhalation Rodent Data – by Order-of-Magnitude Group and Endpoint.

		Rodent Equivalent BMDL (mg/m^3)			
Endpoint	Order-of-magnitude Group	Minimum	5th Percentile	Maximum	n
Inflammation	<0.01 mg/m^3	3.1E-09	3.4E-07	1.0E-02	16
Inflammation	0.01 – 0.1 mg/m^3	2.0E-02	2.0E-02	0.1	5
Inflammation	0.1 – 1.0 mg/m^3	0.2	0.2	1.0	26
Inflammation	1.0 – 10 mg/m^3	1.0	1.2	9.6	19
Inflammation	>10 mg/m^3	13.2	13.2	14.5	4
Fibrosis	<0.01 mg/m^3	0	2.28-06	2.49E-03	10
Fibrosis	0.01 – 0.1 mg/m^3	N/A	N/A	N/A	0
Fibrosis	0.1 – 1.0 mg/m^3	0.27	0.30	0.97	10
Fibrosis	1.0 – 10 mg/m^3	1.38	1.39	9.34	8
Fibrosis	>10 mg/m^3	N/A	N/A	N/A	0
Lung Cell Neoplasia	<0.01 mg/m^3	7.6E-03	7.6E-03	7.6E-03	1
Lung Cell Neoplasia	0.01 – 0.1 mg/m^3	4.8E-02	4.9E-02	0.1	2
Lung Cell Neoplasia	0.1 – 1.0 mg/m^3	0.2	0.2	0.4	7
Lung Cell Neoplasia	1.0 – 10 mg/m^3	1.2	1.3	9.3	5
Lung Cell Neoplasia	>10 mg/m^3	10.5	10.6	159.4	5

For all three endpoints, most materials ended up in hierarchical Cluster 1, the most potent. For lung inflammation, a chronic study will have a lower BMD, indicated by the green points (Figures 3-15 and 3-16). Cobalt metal and antimony trioxide had the most variability in their potency estimates, with indium phosphide having nearly no variability across its eight estimates (two are NA because of inadequate model fits) (Table 3-25).

Table 3-25: Standard Deviation in Lung Inflammation BMD estimates by Material for NTP histopathology data.

Material	# BMDs	Std. Dev.
Cobalt Metal	10	11.8
Antimony trioxide	6	10.2
Nickel (II) oxide	10	3.61
Cobalt sulfate heptahydrate	3	2.89
Nickel Sulfate Hexahydrate	11	0.926
Vanadium Pentoxide	8	0.850
ortho-Phthalaldehyde	4	0.696
Nickel subsulfide	12	0.534
Talc	4	0.358
1020 Long Multiwalled Carbon Nanotube	4	0.317
Gallium arsenide	4	0.197
Indium phosphide	8	0.004
Abrasive blasting agents (coal slag)	1	NA
Abrasive blasting agents (garnet)	1	NA
Abrasive Blasting Agents: Blasting Sand	1	NA
Abrasive Blasting Agents: Specular Hematite	1	NA
Chromium	2	NA
Ferrocene	1	NA
Molybdenum trioxide	2	NA
o-Chlorobenzalmalononitrile (CS)	1	NA

Figure 3-15: Within-material Lung Inflammation Potency (mg/m^3) Variability by Species and Exposure Duration for NTP histopathology data.

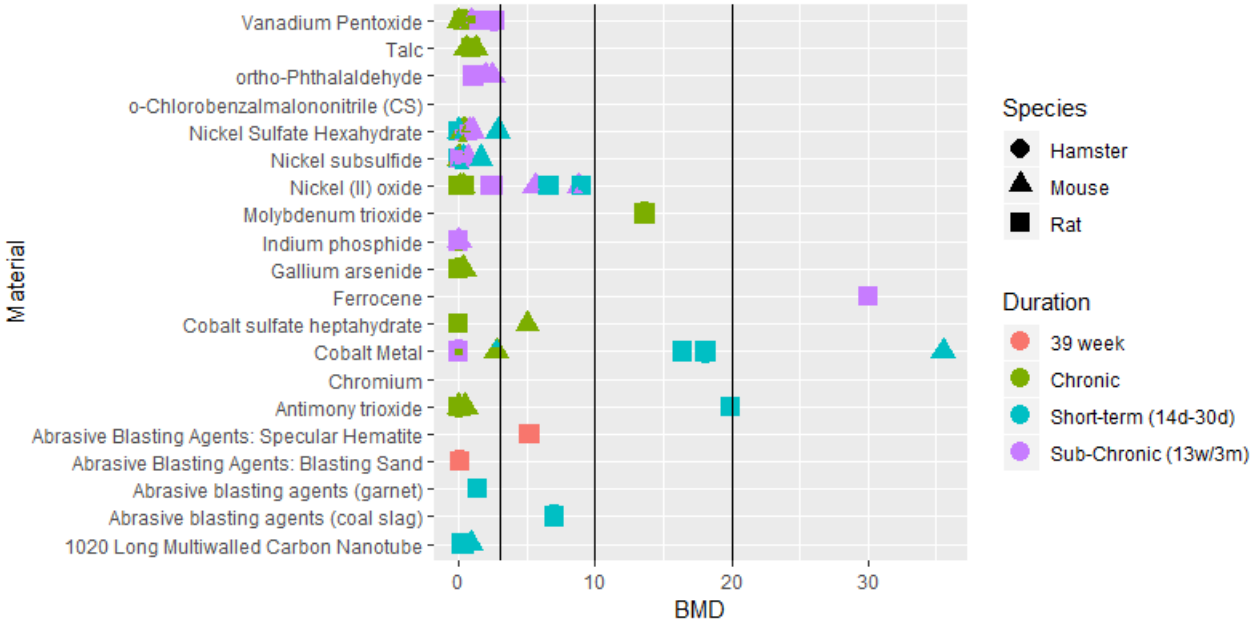

Figure 3-16 provides a closer look at Cluster 1, which contains most of the potency information. Again, the general trend is that a chronic study will have a lower (i.e., more potent) BMD as compared to a shorter-term exposure.

Figure 3-16: Within-material Lung Inflammation Potency (mg/m^3) Variability by Species and Exposure Duration from NTP histopathology data for Cluster 1, the most potent estimates.

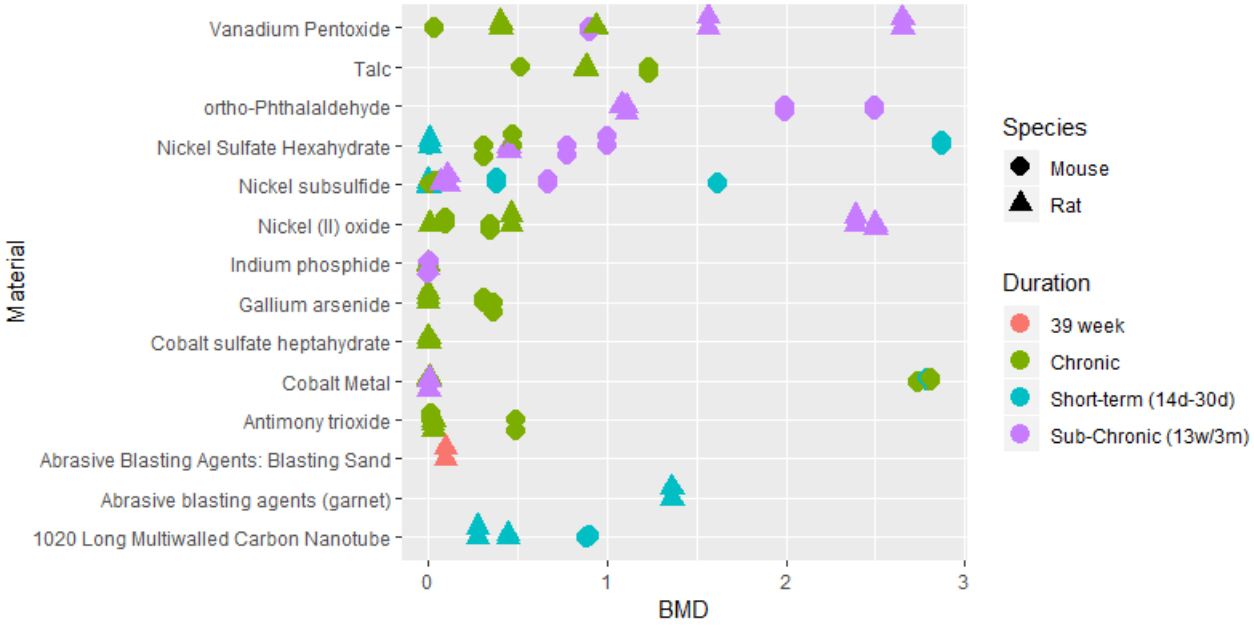

A downside to the NTP data is that although the dose-response data are high quality, experimental and physicochemical information is sparse. Again, in the mindset of predicting the potency for a new material, dose-response data will not be available, so only descriptors of the material may be available. For these data, some experimental design factors are available that may contribute to explaining the variability across potency estimates: material, species, strain, sex, and duration.

To learn about the effect that these experimental factors have on the lung inflammation potency cluster assigned via hierarchical clustering for the NTP histopathological data, exploratory random forest models were created. Because species and strain are correlated, and species can be derived from strain, species was omitted as a factor. Variable importance is measured via Gini impurity, which is a method for measuring predictive error when the predictions are categories.

Material is a useful predictive factor, indicating that a large contributor to the variability across potency estimates is due to characteristics of the materials (Figure 3-17). This is not a new finding, but it echoes the state of the science that not all materials can be considered equally. For these data, the sex of the animal seems to be minimally important. Strain appears more important than species, which indicates that although the species can improve predictions, there are further differences within the species contributing to the increased importance of strain. More specifically, there is only one strain of mouse and hamster, but several rat strains, so knowing the rat strain provides some additional information for prediction. For these data, Sprague-Dawley and F344 rats are two strains that were used in experiments (Table E-1), so differences in their size may be contributing to the

importance of strain for predicting the potency cluster. Some studies have shown that inbred F344 rats are more sensitive to inflammatory agents than are outbred Sprague-Dawley rats [Antonini et al. 2001; Nakano et al. 2014]. Other differences in exposure-response are known to exist between species, and those differences are absorbed by the strain variable when effects of species are omitted.

As an example of rodent species differences, mice have given false negative results more frequently than have rats in bioassays for some particulates that have been classified by the IARC as having limited or sufficient evidence of human carcinogenicity (including crystalline silica and nickel subsulfide). In addition, the mouse lung tumor response to other known human particulate carcinogens (including beryllium, cadmium, nickel oxide, tobacco smoke, asbestos, and diesel exhaust) is substantially less than that in rats [Mauderly 1997].

Figure 3-17: Estimated Experimental Variable Importance for Predicting the Potency Cluster for Lung Inflammation from NTP histopathology data.

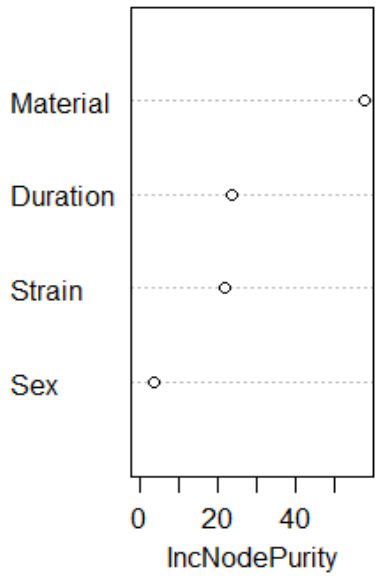

Using the physicochemical database constructed from information in the technical reports and internet searches, exploratory random forest models were also constructed to learn about the utility of the various physicochemical properties for predicting the potency cluster. It should be noted that the relative comparisons of variable importance are very data dependent, as the least important variables are also the ones most sparsely reported (Figure 3-18).

Figure 3-18: Estimated Variable Importance for Predicting the Inflammation Hierarchical Cluster for materials in the NTP histopathology data.

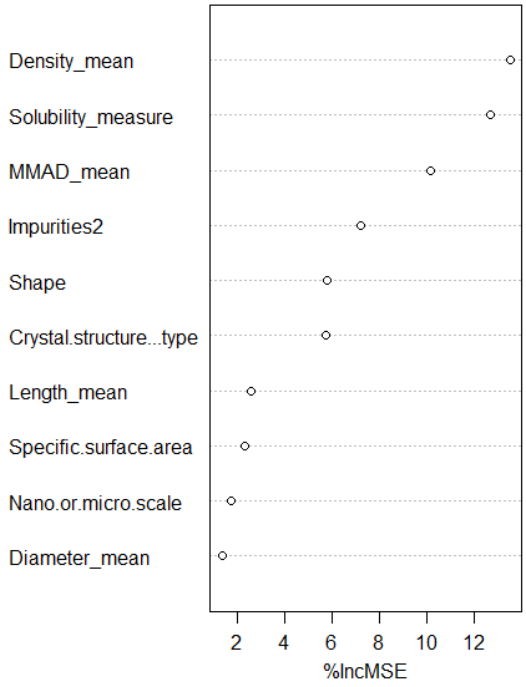

Figure 3-18 illustrates which components make up the relatively high importance of material for predicting the potency cluster. Primary particle characteristics such as density, shape, and crystal structure contribute to the differences in potency across materials, as well as the solubility and whether or not impurities are present in the material.

Because chronic and sub-chronic data are available, we can evaluate UFs, one of which adjusts a sub-chronic point of departure for uncertainty about the chronic PoD, with a maximal value of a factor of 10 [Dankovic et al. 2015]. Another UF is to account for differences in the dose-response across species, such as rodent to human. These factors are compared to suggestions in the NIOSH [2019] *Technical Report: The NIOSH Occupational Exposure Banding Process for Chemical Risk Management* for modifying PoDs on a time basis. Table 3-26 summarizes the relative differences of potency estimates within a given material for different exposure durations. In cases where more than one potency estimate is available for a material and duration (e.g., multiple species or sexes), the average is computed. The 13-week to 2-year adjustment is of most interest, as this reflects the subchronic-to-chronic UF, which has a maximal value of 10. For some of these materials, the maximal UF of 10 would not be protective enough; nickel (II) oxide and indium phosphide would need a factor of approximately 20 to correctly adjust the shorter duration potency estimate. In the NIOSH technical report [NIOSH 2019], a UF of 3 is recommended, which is only met for nickel sulfate hexahydrate and approximately for vanadium pentoxide.

Table 3-26: Lung Inflammation BMDs and BMDLs for materials in the NTP histopathology data–calculated Duration Adjustment Factors.

Material	Duration	Avg. BMD	Avg. BMDL	Adjustment	BMD Factor	BMDL Factor
Cobalt sulfate heptahydrate	2 year	1.67	1.15			
Nickel Sulfate Hexahydrate	16 day	0.96	0.01	16 day to 13 weeks	0.77	50.28
	13 weeks	0.75	0.50	16 day to 2 year	0.41	33.83
	2 year	0.39	0.34	13 weeks to 2 year	0.53	0.67
Ferrocene	3 months	30.00	14.04			
Nickel subsulfide	16 day	0.50	0.64	16 day to 13 weeks	0.56	0.21
	13 weeks	0.28	0.14	16 day to 2year	0.05	0.03
	2 year	0.03	0.02	13 weeks to 2 year	0.09*†	0.15†
Gallium arsenide	2 year	0.17	0.14			
Antimony trioxide	2 weeks	19.95	13.22	2 weeks to 2 year	0.01	0.02
	2 year	0.14	0.31			
Molybdenum trioxide	2 year	13.64	9.60			
Nickel (II) oxide	16 day	7.82	4.31	16 day to 13 weeks	0.61	0.68
	13 weeks	4.81	2.92	16 day to 2 year	0.03	0.03
	2 year	0.23	0.12	13 weeks to 2 year	0.05*†	0.04*
Vanadium Pentoxide	3 months	1.51	0.92	3 months to 2 year	0.30	0.37
	2 year	0.46	0.34			
Talc	2 year	0.88	0.63			
Indium phosphide	3 months	0.003	0.0005	3 months to 2year	0.06*†	0.04*
	2 year	0.0002	1.9E-05			
o-Chlorobenzalmalononitrile (CS)	2 year	NA				
ortho-Phthalaldehyde	3 months	1.67	1.02			
Chromium	2 year	NA				
Cobalt Metal	2 weeks	18.19	8.31	2 weeks to 3 months	0.00	0.00
	3 months	0.004	7.32 E-06	2 weeks to 2 year	0.08	0.13
	2 year	1.39	1.04	3 months to 2 year	351.47	141875.52
Abrasive Blasting Agents: Blasting Sand	39 weeks	0.10	NA			
Abrasive blasting agents (coal slag)	2 weeks	7.02	3.07			
Abrasive blasting agents (garnet)	2 weeks	1.36	0.23			
Abrasive Blasting Agents: Specular Hematite	39 weeks	5.20	3.27			
1020 Long Multiwalled	30 day	0.63	0.28			

Carbon Nanotube						

*Indicates the multiplicative adjustment does not exceed 1/10, the maximal uncertainty factor
†Indicates the multiplicative adjustment does not exceed 1/3, the suggested adjustment for Occupational Exposure Banding

3.6 Across-Assay Comparisons

Although general material classes were explored across the assays (e.g., TiO_2), the particular material and form were not often used in more than one assay. Manufacturers, sizes, or modifications could differ, which adds uncertainty to the understanding of how potent a particular material is under different experimental conditions. Where there were overlaps in materials across assays and endpoints, the connections between various toxicological testing strategies and material potencies were explored in order to develop a better understanding of how to best leverage alternative or short-term information for predicting long-term health effects. Within a given assay, the potency of the exposure material would be estimated and the potencies of numerous nanomaterials across various assay types and endpoints would then be compared.

Data were provided by internal and external researchers from NIOSH, the U.S. Army Center for Environmental Health Research, Oregon State University (OSU), the ENPRA project, and the NanoGo Consortium. Details on the data and analysis of *in vitro* cytotoxicity and zebrafish mortality [Harper et al. 2015] are in Appendices C and D.

SK was used to estimate potencies for the two inflammation assays, where BMRs were 4% above background for the *in vivo* (pulmonary neutrophilic inflammation) assays and 5% above background for the *in vitro* (cytokine IL-1 beta release, human monocytic cell line THP-1) assays. For the *in vitro* cell mortality assay, the BMR was 50% mortality above background. EPA BMDS was used to estimate potencies for the zebrafish mortality.

Dose-response modeling was conducted for relationships exhibiting a statistically significant difference in mean response across dose groups. For the continuous responses, ANOVA was performed. For the dichotomous responses, the Cochran-Armitage trend test was performed. All tests were evaluated at the 5% level of significance.

For inflammation, zinc oxide tended to be the most potent nanomaterial in rodents, whereas it was among the lowest-potency materials for zebrafish mortality. TiO_2 potency was quite variable because of factors such as size, shape, and laboratory. Relative potency rankings were similar between the inflammation assays.

Forty-two potency estimates were created for the *in vivo* rodent inflammation data, showing that the various forms of nanoscale zinc oxide were the most potent and microscale titanium dioxide was the least potent on a mass basis. MWCNTs were moderately potent, and alterations such as purification or functionalization tended to reduce MWCNT potency, which was comparable to that of crystalline silica. Titanium dioxide was the most variable in potency, primarily because of differences in size and shape (Figure 3-19).

Figure 3-19: Variability in the Potency Estimates for Titanium Dioxide for acute rodent pulmonary inflammation from NIOSH/ENPRA/CIIT/NanoGo.

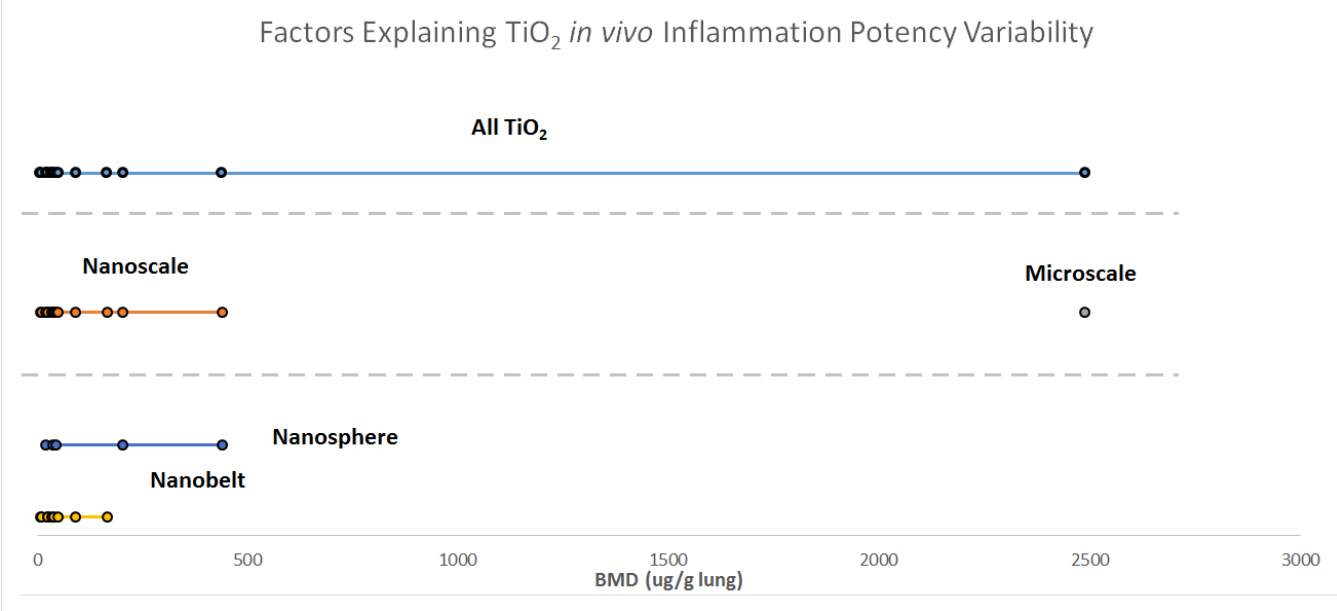

Thirty-one potency estimates were created for the *in vitro* human inflammation data. Potency rankings were similar to those seen in the *in vivo* rodent inflammation data, with ZnO as the most potent, followed by TiO_2 nanobelts, with MWCNT and silica following. The altered forms of MWCNT again tended to be less potent. Zinc oxide was ranked as being highly potent even though BMD estimates could not be created, as it was highly cytotoxic even at the lowest experimental concentration. Figure 3-20 shows the comparison of the mean inflammation potency estimates for all materials.

Figure 3-20: Relative Ranking of Material Potencies Across Inflammation Assays for NIOSH/ENPRA/CIIT/NanoGo.

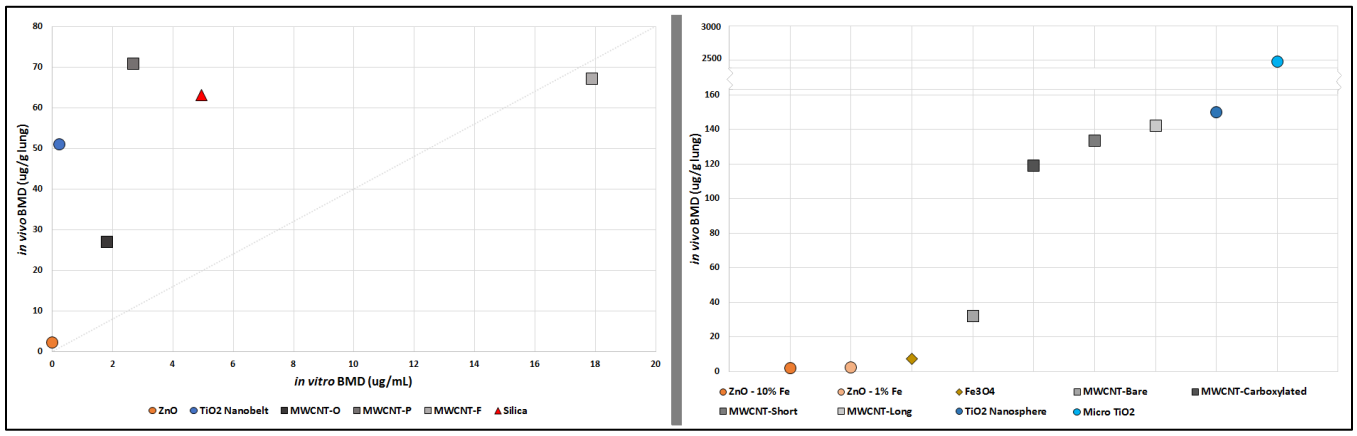

Many types of materials, different to those in the inflammation assays, were investigated in the zebrafish assay, resulting in 39 potency estimates. Although direct material ranking comparisons with the other assays are not easily made, similar meta-potency characteristics can be observed, mainly that within a given material, potency varies because of other factors such as size, shape, or coatings (Figure D-4).

Dose-response data were available for nine materials in the *in vitro* cytotoxicity assay. Only three materials had a statistically significant association: ZnO, coated ZnO, and anatase/rutile TiO_2. Statistically significant differences in cytotoxicity were not observed for the other six materials, which consisted of other forms of TiO_2 as well as MWCNT. A BMD estimate could only be found for ZnO, as the coated ZnO and anatase/rutile TiO_2 did not reach 50% cytotoxicity.

Nanomaterial potency is associated with many factors other than just the chemical composition, so data from all relevant assays should be included when developing hazard potency groups for occupational or environmental safety decision-making. Other factors such as size, shape, and alterations have been seen to affect the potency estimates. Relative potencies were similar between human *in vitro* and acute rodent *in vivo* inflammation, suggesting that prediction of longer-term inflammation effects could be done with alternative testing strategies. Nanoscale materials also tend to be more potent on a mass basis than microscale. Within a given size, other factors contribute to a material's potency (Figure 3-19).

Across the NTP endpoints that were analyzed, material potency varies by endpoint for most materials. Of the materials with a neoplasia potency estimate, the variability is limited, as the least and most potent cluster (represented by Min and Max) are the same; only TiO_2 was placed in more than one cluster, and both were the two least potent (3 and 4). Other factors contribute to the potency estimates, and therefore the hierarchical cluster, such as duration of exposure and species characteristics. The most variability was observed for lung inflammation, specifically cobalt metal which included potency estimates from the most to the least potent clusters.

Table 3-27: Summary of Cluster Variability by Endpoint for NTP Materials.

	Lung Inflammation		**Lung Fibrosis**		**Lung Neoplasia**	
Material	*Min*	*Max*	*Min*	*Max*	*Min*	*Max*
1020 Long Multiwalled Carbon Nanotube*	1	1	N/A	N/A	N/A	N/A
Abrasive blasting agents (coal slag)	2	2	N/A	N/A	N/A	N/A
Abrasive blasting agents (garnet)	1	1	N/A	N/A	N/A	N/A
Abrasive Blasting Agents: Blasting Sand	1	1	1	1	N/A	N/A
Abrasive Blasting Agents: Specular Hematite	2	2	4	4	N/A	N/A
Antimony trioxide	1	3	1	1	2	2
Carbon Black (Elftex-12 furnace black)*	N/A	N/A	N/A	N/A	1	1
Cobalt Metal	1	4	2	3	1	1
Cobalt sulfate heptahydrate	1	2	1	1	1	1
Ferrocene	4	4	N/A	N/A	N/A	N/A
Gallium arsenide	1	1	N/A	N/A	1	1
Indium phosphide	1	1	1	2	1	1
Molybdenum trioxide	3	3	N/A	N/A	2	2
Nickel (II) oxide	1	2	3	3	1	1
Nickel subsulfide	1	1	1	1	1	1
Nickel Sulfate Hexahydrate	1	1	N/A	N/A	N/A	N/A
ortho-Phthalaldehyde	1	1	2	2	N/A	N/A
Talc	1	1	1	2	2	2
TiO_2	N/A	N/A	N/A	N/A	3	4
Vanadium Pentoxide	1	1	1	2	1	1
Wollastonite calcium silicates	N/A	N/A	N/A	N/A	1	1

* Nanoscale

As seen in all of the analyses, there is always a loss of potency information due to lack of trend; or a need to extrapolate beyond the data to reach a chosen BMR limited the ability to compare a given material's potency across assays and endpoints. If a BMR is not estimable, then all data for that material are ignored, providing the opportunity for other methods that can utilize more of the available information. The many differences in material type, supplier, laboratory, assay, and endpoint make ranking comparisons difficult because the similarity or difference in potency is shadowed by the uncertainty around whether the materials can be considered the same.

3.7 Categorical Occupational Exposure Limits

3.7.1 Acute Lung Inflammation

The hazard potency groups for acute pulmonary inflammation based on a hierarchical clustering method using Ward's minimum variance linkage reflect the nature of the data with regard to potency differences. In that analysis, most of the evaluated ENMs clustered into the most potent group (Hazard Potency Group 1). The least potent group was a microscale TiO_2 and a fullerene, which elicited a relatively low acute inflammation response, thus resulting in relatively high animal and human-equivalent single day (8-hour) airborne exposure concentrations (Table 3-28). For more information on the materials within each of the four clusters in the initial analysis and expanded analysis refer to Tables 3-2 and 3-5.

Table 3-28. Categorical OEL Estimates for Acute Inflammation in Rats and Mice (4% PMNs above Background, 0-3 Days Post-Exposure) from NIOSH/ENPRA/CIIT/NanoGo and Swiss-VCI/NIOSHTIC/ATL; Nanoscale and Microscale Particle Lung Dose.

Hazard Potency Group [a]	Rodent Estimated Effect Level [b] (µg/g lung)	Human-Equivalent Lung Dose (mg) [c]	Human-Equivalent Concentration, 8-hr TWA (mg/m^3) [d]	Categorical OEL Estimate for an 8-hr TWA exposure (mg/m^3) [e]
Initial dataset (NIOSH/ENPRA/CIIT)				
1	0.23	0.059	0.0309	0.0021
2	84.7	21.6	11.2	0.75
3	365	93.1	48.4	3.2
4	2,366	603	314	21
More comprehensive dataset - initial plus literature-based dataset				
1	0.0032	0.00082	0.00043	0.000029
2	34.6	8.83	4.6	0.31
3	207	52.9	27.5	1.8
4	2,289	584	304	20

[a] Potency group created using Complete linkage in initial dataset and using Ward's linkage in more comprehensive dataset.

[b] 5th Percentile of the distribution of the BMDLs.

[c] Estimated by assuming rat lung weight of 1 g, then extrapolating the rat particle mass lung dose to humans by normalizing on the lung surface area in humans/rats of (102/0.4) (m^2/m^2).

[d] Estimated as the Human-equivalent Lung Dose (mg) / Worker reference air intake per day (9.6 m^3 [ICRP 1994]) x Alveolar Deposition Fraction Estimate (estimate of 0.2 across respirable particle sizes).

[e] After application of total UF of 15 to the human-equivalent concentration based on lung surface area dose normalization.

Abbreviations: PMNs: Polymorphonuclear leukocyte cells, measured in bronchioalveolar lavage fluid; BMDL: Benchmark dose, 95% lower confidence limit estimate; TWA: Time-Weighted Average.

3.7.2 Short-term to Chronic Lung Inflammation

The categorical OEL estimates for the hierarchical clustering of materials by potency for subchronic lung inflammation are shown in Table 3-29. These cOEL estimates by potency group are based on the BMDL estimate at the 5th percentile of the distribution of BMDL estimates in each group. Comparison of the cOELs estimated from the acute vs. subchronic-chronic inflammation endpoint shows that the cOEL estimates based on acute inflammation are roughly an order of magnitude larger than those based on the subchronic-chronic inflammation endpoints (Table 3-28 and 3-29). This finding makes sense with regard to the expected greater sensitivity to effects with longer exposure.

Alignment of these categorical OEL estimates with the performance-based order-of-magnitude exposure bands would put the materials in potency group 1 into the most stringent band E (<0.01 mg/m^3), although the OEL estimate suggests an even lower exposure (more stringent band) and more rigorous exposure controls may be needed for potency group 1 materials to prevent pulmonary inflammation in workers. Materials in potency group 2 would fall into band D, suggesting the need to control workplace exposures to airborne concentrations from 0.01 to <0.1 mg/m^3. Materials in potency groups 3 and 4 would fall into exposure control band C (0.1 to <1 mg/m^3). Note that most of these materials are assumed to be microscale particles. Because they were selected for study in the NTP cancer bioassays, many of these may have relatively low OELs also (as discussed in the OEB section).

Table 3-29. Categorical OEL Estimates for Subchronic Lung Inflammation in Rats and Mice – Proportion of Animals Observed as Responders by Histopathological Examination; Primarily Microscale Particles from NTP; Airborne Mass Concentration.

Lung Inflam-mation Potency Group	PoD_RODENT (mg/m^3)	DAF (total)	HEC_PoD = PoD_RODENT / DAF (mg/m^3)	UF (total)	cOEL = HEC_PoD / UF (mg/m^3)
1	4.65-06	1	4.65E-06	45	0.00000010
2	2.52		2.52		0.056
3	8.29		8.29		0.18
4	14.06		14.06		0.31

3.7.3 Short-term to Chronic Lung Fibrosis

The categorical OEL estimates for the hierarchical clustering of materials by potency for subchronic fibrosis are shown in Table 3-30. These OEL estimates by potency group are based on the BMDL estimate at the 5th percentile of the distribution of BMDL estimates in each group. Comparison of the cOELs estimated from subchronic-chronic pulmonary inflammation vs. fibrosis shows that the cOEL estimates based on fibrosis are lower than those based on the inflammation endpoints (Table 3-28 and 3-29). This finding suggests that pulmonary fibrosis is a more sensitive endpoint regarding the dose eliciting this response. However, the number of materials eliciting fibrosis was smaller than the materials eliciting inflammation, and so the finding reflects the more severe response among a more limited set of materials (Table 3-23).

Alignment of these categorical OEL estimates with the performance-based order-of-magnitude exposure bands would put the materials in potency group 1 into the most stringent band E (<0.01 mg/m^3), although the OEL estimate suggests an even lower exposure (more stringent band) and more rigorous exposure controls may be needed for potency group 1 materials to prevent pulmonary fibrosis in workers. Materials in potency group 2 would fall into band D, suggesting the need to control workplace exposures to airborne concentrations from 0.01 to <0.1 mg/m^3. Materials in potency groups 3 and 4 would fall into band C (0.1 to <1 mg/m^3).

Table 3-30. Categorical OEL Estimates for Subchronic Lung Fibrosis in Rats and Mice – Proportion of Animals Observed as Responders by Histopathological Examination; Primarily Microscale Particles from NTP; Airborne Mass Concentration.

Lung Fibrosis Potency Group	**PoD$_{_RODENT}$ (mg/m^3)**	**DAF (total)**	**HEC_PoD = PoD$_{_RODENT}$ / DAF (mg/m^3)**	**UF (total)**	**cOEL = HEC_PoD / UF (mg/m^3)**
1	0.000004	1	0.000004	45	9.0x10^{-8}
2	0.79		0.79		0.017
3	4.9		4.9		0.11
4	9.3		9.3		0.21

3.7.4 Chronic Lung Neoplasia

The categorical OEL estimates based on lung cancer in rats or mice following chronic (2-year) inhalation exposure are shown in Table 3-31. These OELs are shown for estimated excess risk of either 0.001 (1/1,000) or 0.0001 (1/10,000) as recommended in the NIOSH cancer policy guidelines [NIOSH 2017]. The categorical OELs based on a 1/1,000 excess risk of lung cancer are about 2 to 10 times higher (less protective) than those based on noncancer endpoint of lung inflammation (Table 3-29). The categorical OELs based on a 1/10,000 excess risk of lung cancer are more similar to those based on lung inflammation (Table 3-29).

The order-of-magnitude exposure control bands associated with these categorical OELs based on a lung cancer excess risk of 1/1,000 for potency groups 1, 2, 3, and 4, respectively, would be bands E, D, B, and B. The control bands associated with these categorical OELs based on a lung cancer excess risk of 1/10,000 would—for potency groups 1, 2, 3, and 4, respectively—be bands E, E, C, and C. Most of these materials are assumed to be microscale inhaled particles. These estimates can serve as benchmarks for comparison to PoD estimates from shorter-term *in vivo* studies of microscale or nanoscale particles. cOEL estimates based on lung cancer excess risk of 1/10,000 are more similar to the cOEL estimates based on subchronic inflammation or fibrosis than are the cOELs based on lung cancer excess risk of 1/1,000.

Table 3-31. Categorical OEL Estimates for Chronic Lung Neoplasia in Rats and Mice (Proportion of Animals Observed as Responders by Histopathological Examination; Primarily Microscale Particles from NTP; Airborne Mass Concentration).

Lung Cancer Potency Group	**PoD_RODENT** *[Excess Risk of 0.1]* **(mg/m³)**	**DAF (total)**	**HEC_PoD = PoD_RODENT / DAF** *[Excess Risk 1/10]* **(mg/m³)**	**Extrapo-lation Factor (from PoD)**	**cOEL = HEC_PoD / EF** *[Excess Risk 1/1,000]* **(mg/m³)**	**Extrapo-lation Factor (from PoD)**	**cOEL = HEC_PoD / EF** *[Excess Risk 1/10,000]* **(mg/m³)**
1	0.0336	1	0.0336	100	0.00034	1,000	**0.000034**
2	9.46		9.46		0.095		**0.0095**
3	154		154		1.54		**0.15**
4	159		159		1.59		**0.16**

Page left blank intentionally

4 Occupational Exposure Banding

4.1 Occupational Exposure Banding Methods

NIOSH recommends occupational exposure banding for materials without authoritative OELs [NIOSH 2019]. As such, estimating an OEB may precede the development of an OEL for emerging materials such as ENMs (Figure 1-1). For these materials, data on humans are not likely to be available. As new materials are developed for potential commercial uses, a tiered toxicology testing program should ideally accompany the development of that material [Oberdörster et al. 2005; Nel et al. 2013]. For materials that lack toxicology testing data, precautionary measures are required to protect workers against potential unknown adverse health effects [Schulte and Salamanca-Buentello 2007]. Toxicology data are used to provide information about potential health hazards and for decisions on exposure control and other risk management options.

In this report, OEBs are developed for nanoscale or microscale materials that meet the Tier 2 data requirements for banding for the longer-term health endpoints of STOT-RE and carcinogenicity [NIOSH 2019]. These OEB estimates are compared to categorical OEL groups estimated from pulmonary inflammation data and to those groups for new materials based on predictive modeling. Most of the ENM data from animal studies are for the endpoint of acute pulmonary inflammation, whereas the longer-term data are primarily for microscale particles. These microscale particle data are relevant because these materials may also be produced in nanoscale forms (Table 2-6).

The microscale particle data are from the NTP chronic bioassay program, which represent high quality (gold standard) data. All of the NTP data on airborne solid particles that were available in the database as of March 2018 have been included in these analyses. These NTP data provide a set of benchmark materials for comparison to the more limited data available on the ENMs. Many of the NTP studies were performed prior to the emergence of the nanotechnology field in the early 2000s and do not specify particle size. Most of the sold particle materials included in the NTP bioassays are metals and metal compounds, including metal oxides.

The database and/or reports usually provide data on the airborne particle size (mass median aerodynamic diameter, or MMAD) but typically do not provide data on the primary particle size. The MMAD particle sizes were in the microscale, respirable size ranges (Table 2-7). Thus, most of the NTP materials are assumed to be microscale particles. An exception is the NTP subchronic study on MWCNT, which is an ENM. In addition to the NTP data, chronic inhalation rodent bioassay data for other nanoscale and microscale particles (TiO_2, toner,

carbon black) are included from earlier analyses [Kuempel et al. 2006; NIOSH 2011]. The nanoscale particle data are used to derive an OEB for the specific material directly, and the microscale particles data are used to derive an OEB that is adjusted for the nanoscale form of those materials, based on the NIOSH [2019] banding criteria.

The data used in applying the NIOSH [2019] occupational exposure banding process includes the potency estimates (BMDL, NOAEL) from the analyses of the dose-response relationships for pulmonary inflammation, fibrosis, or lung tumors in rats or mice in the NTP studies (subchronic or chronic inhalation exposure data). The entire Tier 2 banding process was not applied, but the focus was on two of the most relevant endpoints for occupational lung diseases associated with inhaled particles: Specific Target Organ Toxicity–Repeated Exposure (STOT-RE) and carcinogenicity. The criteria for banding materials based on these endpoints are shown from NIOSH [2019] in Table 4-4 for carcinogenicity and in Table 4-1 for STOT-RE. BMDLs and NOAELs are examples of points of departure that are used in the Tier 2 banding.

Data on the nanoscale form of a material are preferred for banding, if available. However, if the data available on a nanoscale material are not adequate for banding, then the data on a microscale form of the material can be used with adjustment (Section 3.14 of NIOSH [2019]). First, a band is created by using the data for the microscale material that meet the data sufficiency criteria (Section 3.2 of NIOSH [2019]); then, that band is shifted to the next more stringent band to account for the potentially greater toxicity of the nanoscale form of the material. This guidance applies to all nanomaterials, including soluble and poorly soluble substances. In the current application of the banding guidance, the data criteria for the STOT-RE and carcinogenicity endpoints are used (Sections 3.3 and 3.5 of NIOSH [2019]).

An objective of this current analysis is to use these available data from rodent studies to determine if new information can be gleaned pertaining to these initial banding recommendations. Eventually, a predictive model using data from physicochemical properties of nanomaterials and from in vitro assays would be used to augment the rodent study data and to extend the banding capability by using information about *in vitro* potency to predict *in vivo* potency (*in vitro–in vivo* extrapolation, or IVIVE) after an exposure of at least 28 days. Presently, the data are insufficient to build an IVIVE model because assays on the same materials are not available across the different assays.

The STOT-RE criteria refer to doses or exposure concentrations from standard 90-day toxicity studies in rats (Section 3.5 of NIOSH [2019]). As recommended in the occupational exposure banding framework, the most sensitive PoD was identified, based on either the NOAEL or the BMDL. Also, as recommended, if the duration

of exposure was less than 90 days (but at least 28 days), then the NOAEL and BMDL estimates were divided by a factor of 3 to adjust toward a PoD from a study with exposure duration of at least 90 days. This factor is less stringent than a factor of 10, which Lampe et al. [2018] concluded was a sufficient factor "to account for the uncertainty associated with evaluating human health risk based on results from a 28-day study in the absence of results from a 90-day study." If no NOAEL was available, the LOAEL was divided by 10 to adjust toward a NOAEL (which is the maximum typical value for that UF [Dankovic et al. 2015]). The lowest of the adjusted NOAEL or BMDL was chosen for placement into a STOT-RE band, and the LOAEL was used only if neither a BMDL nor a NOAEL was available.

The banding criteria applied to the NTP lung inflammation results are those for "Inhalation (dust/particles)" (Table 3-12 of NIOSH 2019). These criteria for assigning a material to one of five bands are as follows, from lowest to highest potency, corresponding to the PoD: band A (>30,000 µg/m^3), band B (>3,000 to ≤30,000 µg/m^3), band C (>300 to ≤3,000 µg/m^3), band D (>30 to ≤300 µg/m^3), or band E (≤30 µg/m^3) (Table 3-12 of NIOSH 2019). These concentration ranges refer to airborne exposure concentrations that include the PoD (NOAEL or BMDL) from a standard 90-day toxicity study in rats, or they refer to the adjusted PoD if the estimate was derived from a study that was less than 90 days (but at least 28 days) or if a LOAEL was used as the PoD (as discussed above). Because a given material may have potency estimates from multiple exposure durations, the final STOT-RE band for a given material was chosen to be the most stringent band.

For the carcinogenicity band, the NIOSH guidance recommends using a BMDL from a BMR of 5% [NIOSH 2019]. Because a BMR of 10% was used in modeling, a linear extrapolation to the origin was assumed so that the 5% BMDL could be found by dividing the 10% BMDL by 2. This adjusted BMDL was then placed into the corresponding cancer band on the basis of the following recommended criteria: band C (>16,700 µg/m^3), band D (>5 to ≤16,700 µg/m^3), or band E (≤5 µg/m^3) (Table 3-7 of NIOSH 2019). According to NIOSH [2019] guidance, only the three more stringent bands (i.e., bands C, D, and E) are used to band materials for which cancer endpoints are reported. These ranges refer to airborne exposure concentrations that include the PoD (BMR of 5%) from a standard 2-year cancer bioassay in rats. A term that is equivalent to a 5% BMR, and which was used in the technical report, is the tumorigenic concentration for 5% of the population (TC_{05}) [NIOSH 2019].

4.2 Occupational Exposure Banding Results

In this investigation, the occupational exposure banding process developed by NIOSH [2019] was followed for the endpoints STOT-RE (Inhalation [dusts/particles)]) (Table 4-1) and carcinogenicity (quantitative analysis) (Table 4-4). The rat potency estimates were used in banding the NTP materials on the basis of subchronic or

chronic lung inflammation and fibrosis (STOT-RE) or lung neoplasia (carcinogenicity) endpoints. In the cases where for a given endpoint a material was classified into more than one band because of having multiple potency estimates in male and female rats, the most stringent band was chosen (see Methods for more details on the banding criteria).

OEB assignments depend on the endpoint (STOT-RE or carcinogenicity). For the lung inflammation endpoint, following 90-day inhalation exposure in rats, seven of the 23 NTP materials were assigned to band E, which is the most stringent band. Six materials were assigned to band D, the next most stringent band. Four materials were assigned to band C, and six materials were assigned to band B. No materials were assigned to the least stringent band A (Table 4-2). The worker-equivalent airborne exposure concentrations corresponding to these bands are discussed in Section 5 (Table 5-1). For the fibrosis endpoint, four materials were assigned to band E, one to band D, seven to band C, four to band B, and one to band A (Table 4-3).

The STOT-RE bands for inflammation and fibrosis are based on the NTP data only (not the acute inflammation data) in order to align with the NIOSH [2019] OEB STOT-RE criteria that are based on a standard 90-day rat study. Most of the OEBs were based on the rat data (Table 4-2), as PoDs were not estimable from the mouse data for many materials (e.g., because of lack of dose-response trend). For the carcinogenicity response to talc and vanadium pentoxide, the mouse was more sensitive than the rat, and the PoDs based on the mouse data resulted in more stringent OEBs (E vs. C) for those two materials (Table 4-2).

Table 4-1. Criteria for Specific Target Organ Toxicity – Repeated Exposure (STOT-RE) Endpoint [Table 3-12 of NIOSH 2019].

NIOSH banding criteria for Specific Target Organ Toxicity (NOAEL/BMDL/BMCL)					
Exposure/ dosing route	**Endpoint Band A**	**Endpoint Band B**	**Endpoint Band C**	**Endpoint Band D**	**Endpoint Band E**
Oral, Dermal	>1,000 mg/ kg-day	>100 to ≤1,000 mg/ kg-day	>10 to ≤100 mg/kg-day	>1 to ≤10 mg/kg-day	≤1 mg/kg-day
Inhalation (dust/ particles)	>30,000 µg/m³	>3,000 to ≤30,000 µg/ m³	>300 to ≤3,000 µg/m³	>30 to ≤300 µg/m³	≤30 µg/m³
Inhalation (gases/ vapors)	>30,000 ppm	>3,000 to ≤30,000 ppm	>300 to ≤3,000 ppm	>30 to ≤300 ppm	≤30 ppm

Table 4-2: Example STOT-RE Banding for Inflammation based on NTP rat data for Microscale Materials.

Chemical Name	Most Stringent STOT-RE Band
1020 Long Multiwalled Carbon Nanotube *	D
Abrasive blasting agents (coal slag)	C
Abrasive blasting agents (garnet)	D
Abrasive Blasting Agents: Blasting Sand	D
Abrasive blasting agents (crushed glass)	B
Abrasive Blasting Agents: Specular Hematite	B
Antimony trioxide	D
Calcium chromate	B
Chromium	C
Cobalt	E
Cobalt sulfate heptahydrate	E
Ferrocene	B
Gallium arsenide	E
Indium phosphide	E
Molybdenum trioxide	B (or C with mice & rat data)
Nickel (II) oxide	E
Nickel subsulfide	E
Nickel sulfate hexahydrate	D
o-Chlorobenzalmalononitrile (CS)	D
ortho-Phthalaldehyde	E
Talc	C (or E with mice & rat data)
Vanadium pentoxide	C (or E with mice & rat data)
Wollastonite calcium silicates	B

* Nanoscale

Table 4-3: Example STOT-RE Banding for Fibrosis based on NTP rat data for Microscale Materials.

Chemical Name	Most Stringent STOT-RE Band
1020 Long Multiwalled Carbon Nanotube*	NA
Abrasive blasting agents (coal slag)	NA
Abrasive blasting agents (crushed glass)	NA
Abrasive blasting agents (garnet)	NA
Abrasive Blasting Agents: Blasting Sand	C
Abrasive Blasting Agents: Specular Hematite	B
Antimony trioxide	E
Calcium chromate	B
Chromium	B
Cobalt	B
Cobalt sulfate heptahydrate	E
Ferrocene	NA
Gallium arsenide	NA
Indium phosphide	E
Molybdenum trioxide	A
Nickel (II) oxide	C
Nickel subsulfide	E
Nickel sulfate hexahydrate	D
o-Chlorobenzalmalononitrile (CS)	NA (or C with mouse & rat data)
ortho-Phthalaldehyde	C
Talc	C
Vanadium pentoxide	C
Wollastonite calcium silicates	C

* Nanoscale

The NIOSH occupational exposure banding criteria for carcinogenicity (Table 4-4) were used for the lung neoplasia endpoint observed in rats in the NTP and other chronic bioassay data. On the basis of these criteria, most of these materials were assigned to band D (nine of 11 materials); one material (microscale TiO_2) was assigned to band C and one to band E (Indium Phosphide) (Table 4-5). The worker-equivalent airborne exposure concentrations corresponding to these bands are shown in Table 5-1.

The OEBs derived for carcinogenicity were based primarily on the NTP data in rats. The banding changed for only one material (molybdenum trioxide) depending on rodent species. For molybdenum trioxide, a PoD was not estimable from the rat data but was assigned to band D on the basis of the mouse data (Table 4-5). For TiO_2 P25, a PoD was not estimable because that study [Heinrich et al. 1995] included only one exposure concentration for the material. Previously, NIOSH had converted the particle mass exposure concentrations to particle surface area lung doses in order to combine the nanoscale and microscale TiO_2 data for dose-response modeling and derivation of a recommended exposure limit [NIOSH 2011]. In the standardized methods used in this analysis, the particle mass exposure data as reported in the publications are used in the dose-response modeling.

Table 4-4. Criteria for Carcinogenicity (Quantitative Analysis [Table 3-7 from NIOSH 2019].

NIOSH banding criteria for carcinogenicity			
Exposure/ dosing route	**Endpoint Band C**	**Endpoint Band D**	**Endpoint Band E**
Slope Factor	<0.01 $(mg/kg\text{-}day)^{-1}$	≥ 0.01 to <10 $(mg/kg\text{-}day)^{-1}$	≥ 10 $(mg/kg\text{-}day)^{-1}$
Inhalation Unit Risk	$<3 \times 10^{-6}$ $(\mu g/m^3)^{-1}$	$\geq 3 \times 10^{-6}$ to <0.01 $(\mu g/m^3)^{-1}$	≥ 0.01 $(\mu g/m^3)^{-1}$
TD_{05}	>5 mg/kg-day	>0.005 to ≤5 mg/kg-day	≤0.005 mg/kg-day
TC_{05}	>16,700 µg/m³	>5 to ≤16,700 µg/m³	≤5 µg/m³

Table 4-5. Example Banding for Lung Cancer based on NTP Rat Studies (Microscale Materials, unless noted otherwise).

Material	Most Stringent Cancer Band
Antimony trioxide	D
Carbon Black (Elftex-12 furnace black)*	D
Cobalt	D
Cobalt sulfate heptahydrate	D
Gallium arsenide	D
Indium phosphide	E
Nickel (II) oxide	D
Nickel subsulfide	D
Talc	D
TiO_2	C
Vanadium pentoxide	D
Abrasive blasting agents: Blasting sand	NA
Calcium chromate	NA
CB P90*	NA
Molybdenum trioxide	NA (was D with mice & rat data)
Nickel sulfate hexahydrate	NA
o-Chlorobenzalmalononitrile (CS)	NA
TiO_2 P25*	NA
Vanadium pentoxide	NA
Wollastonite calcium silicates	NA

NA: Not available
* Nanoscale

The occupational exposure banding guidance recommends that nine standard toxicological endpoints should be considered when deriving a Tier 2 band, with the banding result representing the most stringent band across endpoints. In the analysis of the NTP materials, the three endpoints – inflammation, fibrosis, and carcinogenicity – were chosen *a priori* to be most relevant for workers and represent two of the recommended outcomes (carcinogenicity and STOT-RE); the other five endpoints were not pursued here. With the additional data and

banding results for those additional five endpoints, the most stringent band could change. The most stringent band was determined for these materials across the three end points (Table 4-6).

Table 4-6. Examples of Most Stringent Bands for Lung Endpoints based on NTP Rat Studies (of Microscale Materials unless noted otherwise).

Material	Most Stringent Band
1020 Long Multiwalled Carbon Nanotube*	D
Abrasive blasting agents (coal slag)	C
Abrasive blasting agents (crushed glass)	B
Abrasive blasting agents (garnet)	D
Abrasive Blasting Agents: Blasting Sand	D
Abrasive Blasting Agents: Specular Hematite	B
Antimony trioxide	E
Calcium chromate	B
Carbon Black (Elftex-12 furnace black)*	D
CB P90*	NA
Chromium	C
Cobalt	E
Cobalt sulfate heptahydrate	E
Ferrocene	B
Gallium arsenide	E
Indium phosphide	E
Molybdenum trioxide	D†
Nickel (II) oxide	E
Nickel subsulfide	E
Nickel sulfate hexahydrate	D
o-Chlorobenzalmalononitrile (CS)	D
ortho-Phthalaldehyde	E
Talc	E†
TiO_2	C
TiO_2 P25*	NA
Vanadium pentoxide	E†
Wollastonite calcium silicates	C

* Nanoscale

† Mouse

Page intentionally left blank

5 Discussion

In general, these analyses found that potency of several materials varies greatly between the nanoscale and microscale particles and that the variation is explained by factors such as the material and its physicochemical properties, the experimental design choices such as route of exposure or exposure duration, and the health endpoint. The experimental differences were taken into account to the extent feasible. In particular, the inhalation exposure or administered dose was converted to the particle mass deposited per gram of wet lung tissue, which normalizes the dose by route of exposure, exposure duration, and rodent body weight. In addition, analyses were performed within strata of the key variables of post-exposure duration (focusing on the 0- to 3-day post-exposure time point) and endpoint (i.e., dose-response relationships evaluated by health endpoint, including pulmonary inflammation, fibrosis, or lung cancer). Materials with similar potencies can be identified by data-driven clustering methods like hierarchical clustering or by *a priori* groupings like order-of-magnitude bands. If sufficient physicochemical data are available, potency group (specifically cluster) predictions appear promising, using classification methods from statistical learning like random forests.

Gaps in the available data make across-assay comparisons difficult, as the same material was rarely available across the different datasets analyzed here. The sparse physicochemical information also makes the development and testing of predictive models difficult, as it is uncertain which properties are actually the most important to have in a predictive model. The differences in available materials contribute to uncertainty about how to best leverage data from assays other than sub-chronic or chronic inhalation exposures. Hypothetically, a large set of varied materials with dose-response data from *in vitro*, acute *in vivo*, sub-chronic *in vivo*, and chronic *in vivo* exposures should be able to provide insight into tools like UFs or other adjustments for estimating chronic effects from short-term potency estimates. New datasets are currently being explored to evaluate their utility for analyses such as these (Appendix F).

Building on the current framework with additional data and analyses would increase the coverage of materials and experimental data, expanding opportunities to investigate linkages among assay types in developing predictive models. The currently limited and preliminary estimates of categorical OELs or OEBs can be expanded and uncertainties reduced. A strength of this methodology is that hazard potency is estimated with standard quantitative analyses across a range of materials, including benchmark materials (relatively well-studied and with more complete data). A predictive model would also provide useful information regarding a minimum set of toxicity assays needed to assess hazard potency. These categorical OELs and OEBs, which are based on the hazard potency estimates, provide evidence-based input needed to select the appropriate workplace exposure controls and are compatible with the use of exposure banding processes for occupational health decision-making.

These methods comprise the main components of the data analysis framework used in the analyses in this TR for evaluating the available data and exploring the utility of the results with regard to risk management decision-making. This framework will also be useful in further analyses as more data become available and for additional development and testing of predictive tools. This framework for evidence-based grouping is consistent with 21st-

century toxicological testing goals to utilize alternative information and testing strategies. Such a comprehensive set of experimental data would include a core set of physicochemical properties and an array of *in vitro* assays, along with comprehensive information for a set of microscale and nanoscale benchmark materials, including acute to chronic *in vivo* assays and associated *in vitro* assays. Reaching the goal of achieving a predictive model for hazard categorization across a wide variety of ENMs will require a sufficiently comprehensive database to evaluate inter-assay associations.

The data analysis framework developed and applied in this document provides insights toward achieving this ultimate goal of a predictive model for evidence-based hazard categorization. A fully validated grouping framework will require a more comprehensive dataset and further model development and cross-validation. The strengths and limitations of the current data and methods are described, as well as next steps needed toward extension and validation of the current framework. Developing efficient evidence-based categorization of ENMs regarding potential health hazard is a global research effort. Further collaborative efforts that will be useful include experimental data sharing from standardized sets and cross-validation of the data and methods used in this and other grouping frameworks.

5.1 Comparison of Hazard Potency In vitro and In vivo

In these analyses, the hazard potency groupings and relative ranking results for nanoscale and microscale materials showed similar findings in the rodent and cellular studies. Nanoscale materials tended to be more potent on a mass basis than microscale materials. Within a given particle size category (nanoscale or microscale), other physicochemical factors contributed to ENM potency, including shape and surface modification. These results are consistent with previous findings, which suggest that chemical composition alone is not sufficient to predict the toxicity across various forms of a material. The relative ranking of hazard potency across the materials studied was similar between the rodent *in vivo* and the rodent or human *in vitro* assays for inflammation. These results are also consistent with previous findings suggesting that *in vitro* assays may be useful in predicting acute pulmonary inflammation.

5.2 Strengths and Limitations

The large amount of data allows for numerous exploratory insights; however, several common data limitations became apparent, and additional research questions were identified. The set of materials analyzed in the document may not be representative of the universe of materials to which workers are exposed, resulting in uncertainty regarding the potential hazard of unstudied materials. Many factors contribute to the estimation of a material's hazard, including experimental design (route and duration of exposure, exposed organism, biological endpoint/assay) and intrinsic material properties (e.g., specific surface area, modification). It was rare to have relevant data for a given material across all of the different assays and endpoints explored here, leading to uncertainty in the effects of these factors on material hazard (Figure A-1). Because of the available data, health hazards were estimated on a particle mass-basis, whereas other metrics such as surface area may be better suited

for hazard identification across a range of particle sizes and types. Physicochemical properties were considered the information most likely to be available for new ENMs yet exploring the utility of these properties was hampered by inconsistent reporting of the properties themselves or inconsistent methods of measurement. In addition, various experimental factors were found to contribute to the variability in hazard potency estimates, including differences in assay type (Table 5-5), laboratory (Table A-2), material type (Figure 3-2), species/strain and duration of exposure (Figure 3-15), and the specific health endpoint (Table E-4). These results indicate that in addition to differences in physicochemical properties of the materials, these various experimental factors need to be taken into account in any evaluation of relative potency across materials.

To the extent feasible, the experimental factors were taken into account in these analyses by stratification or normalization. Dose was normalized across exposure route (inhalation, IT, aspiration) by expressing dose as the total deposited mass particle dose per gram of wet lung tissue. This normalization also accounted for dose differences across species/strain/sex. Stratification was used in performing the dose-response analyses by health endpoint (inflammation, lung cancer), and the 0- to 3-day post-exposure time point was selected as reflecting the immediate response to exposure. In some cases, insufficient information was available to fully account for experimental factors that may affect the potency estimates. For example, inter-individual laboratory effects were shown in the NanoGo studies [Xia et al. 2013; Bonner et al. 2013], especially for the *in vitro* data. However, no clear adjustment for laboratory effect was available, although the initial inter-laboratory differences in the *in vitro* studies were mitigated in re-testing after an evaluation of methods [Xia et al. 2013]. In the current analyses, any residual effects of laboratory were absorbed by the potency groups, while attempting to attribute the potency differences to the physicochemical properties. To the extent that laboratories conducted experiments by standardized protocols, the potential effect of laboratory may be to contribute random variability; however, some bias by laboratory is also possible.

Across the four main analyses (acute *in vivo* lung inflammation, *in vitro* inflammation, zebrafish mortality, NTP lung inflammation, and lung cell neoplasia), approximately 300 materials were investigated (Table B-1). However, most of the materials in a given analysis were not found in the other analyses because of their specific characteristics such as size or modifications. Carbon nanotubes were present in all of the analyses, yet they are not necessarily the same carbon nanotubes—long, short, carboxylated, bare, and different manufacturers are examples of the differing material descriptors. This introduces uncertainty into the understanding of how a given material's potency changes across its lifecycle (short-term *in vitro* exposures up to chronic *in vivo* exposures) as well as across endpoints. Furthermore, it was rare to have information for a given material in both a nanoscale and microscale form. If such data were available, establishing a basis for a UF for nanoscale to microscale particle size may be possible.

It was shown in these analyses that on a mass basis, nanoscale materials tended to be more potent than microscale. However, if potency information was known for a microscale version of a new material and there was interest in an exposure limit for a nanoscale version, there is uncertainty around how to best adjust the microscale information. In the absence of specific information, default recommendation of one or more factors of 10 has

been proposed, e.g., in the derivation of a nanoscale OEB based on hazard data for a microscale form of that material [ANSES 2010; ISO 2014a; NIOSH 2021]. These current analyses enabled an evaluation of the data available to develop a predictive model of ENM hazard potency. Because of the disparate nature of the available data, there was little overlap in the data for nanoscale and microscale particles of the same chemical composition within studies of comparable design. For PSLT, a factor of 2 to 2.5 was proposed, based on an evaluation of lung tumor data in rats exposed to microscale or nanoscale particles of poor solubility and low toxicity (PSLT) [Gebel 2012]. However, the statistical methods that were used in pooling those data and deriving an adjustment factor have been questioned and discussed [Morfeld 2013; Gebel 2013]. The derivation of an evidence-based adjustment factor for microscale to nanoscale particles remains unresolved for PSLT, as well as for other types of particles.

In this report, typically much more data were available at the onset of an analysis than were analyzed. Several requirements must be met when conducting dose-response modeling: there must be a statistically significant trend; for those dose-response relationships with a trend, a best-fitting model must be found; and for those relationships with a best-fitting model, the potency estimate must be within the scope of the data and not extrapolated. These requirements caused a large portion of the dose-response relationships to be removed from analysis, as a potency estimate could not be derived. This harsh treatment, ignoring the data that do not meet the requirements as if there were no information to be had, is an area for future research. For example, in cases where a potency estimate requires extrapolation, this reveals that the potency estimate is at least the highest dose group of the study, which is much different from the current treatment of "unknown potency." The utility of other PoDs, such as NOAELs or LOAELs, presents another avenue for additional research. When a BMD is not estimable, a NOAEL or LOAEL usually can be estimated, providing some information about a material's potency. Statistically, NOAELs and LOAELs are inferior to a BMD, but by investigating the tradeoff between the statistical drawbacks and the increase in information gleaned from the data, uncertainties around categorizing materials may be reduced.

Although a BMD may be preferred statistically over a NOAEL or LOAEL, the BMD for a given material is influenced by the choice of the benchmark response (BMR). As the BMR changes, the BMD will change and as a result many of the results here would change; for example, clusters based on BMDs would change, and therefore the composition and performance of random forest models would also be affected. The BMD was typically treated as the best representation of a material's hazard, but the BMD is an estimate with uncertainty and is essentially a distillation of experimental and dose-response information into a single point.

In each of the analyses, dose-response relationships were typically investigated individually by study/experiment and endpoint. These analyses were stratified by post-exposure duration, with the 0- to 3-day post-exposure timepoint selected as representing the most immediate effects following exposure (vs. later post-exposure time points representing recovery). Normalization of dose (as total deposited dose per gram of wet lung tissue) accounted for differences in the route of exposure, as well as differences in lung weight by species, strain, and sex. It would be of interest to investigate alternative dose metrics, including particle surface area and particle

volume dose. These metrics were not investigated since information was limited across the materials to estimate these metrics. It may be that density is an important factor that is not taken into account with the mass dose but may be with volume dose [Pauluhn 2014]. It is also known that particle surface area explains the difference in hazard potency by mass dose of TiO_2 for pulmonary inflammation and cancer endpoints [NIOSH 2011]. These considerations do not represent limitations in the current analysis, because the purpose was to group potency by mass concentration, which is most directly relevant to the airborne mass concentrations to which OELs typically refer.

More comprehensive data are needed to further evaluate this framework across a larger set of materials, dose metrics, and response endpoints. When a new material is identified, it is possible that information other than physicochemical information may be available—for example, an *in vitro* assay may have been completed. This creates a future research need in the development of models that allow for the incorporation of physicochemical properties and assay-specific potency estimates for predicting chronic effects. More generally, research into multiple covariate and multiple response models may make better use of the data by pooling. In some cases, several dose-response relationships, which were not useful for potency estimation independently, may allow for estimation when they are combined. The use of multiple regression models may also lead to a better understanding of the associations between dose and response by allowing the inclusion of other factors, such as case effects or other biological characteristics that are associated with the response. For example, in the *in vitro* inflammation analyses, the inflammatory response was modeled by using only the dose, although it was identified that cytotoxicity is also important for understanding changes in inflammatory response. However, cytotoxicity was not quantitatively included in the modeling process.

In the current analyses, the method for pooling data from experiments using different routes of exposure was to estimate the deposited lung doses from inhalation exposures for comparison to studies with administered lung doses by intratracheal instillation or pharyngeal aspiration. Because the deposited lung doses in rats were estimated by using the MPPD model [ARA 2011], further evaluation of the MPPD model estimates with those from other models (e.g., Raabe et al. [1988]) or from measured lung doses would help to characterize uncertainty in these estimates.

Many of the identified data gaps—different materials in different assays or experimental designs, inconsistent physicochemical property reporting, lack of available individual animal data or sufficient summary data—could be alleviated by a uniform, large-scale data sharing initiative. Some progress toward accessible data in the United States has been made within the gene expression community by the NIH Gene Expression Omnibus (GEO) database, which archives and freely distributes genomic data. Journals in the field typically require the submission of data to GEO, which enables peer review and replication. Within the EPA, ToxCast is a large database of approximately 1,800 materials tested across 700 high-throughput assays. In the European Union, data sharing appears to be more at the forefront of research, as it allows the various research institutes to pool their data and findings. Within NIOSH, availability of data is dependent on its nature [NIOSH 2011]. As a result, tools like meta-analyses can be used to derive new findings from the combined information sources.

In addition to the models and methods used to analyze the data in this report to estimate hazard potency groups, other methods could be investigated. For example, principal components analysis has been used for dimension reduction, which identifies combinations of predictor variables that are statistically useful for classification or prediction tasks [Lamon et al. 2018; Aschberger et al. 2019]. Other uncertainties are also present in the methodologies used here. When PoDs are summarized, in either groupings or descriptions, the study size is not included as a weight of evidence, leading to an equal contribution and consideration of all estimates. As a result, estimates from small studies may be biased toward hazards more severe than they really are. For estimating BMDs, SK or the EPA BMDS model suite was used for modeling and estimation. Other approaches are available, such as non-parametric spline models and model averaging, but it is uncertain which if any of these modeling methods would make more efficient use of the available data and lead to more accurate estimates. For the classification tasks, various alternate tools are available in addition to random forests: a single classification tree; gradient boosted decision trees; logistic regression; and neural networks. More advanced methods have been used recently (Wheeler 2018) to predict the entire dose-response curve rather than a single point (e.g. BMD) using nonparametric Bayesian techniques. Along the similar vein of predicting potency directly rather than predicting a potency group (classification), meta-analytical techniques could be used to model the relative potency while accounting for factors other than dose (e.g., route of exposure, duration of exposure, material, and laboratory) and to further evaluate the sensitivity of results to the choice of BMR. Typically, default options were chosen for the various statistical methods. For example, in building random forests, the default number of trees to be constructed and the default number of predictor variables sampled at each split in the process of constructing trees were used. It is uncertain if tuning these parameters to identify the values that are optimal for classification would be advantageous. Further evaluation of statistical methods and these uncertainties will be more feasible once a more comprehensive dataset is compiled across a range of nanoscale and microscale materials in studies with the most relevant experimental design for use in dose-response assessments for human health risk assessment.

5.3 Occupational Exposure Banding

The workplace airborne exposure concentrations corresponding to the NIOSH OEBs are shown in Table 5-1. These NIOSH OEBs are comparable to those from other agencies and organizations [ISO 2016]. OEBs correspond to airborne concentration ranges. These order-of-magnitude concentration ranges have been aligned to performance-based engineering controls, which are designed to control workplace airborne concentrations of particulates within those concentration ranges [Naumann et al. 1996; HSE 2009; Dunn et al. 2018]. A difference in the NIOSH OEBs is that these order-of-magnitude bands are shifted one band toward the less stringent band (A); this means that the most stringent band E includes the *two* most stringent order-of-magnitude bands in the performance-based control banding frameworks [Naumann et al. 1996; Brooke 1998; Ader et al. 2005; Zalk and Nelson 2008; HSE 2009; ANSES 2010; ISO 2014a].

Table 5-1. Airborne concentration ranges associated with occupational exposure bands* [Table 1-1 of NIOSH 2019].

Occupational exposure band	Airborne target range for dust or particle concentration (milligrams per cubic meter of air [mg/m^3])	Airborne target range for gas or vapor concentration (parts per million [ppm])
A	>10	>100
B	>1 to 10	>10 to 100
C	>0.1 to 1	>1 to 10
D	>0.01 to 0.1	>0.1 to 1
E	≤0.01	≤0.1

* 8-hr time-weighted average concentrations

The OEBs for the NTP materials based on lung inflammation are shown in Table 5-2, OEBs based on lung fibrosis are shown in Table 5-3, and OEBs based on lung cancer are shown in Table 5-4. Indium phosphide is in the lowest and most stringent band (band E), on the basis of both the STOT-RE (lung inflammation) and cancer (lung cancer) endpoints. Most of the other materials that are assigned to band D on the basis of lung cancer are assigned to band E on the basis of lung inflammation.

These results provide information about the relationship of earlier endpoints to later, more severe, endpoints. Based on the earlier, non-cancer response of lung inflammation in the 90-day rat studies, the OEBs would be more protective than banding based on the chronic bioassay results for lung cancer. This would make biological sense if lung inflammation were a precursor to lung cancer, as has been hypothesized for respirable poorly soluble particles such as TiO_2 [NIOSH 2011]. In contrast, talc and vanadium pentoxide were assigned to a lower (more stringent) band (band D) on the basis of lung cancer, compared to the band assignment (band C) based on lung inflammation. In this case, the banding based on lung inflammation would be less sensitive than the banding based on lung cancer. For ortho-phthalaldehyde, a PoD was not estimable for cancer because no chronic data were available.

The only NTP material known to be nanoscale is the 1020 L-MWCNT, which was assigned to band D on the basis of lung inflammation (only the 90-day study data were available at the time of these analyses). Band D is less stringent than the NIOSH REL of 1 µg/m^3 (0.001 mg/m^3) for carbon nanotubes and nanofibers based on lung fibrosis in rats from 90-day inhalation studies [NIOSH 2013], which would be associated with band E. This NIOSH REL also suggests that a lower band (e.g., a hypothetical "band F," ≤0.001 mg/m^3) may be warranted for

some nanoscale materials, i.e., carbon nanotubes, as well as silver nanoparticles, for which the NIOSH REL is also approximately 1 µg/m^3 [NIOSH 2021].

It is not known whether some of the other NTP materials may have had particle size distributions that included nanoscale primary particles, as this information was not reported in the NTP database or in the technical reports for most of these materials. The vanadium pentoxide technical report did provide some information about the primary particle size distribution, which indicated it included a nanoscale fraction (Table 2-7).

According to the NIOSH draft OEB guidance, when microscale particle data are used to estimate an OEB for a nanoscale material of the same chemical composition, the next lower band should be assigned to the nanoscale form. This means that for nanoscale forms of the materials shown in Tables 5-2 to 5-4, the bands would all be shifted to the next more stringent band (except for those in band E, which is the lowest, again suggesting the possible need for a new "band F"). A critical question regarding a possible band lower than E is what additional exposure control options are available to reduce exposures further. Because these OEBs are all 8-hour time-weighted average (TWA) concentrations, one option may be to reduce exposure times (e.g., 15-minute short-term exposure limit, STEL [NIOSH 2007]). Another option aligned with performance-based controls would be closed systems and robotics (Figure 1-5).

In the case of TiO_2, the NIOSH REL for the microscale form is 2.4 mg/m^3 [NIOSH 2011], so the assigned band C (>0.1 to 1 mg/m^3) based on lung cancer is one band more stringent. It should be noted that the TiO_2 data are not from the NTP database but from another 2-year bioassay in rats [Lee et al. 1985]. According to the NIOSH OEB guidance, the OEB for the nanoscale form would be the next most stringent band, or band D (>0.01 to 0.1 mg/m^3). The NIOSH REL for nanoscale TiO_2 is 0.3 mg/m^3, which indicates that the OEB for nanoscale TiO_2 would also be more protective than the REL. Given that an OEB framework is intended for substances that have inadequate data to derive a REL, a more stringent band in the absence of specific data is prudent practice [Schulte et al. 2010].

Table 5-2. Example Occupational Exposure Bands in Workers and Material Assignments based on Lung Inflammation Endpoint in Rats following Chronic Inhalation Exposure; NTP and Similar Studies (alignment of Tables 4-2 and 5-1) – Primarily Microscale Materials.

Occupational Exposure Band and Airborne Exposure Concentrations (8-hr time-weighted average concentration)				
A (>10 mg/m^3)	B (>1 – 10 mg/m^3)	C (>0.1 – 1 mg/m^3)	D (>0.01 – 0.1 mg/m^3)	E (≤0.01 mg/m^3)
	Abrasive Blasting Agent: Specular Hematite	Abrasive blasting agent: Coal slag	1020 Long Multiwalled Carbon Nanotube*	Cobalt
	Calcium chromate	Chromium	Abrasive blasting agent: Garnet	Cobalt sulfate heptahydrate
	Ferrocene	Talc	Abrasive Blasting Agent: Blasting Sand	Gallium arsenide
	Molybdenum trioxide	Vanadium pentoxide	Antimony trioxide	Indium phosphide
	Abrasive Blasting Agent : Crushed Glass		Nickel sulfate hexahydrate	Nickel (II) oxide
	Wollastonite calcium silicates		o-Chlorobenzal-malononitrile (CS)	Nickel subsulfide
				ortho-Phthalaldehyde

* Nanoscale

Table 5-3. Example Occupational Exposure Bands in Workers and Material Assignments based on Lung Fibrosis Endpoint in Rats following Chronic Inhalation Exposure; NTP and Similar Studies (alignment of Tables 4-3 and 5-1) – Primarily Microscale Materials.

Occupational Exposure Band and Airborne Exposure Concentrations (8-hr time-weighted average concentration)				
A (>10 mg/m^3)	B (>1 – 10 mg/m^3)	C (>0.1 – 1 mg/m^3)	D (>0.01 – 0.1 mg/m^3)	E (≤0.01 mg/m^3)
Molybdenum trioxide	Abrasive Blasting Agents: Specular Hematite	Abrasive Blasting Agents: Blasting Sand	Nickel sulfate hexahydrate	Antimony trioxide
	Calcium chromate	Nickel (II) oxide		Cobalt sulfate heptahydrate
	Chromium	ortho-Phthalaldehyde		Indium phosphide
	Cobalt	Talc		Nickel subsulfide
		Vanadium pentoxide		
		Wollastonite calcium silicates		

Table 5-4. Example Occupational Exposure Bands in Workers and Material Assignments based on Lung Cancer Endpoint in Rats in Chronic Bioassays by NTP and Similar Studies (Alignment of Tables 4-5 and 5-1) – Primarily Microscale Materials.

Occupational Exposure Band and Airborne Exposure Concentrations (8-hr time-weighted average concentration)		
C ($>0.1 – 1$ mg/m^3)	D ($>0.01 – 0.1$ mg/m^3)	E (≤ 0.01 mg/m^3)
Titanium dioxide (fine)	Antimony trioxide	Indium phosphide
	Carbon Black (Elftex-12 furnace black)*	
	Cobalt	
	Cobalt sulfate heptahydrate	
	Gallium arsenide	
	Nickel (II) oxide	
	Nickel subsulfide	
	Talc	
	Vanadium pentoxide	

* Nanoscale

An additional dataset used in the estimation of OEBs for ENMs is from the OECD (Table 5-5). In this case, the PoDs were the NOAELs or LOAELs reported from a systematic review of the literature [OECD 2015] and which were compiled as part of a separate analysis [Davidson 2016]. These data provide a relatively large set of nanomaterials for banding, including various types of TiO_2, MWCNT, cerium oxide, silica, and other nanomaterials. The only microscale primary particle included was P-TiO_2 (Fine).

In these data, both nanoscale and fine titanium dioxide were assigned to band C (OEB of >0.1 to 1 mg/m^3) (Table 5-5). This is consistent with the NIOSH REL for nanoscale (ultrafine) TiO_2 of 0.3 mg/m^3 and is more protective than the NIOSH REL of 2.4 mg/m^3 for fine TiO_2. All the MWCNT and SWCNT were assigned to band D or E, with one exception, which was in band B. The estimate for that material was identified *post hoc* as being of insufficient quality for use in banding because of the nature of the data available from that study: a single high mass concentration (32.6 mg/m^3, 6 hr/d, for 30 out of 60 days), which was the LOAEL in that study. The true LOAEL is unknown, but other data suggest it could be a much lower mass concentration. For example, a LOAEL of 32.6 mg/m^3 is approximately two orders of magnitude higher than the LOAELs reported in some subchronic

inhalation studies of MWCNT in rats [Ma-Hock et al. 2009; Pauluhn 2010a]. A lower LOAEL for that study would result in a lower OEB estimate.

Silver nanomaterials were assigned to band D or band E (Table 5-5). These OEB estimates are similar to, respectively, the existing NIOSH REL for total silver (particle size not specified) of 0.01 mg/m^3 and the NIOSH REL for silver nanomaterials of 0.09 µg/m^3 [NIOSH 2021]. (Because <0.01 mg/m^3 is the lowest OEB in the NIOSH hazard banding guidance [NIOSH 2019], estimation of lower OEBs is not available in the draft OEB framework). Two types of spherical, nanoscale carbon black (Printex 90 and HSCb) were assigned to band D (OEB of >0.01 to 0.1 mg/m^3) and band E (OEB of <0.01 mg/m^3), respectively. These OEBs are approximately one or two orders of magnitude lower than the existing NIOSH REL of 3.5 mg/m^3 for carbon black (particle size not specified) [NIOSH 2007]. Three forms of nanoscale silica (SiO_2), which are likely amorphous, were assigned to band C (OEB of >0.1 to 1 mg/m^3), which is lower than the NIOSH REL of 6 mg/m^3 for amorphous silica (particle size not specified). These findings are consistent with the recommendation to reduce the OEB by at least an order of magnitude if microscale data are used to estimate an OEB for the nanoscale form of the material [ISO 2016; NIOSH 2019].

Several nanomaterials without RELs (for any particle size) were assigned OEBs (Table 5-5). Nanoscale Au was assigned to band E (OEB of ≤0.01 mg/m^3). Five different cerium oxide (CeO_2) materials were assigned to either band C (OEB of >0.1 to 1 mg/m^3) or band D (OEB of >0.01 to 0.1 mg/m^3). Fullerene, also without a REL, was assigned to band D (OEB of >0.01 to 0.1 mg/m^3).

Table 5-5. Example Occupational Exposure Bands in Workers and Material Assignments based on Lung Inflammation Endpoint in Rodents, using NOAELs and LOAELs from OECD [2015] and Systematic Literature Searches – Primarily Nanoscale Materials.

Occupational Exposure Band and Airborne Exposure Concentrations (8-hr time-weighted average concentration)				
A (>10 mg/m^3)	B (>1 – 10 mg/m^3)	C (>0.1 – 1 mg/m^3)	D (>0.01 – 0.1 mg/m^3)	E (≤0.01 mg/m^3)
	[MWCNT][a]	CeO_2 in aliphatic hydrocarbons (Envirox)	Nanosized silver	Nanosized silver
		CeO_2 NM-213	C60 fullerene	Nanosized gold
		SiO_2 NM-201 Sipernat 22S	CeO_2	HSCb[b]
		SiO_2 NM-203 Aerosil 200	CeO_2 NM-211 (Ceria Dry)	Magnetite[c]
		SiO_2 (Aerosil R 974)	CeO_2 NM-211(Nanograin Ceria)	MWCNT
		TiO_2 NM-103 (UV TITAN M212)	Fe_3O_4[c]	MWCNT-7
		TiO_2 NM-104 (UV TITAN M262)	MWCNT Baytubes	MWCNT Nanocyl NC 7000
		TiO_2 NM-105 (P25)	MWCNT Graphistrength C100	Siderite[c]
		TiO_2 P25	MWCNT	
		ZnO NM-111 Z-COTE® HP1	MWCNT-7	
		P-TiO_2 (Fine)[c]	Printex 90	
			SWCNT	

Footnotes on next page.

Footnotes to Table 5-5:

[a] This estimate was identified *post hoc* as being of insufficient quality for use in OEB estimation because of the nature of the data available: this study of MWCNT inhalation in mice had one exposure concentration, 32.6 mg/m^3, 6 hr/d, every other day over 60 days [Li et al. 2009]. Adverse pulmonary effects were observed in the exposed mice, and thus this exposure concentration was the LOAEL in that study. However, the true LOAEL is unknown and could be a much lower mass concentration, which would result in a lower OEB (see text for further discussion).

[b] High surface area carbon black (nanoscale) [Elder et al. 2005].

[c] Microscale.

If no specific chemical characteristics are known other than type (e.g., a cerium oxide material), an initial band may be found by summarizing Tables 5-2 through 5-5. This initial band is a starting point for identifying the hazard of a new material; if additional information is known (e.g., physicochemical properties), then that information should be incorporated into the banding. All materials of a similar type were combined, and the most stringent OEB was identified for each group of materials (Table 5-6). The physicochemical property group in Table 5-6 is adapted from the biological mode-of-action groups reported earlier (e.g., BSI [2007]; Kuempel et al. [2012]; SER [2012]). The definition of high toxicity for poorly soluble materials was based on the general criteria from Guest [1998], which has been used subsequently, e.g., in NanoSafer, as described in Brouwer [2012]. Guest [1998] described materials as very toxic if the OEL is less than 0.1 mg/m^3 and toxic if the OEL is 0.1 to 1 mg/m^3. In Table 5-6, low or poorly soluble materials that have an OEL less than 1 mg/m^3 are listed as high toxicity materials. Soluble materials may include a range of toxicities (including according to criteria from Guest [1998]) but are not further defined here since soluble substances are typically assessed separately in control banding tools for nanomaterials.

It should be noted that the individual bands comprise differing experimental designs, health endpoints, and physicochemical properties. A table showing the collected individual results by material is in the Appendix (Table E-5) and is visually represented in Figure 5-1.

Table 5-6. Examples of Most Stringent Occupational Exposure Bands in Workers and Material Assignments Across Lung Endpoints in Rodents, using NOAELs, LOAELs or BMDLs from NTP and similar studies, OECD, and systematic literature searches.

Physicochemical Property Group*	Nanoscale or microscale with nanoscale uses (Table 2-6)**	Material	Most Stringent Band	Health Endpoint(s)
Fiber	NP	Multiwalled carbon nanotube	E	Lung Inflammation
Fiber	NP	Single walled carbon nanotube	D	Lung Inflammation
Fiber (Sol: L)	Micro***	Wollastonite calcium silicates	C	Lung Fibrosis
Sol (L), Tox (H)	Micro	Antimony trioxide	E	Lung Fibrosis
Sol (L), Tox (H)	Micro	Cobalt	E†	Lung Inflammation
Sol (L), Tox (H)	Micro	Gallium arsenide	E†	Lung Inflammation
PS, Tox (H)	Micro	Indium phosphide	E†	Lung Neoplasia; Fibrosis; Inflammation
Sol (VL), Tox (H)	Micro	Nickel (II) oxide	E†	Lung Inflammation
Sol (L), Tox (H)	Micro	Nickel subsulfide	E†	Lung Inflammation; Fibrosis
PS, High tox	Micro***	Sand blasting agents	C	Lung Fibrosis
Sol (VL), Tox (H)	Micro	Vanadium pentoxide	D	Lung Neoplasia
PSLT	NP	(C60) Fullerene	D	Lung Inflammation
PSLT	NP	(Au) Gold	E†	Lung Inflammation
PSLT	NP	Carbon black	E	Lung Inflammation
PSLT	NP	Cerium oxide	D	Lung Inflammation
PSLT	NP	Ferrous carbonate ($FeCO_3$, Siderite)	E	Lung Inflammation
PSLT	NP	Iron oxide (Fe_3O_4, Magnetite)	E	Lung Inflammation
PSLT	NP	Silicon dioxide, amorphous (Nano)	C	Lung Inflammation
PSLT	NP	Titanium dioxide (Nano)	C	Lung Inflammation
PSLT (Sol: VL)	Micro	Calcium chromate	B	Lung Inflammation; Fibrosis
Sol (L), Tox (L)	Micro	Molybdenum trioxide	B	Lung Inflammation
Sol (L)	Micro***	o-Chlorobenzalmalonitrile	D	Lung Inflammation
PSLT (Sol: L)	Micro***	Talc	D	Lung Neoplasia
PSLT	Micro	Titanium dioxide (Micro)	C	Lung Neoplasia
Soluble	NP	(Ag) Silver	E	Lung Inflammation
Soluble	NP	Zinc oxide	C	Lung Inflammation
Soluble	Micro	Chromium, hexavalent	C	Lung Inflammation
Sol (H)	Micro	Cobalt sulfate heptahydrate	E†	Lung Inflammation; Fibrosis
Sol (Med)	Micro	Ferrocene	B	Lung Inflammation
Sol (H)	Micro	Nickel sulfate hexahydrate	D	Lung Inflammation; Fibrosis

Sol (UK)	Micro***	ortho-Phthalaldehyde	E†	Lung Inflammation

Footnotes to Table 5-6:
* As relates to (four) broad biological mode-of-action groups (e.g., BSI [2007]; Kuempel et al. [2012]; SER [2012]). Solubility group defined in Table 2-7 (PS: poorly soluble; VL: very low; L: low; Med: medium: H: high: UK: unknown); assigned "soluble" if generally known to be soluble. [A difference between Tables 2-7 and 5-6 is that hexavalent chromium is reported to be soluble, while other forms of chromium are reported as poorly soluble]. Toxicity groups are based on definitions by Guest [1998]. High toxicity (Tox H) assigned here for poorly soluble materials with an OEL <1 mg/m^3 for the same or similar material, including OELs for non-nanoscale (bulk) materials.
** No nanoscale commercial form found.
*** High toxicity assumption based on analogy to crystalline silica.
† Adjusted points of departure below 0.001 mg/m^3, suggesting a hypothetical lower band F.

A qualitative view of exposure band results across endpoints and durations additionally illustrates the sparsity of data for understanding hazard; multiple endpoints were not available for several materials. Chronic studies were less common than sub-chronic, and multiple durations were also not available for many of the materials. For the 31 material groups that were banded (Table 5-6), only one exposure duration or response endpoint was available for 14 material groups, resulting in only one band. There were four material groups where information from multiple durations or endpoints resulted in the same band, indicated by a single point in Figure 5-1: antimony trioxide, indium phosphide, synthetic amorphous silica, and nanoscale titanium dioxide. These and other instances where multiple studies, endpoints, or durations resulted in the same band are indicated by the triangles (2 results) or squares (3+ results). No materials were placed in band A, which contains materials of the lowest hazard. Of the materials placed in band E (<0.01 mg/m^3), several materials would potentially fit into a possible additional "band F," which would include materials with adjusted points of departure below 0.001 mg/m^3: gold, cobalt, cobalt sulfate heptahydrate, gallium arsenide, indium phosphide, nickel (ii) oxide, nickel subsulfide, and ortho-phthalaldehyde (Table E-6). Some banding results are based on a microscale version of a material, and if an initial band is sought for a nanoscale version, it is recommended to use the next more stringent band, which is reflective of an adjustment of a factor of 10. For materials with both lung inflammation and lung neoplasia endpoints, the lung neoplasia band was less stringent than or equal to the lung inflammation band in all cases except talc and vanadium pentoxide. Durations of exposure range from 28 days to 2 years, and studies with durations of less than 28 days were not included because there is not currently a recommended adjustment for the point of departure. Figure 5-2 focuses the view on the nanomaterials with the highest commercial production volume [Schulte et al. 2019; WHO 2017], where these materials were placed in band C or higher. Banding results were available for all but two of the highest commercial production-volume materials, barium titanate and aluminum oxide.

Figure 5-1: Example Hazard Bands by Material from NTP and similar studies, OECD, and systematic literature searches

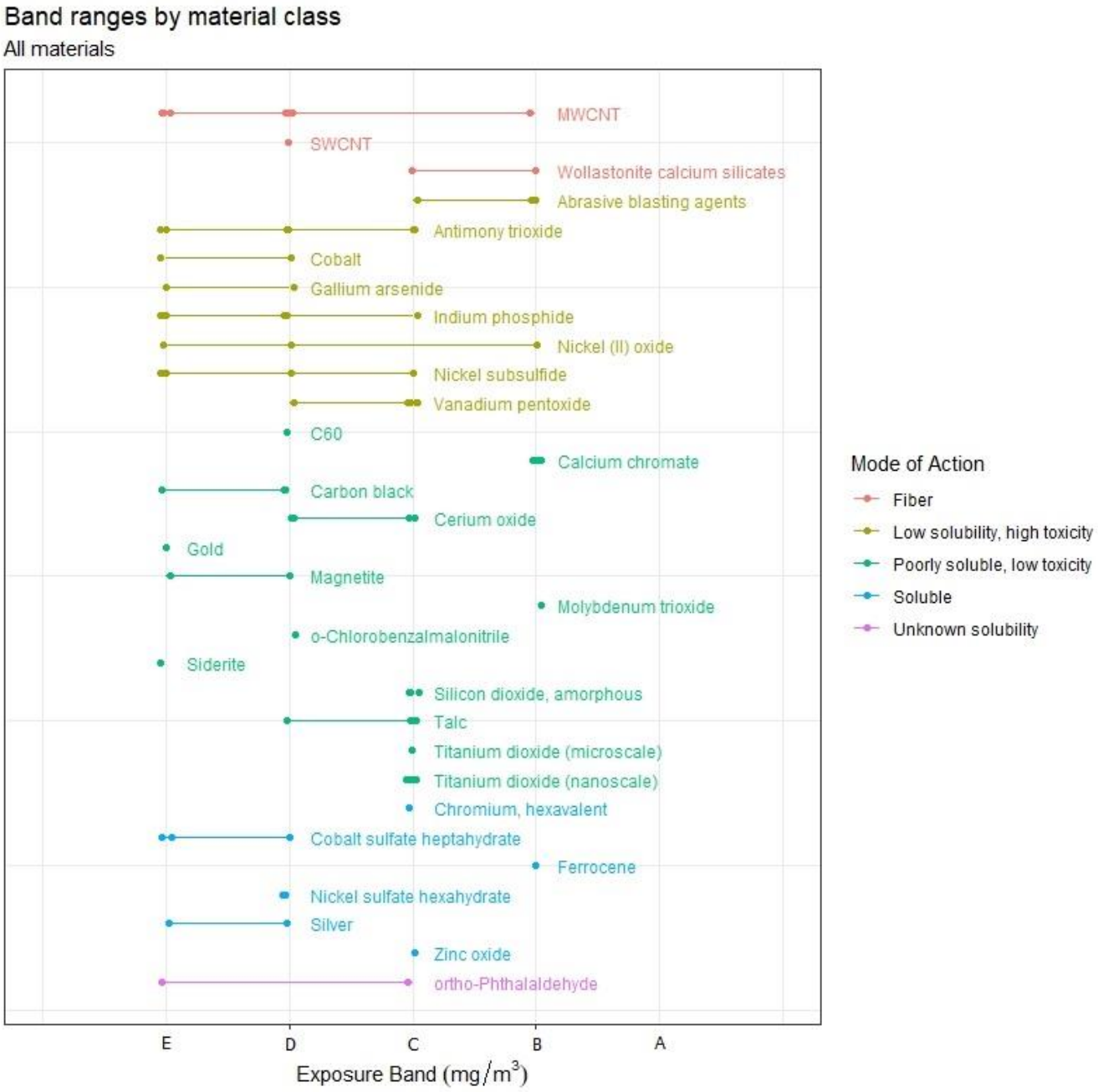

Figure 5-2: Example Hazard Bands for Nanomaterials with Highest Commercial Volume

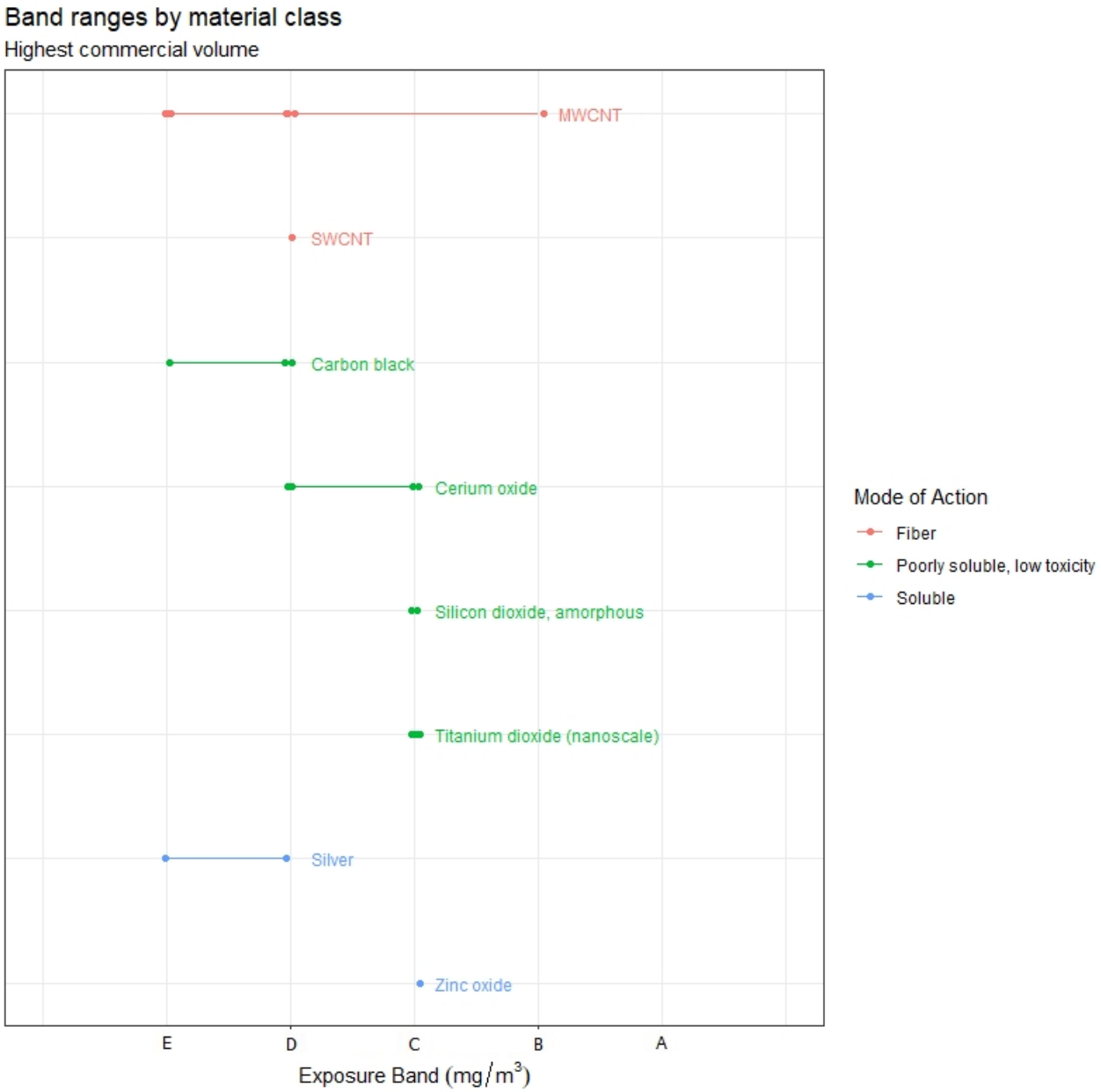

5.4 Categorical Occupational Exposure Limit Estimation

5.4.1 Acute Lung Inflammation

The categorical OEL estimates based on prevention of acute pulmonary inflammation (i.e., 0–3 days post-exposure) are similar in concept to the acute exposure guidance limits (AEGLs) [OEHHA 2008]. For those materials for which the pulmonary inflammation response was reversible after the end of exposure (which was generally the case in these data), the most closely aligned AEGLs would be for "severity level 1" (reversible irritation or mild effects).

The NIOSH recommended exposure limits (RELs) for acute effects are short-term exposure limits (STELs), which are typically 15-minute airborne exposure concentrations. These STELs are typically aimed at preventing respiratory irritant effects. Although these OEL estimates based on acute pulmonary inflammation differ in endpoint and exposure duration from the NIOSH STELs, they are illustrative of the relative potency of these groups of nanoscale and microscale materials with regard to an acute respiratory response of relevance to workers. It is important to note that OELs based on repeated exposure (sub-chronic or chronic) would likely be lower. For example, the acute OEL estimate for microscale TiO_2 in this example is 35 mg/m^3 for a single 8-hour TWA (Table 4-6), whereas the NIOSH REL for microscale (fine) TiO_2 is 2.4 mg/m^3 as an 8-hour TWA exposure for up to a 45-year working lifetime [NIOSH 2011]. In addition to the different exposure duration and response endpoints, the risk assessment methods and models also differed in these analyses, which had an influence on the OEL estimates. Generally, chronic exposure data are more applicable to risk estimation of the repeated exposures that may be experienced by workers than are shorter-term exposure data, as described in this example. Analysis of shorter-term exposure data are relevant to risk estimation of nanomaterials because chronic data are typically not available for most ENMs. Comparative potency analyses may be useful in estimating the risk of long-term exposure to nanomaterials based on comparison of shorter-term dose-response data of a well-studied benchmark material and a new ENM, along with longer-term data for the benchmark material (i.e., the "parallelogram approach") [Sobels 1977; Kuempel et al. 2012].

5.4.2 Sub-chronic/Chronic Lung Inflammation and Neoplasia

The categorical OEL estimates based on the lung inflammation or lung neoplasia responses in the NTP studies are assumed to be primarily for microscale materials (based on MMAD data), because the primary particle size data are typically not reported in the NTP database or reports. The estimates for these materials can serve as benchmarks for comparison to potency or PoD estimates from shorter-term *in vivo* or *in vitro* studies of other microscale or nanoscale particles. The limited data on the physicochemical properties and experimental factors

that are associated with materials in each potency group provide some information on important factors that influence the potency estimates, although these are too limited for current use in predictive modeling.

Most of the BMD and BMDL estimates are from rats, but some are from mice. This interspecies dose adjustment was addressed in the acute inflammation data of nanoscale and microscale particles by first estimating the deposited mass dose concentrations in the lungs (i.e., µg/g lung, which normalized the dose across species). That dose unit also allowed for normalization across route of exposure (because the dose metric µg/g lung was computed regardless of route of exposure to the lungs). Because the dosimetric adjustment of the single-day deposited lung dose of microscale airborne particles was shown above to be ~1 from rats to humans, it was considered reasonable to assume that the dosimetric adjustment of these inhaled particle exposures between rats and mice would also be ~1. Thus, the pooling of the rat and mouse data may have not had much effect on the grouping of potency estimates for these airborne particles. Data for both sexes of rodent species were also pooled, which seems reasonable because differences in male and female rodents were not expected, nor were they generally observed with regard to lung inflammation or neoplasia in response to inhaled respirable particles. The influence of these various experimental factors on the potency grouping or categorical OELs may be relatively small because most of the estimates were based on the rat sub-chronic or chronic data, but it is an area to explore regarding dose normalization across species in categorical analysis. In addition, these potency estimates (BMDs and BMDLs) from the NTP inhalation studies were found to be too sparse for grouping when those data were stratified by species and duration of exposure.

5.5 Use of Categorical OELs or OEBs in Control Banding

Hazard and control banding tools have been used for many years to make decisions on workplace exposure controls and to support other risk management and risk communication needs when substance-specific OELs are not available for chemicals in general [HSE 2009; UNECE 2015; OSHA 2012; NIOSH 2019] and, more recently, for nanomaterials [ISO 2014a; ANSES 2010; Van Duuren-Stuurman et al. 2012]. The control banding strategies for ENMs have been reviewed [Liguori et al. 2016; Dunn et al. 2018]. Control banding is a pragmatic tool that can be used to identify the types of engineering controls and performance capabilities to achieve the specified levels of exposure control (e.g., order-of-magnitude bands).

The typical control banding framework is a matrix consisting of hazard bands and exposure/emission potential bands to indicate the appropriate control band for a chemical substance, given its properties and production/use. Hazard bands are typically derived from toxicological data of adverse responses associated with acute or chronic exposures to hazardous substances in experimental animal studies, as well as data on humans when available.

Some hazard banding systems include associated exposure concentration ranges [HSE 2009; ANSES 2010; ISO 2014a], as discussed in ISO [2016] and Dunn et al. [2018]. Emission potential bands are qualitative descriptors of potential exposure levels, given the factors that influence exposure such as dustiness (propensity of the material to become airborne), type of process or task being performed, and amount of material being handled [ISO 2014a]. The level of hazard and the emission/exposure potential determine the control band and associated exposure control options (Figure 1-5). Categorical OELs or OEBs derived for ENMs, as described in this document, can provide the information needed in hazard banding for use in exposure control decision-making.

Note that the exposure concentration bands in Figure 1-5 are shifted lower by one order of magnitude compared to the bands in the NIOSH [2019] hazard banding framework. The exposure concentration ranges associated with ENMs (Section 5.3; Tables 5-6 and E-6) appear to be better aligned with the hazard bands in other frameworks [Brooke 1998; HSE 2009; ANSES 2010; ISO 2014a] and to the performance-based engineering controls shown in Figure 1-5 [Dunn et al. 2018]. These findings (Section 5.3; Table 5-6) suggest that the addition of a band "F" ($\leq$0.001 mg/m^3) would better reflect the data showing greater hazard potency of ENMs for adverse lung effects (inflammation and cancer), compared to the hazard potency of microscale particles.

5.6 Adjusting for Scale: Relationship between Nanoscale and Microscale Hazard

PSLT is the most highly represented material category in the data analyzed for OEBs in this report (Table 5-6). Studies of the PSLT materials TiO_2 and carbon black have shown that the nanoscale form of these materials elicits a greater pulmonary inflammation response in rodents than an equivalent mass of the microscale form of the same material [NIOSH 2011; Elder et al. 2006]. However, the quantitative evidence to estimate a potency factor for microscale to nanoscale particles is limited and is primarily focused on PSLT materials. The lung cancer incidence in rats after chronic inhalation exposure to TiO_2 was estimated to be approximately eight times greater for nanoscale than microscale particles at an equivalent mass dose. That factor of eight reflects the difference in the specific surface areas (m^2/g) of those materials. In other analyses of PSLT materials based on rodent lung tumors or inflammation response, a factor of two to four has been proposed to adjust the microscale OELs to nanoscale OELs [Gebel 2012; Gebel et al. 2014; BAuA 2015].

The NIOSH [2019] hazard banding guidance for ENMs is to adjust the OEB for a microscale particle to the next most stringent band (a factor of 10) to estimate an OEB for the nanoscale form of the chemical substance. That recommendation is based on the limited evidence for PSLT and the uncertainty in those estimates and about other types of nanoscale materials. Other hazard banding strategies also recommend adjusting the ENM OEB by one or

more bands more stringent when using data from the microscale form of the material (as discussed in Section 3.14 of NIOSH [2019]).

Findings in this report tend to support the current NIOSH [2019] recommendations for banding ENMs. Among the PSLT materials, the most protective OEB tend to be more stringent for nanoscale than for microscale PSLTs, by one to two bands (i.e., one to two orders of magnitude) (Table 5-5). On average, the band was D to E for nanoscale PSLT versus B to C for microscale PSLT. The data available for the other material classes are too sparse for assessment of particle size effects in those classes (Table 5-5).

In a separate analysis of the hazard potency estimates of ENMs based on summary data from the literature [Boots et al., submitted], the main predictor of hazard potency was chemical composition, whereas factors such as size or shape did not have statistically significant effects. In general, the physicochemical property data were more limited in the literature-based data [Boots et al., submitted] than in a previous analysis that used a smaller set of individual experimental datasets [Drew et al. 2017]. Thus, the addition of the literature-based data did not provide clear new evidence regarding the relationship between particle size and hazard potency. Those literature-based data are included in the more comprehensive dataset evaluated in this report.

In conclusion, the data analyzed in this report did not provide any clear evidence for altering the NIOSH-recommended default approach to banding ENMs [NIOSH 2019]. Exploring whether a factor of 10 is sufficient for a variety of materials, not just PSLT, is an area of future research.

5.7 Hazard Ranking

In looking qualitatively at potency rankings across assays, there are some commonalities in material types despite the lack of identical materials. Metals, such as indium phosphide, tend to be more potent than metal oxides; metal oxides tend to be more potent than carbon nanotubes, and crystalline silica tends to have a potency similar to carbon nanotubes. Particulate TiO_2 tends to be less potent than other materials, but modifications to TiO_2 such as the nanobelts tend to increase its potency (Table 5-7). Not all metal oxides can be considered equally, however, as zinc oxide tended to have little variability across its potency estimates whereas titanium dioxide potency estimates were more variable. These findings suggest some concordance across assays, which tends to support the potential utility of *in vitro* and shorter-term *in vivo* studies to predict adverse lung effects in chronic bioassays in rodents. The low potency of microscale (fine) TiO_2 relative to other materials is consistent with previous findings for TiO_2 and other PSLT [NIOSH 2011].

Tables 5-2 through 5-5 provide a set of empirical-based estimates of OEBs across a range of nanoscale and microscale materials. As more data become available, these initial estimates could be reevaluated, ideally through the use of a predictive model. The currently available data are still too limited to develop a validated

model to predict *in vivo* toxicity based on only physicochemical data or *in vitro* assay results, although some proof-of-concept and limited-application models have been developed to date [Burello and Worth 2011b, 2015; Gernand and Casman 2014; Drew et al. 2017].

Table 5-7: Relative rankings of material potencies (BMD) across assays for adverse pulmonary endpoints from NIOSH/ENPRA/CIIT/NanoGo and NTP histopathology

	Neoplasia, Chronic	**Fibrosis, Subchronic to Chronic**	**Subchronic to Chronic Inflammation**	***in vivo* Acute to Subchronic Inflammation [Drew et al. 2017]**	***in vitro* Inflammation, Acute**
Most Potent	Indium phosphide	Indium Phosphide	Cobalt sulfate heptahydrate	ZnO 10% Fe	ZnO
	Cobalt	Cobalt sulfate hexahydrate	Indium phosphide	ZnO Pure	TiO_2 Nanobelt
	Vanadium pentoxide	Antimony trioxide	Gallium arsenide	ZnO 1% Fe	Original MWCNT
	Gallium arsenide	Abrasive Blasting Agents: Blasting Sand	Cobalt	Fe_3O_4 pure	Crystalline Silica
	Cobalt sulfate heptahydrate	Nickel subsulfide	Nickel (II) oxide	TiO_2 Long Nanobelt	Purified MWCNT
	Nickel subsulfide	Vanadium pentoxide	Nickel subsulfide	TiO_2 Short Nanobelt	Functionalized MWCNT
	Wollastonite calcium silicates	Talc	Antimony trioxide	Short MWCNT	
	Nickel (II) oxide	ortho-Phthalaldehyde	Vanadium pentoxide	Crystalline Silica	
	Carbon Black	Cobalt	Abrasive Blasting Agents: Blasting Sand	Bare MWCNT	
	Talc	Nickel (II) oxide	1020 Long Multiwalled Carbon Nanotube	Long MWCNT	
	Antimony trioxide	Abrasive Blasting Agents: Specular Hematite	Nickel sulfate hexahydrate	Carboxylated MWCNT	
	Molybdenum trioxide		Talc	Ultrafine TiO_2	
	Fine TiO_2		ortho-Phthalaldehyde	Fine TiO_2	
			Abrasive blasting agents (garnet)		
			Abrasive Blasting Agents: Specular Hematite		
			Abrasive blasting agents (coal slag)		
			Molybdenum trioxide		
Least Potent			Ferrocene		

5.8 Recommendations

The objectives of this report are to describe state-of-the-science approaches for developing cOELs or OEBs for ENMs that lack sufficient experimental data to develop substance-specific OELs. Current approaches have been described herein. This information is intended for occupational safety and health professionals and researchers assessing the data and methods available to estimate the potential occupational health risks of exposure to airborne ENMs.

Several options are available for estimating safe workplace exposure limits (Figure 1-4). OELs have been derived for an increasing number of ENMs (reviewed in Mihalache et al. [2017]). For these materials, the OEL can be used directly to evaluate and select exposure control measures based on performance (Figure 1-5). For ENMs without specific OELs, the available literature can be used to identify a PoD as a starting point to estimating an OEL or OEB. Generally speaking, derivation of an OEL requires a greater level of evidence regarding the biological mode of action as well as data describing the dose-response relationship in standard rodent bioassays [NIOSH 2020]. Generally, fewer data are needed to estimate an OEB, although a PoD estimate from a standard toxicology study is still required [NIOSH 2019]. If a PoD estimate is not available for the specific nanomaterial, data from a microscale form of the material can be used along with a UF adjustment, which is currently recommended as a factor of 10 (i.e., move material assignment one band lower) [NIOSH 2019]. If these minimum data are not available to estimate an OEL or OEB, then prudent occupational health practices should be followed until sufficient data are available for re-evaluation of available evidence [Schulte and Salamanca-Buentello 2007].

In addition, the OEB estimates presented in the current study (Tables 5-2 through 5-4) provide results based on the application of standard methods and health endpoints of relevance to workers. These OEB estimates could be used as initial OEB estimates for similar nanoscale materials, including through read-across methods. As described earlier, if only data on a microscale form are used, then an adjustment factor of 10 is recommended on the basis of current data (i.e., the OEB assigned would become one band more stringent for the nanoscale form) [NIOSH 2019].

The findings of these analyses lead to the following recommendations:

- Examine the evidence for the utility of a lower order-of-magnitude band below the current band E in the NIOSH [2019] hazard banding guidance.

- Extend coordination among NIOSH and external researchers to develop a more comprehensive database for further analyses, e.g., NanoInformaTIX (http://www.nanoinformatix.eu/).
- Utilize a level of evidence–based approach to deriving OELs or OEBs for ENMs (Figure 1-4).

Comparing the OEBs in Table 5-1 and Figure 1-5 shows a shift in the order-of-magnitude OEBs toward higher OEBs in the NIOSH recommendations [NIOSH 2019], compared to those proposed in previous hazard and control banding frameworks (summarized in Figure 1-5). Performance-based controls have been associated with those order-of-magnitude exposure bands in Figure 1-5. In addition, none of the nanoscale or microscale particles evaluated in these analyses were assigned to the NIOSH band A, which indicates a lack of utility for that band in evaluating the hazard potency of these materials. However, many nanomaterials as well as microscale materials were assigned to band E, and further evaluation of hazard potency within that band would be useful.

5.9 Conclusions and Next Steps

The data analysis framework developed and applied in this document shows progress toward achieving the ultimate goal of a predictive model for evidence-based hazard categorization. In general, the ENM data available for analysis, as reported here, tended to be for a small set of materials, such as TiO_2 and CNTs. A fully validated grouping framework will require a more comprehensive database—with wider coverage of data to include more ENM types—and further model development and cross-validation. Such a comprehensive set of experimental data would include a core set of physicochemical properties and an array of *in vitro* dose-response assays, as well as comprehensive information for a varied set of microscale and nanoscale benchmark materials ideally representing the universe of materials, including acute to chronic *in vivo* assays and associated *in vitro* assays. Several datasets have been created or identified to meet these requirements (Appendix F).

These analyses generated useful insights into understanding the health hazards of numerous materials, both nanoscale and microscale. The goal of identifying groups of materials with similar potency appears reachable from the findings in this document, as does the goal of predicting the health hazard of a new material for which experimental data are lacking. However, further data and analyses are needed to develop predictive models of hazard potency across a range of nanomaterials, including comparison to microscale benchmark materials. Collaboration, both locally and globally, through data sharing and validation of methods would facilitate the development of evidence-based approaches for accurately categorizing materials and protecting the health of workers.

Page intentionally left blank

6 References

ACGIH [2001]. Silver and compounds. In: Documentation of threshold limit values and biological exposure indices. 7th ed. Vol. 1. Cincinnati, OH: American Conference of Governmental Industrial Hygienists.

ACGIH [2014]. Threshold Limit Values for Chemical Substances and Physical Agents and Biological Exposure Indices. Cincinnati, OH: American Conference of Governmental Industrial Hygienists.

Ader AW, Farris JP, Ku RH [2005]. Occupational health categorization and compound handling practice systems—roots, application and future. Chem Health Safety *12*:20–26.

ANSES [2010]. Development of a specific control banding tool for nanomaterials. Maisons-Alfort Cedex, France: Agence nationale de sécurité sanitaire, the French Agency for Food, Environmental and Occupational Health & Safety. Request no. 2008-SA-0407, https://www.anses.fr/en/system/files/AP2008sa0407RaEN.pdf.

Antonini JM, Roberts JR, Clarke RW [2001]. Strain-related differences of nonspecific respiratory defense mechanisms in rats using a pulmonary infectivity model. Inhal Toxicol *13*(1):85-102. doi: 10.1080/08958370119500. PMID: 11153062.

ARA [2011]. Multiple-path particle deposition (MPPD 2.1): a model for human and rat airway particle dosimetry. Raleigh, NC: Applied Research Associates, Inc.

ARA [2015]. Multiple-path particle dosimetry model (MPPD 3.04). Raleigh, NC: Applied Research Associates, Inc. Available from: http://www.ara.com/mppd/.

Arts JH, Hadi M, Irfan MA, Keene AM, Kreiling R, Lyon D, Maier M, Michel K, Petry T, Sauer UG, Warheit D, Wiench K, Wohlleben W, Landsiedel R [2015]. A decision-making framework for the grouping and testing of nanomaterials (DF4nanoGrouping). Regul Toxicol Pharmacol *71*(2 Suppl):S1–S27.

Arts JH, Irfan MA, Keene AM, Kreiling R, Lyon D, Maier M, Michel K, Neubauer N, Petry T, Sauer UG, Warheit D, Wiench K, Wohlleben W, Landsiedel R [2016]. Case studies putting the decision-making framework for the grouping and testing of nanomaterials (DF4nanoGrouping) into practice. Regul Toxicol Pharmacol *76*:234–261.

Aschberger K, Johnston HJ, Stone V, Aitken RJ, Hankin SM, Peters SA [2010]. Review of carbon nanotubes toxicity and exposure — Appraisal of human health risk assessment based on open literature. Crit Rev Toxicol *40*(9):759–790.

Aschberger K, Micheletti C, Sokull-Klüttgen B, Christensen FM [2011]. Analysis of currently available data for characterising the risk of engineered nanomaterials to the environment and human health — Lessons learned from four case studies. Environ Int *37*(6):1143–1156.

Aschberger K, Asturiol D, Lamon L, Richarz A, Gerloff K, Worth A [2019]. Grouping of multi-walled carbon nanotubes to read-across genotoxicity: a case study to evaluate the applicability of regulatory guidance. Comput Toxicol *9*:22–35.

Asgharian B, Price OT, Oldham M, Chen LC, Saunders EL, Gordon T, Mikheev VB, Minard KR, Teeguarden JG [2014]. Computational modeling of nanoscale and microscale particle deposition, retention and dosimetry in the mouse respiratory tract. Inhal Toxicol *26*(14):829–842.

BAuA [2013]. Bundesanstalt für Arbeitsschutz und Arbeitsmedizin. Bekanntmachung zu Gefahrstoffen. Hergestellte Nanomatierialien, the German Federal Institute for Occupational Safety and Health. Announcement regarding hazardous substances. Manufactured nanomaterials: BekGS 527. BMBl *25*:498–511, http://www.baua.de/de/Themen-von-A-Z/Gefahrstoffe/TRGS/Bekanntmachung-527.html.

BAuA [2015]. Assessment criterion (reference value) for nanoscaled GBP. Version 3 of June 2015. Committee on Hazardous Substances—AGS Management— Bundesanstalt für Arbeitsschutz und Arbeitsmedizin (BAuA), http://www.baua.de/ags.

Bermudez E, Mangum JB, Asgharian B, Wong BA, Reverdy EE, Janszen DB, Hext PM, Warheit DB, Everitt JI [2002]. Long-term pulmonary responses of three laboratory rodent species to subchronic inhalation of pigmentary titanium dioxide particles. Toxicol Sci *70*:86–97.

Bermudez E, Mangum JB, Wong BA, Asgharian B, Hext PM, Warheit DB, Everitt JI [2004]. Pulmonary responses of mice, rats, and hamsters to subchronic inhalation of ultrafine titanium dioxide particles. Toxicol Sci *77*:347–357.

Bonner JC, Silva RM, Taylor AJ, Brown JM, Hilderbrand SC, Castranova V, Porter D, Elder A, Oberdörster G, Harkema JR, Bramble LA, Kavanagh TJ, Botta D, Nel A, Pinkerton KE [2013]. Interlaboratory evaluation of rodent pulmonary responses to engineered nanomaterials: the NIEHS Nano GO Consortium. Environ Health Perspect *121*(6):676–682.

Boots TE, Kogel A, Drew NM, Kuempel ED. [Submitted]. Utilizing literature-based rodent toxicology data to derive potency estimates for quantitative risk assessment.

Bos PM, Gottardo S, Scott-Fordsmand JJ, van Tongeren M, Semenzin E, Fernandes TF, Hristozov D, Hund-Rinke K, Hunt N, Irfan MA, Landsiedel R, Peijnenburg WJ, Sánchez Jiménez A, van Kesteren PC, Oomen AG [2015]. The MARINA risk assessment strategy: a flexible strategy for efficient information collection and risk assessment of nanomaterials. Int J Environ Res Public Health *12*(12):15007–15021.

Braakhuis HM, Oomen AG, Cassee FR [2016]. Grouping nanomaterials to predict their potential to induce pulmonary inflammation. Toxicol Appl Pharmacol *299*:3–7.

Breiman L, Freidman JH, Olshen RA, Stone CJ [1984]. Classification and regression trees. New York: Chapman and Hall.

Breiman L [2001]. Random forests. Machine Learning *45*(1):5–32.

Brooke IM [1998]. A UK scheme to help small firms control health risks from chemicals: toxicological considerations. Ann Occup Hyg *42*(6):377–390.

Brouwer DH [2012]. Control banding approaches for nanomaterials. Ann Occup Hyg *56*(5):506–514.

BSI [2007]. Nanotechnologies, part 2. PD 6699-2:2007: guide to safe handling and disposal of manufactured nanomaterials. London: British Standards Institution.

Burello E, Worth AP [2011a]. QSAR modeling of nanomaterials. Nanomed Nanobiotechnol *3*:298–306.

Burello E, Worth AP [2011b]. A theoretical framework for predicting the oxidative stress potential of oxide nanoparticles. Nanotoxicology *5*(2):228–235.

Burello E, Worth AP [2015]. A rule for designing safer nanomaterials: do not interfere with the cellular redox equilibrium. Nanotoxicology *9*(Suppl 1):116–117.

Chen C, Liaw A, Breiman L [2004]. Using random forest to learn unbalanced data. Technical report 666. Berkeley, CA: University of California at Berkeley, Department of Statistics, http://statistics.berkeley.edu/sites/default/files/tech-reports/666.pdf.

Cohen Y, Rallo R, Liu R, Liu HH [2013]. In silico analysis of nanomaterials hazard and risk. Acc Chem Res *46*(3):802–812.

Cote I, Anastas PT, Birnbaum LS, Clark RM, Dix DJ, Edwards SW, Preuss PW [2012]. Advancing the next generation of health risk assessment. Environ Health Perspect *120*:1499–1502.

Crump KS [1984]. A new method for determining allowable daily intakes. Fund Appl Toxicol *4*:854–871.

Crump KS [1995]. Calculation of benchmark doses from continuous data. Risk Analysis *15*(1).

Crump KS [2002]. Critical issues in benchmark calculations from continuous data. Crit Rev Toxicol *32*(3):133–153.

Crump KS, Chen C, Louis TA [2010]. The future use of in vitro data in risk assessment to set human exposure standards: challenging problems and familiar solutions. Environ Health Perspect *118*(10):1350–1354.

Crystal RG, Gadek JE, Ferrans VJ, Fulmer JD, Line BR, Hunninghake GW [1981]. Interstitial lung disease: current concepts of pathogenesis, staging, and therapy. Am J Med *70*:542–568.

Dankovic DA, Naumann BD, Maier A, Dourson ML, Levy LS [2015]. The scientific basis of uncertainty factors used in setting occupational exposure limits. J Occup Environ Hyg *12*(Suppl 1):S55–S68.

Davidson SE [2016]. Benchmark dose modeling with covariates for nanomaterials: mathematics. Paper 3, http://www.exhibit.xavier.edu/undergrad_mathematics/3.

Degenhardt F, Seifert S, Szymczak S [2019]. Evaluation of variable selection methods for random forests and omics data sets. Brief Bioinform *20*(2):492–503, doi:10.1093/bib/bbx124.

Dekkers S, Ma-Hock L, Lynch I, Russ M, Miller MR, Schins RPF, Keller J, Römer I, Küttler K, Strauss V, De Jong WH, Landsiedel R, Cassee FR [2018]. Differences in the toxicity of cerium dioxide nanomaterials after inhalation can be explained by lung deposition, animal species and nanoforms. Inhal Toxicol *30*(7–8):273–286, doi:10.1080/08958378.2018.1516834.

Donaldson K, Borm PJ, Oberdörster G, Pinkerton KE, Stone V, Tran CL [2008]. Concordance between in vitro and in vivo dosimetry in the proinflammatory effects of low-toxicity, low-solubility particles: the key role of the proximal alveolar region. Inhal Toxicol *20*:53–62.

Drew N, Kuempel E, Pei Y, Yang F [2017]. A quantitative framework to group nanoscale and microscale particles by hazard potency to derive occupational exposure limits: Proof of concept evaluation. Reg Tox Pharm *89*:253–267.

Drew NM, Kuempel ED [2018]. Relative ranking of nanomaterial potencies across toxicological assays and endpoint. Toxicology and Risk Assessment Conference, April 24, Cincinnati, Ohio.

Dunn KH, Eastlake AC, Story M, Kuempel ED [2018]. Control banding tools for engineered nanoparticles: what the practitioner needs to know. Ann Work Expo Health *62*(3):362–388, https://doi.org/10.1093/annweh/wxy002.

Eastlake A, Zumwalde R, Geraci C [2016]. Can control banding be useful for the safe handling of nanomaterials? A systematic review. J Nanopart Res *18*:1–24.

ECHA [2012]. Guidance on information requirements and chemicals safety assessment. Chapter R.8: Characterisation of dose [concentration]-response for human health. Version 2.1. Reference No. ECHA-2010-G-19-EN. Helskinki, Finland: European Chemicals Agency (ECHA), http://echa.europa.eu/.

ECHA [2017]. Read-Across Assessment Framework (RAAF). ECHA-17-R-01-EN. Helsinki, Finland: European Chemicals Agency (ECHA).

ECHA [2019]. Guidance on information requirements and chemical safety assessment. Appendix R.6-1 for nanoforms applicable to the guidance on QSARs and grouping of chemicals. Version 2.0. ECHA-19-H-15-EN. Helsinki, Finland: European Chemicals Agency (ECHA).

Elder A, Gelein R, Finkelstein JN, Driscoll KE, Harkema J, Oberdörster G [2005]. Effects of subchronically inhaled carbon black in three species. I. Retention kinetics, lung inflammation, and histopathology. Toxicol Sci *88*(2):614–629.

ENPRA [2013]. Final report summary—ENPRA (Risk Assessment of Engineered Nanoparticles). April 29, 2013. Engineered NanoParticle Risk Assessment. European Commission Community Research and Development Information Service, http://cordis.europa.eu/result/rcn/56040_en.html.

Environmental Defense–DuPont Nano Partnership [2007]. Nano risk framework. Washington, DC: Environmental Defense Fund, https://nanotech.law.asu.edu/Documents/2011/06/6496_Nano%20Risk%20Framework_534_2973.pdf.

Fox EW, Hill RA, Leibowitz SG, Olsen AR, Thornburgh DJ, Weber MH [2017]. Assessing the accuracy and stability of variable selection methods for random forest modeling in ecology. Environ Monit Assess *189*(7), doi:10.1007/s10661-017-6025-0.

Gamo M, ed. [2011]. Risk assessment of manufactured nanomaterials: Titanium dioxide (TiO2). Final report issued on July 22, 2011. New Energy and Industrial Technology Development Organization (NEDO) project

(P06041) "Research and Development of Nanoparticle Characterization Methods." National Institute of Advanced Industrial Science and Technology (AIST). http://en.aist-riss.jp/assessment/2721/

Gangwal S, Brown JS, Wang A, Houck KA, Dix DJ, Kavlock RJ, Hubal EA [2011]. Informing selection of nanomaterial concentrations for ToxCast in vitro testing based on occupational exposure potential. Environ Health Perspect *119*:1539–1546.

Gebel T [2012]. Small difference in carcinogenic potency between GBP nanomaterials and GBP nanomaterials. Arch Toxicol *86*:995–1007, doi:10.1007/s00204-012-0835-1.

Gebel T [2013]. Response to Morfeld 2013: commentary to Gebel 2012: a quantitative review should apply meta-analytical methods. Arch Toxicol *87*(5):923–924.

Gebel T, Foth H, Damm G, Freyberger A, Kramer PJ, Lilienblum W, Röhl C, Schupp T, Weiss C, Wollin KM, Hengstler JG [2014]. Manufactured nanomaterials: categorization and approaches to hazard assessment. Arch Toxicol *88*(12):2191–2211.

Gernand JM, Casman EA [2014]. A meta-analysis of carbon nanotube pulmonary toxicity studies—how physical dimensions and impurities affect the toxicity of carbon nanotubes. Risk Anal *34*(3):583–597.

Gernand JM, Casman EA [2016]. Nanoparticle characteristic interaction effects on pulmonary toxicity: a random forest modeling framework to compare risks of nanomaterial variants, J Risk Uncertainty Engin Sys *2*(2):021002, doi:10.1115/1.4031216.

Gkika DA, Nolan JW, Vansant EF, Vordos N, Kontogoulidou C, Mitropoulos AC, Cool P, Braet J [2017]. A framework for health-related nanomaterial grouping. Biochim Biophys Acta *1861*(6):1478–1485, https://www.sciencedirect.com/science/article/pii/S0304416516303038.

Godwin H, Nameth C, Avery D, Bergeson LL, Bernard D, Beryt E, Boyes W, Brown S, Clippinger AJ, Cohen Y, Doa M, Hendren CO, Holden P, Houck K, Kane AB, Klaessig F, Kodas T, Landsiedel R, Lynch I, Malloy T, Miller MB, Muller J, Oberdorster G, Petersen EJ, Pleus RC, Sayre P, Stone V, Sullivan KM, Tentschert J, Wallis P, Nel AE [2015]. Nanomaterial categorization for assessing risk potential to facilitate regulatory decision-making. ACS Nano *9*(4):3409–3417.

Gordon SC, Butala JH, Carter JM, Elder A, Gordon T, Gray G, Sayre PG, Schulte PA, Tsai CS, West J [2014]. Workshop report: strategies for setting occupational exposure limits for engineered nanomaterials. Regul Toxicol Pharmacol *68*(3):305–311.

Gregoratto D, Bailey MR, Marsh JW [2010]. Modelling particle retention in the alveolar-interstitial region of the human lungs. J Radiol Prot *30*(3):491–512.

Grieger KD, Redmon JH, Money ES, Widder MW, van der Schalie WH, Beaulieu SM, Womak D [2015]. A relative ranking approach for nano-enabled applications to improve risk-based decision making: a case study of Army materiel. Environ Syst Decis *35*:42–53.

Guest I [1998]. The Chemical Industries Association guidance on allocationg occupational exposure bands. Ann Occup Hyg *42*(6):407-411.

Harper B, Thomas D, Chikkagoudar S, Baker N, Tang K, Heredia-Langner A, Lins R, Harper S [2015]. Comparative hazard analysis and toxicological modeling of diverse nanomaterials using the embryonic zebrafish (EZ) metric of toxicity. J Nanopart Res *17*:250.

Henry BJ, Schaper KL [1990]. PPG's safety and health index system: a 10-year update of an in-plant hazardous materials identification system and its relationship to finished product labeling, industrial hygiene and medical programs. Am Ind Hyg Assoc J *51*:475–484.

Heinrich U, Fuhst R, Rittinghausen S, Creutzenberg O, Bellmann B, Koch W, Levsen K [1995]. Chronic inhalation exposure of Wistar rats and two different strains of mice to diesel engine exhaust, carbon black, and titanium dioxide. Inhal Toxicol *7*(4):533–556.

Höck J, Epprecht T, Furer E, Gautschi M, Hofmann H, Hohener K, Knauer K, Krug H, Limbaugh L, Gehr P, et al. [2013]. Guidelines on the precautionary matrix for synthetic nanomaterials, verison 3.0. Federal Office for Public Health and Federal Office for the Environment, Berne.

Hristozov D, Zabeo A, Alstrup Jensen K, Gottardo S, Isigonis P, Maccalman L, Critto A, Marcomini A [2016]. Demonstration of a modelling-based multi-criteria decision analysis procedure for prioritization of occupational risks from manufactured nanomaterials. Nanotoxicology *10*(9):1215–1228.

Hristozov DR, Zabeo A, Foran C, Isigonis P, Critto A, Marcomini A, Linkov I [2014]. A weight of evidence approach for hazard screening of engineered nanomaterials. Nanotoxicology *8*(1):72–87.

HSE [2009]. The technical basis for COSHH essentials: easy steps to control chemicals. Health and Safety Executive, http://www.hse.gov.uk/pubns/guidance/coshh-technical-basis.pdf.

Hubbs AF, Minhas NS, Jones W, Greskevitch M, Battelli LA, Porter DW, Goldsmith WT, Frazer D, Landsittel DP, Ma JYC, Barger M, Hill K, Schwegler-Berry D, Robinson VA, Castranova V [2001]. Comparative pulmonary toxicity of 6 abrasive blasting agents. Tox Sci *61*(1):135–143.

IARC [2010]. IARC monographs on the evaluation of carcinogenic risks to humans. Volume 93. Carbon black, titanium dioxide, and talc. International Agency for Research on Cancer, World Health Organization. Geneva, Switzerland: WHO Press.

ICRP [1994]. Human respiratory tract model for radiological protection: a report of a task group of the International Commission on Radiological Protection. ICRP Publication 66. Ann ICRP *24*(1–3):1–482.

ICRP [2002]. Annals of the ICRP (The International Commission on Radiological Protection). In: Valentin J, ed. Basic Anatomical and Physiological Data for Use in Radiological Protection: Reference Values. ICRP Publication 89. Oxford, U.K.: Pergamon. Available from: https://doi.org/10.1016/S0146-6453(03)00002-2.

ICRP [2015]. Occupational intakes of radionuclides: part 1. The International Commission on Radiological Protection (ICRP), Publication 130. Ann ICRP *44*(2).

ILSI (International Life Sciences Institute) [2000]. The relevance of the rat lung response to particle overload for human risk assessment: a workshop consensus report. Inhal Toxicol *12*:1–17.

ISO [2007]. ISO/TR 27628:2007. Workplace atmospheres—ultrafine, nanoparticle and nano-structured aerosols—inhalation exposure characterization and assessment. Geneva, Switzerland: International Organization for Standardization.

ISO [2014a]. ISO/TS 12901-2:2014. Nanotechnologies—occupational risk management applied to engineered nanomaterials. Part 2: use of the control banding approach. Geneva, Switzerland: International Organization for Standardization.

ISO [2014b]. ISO/TS 80004-2. Terminology and definitions for nano-objects—nanoparticle, nanofibre and nanoplate [draft]. Geneva, Switzerland: International Organization for Standardization.

ISO [2016]. ISO/TR 18637. Nanotechnologies—overview of available frameworks for the development of occupational exposure limits and bands for nano-objects and their aggregates and agglomerates (NOAAs). Published Nov. 21. Geneva, Switzerland: International Organization for Standardization.

JSOH (The Japan Society for Occupational Health) [2013]. Recommendation of occupational exposure limits (2013–2014). J Occup Health, pp. 421–439.

Kobayashi N1, Naya M, Endoh S, Maru J, Yamamoto K, Nakanishi J [2009]. Comparative pulmonary toxicity study of nano-TiO(2) particles of different sizes and agglomerations in rats: different short- and long-term post-instillation results. Toxicology *264*(1–2):110–118.

Kuempel ED, O'Flaherty EJ, Stayner LT, Smith RJ, Green FHY, Vallyathan V [2001]. A biomathematical model of particle clearance and retention in the lungs of coal miners: part I. Model development. Regul Toxicol Pharmacol *34*(1):69–87.

Kuempel ED, Tran CL, Castranova V, Bailer AJ [2006]. Lung dosimetry and risk assessment of nanoparticles: evaluating and extending current models in rats and humans. Inhal Toxicol *18*(10):717–724.

Kuempel ED, Castranova V, Geraci CL, Schulte PA [2012]. Development of risk-based nanomaterial groups for occupational exposure control. J Nanopart Res *14*:1029.

Kuempel ED, Sweeney LM, Morris JB, Jarabek AM [2015]. Advances in inhalation dosimetry models and methods for occupational risk assessment and exposure limit derivation. J Occup Environ Hyg *12*(Suppl 1):S18–S40.

Lamon L, Asturiol D, Richarz A, Joossens E, Graepel R, Aschberger K, Worth A (2018). Grouping of nanomaterials to read-across hazard endpoints: from data collection to assessment of the grouping hypothesis by application of chemoinformatic techniques. Particle Fibre Toxicol *15*:37, https://doi.org/10.1186/s12989-018-0273-1.

Lampe BJ, Fuller E, Senthilkumar P, Kuppusamy B (2018). A quantitative comparison of points of departure between 28-day and 90-day repeated dose studies with a proposed extrapolation factor. Reg Tox Pharm *92*:189–200.

Landsiedel R, Ma-Hock L, Wiench K, Wohlleben W, Sauer UG [2017]. Safety assessment of nanomaterials using an advance decision-making framework, the DF4nanoGrouping. JNR *19*:171.

Lee KP, Trochimowicz HJ, Reinhardt CF [1985]. Pulmonary response of rats exposed to titanium dioxide (TiO2) by inhalation for two years. Toxicol Appl Pharmacol *79*:179–192.

Li JG, Li QN, Xu JY, Cai XQ, Liu RL, Li YJ, Ma JF, Li WX [2009]. The pulmonary toxicity of multi-wall carbon nanotubes in mice 30 and 60 days after inhalation exposure. J Nanosci Nanotechnol *9*(2):1384–1387.

Liguori B, Hansen SF, Baun A, Jensen KA [2016]. Control banding tools for occupational exposure assessment of nanomaterials—ready for use in a regulatory context? NanoImpact 2:1–17.

Liu R, Rallo R, George S, Ji Z, Nair S, Nel AE, Cohen Y [2011]. Classification NanoSAR development for cytotoxicity of metal oxide nanoparticles. Small *7*(8):1118–1126.

Liu R, Zhang HY, Ji ZX, Rallo R, Xia T, Chang CH, Nel A, Cohen Y [2013a]. Development of structure-activity relationship for metal oxide nanoparticles. Nanoscale *5*(12):5644–5653.

Liu R, Rallo R, Weissleder R, Tassa C, Shaw S, Cohen Y [2013b]. Nano-SAR development for bioactivity of nanoparticles with considerations of decision boundaries. Small *9*(9):1842–1852, doi:10.1002/smll.201201903.

Ma-Hock L, Treumann S, Strauss V, Brill S, Luizi F, Mertler M, Wiench K, Gamer AO, Ravenzwaay B, Landsiedel R [2009]. Inhalation toxicity of multi-wall carbon nanotubes in rats exposed for 3 months. Toxicol Sci *112*(2):468–481.

Maier MS [2011]. Setting occupational exposure limits for unstudied pharmaceutical intermediates using an in vitro parallelogram approach. Toxicol Mech Methods *21*(2):76–85.

MATLAB [2016]. MATLAB and statistics toolbox, release 2016a. Natick, MA: The MathWorks, Inc.

Martin TR, Ganesh R, Maunder RJ, Springmeyer SC [1985]. The effects of chronic bronchitis and chronic air-flow obstruction on lung cell populations recovered by bronchoalveolar lavage. Am Rev Respir Dis *132*:254–260.

Mauderly JL [1997]. Relevance of particle-induced rat lung tumors for assessing lung carcinogenic hazard and human lung cancer risk. Environ Health Perspect *105*(Suppl 5):1337–1346.

Mercer RR, Russell ML, Roggli VL, Crapo JD [1994]. Cell number and distribution in human and rat airways. Am J Respir Cell Mol Biol *10*:613–624.

Mihalache R, Verbeek J, Graczyk H, Murashov V, van Broekhuizen P [2017]. Occupational exposure limits for manufactured nanomaterials, a systematic review. Nanotoxicology *9*:1–13.

Monteiller C, Tran L, MacNee W, Faux S, Jones A, Miller B, Donaldson K [2007]. The pro-inflammatory effects of low-toxicity low-solubility particles, nanoparticles and fine particles, on epithelial cells in vitro: the role of surface area. Occup Environ Med *64*(9):609–615.

Morfeld P [2013] Commentary to Gebel 2012: a quantitative review should apply meta-analytical methods—and this applies also to quantitative toxicological reviews. Arch Toxicol 87(11):2023–2025.

Morfeld P, Bruch J, Levy L, Ngiewih Y, Chaudhuri I, Muranko HJ, Myerson R, McCunney RJ [2015]. Translational toxicology in setting occupational exposure limits for dusts and hazard classification: a critical evaluation of a recent approach to translate dust overload findings from rats to humans. Part Fibre Toxicol*12*:3.

Morrow PE [1988]. Possible mechanisms to explain dust overloading of the lungs. Fund Appl Toxicol *10*:369–384.

Muhle H, Bellmann B, Creutzenberg O, Dasenbrock C, Ernst H, Kilpper R, MacKenzie JC, Morrow P, Mohr U, Takenaka S, Mermelstein R [1991]. Pulmonary response to toner upon chronic inhalation exposure in rats. Fund Appl Toxicol *17*:280–299.

Munro IC, Ford RA, Kennepohl E, Sprenger JG [1996]. Correlation of structural class with no-observed-effect levels: a proposal for establishing a threshold of concern. Food Chem Toxicol *34*:829–867.

Nakanishi J, ed. [2011]. Risk assessment of manufactured nanomaterials: "Approaches" - Overview of approaches and results. Final report issued on August 17, 2011. New Energy and Industrial Technology Development Organization (NEDO) project (P06041) "Research and Development of Nanoparticle Characterization Methods." National Institute of Advanced Industrial Science and Technology (AIST). http://en.aist-riss.jp/assessment/2721/

Nakano Y, Yokohira M, Hashimoto N, Yamakawa K, Kishi S, Ninomiya F, Kanie S, Saoo K, Imaida K [2014]. Rat strain differences in levels and effects of chronic inflammation due to intratracheal instillation of quartz on lung tumorigenesis induced by DHPN. Exp Toxicol Pathol *66*(8):391-401. doi: 10.1016/j.etp.2014.06.002. PMID: 25024166.

NAS [1983]. Risk assessment in the federal government: managing the process. Committee on the Institutional Means for Assessment of Risks to Public Health, Commission on Life Sciences, National Research Council, National Academy of Sciences. Washington, DC: National Academies Press.

NAS [2007]. Toxicity testing in the 21st century: a vision and a strategy. National Academy of Sciences. Washington, DC: National Academies Press.

NAS [2009]. Science and decisions: advancing risk assessment. Committee on Improving Risk Analysis Approaches Used by the U.S. EPA, Board on Environmental Studies and Toxicology, Division of Earth and Life Studies, National Research Council, National Academy of Sciences. Washington, DC: National Academies Press.

NAS [2017]. Using 21st century science to improve risk-related evaluation. National Academy of Sciences. Washington, DC: National Academies Press.

Naumann BD, Sargent EV, Starkman BS, Fraser WJ, Becker GT, Kirk GD [1996]. Performance-based exposure control limits for pharmaceutical active ingredients. Am Ind Hyg Assoc J 57:33–42.

Nel AE, Nasser E, Godwin H, Avery D, Bahadori T, Bergeson L, Beryt E, Bonner JC, Boverhof D, Carter J, Castranova V, Deshazo JR, Hussain SM, Kane AB, Klaessig F, Kuempel E, Lafranconi M, Landsiedel R, Malloy T, Miller MB, Morris J, Moss K, Oberdorster G, Pinkerton K, Pleus RC, Shatkin JA, Thomas R, Tolaymat T, Wang A, Wong J [2013]. A multi-stakeholder perspective on the use of alternative test strategies for nanomaterial safety assessment. ACS Nano *7*(8):6422–6433.

Nikula KJ, Snipes MB, Barr EB, Griffith WC, Henderson RF, Mauderly JL [1995]. Comparative pulmonary toxicities and carcinogenicities of chronically inhaled diesel exhaust and carbon black in F344 rats. Fundam Appl Toxicol *25*:80–94.

NIOSH [2007]. NIOSH pocket guide to chemical hazards. Cincinnati, OH: U.S. Department of Health and Human Services, Centers for Disease Control and Prevention, National Institute for Occupational Safety and Health, DHHS (NIOSH) Publication No. 2005–149. https://www.cdc.gov/niosh/npg

NIOSH [2009]. Quantitative risk characterization and management of occupational hazards: control banding (CB)—a literature review and critical analysis. Cincinnati, OH: U.S. Department of Health and Human Services, Centers for Disease Control and Prevention, National Institute for Occupational Safety and Health, DHHS (NIOSH) Publication No. 2009–152.

NIOSH [2011]. Current intelligence bulletin 63: occupational exposure to titanium dioxide. Cincinnati, OH: U.S. Department of Health and Human Services, Centers for Disease Control and Prevention, National Institute for Occupational Safety and Health, DHHS (NIOSH) Publication No. 2011-160.

NIOSH [2013]. Current intelligence bulletin 65: occupational exposure to carbon nanotubes and nanofibers. Cincinnati, OH: U.S. Department of Health and Human Services, Centers for Disease Control and Prevention, National Institute for Occupational Safety and Health, DHHS (NIOSH) Publication No. 2013-14.

NIOSH [2017]. Current intelligence bulletin 68: NIOSH chemical carcinogen policy. Cincinnati, OH: U.S. Department of Health and Human Services, Centers for Disease Control and Prevention, National Institute for Occupational Safety and Health, DHHS (NIOSH) Publication No. 2017–2100.

NIOSH [2019]. Technical report: the NIOSH occupational exposure banding process for chemical risk management. By Lentz TJ, Seaton M, Rane P, Gilbert SJ, McKernan LT, Whittaker C. Cincinnati, OH: U.S. Department of Health and Human Services, Centers for Disease Control and Prevention, National Institute for Occupational Safety and Health, DHHS (NIOSH) Publication No. 2019-132. https://doi.org/10.26616/NIOSHPUB2019132.

NIOSH [2020]. Current intelligence bulletin 69: NIOSH practices in occupational risk assessment. By Daniels RD, Gilbert SJ, Kuppusamy SP, Kuempel ED, Park RM, Pandalai SP, Smith RJ, Wheeler MW, Whittaker C, Schulte PA. Cincinnati, OH: U.S. Department of Health and Human Services, Centers for Disease Control and Prevention, National Institute for Occupational Safety and Health. DHHS (NIOSH) Publication No. 2020-106 (revised 03/2020), https://doi.org/10.26616/NIOSHPUB2020106revised032020.

NIOSH [2021]. Current intelligence bulletin 70: health effects of occupational exposure to silver nanomaterials. Cincinnati, OH: U.S. Department of Health and Human Services, Centers for Disease Control and Prevention, National Institute for Occupational Safety and Health, DHHS (NIOSH) Publication No. 2021-112.

Oberdörster G, Ferin J, Soderholm S, Gelein R, Cox C, Baggs R, Morrow PE [1994]. Increased pulmonary toxicity of inhaled ultrafine particles: due to lung overload alone? Ann Occup Hyg *38*:295–302.

Oberdörster G, Maynard A, Donaldson K, Castranova V, Fitzpatrick J, Ausman K, Carter J, Karn B, Kreyling W, Lai D, Olin S, Monteiro-Riviere N, Warheit D, Yang H [2005]. Principles for characterizing the potential human health effects from exposure to nanomaterials: elements of a screening strategy. Part Fibre Toxicol *2*:1–35.

OECD [2007]. Guidance on grouping of chemicals. Series on testing and assessment, no. 80. ENV/JM/MONO(2007)28. Paris: Organization for Economic Cooperation and Development, Environmental Health and Safety Publications.

OECD [2012]. Important issues on risk assessment of manufactured nanomaterials. Series on the safety of manufactured nanomaterials, no. 33. ENV/JM/MONO(2012)8. Paris, France: Organization for Economic Cooperation and Development, Environmental Health and Safety Publications.

OECD [2014a]. OECD series on the safety of manufactured nanomaterials, No. 41. Report of the OECD Expert Meeting on the Physico-chemical Properties of Manufactured Nanomaterials and Test Guidelines. OECD, Paris, France, pp. 56. ENV/JM/MONO (2014)15. https://www.oecd.org/officialdocuments/publicdisplaydocumentpdf/?cote=ENV/JM/MONO(2014)15&docLanguage=En.

OECD [2014b]. Guidance on grouping of chemicals, second edition. Series on testing and assessment, no. 194. ENV/JM/MONO(2014)4. Paris, France: Organization for Economic Cooperation and Development, Environmental Health and Safety Publications.

OECD [2015]. Guidance notes on nanomaterials: interspecies variability factors in human health risk assessment. 18-Dec-2014. ENV/CHEM/NANO(2015)4. Paris, France: Working Party on Manufactured Nanomaterials, Organisation for Economic Co-operation and Development, Environmental Health and Safety Publications.

OECD [2016]. Alternative testing strategies in risk assessment of manufactured nanomaterials: current state of knowledge and research needs to advance their use. Series on the safety of manufactured nanomaterials, no. 80. ENV/JM/MONO(2016)63. Paris, France: Organization for Economic Cooperation and Development, Environmental Health and Safety Publications.

OEHHA [2008]. Air toxics hot spots risk assessment guidelines - technical support document for the derivation of noncancer reference exposure levels. Air Toxicology and Epidemiology Branch, Office of Environmental Health Hazard Assessment, California Environmental Protection Agency.

Ogura I, Gamo M, Kobayashi N, Ema M, Adachi K, Yamada N, Yamamoto O [2011]. Risk assessment of manufactured nanomaterials, TiO2. Tsukuba, Japan: NEDO reports.

Oh E, Liu R, Nel A, Gemill KB, Bilal M, Cohen Y, Medintz IL [2016]. Meta-analysis of cellular toxicity for cadmium-containing quantum dots. Nat Nanotechnol *11*(5):479–486.

Oomen AG, Bleeker EA, Bos PM, van Broekhuizen F, Gottardo S, Groenewold M, Hristozov D, Hund-Rinke K, Irfan MA, Marcomini A, Peijnenburg WJ, Rasmussen K, Jiménez AS, Scott-Fordsmand JJ, van Tongeren M, Wiench K, Wohlleben W, Landsiedel R [2015]. Grouping and read-across approaches for risk assessment of nanomaterials. Int J Environ Res Public Health *12*(10):13415–13434.

Oosterwijk MT, Feber ML, Burello E [2016]. Proposal for a risk banding framework for inhaled low aspect ratio nanoparticles based on physicochemical properties. Nanotoxicology *10*(6):780–793.

OSHA [2012]. Appendix A to §1910.1200—Health Hazard Criteria. 17574 Federal Register/Vol. 77, No. 58/Monday, 26 March, 2012.

Park, MV, Catalán J, Ferraz N, Cabellos J, Vanhauten R, Vázquez-Campos S, Janer G [2018]. Development of a systematic method to assess similarity between nanomaterials for human hazard evaluation purposes: lessons learnt. Nanotoxicology *12*:7:652–676, doi: 10.1080/17435390.2018.1465142.

Pauluhn J [2010a]. Subchronic 13-week inhalation exposure of rats to multiwalled carbon nanotubes: Toxic effects are determined by density of agglomerate structures, not fibrillar structures. Toxicol Sci *13*(1):226–242.

Pauluhn J [2010b]. Multi-walled carbon nanotubes (Baytubes): approach for derivation of occupational exposure limit. Regul Toxicol Pharmacol *57*(1):78–89.

Pauluhn J [2011]. Poorly soluble particulates: searching for a unifying denominator of nanoparticles and fine particles for DNEL estimation. Toxicology *279*(1–3):176–188.

Pauluhn J [2012]. Subchronic inhalation toxicity of iron oxide (magnetite, Fe3O4) in rats: pulmonary toxicity is determined by the particle kinetics typical of poorly soluble particles. J Appl Toxicol *32*:488–504.

Pauluhn J [2014]. Derivation of occupational exposure levels (OELs) of low-toxicity isometric biopersistent particles: how can the kinetic lung overload paradigm be used for improved inhalation toxicity study design and OEL-derivation? Part Fibre Toxicol *11*:72.

Porter DW, Ramsey D, Hubbs AF, Battelli L, Ma J, Barger M, Landsittel D, Robinson VA, McLaurin J, Khan A, Jones W, Teass A, Castranova V [2001]. Time course of pulmonary response of rats to inhalation of crystalline silica: histological results and biochemical indices of damage, lipidosis, and fibrosis. J Environ Pathol Toxicol Oncol *20*(Suppl 1):1–14.

Porter DW, Hubbs AF, Robinson VA, Battelli LA, Greskevitch M, Barger M, Landsittel D, Jones W, Castranova V [2002]. Comparative pulmonary toxicity of blasting sand and five substitute blasting agents. J Toxicol Environ Health Part A *65*(16):1121–1140.

Porter DW, Hubbs AF, Mercer R, Robinson VA, Ramsey D, McLaurin K, Khan A, Battelli L, Brumbaugh K, Teass A, Castranova V [2004]. Progression of lung inflammation and damage in rats after cessation of silica inhalation. Toxicol Sci *79*:370–380.

Porter DW, Wu N, Hubb AF, Mercer RR, Funk K, Meng F, Li J, Wolfarth MG, Battelli L, Friend S, Andrew M, Hamilton R, Sriram K, Yang F, Castranova V, Holian A [2013]. Differential mouse pulmonary dose and time course responses to titanium dioxide nanospheres and nanobelts. Toxicol Sci *131*(1):179–193.

R Core Team [2014]. R: A language and environment for statistical computing. Vienna, Austria: R Foundation for Statistical Computing, http://www.R-project.org/.

Raabe OG, Al-Bayati MA, Teague SV, Rasolt A [1988]. Regional deposition of inhaled monodisperse coarse and fine aerosol particles in small laboratory animals. Ann Occup Hyg *32*:53–63.

Ramchandran V, Gernand JM [2019]. A dose-response-recovery clustering algorithm for categorizing carbon nanotube variants into toxicologically distinct groups. Comput Toxicol *11*:25–32.

Ramchandran V, Gernand JM [2020]. Examining the in vivo pulmonary toxicity of engineered metal oxide nanomaterials using a genetic algorithm-based dose-response-recovery clustering model. Comput Toxicol *13*:100–113.

Rasmussen CE, Christopher KIW [2006]. Gaussian processes for machine learning. Cambridge, MA: The MIT Press.

Rasmussen K, Rauscher H, Mech A, Riego Sintes J, Gilliland D, González M, Kearns P, Moss K, Visser M, Groenewold M, Bleeker EAJ [2018]. Physico-chemical properties of manufactured nanomaterials - Characterisation and relevant methods. An outlook based on the OECD Testing Programme. Regul Toxicol Pharmacol 92:8-28.

Roberts JR, McKinney W, Kan H, Krajnak K, Frazer DG, Thomas TA, Waugh S, Kenyon A, MacCuspie RI, Hackley VA, Castranova V [2013]. Pulmonary and cardiovascular responses of rats to inhalation of silver nanoparticles. J Toxicol Environ Health A *76*(11):651–668.

Rodriguez-Ibarra C, Deciga-Alcaraz A, Ispanixtlahuatl-Meraz O, Medina-Reyes EI, Delgado-Buenrostro NL, Chirino YI [2020]. International landscape of limits and recommendations for occupational exposure to engineered nanomaterials. Toxicology letters *322*:111–119. https://doi.org/doi:10.1016/j.toxlet.2020.01.016

Rom WL [1991]. Relationship of inflammatory cell cytokines to disease severity in individuals with occupational inorganic dust exposure. Am J Ind Med *19*(1):15–27.

Rushton EK, Jiang J, Leonard SS, Eberly S, Castranova V, Biswas P, Elder A, Han X, Gelein R, Finkelstein J, Oberdörster G [2010]. Concept of assessing nanoparticle hazards considering nanoparticle dosemetric and chemical/biological response metrics. J Toxicol Environ Health A *73*(5):445–461.

Ryman-Rasmussen JP, Cesta MF, Brody AR, Shipley-Phillips JK, Everitt JI, Tewksbury EW, Moss OR, Wong BA, Dodd DE, Andersen ME, Bonner JC [2009]. Inhaled carbon nanotubes reach the subpleural tissue in mice. Nat Nanotechnol *4*(11):747–751. http://dx.doi.org/10.1038/NNANO.2009.305.

Sager TM, Wolfarth MW, Andrew M, Hubbs A, Friend S, Chen T, Porter DW, Wu N, Yang F, Hamilton RF, Holian A [2013]. Effect of multi-walled carbon nanotube surface modification on bioactivity in the C57BL/6 mouse model. Nanotoxicology *8*(3):317–327.

Sánchez Jiménez A, Varet J, Poland C, Fern GJ, Hankin SM, van Tongeren M [2016]. A comparison of control banding tools for nanomaterials. J Occup Environ Hyg *13*(12):936–949. doi: 10.1080/15459624.2016.1200191. PMID: 27314531.

Schmid O, Stoeger T [2016]. Surface area is the biologically most effective dose metric for acute nanoparticle toxicity in the lung. J Aerosol Sci *99*:133–143.

Schulte PA, Salamanca-Buentello F [2007]. Ethical and scientific issues of nanotechnology in the workplace. Environ Health Perspect *115*(1):5–12.

Schulte PA, Murashov V, Zumwalde R, Kuempel ED, Geraci CL [2010]. Occupational exposure limits for nanomaterials: state of the art. J Nanopart Res *12*(6):1971–1987.

Schulte PA, Kuempel ED, Drew NM [2018]. Characterizing risk assessments for the development of occupational exposure limits for engineered nanomaterials. Regul Toxicol Pharmacol *95*:207–219.

Schulte PA, Leso V, Niang M, Iavicoli I [2019]. Current state of knowledge on the health effects of engineered nanomaterials in workers: a systematic review of human studies and epidemiological investigations. Scand J Work Environ Health *45*(3):217–238.

Scott-Fordsmand JJ, Amorim MJB, Sorensen PB [2018]. Implementing the DF4 in a robust model, allowing for enhanced comparison, prioritization and grouping of nanomaterials. Reg Tox Pharm *92*:207–212.

SER [2012]. Provisional nano reference values for engineered nanomaterials. Advisory report 12/01. Sociaal-Economische Raad (Social and Economic Council), The Netherlands.

Shao K, Shapiro A [2016]. A next generation benchmark dose computation system. Abstract #2165. Poster presentation at Society of Toxicology 55th Annual Meeting, March 13–16, New Orleans, LA. The Toxicologist *150*(1):274.

Shatkin J, ed. [2013]. Nanotechnology health and environmental risks, 2nd ed. Boca Raton, FL: CRC Press, Taylor & Francis.

Sheehan B, Murphy F, Mullins M, Furxhi I, Costa AL, Simeone FC, Mantecca P [2018]. Hazard screening methods for nanomaterials: a comparative study. Int J Mol Sci *19*:649, doi:10.3390/ijms19030649.

Sneath PHA, Sokal RR [1973]. Numerical taxonomy. San Francisco, CA: Freeman.

Snipes MB [1989]. Long-term retention and clearance of particles inhaled by mammalian species. Crit Rev Toxicol *20*(3):175–211.

Sobels FH [1977]. Some problems associated with the testing for environmental mutagens and a perspective for studies in "comparative mutagenesis." Mutat Res *46*(4):245–260.

Sorensen T [1948]. A method of establishing groups of equal amplitude in plant sociology based on similarity of species content and its application to analyses of the vegetation on Danish commons. The Royal Danish Science Company *5*(4).

Stockmann-Juvala H, Taxell P, Santonen T [2014]. Formulating occupational exposure limits values (OELs) (Inhalation & Dermal). Helsinki: Finnish Institute of Occupational Health. Scaffold Public Documents - SPD7.

Stone KC, Mercer RR, Freeman BA, Chang LY, Crapo JD [1992]. Distribution of lung cell numbers and volumes between alveolar and nonalveolar tissue. Am Rev Respir Dis *146*(2):454–456.

Stone V [2009]. Engineered nanoparticles: review of health and environmental safety. Edinburgh: ENRHES EU project report.

Stone V, Pozzi-Mucelli S, Tran L, Aschberger K, Sabella S, Vogel UB, Poland C, Balharry D, Fernandes T, Gottardo S, Hankin S, Hartl MG, Hartmann N, Hristozov D, Hund-Rinke K, Johnston H, Marcomini A, Panzer O, Roncato D, Saber AT, Wallin H, Scott-Fordsmand JJ [2014]. ITS-NANO: prioritizing nanosafety research to develop a stakeholder driven intelligent testing strategy. Part Fibre Toxicol *11*:9.

Strobl C, Boulesteix A, Kneib T, Augustin T, Zeileis A [2008]. Conditional variable importance for random forests. BMC Bioinformatics *9*:307.

Swidwinska-Gajewska AM, Czerczak S [2014]. Titanium dioxide nanoparticles: occupational exposure limits. Medycyna Pracy *65*:407 [in Polish].

Swidwinska-Gajewska AM, Czerczak S [2015]. Nanosilver-Occupational exposure limits. Med Pr *66*:429–442 [in Polish].

Tran CL, Cullen RT, Buchanan D, Jones AD, Miller BG, Searl A, Davis JMG, Donaldson K [1999]. Investigation and prediction of pulmonary responses to dust. Part II. In: Investigations into the pulmonary effects of low toxicity dusts. Parts I and II. Suffolk, UK: Health and Safety Executive, Contract Research Report 216/1999.

Tran CL, Buchanan D, Cullen RT, Searl A, Jones AD, Donaldson K [2000]. Inhalation of poorly soluble particles. II. Influence of particle surface area on inflammation and clearance. Inhal Toxicol *12*(12):1113–1126.

Tran CL, Kuempel ED, Castranova V [2002]. A rat lung model of exposure, dose, and response to inhaled silica. Ann Occup Hyg *46*(Suppl 1):14–17.

UNECE [2015]. Globally harmonized system of classification and labelling of chemicals (GHS). 6th rev. ed. Geneva, Switzerland: United Nations Economic Commission for Europe, https://www.unece.org/fileadmin/DAM/trans/danger/publi/ghs/ghs_rev06/English/ST-SG-AC10-30-Rev6e.pdf.

U.S. EPA [1994]. Methods for derivation of inhalation reference concentrations and application of inhalation dosimetry. EPA/600/8-90/066F. Research Triangle Park, NC: U.S. Environmental Protection Agency, Environmental Criteria and Assessment Office.

U.S. EPA [2002]. A review of the reference dose and reference concentration processes. EPA/630/P-02/002F. Washington, DC: Risk Assessment Forum, U.S. Environmental Protection Agency.

U.S. EPA [2005]. Guidelines for carcinogen risk assessment. EPA/630/P-03/001F. Washington, DC: U.S. Environmental Protection Agency, Risk Assessment Forum.

U.S. EPA [2012]. Benchmark dose technical guidance. EPA/100/R-12/001. Washington, DC: U.S. Environmental Protection Agency.

U.S. EPA [2014]. Next generation risk assessment: incorporation of recent advances in molecular, computational, and systems biology. EPA/600/R-14/004. Washington, DC: U.S. Environmental Protection Agency, National Center for Environmental Assessment, Office of Research and Development.

U.S. EPA [2015]. Benchmark dose software (BMDS), version 2.6. Washington, DC: U.S. Environmental Protection Agency, National Center for Environmental Assessment.

Van Duuren-Stuurman B, Vink SR, Verbist KJ, Heussen HG, Brouwer DH, Kroese DE [2012]. Stoffenmanager Nano version 1.0: a web-based tool for risk prioritization of airborne manufactured nano objects. Ann Occup Hyg *56*(5):525–541.

Walser T, Studer C [2015]. Sameness: the regulatory crux with nanomaterial identity and grouping schemes for hazard assessment. Regul Toxicol Pharmacol *72*(3):569–571.

Wang K, Chen X, Yang F, Porter DW, Wu N [2014]. A new stochastic kriging method for modeling multi-source exposure-response data in toxicology studies. ACS Sustain Chem Eng *2*:1581–1591.

Ward JH Jr [1963]. Hierarchical grouping to optimize an objective function. J Am Stat Assoc *58*(301):236–244.

Warheit DB [2013]. How to measure hazards/risks following exposures to nanoscale or pigment-grade titanium dioxide particles. Toxicol Lett *220*:193–204.

Weldon BA, Faustman EM, Oberdörster G, Workman T, Griffith WC, Kneuer C, Yu IJ [2016]. Occupational exposure limit for silver nanoparticles: considerations on the derivation of a general health-based value. Nanotoxicology *10*(7):945–956.

Wheeler MW [2018]. Bayesian additive adaptive basis tensor product models for modeling high dimensional surfaces: an application to high-throughput toxicity testing. Biometric Methodol *75*(1):193–201, doi:10.1111/biom.12942.

WHO [2017]. WHO guidelines on protecting workers from potential risks of manufactured nanomaterials. Licence: CC BY-NC-SA 3.0 IGO. Geneva: World Health Organization.

Wignall JA, Shapiro AJ, Wright FA, Woodruff TJ, Chiu WA, Guyton KZ, Rusyn I [2014]. Standardizing benchmark dose calculations to improve science-based decisions in human health assessments. Environ Health Perspect *122*(5):499–505.

Xia T, Zhao Y, Sager T, George A, Pokhrel S, Li N, Schoenfeld D, Meng H, Lin S, Wang X, Wang M, Ji Z, Zink JI, Madler L, Castranova V, Lin S, Nel AE [2011]. Decreased dissolution of ZnO by iron doping yields nanoparticles with reduced toxicity in the rodent lung and zebrafish embryos. ACS Nano *5*(2):1223–1235.

Xia T, Hamilton RF, Bonner JC, Crandall ED, Elder A, Fazlollahi F, Girtsman TA, Kim K, Mitra S, Ntim SA, Orr G, Tagmount M, Taylor AJ, Telesca D, Tolic A, Vulpe CD, Walker AJ, Wang X, Witzmann FA, Wu N, Xie Y, Zink JI, Nel A, Holian A [2013]. Interlaboratory evaluation of in vitro cytotoxicity and inflammatory responses to engineered nanomaterials: the NIEHS Nano GO Consortium. Environ Health Perspect *121*(6):683–690.

Yanamala N, Desai IC, Miller W, Kodali VK, Syamlal G, Roberts JR, Erdely AD [2019]. Grouping of carbonaceous nanomaterials based on association of patterns of inflammatory markers in BAL fluid with adverse outcomes in lungs. Nanotoxicol *13*(8):1102–1116.

Zalk DM, Nelson DI [2008]. History and evolution of control banding: a review. J Occup Environ Hyg *5*:330–346.

Zhang H, Ji Z, Xia T, Meng H, Low-Kam C, Liu R, Pokhrel S, Lin S, Wang X, Liao YP, Wang M, Li L, Rallo R, Damoiseaux R, Telesca D, Mädler L, Cohen Y, Zink JI, Nel AE [2012]. Use of metal oxide nanoparticle band gap to develop a predictive paradigm for oxidative stress and acute pulmonary inflammation. ACS Nano *6*(5):4349–4368.

Zuin S, Micheletti C, Critto A, Pojana G, Johnston H, Stone V, Tran L, Marcomini A [2011]. Weight of evidence approach for the relative hazard ranking of nanomaterials. Nanotoxicology *5*(3):445–458.

Page intentionally left blank

Appendices to NIOSH Draft Technical Report:

Approaches to Developing Occupational Exposure Limits or Bands for Engineered Nanomaterials

7 Appendices

Appendix A: Acute Inflammation

Appendix B: General Descriptive Results

Appendix C: In Vitro Inflammation and Cytotoxicity

Appendix D: Zebrafish Mortality

Appendix A: Acute Inflammation

Figure A-1: Summary of Physicochemical Properties and other Factors Available in the NIOSH/ENPRA/CIIT Dataset.

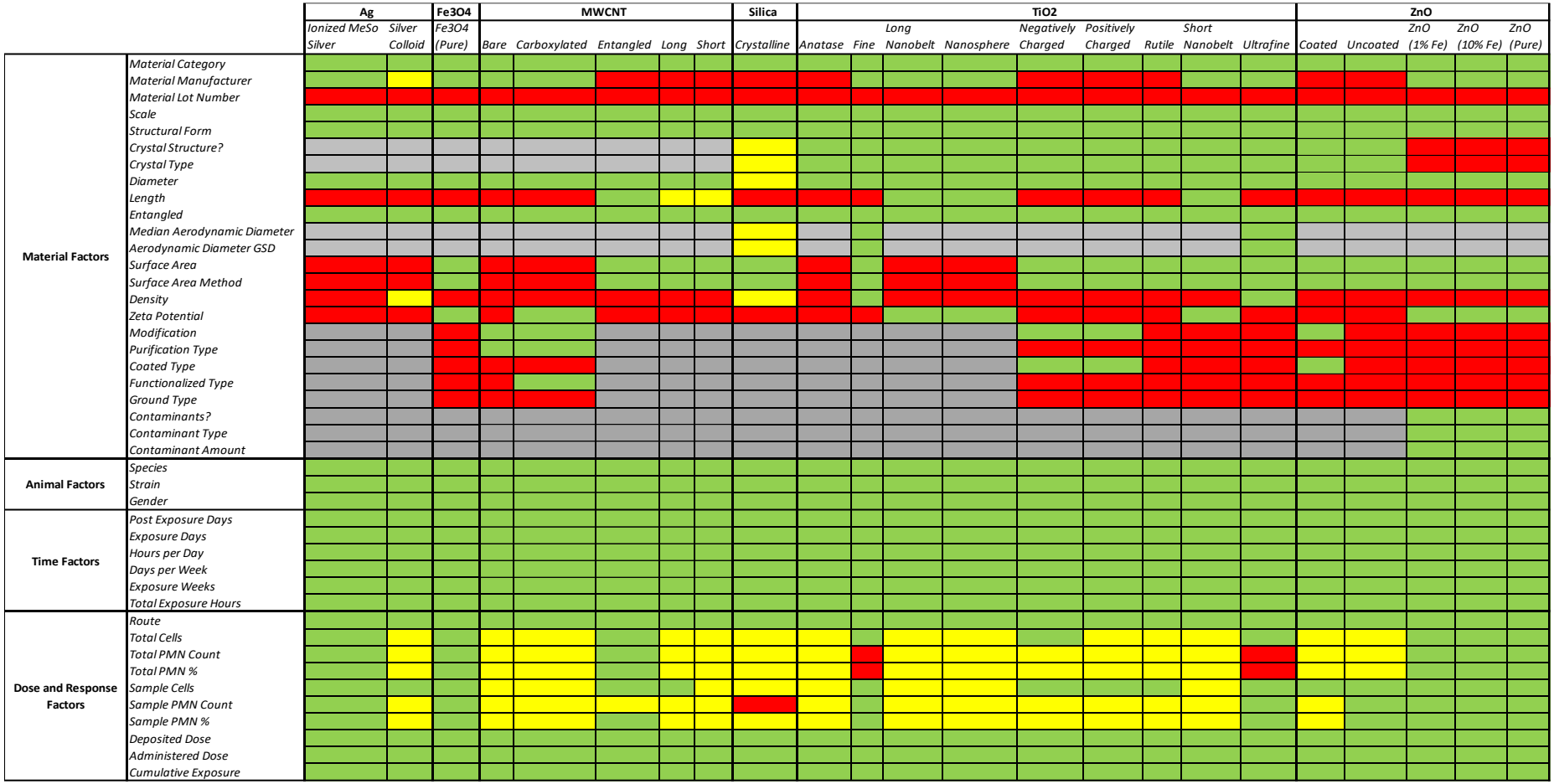

Color Key: Red = Missing; Yellow = Partially Missing; Green = Not Missing; Grey = Not Applicable

Properties Considered but Missing Values for All Materials: Volume, Solubility, Solubility Measurement Method, Surface Charge, Rigidity, Material Lot Number, Measure of Agglomeration

Figure A-2: Stochastic Kriging Fits for NIOSH/CIIT/ENPRA Dataset; BMR=Background + 4% PMNs, 0-3 Days Post-Exposure

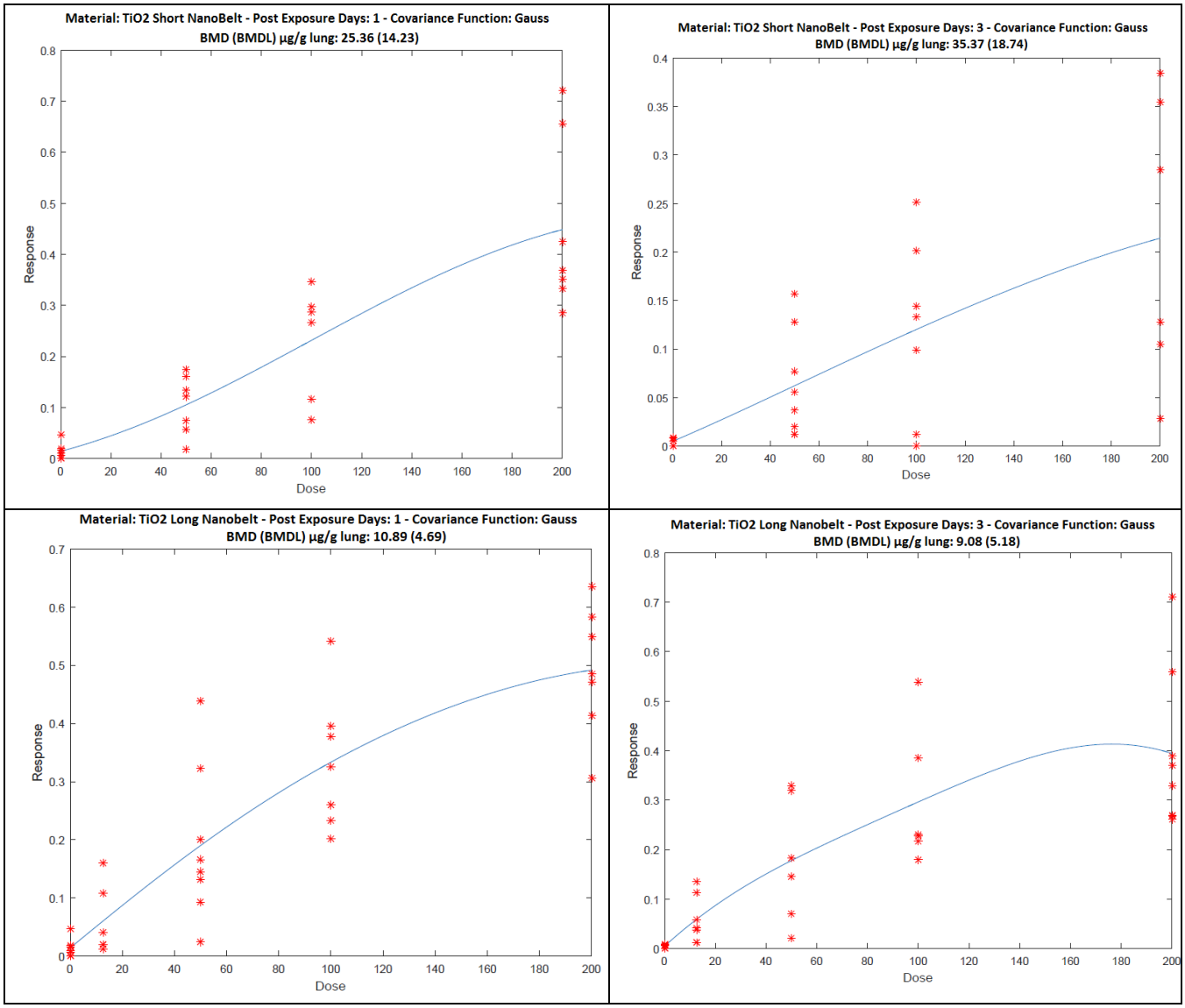

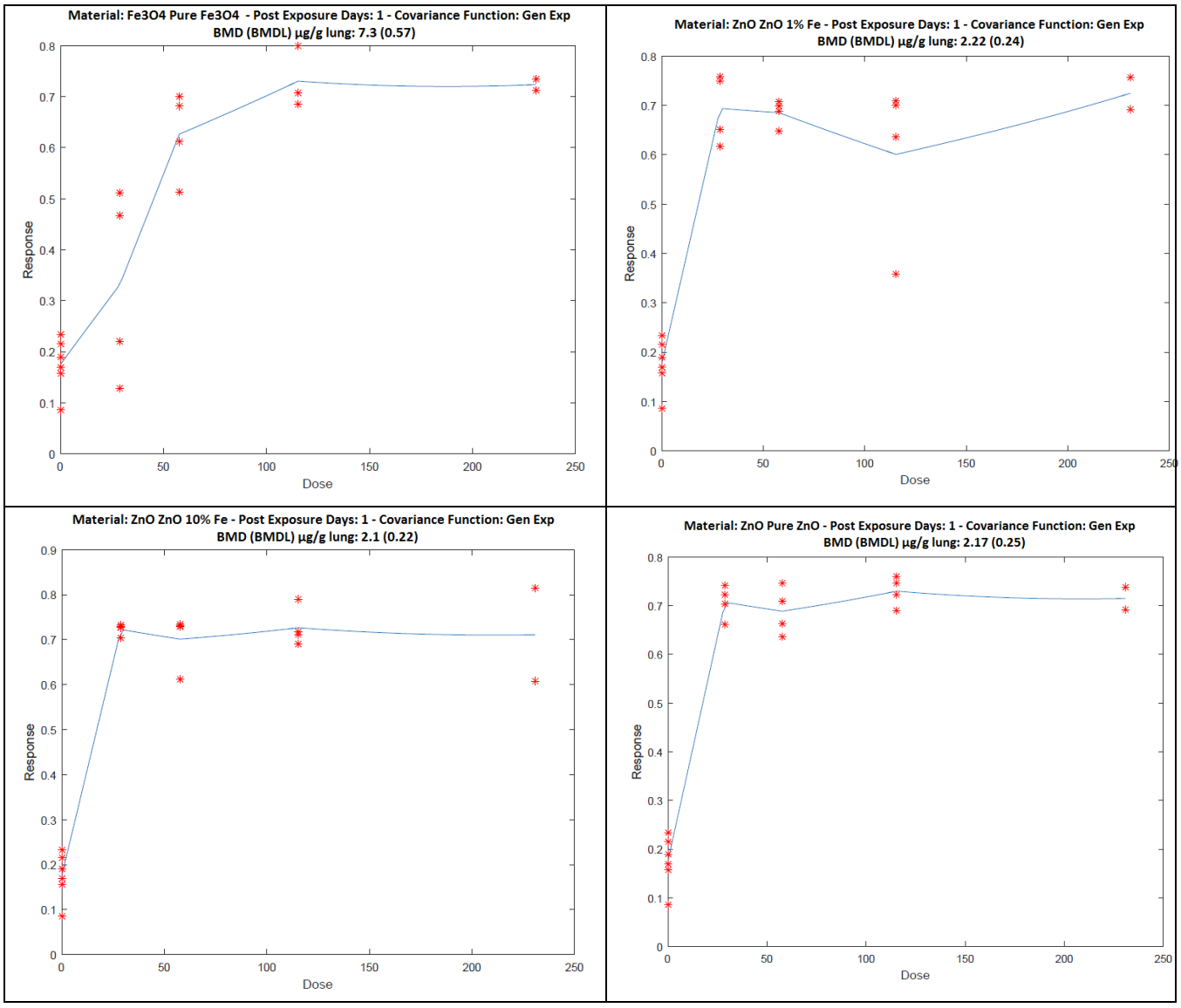

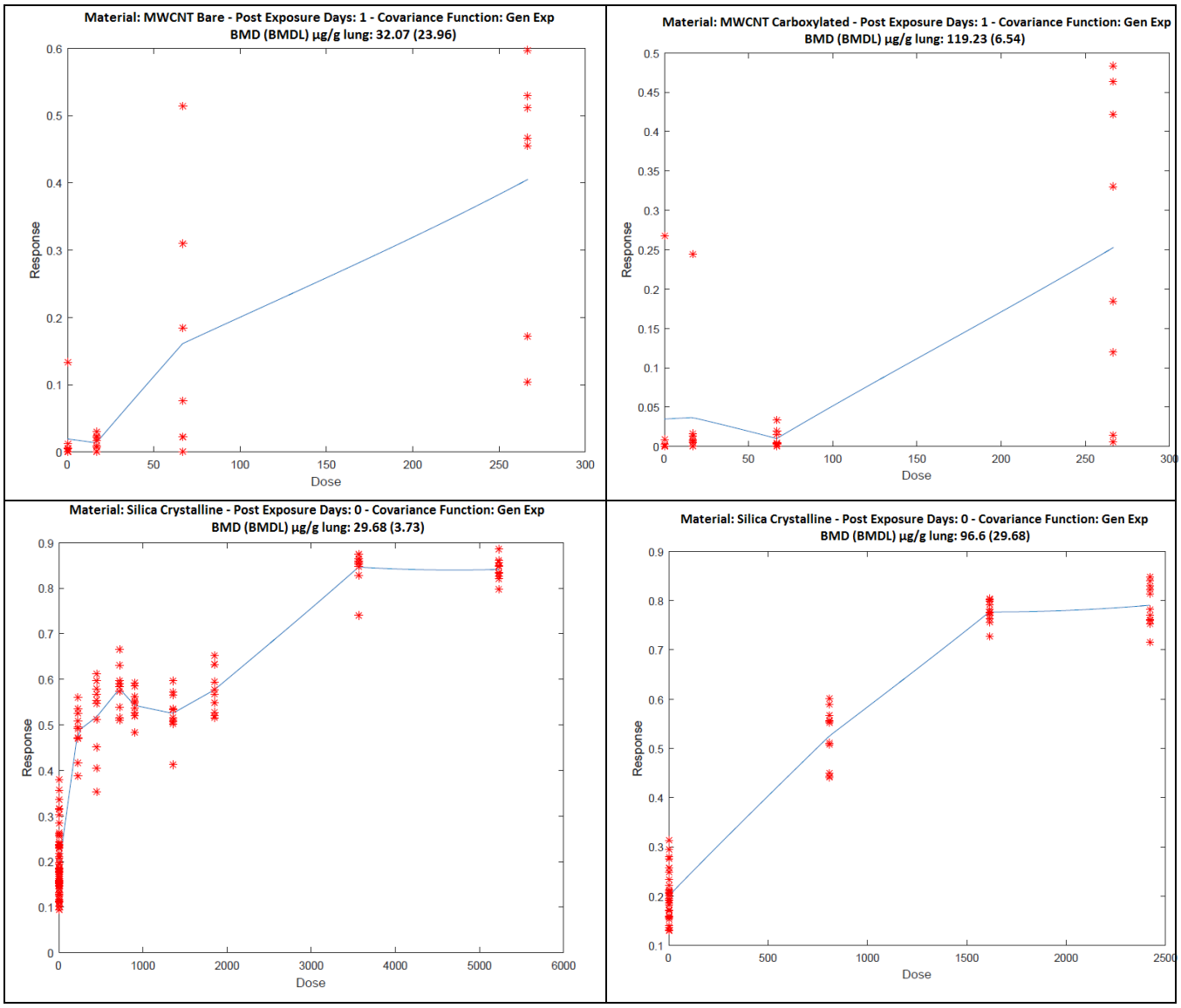

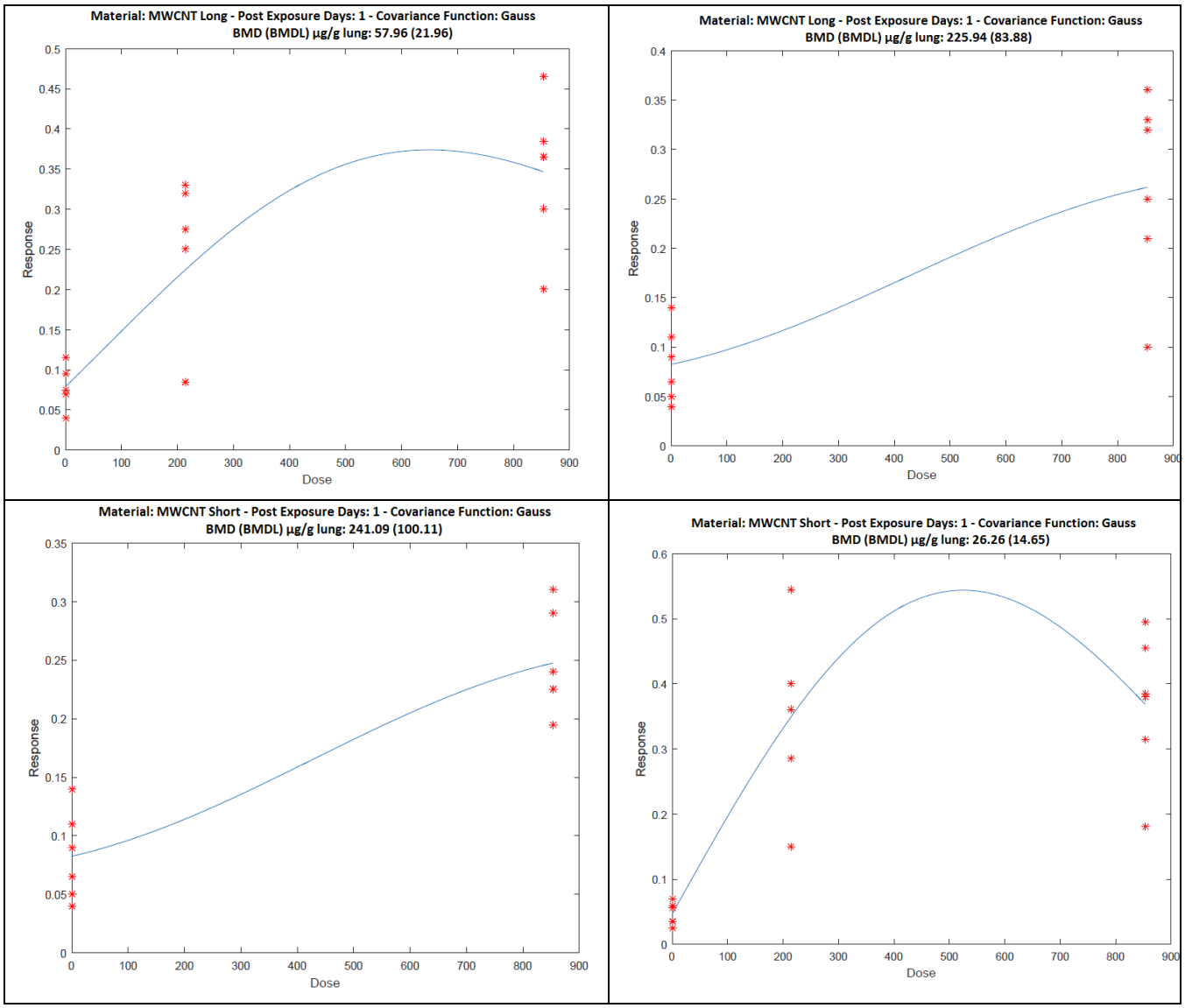

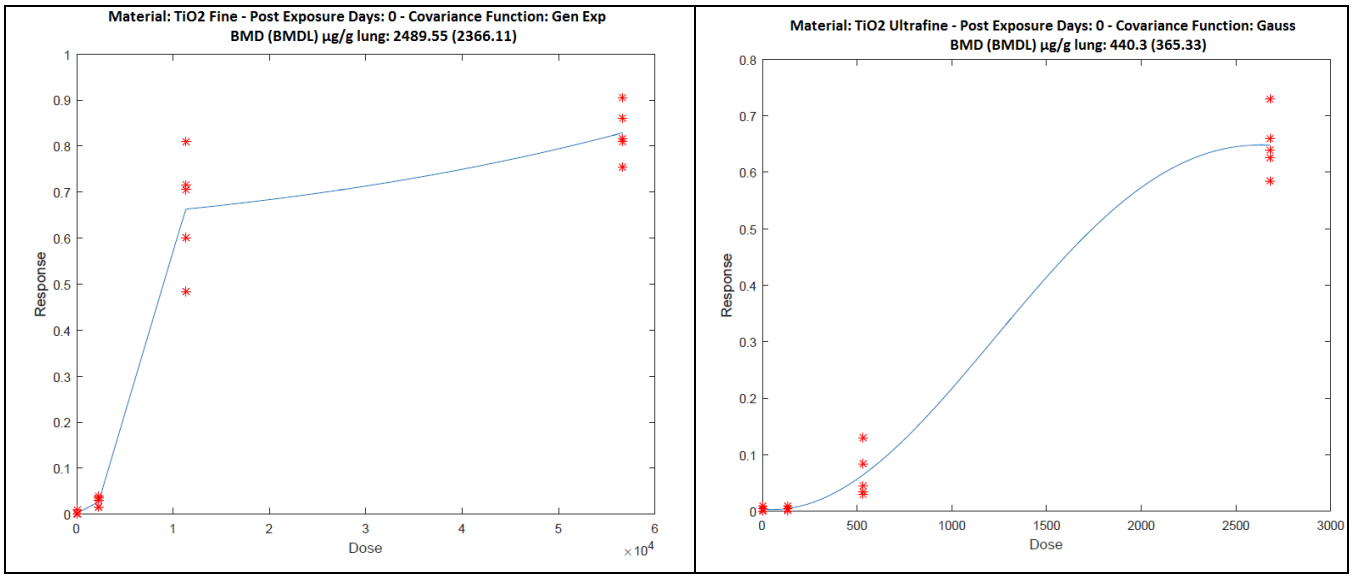

Figure A-3: Complete Linkage Clusters, Linear and Logarithmic Axes

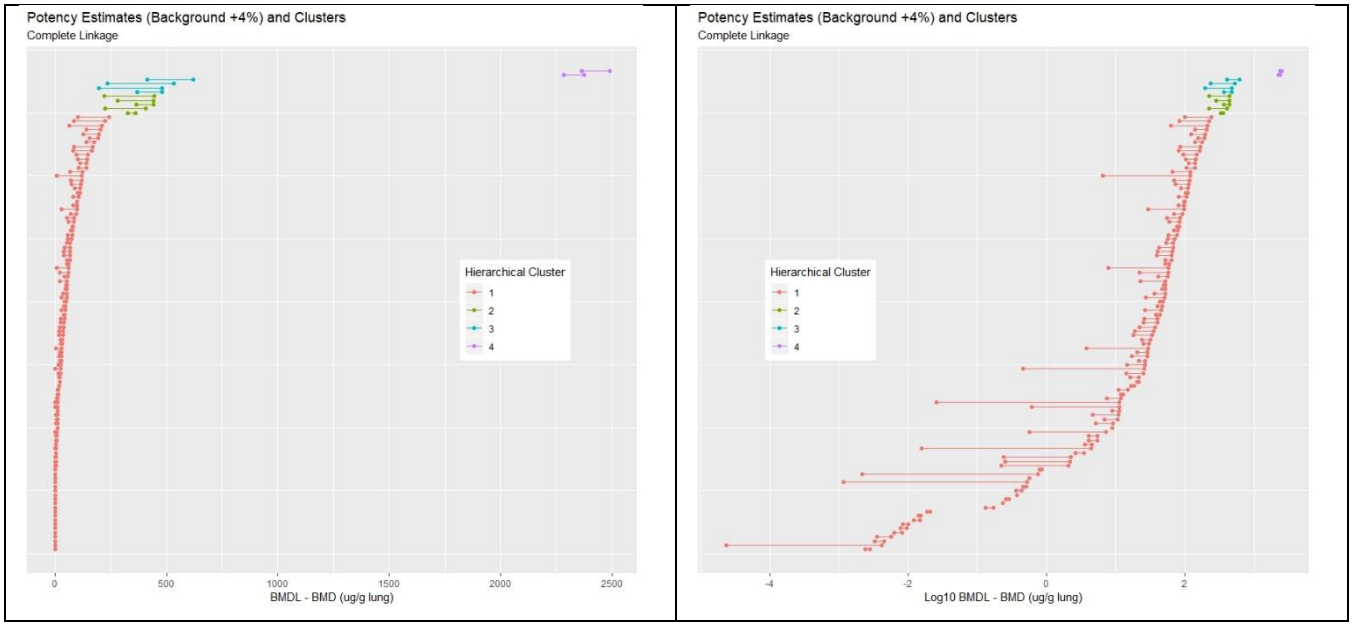

Figure A-4: Ward's Method Clusters, Linear and Logarithmic Axes

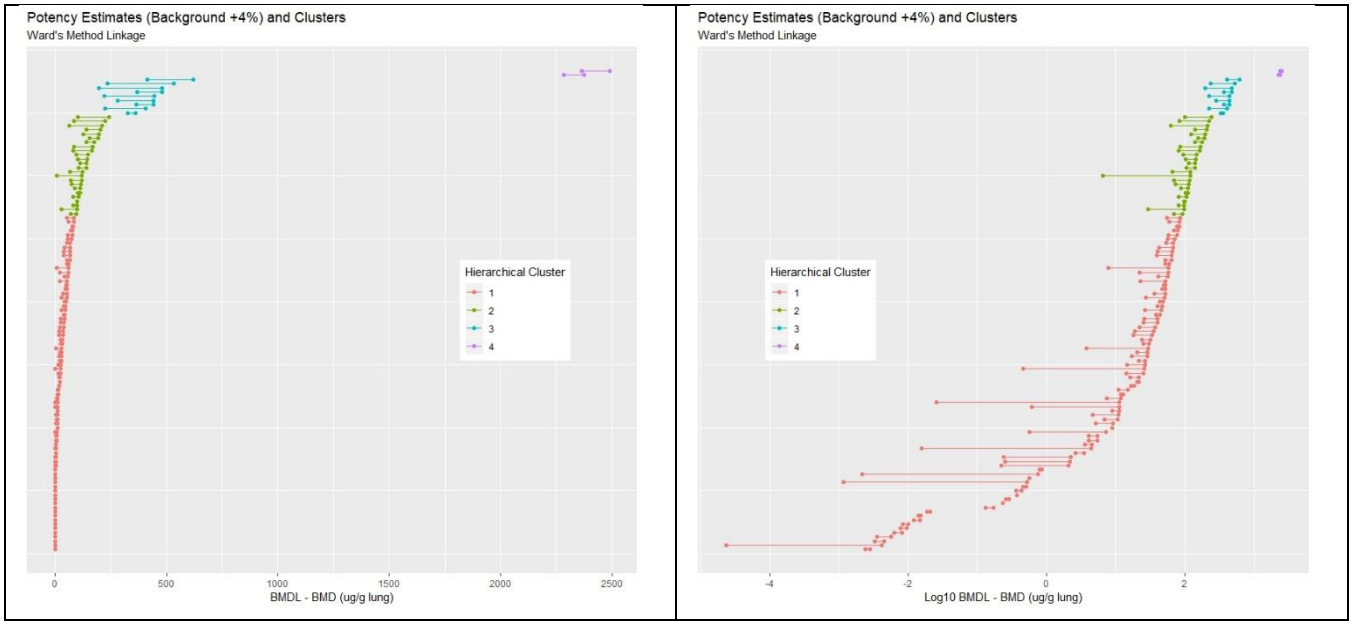

Figure A-5: Order of Magnitude Groups, Linear and Logarithmic Axes

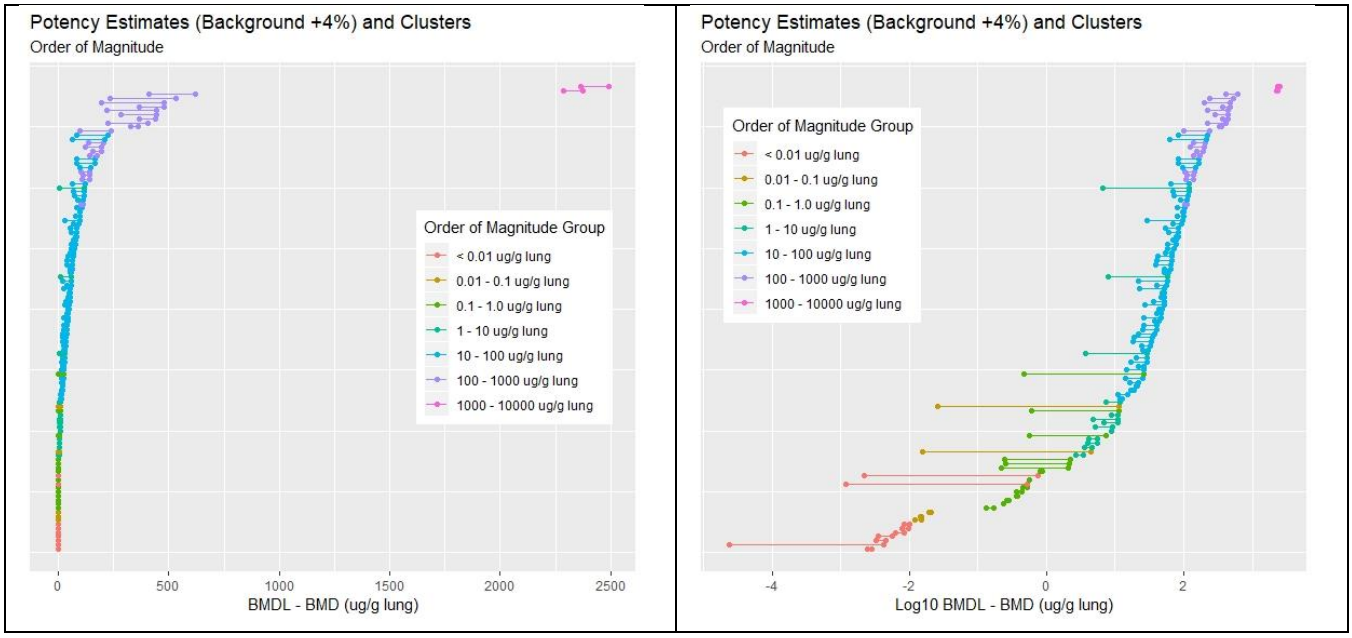

Table A-1: Potency Estimates and Clusters for the NIOSH/CIIT/ENPRA Dataset, based on Stochastic Kriging Modeling; BMR=Background + 4% PMNs, 0-3 Days Post-Exposure

Reference	Material	Material Type	Post Exposure	Route	BMD (µg / g lung)	BMDL (µg / g lung)	Potency Group
Xia 2011	ZnO	ZnO 10% Fe	1	IT	2.1	0.22	1
Xia 2011	ZnO	ZnO Pure	1	IT	2.17	0.25	1
Xia 2011	ZnO	ZnO 1% Fe	1	IT	2.22	0.24	1
Xia 2011	Fe_3O_4	Fe3O4 pure	1	IT	7.3	0.57	1
Porter 2013	TiO_2	NB2	3	PA	9.08	5.18	1
Porter 2013	TiO_2	NB2	1	PA	10.89	4.69	1
Porter 2013	TiO_2	NB1	1	PA	25.36	14.23	1
ENPRA-NRCWE	MWCNT	Short	1	IT	26.26	14.65	1
Porter 2001	Silica	Crystalline	0	Inh	29.68	3.73	1
Sager 2013	MWCNT	Bare	1	PA	32.07	23.96	1
Porter 2013	TiO_2	NB1	3	PA	35.37	18.74	1
ENPRA-NRCWE	MWCNT	Long	1	IT	57.96	21.96	1
Porter 2004	Silica	Crystalline	0	Inh	96.6	29.68	1
Sager 2013	MWCNT	Carboxylated	1	PA	119.23	6.54	1
ENPRA-NRCWE	MWCNT	Long	1	IT	225.94	83.88	2
ENPRA-NRCWE	MWCNT	Short	1	IT	241.09	100.11	2
Bermudez 2004	TiO_2	Ultrafine	0	Inh	440.3	365.33	3
Bermudez 2002	TiO_2	Fine	0	Inh	2489.55	2366.11	4

Table A-2: Summary of NanoGo Dose-Response Data by Experiment; BMR = Background + 4% PMNs, 0-3 Days Post-Exposure, based on Stochastic Kriging Modeling

Case Number	Study Reference	Material	Material Type	Difference in Mean Response?	BMD (µg / g lung)	BMDL (µg / g lung)	Covariance Structure
1	NanoGo-NIOSH	TiO_2	Anatase Nanobelt	N	---	---	
2	NanoGo-NIOSH	MWCNT	Functionalized MWCNT	Y	11.17	0.61	General Exponential
3	NanoGo-NIOSH	MWCNT	Original MWCNT	Y	4.43	0.02	General Exponential
4	NanoGo-NIOSH	MWCNT	Purified MWCNT	Y	58.21	7.88	General Exponential
5	NanoGo-UCD	TiO_2	Anatase Nanosphere	N	---	---	
6	NanoGo-UCD	TiO_2	Anatase/Rutile Nanosphere	N	---	---	
7	NanoGo-UR	TiO_2	Anatase Nanobelt	Y	93.10	69.81	Gaussian
8	NanoGo-UR	TiO_2	Anatase Nanosphere	N	---	---	
9	NanoGo-UR	TiO_2	Anatase/Rutile Nanosphere	N	---	---	
10	NanoGo-UR	MWCNT	Functionalized MWCNT	Y	98.36	80.44	Gaussian
11	NanoGo-UR	MWCNT	Original MWCNT	Y	47.97	43.66	General Exponential
12	NanoGo-UR	MWCNT	Purified MWCNT	Y	77.10	57.20	Gaussian
13	NanoGo-ECU	TiO_2	Anatase Nanobelt	Y	51.48	27.46	General Exponential
14	NanoGo-ECU	TiO_2	Anatase Nanosphere	N	---	---	

15	NanoGo-ECU	TiO_2	Anatase/Rutile Nanosphere	Y	21.39	20.55	General Exponential
16	NanoGo-MSU	TiO_2	Anatase Nanobelt	Y	40.71	26.00	General Exponential
17	NanoGo-MSU	TiO_2	Anatase Nanosphere	Y	204.68	139.25	Gaussian
18	NanoGo-MSU	TiO_2	Anatase/Rutile Nanosphere	Y	46.37	26.31	General Exponential
19	NanoGo-NCSU	TiO_2	Anatase Nanobelt	Y	26.02	0.46	General Exponential
20	NanoGo-NCSU	TiO_2	Anatase Nanosphere	N	---	---	
21	NanoGo-NCSU	TiO_2	Anatase/Rutile Nanosphere	N	---	---	
22	NanoGo-UW	TiO_2	Anatase Nanobelt	Y	167.53	84.83	General Exponential
23	NanoGo-UW	TiO_2	Anatase Nanosphere	N	---	---	
24	NanoGo-UW	TiO_2	Anatase/Rutile Nanosphere	Y	37.19	22.02	General Exponential
25	NanoGo-ECU	MWCNT	Functionalized MWCNT	Y	52.16	46.48	General Exponential
26	NanoGo-ECU	MWCNT	Original MWCNT	N	---	---	
27	NanoGo-ECU	MWCNT	Purified MWCNT	Y	67.54	53.05	General Exponential
28	NanoGo-MSU	MWCNT	Functionalized MWCNT	Y	52.62	22.77	General Exponential
29	NanoGo-MSU	MWCNT	Original MWCNT	Y	28.83	17.04	General Exponential

30	NanoGo-MSU	MWCNT	Purified MWCNT	Y	33.47	18.09	General Exponential
31	NanoGo-NCSU	MWCNT	Functionalized MWCNT	N	---	---	
32	NanoGo-NCSU	MWCNT	Original MWCNT	Y	26.39	21.57	General Exponential
33	NanoGo-NCSU	MWCNT	Purified MWCNT	Y	40.16	25.16	General Exponential
34	NanoGo-UW	MWCNT	Functionalized MWCNT	Y	121.43	65.15	General Exponential
35	NanoGo-UW	MWCNT	Original MWCNT	N	---	---	
36	NanoGo-UW	MWCNT	Purified MWCNT	Y	148.84	96.13	Gaussian

Table A-3: NIOSH/CIIT/ENPRA Potency Estimates for BMR=10% PMNs Total, 0-3 Days Post-Exposure, based on Stochastic Kriging Modeling with EPA BMDS Comparisons

					Stochastic Kriging			EPA BMDS	
Reference	Material	Material Type	Post Exposure	Route	BMD (µg / g lung)	BMDL (µg / g lung)	Potency Group	BMD (µg / g lung)	BMDL (µg / g lung)
Porter 2013	TiO_2	NB2	1	PA	23.55	12.26	1	23.20	17.28
Porter 2013	TiO_2	NB2	3	PA	23.63	13.99	1	22.24	16.31
ENPRA-NRCWE	MWCNT	Long	1	IT	30.35	1.66	1	105.26	0.78
ENPRA-NRCWE	MWCNT	Short	1	IT	37.51	23.29	1	16.27	0.04
Sager 2013	MWCNT	Bare	1	PA	45.79	31.37	1	63.24	43.70
Porter 2013	TiO_2	NB1	1	PA	47.63	32.83	1	47.69	40.67
ENPRA-NRCWE	MWCNT	Long	1	IT	78.60	0.91	2	476.28	346.01
Porter 2013	TiO_2	NB1	3	PA	82.11	50.71	2	87.70	68.93
ENPRA-NRCWE	MWCNT	Short	1	IT	85.49	0.94	2	517.17	421.06
Sager 2013	MWCNT	Carboxylated	1	PA	140.19	110.14	2	254.76	178.95
Bermudez 2004	TiO_2	Ultrafine	0	Inh	661.85	547.48	3	594.82	537.08
Bermudez 2002	TiO_2	Fine	0	Inh	3309.27	3104.00	4	3774.58	3368.74

Table A-4: NanoGo Potency Estimates for BMR=10% PMN Total, 0-3 Days Post-Exposure, based on Stochastic Kriging Modeling

Case Number	Study Reference	Material	Material Type	Difference in Mean Response?	BMD (µg / g lung)	BMDL (µg / g lung)
1	NanoGo-NIOSH	TiO_2	Anatase Nanobelt	N	---	---
2	NanoGo-NIOSH	MWCNT	Functionalized MWCNT	Y	Not Estimable	Not Estimable
3	NanoGo-NIOSH	MWCNT	Original MWCNT	Y	Not Estimable	Not Estimable
4	NanoGo-NIOSH	MWCNT	Purified MWCNT	Y	Not Estimable	Not Estimable
5	NanoGo-UCD	TiO_2	Anatase Nanosphere	N	---	---
6	NanoGo-UCD	TiO_2	Anatase/Rutile Nanosphere	N	---	---
7	NanoGo-UR	TiO_2	Anatase Nanobelt	Y	145.73	133.4
8	NanoGo-UR	TiO_2	Anatase Nanosphere	N	---	---
9	NanoGo-UR	TiO_2	Anatase/Rutile Nanosphere	N	---	---
10	NanoGo-UR	MWCNT	Functionalized MWCNT	Y	126.86	93.49
11	NanoGo-UR	MWCNT	Original MWCNT	Y	75.84	68.97
12	NanoGo-UR	MWCNT	Purified MWCNT	Y	118.34	90.8
13	NanoGo-ECU	TiO_2	Anatase Nanobelt	Y	111.57	69.46
14	NanoGo-ECU	TiO_2	Anatase Nanosphere	N	---	---

15	NanoGo-ECU	TiO_2	Anatase/Rutile Nanosphere	Y	59.42	44.36
16	NanoGo-MSU	TiO_2	Anatase Nanobelt	Y	93.65	54.45
17	NanoGo-MSU	TiO_2	Anatase Nanosphere	Y	Not Estimable	Not Estimable
18	NanoGo-MSU	TiO_2	Anatase/Rutile Nanosphere	Y	95.5	53.77
19	NanoGo-NCSU	TiO_2	Anatase Nanobelt	Y	53.88	8.9
20	NanoGo-NCSU	TiO_2	Anatase Nanosphere	N	111.57	24.56
21	NanoGo-NCSU	TiO_2	Anatase/Rutile Nanosphere	N	---	---
22	NanoGo-UW	TiO_2	Anatase Nanobelt	Y	Not Estimable	Not Estimable
23	NanoGo-UW	TiO_2	Anatase Nanosphere	N	---	---
24	NanoGo-UW	TiO_2	Anatase/Rutile Nanosphere	Y	108.87	55.96
25	NanoGo-ECU	MWCNT	Functionalized MWCNT	Y	127.64	119.4
26	NanoGo-ECU	MWCNT	Original MWCNT	N	91.43	47.53
27	NanoGo-ECU	MWCNT	Purified MWCNT	Y	175.85	143.6
28	NanoGo-MSU	MWCNT	Functionalized MWCNT	Y	104	48.88
29	NanoGo-MSU	MWCNT	Original MWCNT	Y	68.35	38.82
30	NanoGo-MSU	MWCNT	Purified MWCNT	Y	78.21	42.69

31	NanoGo-NCSU	MWCNT	Functionalized MWCNT	N	194.19	125
32	NanoGo-NCSU	MWCNT	Original MWCNT	Y	84.76	60.83
33	NanoGo-NCSU	MWCNT	Purified MWCNT	Y	136.11	75.76
34	NanoGo-UW	MWCNT	Functionalized MWCNT	Y	Not Estimable	Not Estimable
35	NanoGo-UW	MWCNT	Original MWCNT	N	---	---
36	NanoGo-UW	MWCNT	Purified MWCNT	Y	Not Estimable	Not Estimable

Table A-5: Evaluation of Random Forest Model for BMR=10% PMN Total

Material	Median BMD	Actual Cluster	Predicted Cluster
Anatase Nanospheres	N/A	N/A	1
Anatase Nanobelt	102.61	2	1
Anatase/Rutile Nanospheres	95.5	2	1
Original MWCNT	75.84	2	1
Functionalized MWCNT	126.86	2	2
Purified MWCNT	127.23	2	1

Table A-6: Description of NanoGo Experimental Designs

Reference	Route	Species	Strain	Material	Material Type	Animals	Dose Groups (Not including control)[d]
NanoGo-NIOSH	IT	Male Rat	Sprague-Dawley	TiO_2	Anatase Nanobelt	18	3
					Control	6	
NanoGo-NIOSH*	IT	Male Rat	Sprague-Dawley	MWCNT	Functionalized MWCNT	18	3
					Control	6	
NanoGo-NIOSH	IT	Male Rat	Sprague-Dawley	MWCNT	Original MWCNT	18	3
					Control	6	
NanoGo-NIOSH*	IT	Male Rat	Sprague-Dawley	MWCNT	Purified MWCNT	18	3
					Control	6	
NanoGo-UCD	IT	Male Rat	Sprague-Dawley	TiO_2	Anatase Nanospheres	18	3
					Control	6	
NanoGo-UCD	IT	Male Rat	Sprague-Dawley	TiO_2	Anatase/Rutile Nanospheres	18	3
					Control	6	
NanoGo-UR	IT	Male Rat	Sprague-Dawley	TiO_2	Anatase Nanobelt	18	3
					Control	6	
NanoGo-UR**	IT	Male Rat	Sprague-Dawley	TiO_2	Anatase Nanospheres	18	3
					Control	6	
NanoGo-UR**	IT	Male Rat	Sprague-Dawley	TiO_2	Anatase/Rutile Nanospheres	18	3
					Control	6	
NanoGo-UR†	IT	Male Rat	Sprague-Dawley	MWCNT	Functionalized MWCNT	18	3

					Control	6	
NanoGo-UR	IT	Male Rat	Sprague-Dawley	MWCNT	Original MWCNT	18	3
					Control	6	
NanoGo-UR†	IT	Male Rat	Sprague-Dawley	MWCNT	Purified MWCNT	18	3
					Control	6	
NanoGo-ECU	IT	Male Mouse•	C57BL/6	TiO_2	Anatase Nanospheres	4	1
					Control	3	
NanoGo-ECU	IT	Male Mouse•	C57BL/6	TiO_2	Anatase/Rutile Nanospheres	4	1
					Control	3	
NanoGo-ECU	IT	Male Mouse•	C57BL/6	TiO_2	Anatase Nanobelt	4	1
					Control	3	
NanoGo-MSU	IT	Male Mouse•	C57BL/6	TiO_2	Anatase Nanospheres	4	1
					Control	4	
NanoGo-MSU	IT	Male Mouse•	C57BL/6	TiO_2	Anatase/Rutile Nanospheres	4	1
					Control	4	
NanoGo-MSU	IT	Male Mouse•	C57BL/6	TiO_2	Anatase Nanobelt	4	1
					Control	4	
NanoGo-NCSU	IT	Male Mouse•	C57BL/6	TiO_2	Anatase Nanospheres	6	1
					Control	5	
NanoGo-NCSU	IT	Male Mouse•	C57BL/6	TiO_2	Anatase/Rutile Nanospheres	6	1
					Control	5	
NanoGo-NCSU	IT	Male Mouse•	C57BL/6	TiO_2	Anatase Nanobelt	6	1
					Control	5	

NanoGo-UW	IT	Male Mouse•	C57BL/6	TiO_2	Anatase Nanobelt	4	1
					Control	6	
NanoGo-UW	IT	Male Mouse•	C57BL/6	TiO_2	Anatase Nanospheres	4	1
					Control	6	
NanoGo-UW	IT	Male Mouse•	C57BL/6	TiO_2	Anatase/Rutile Nanospheres	5	1
					Control	6	
NanoGo-ECU‡	IT	Male Mouse•	C57BL/6	MWCNT	Functionalized MWCNT	3	1
					Control	3	
NanoGo-ECU	IT	Male Mouse•	C57BL/6	MWCNT	Original MWCNT	3	1
					Control	3	
NanoGo-ECU‡	IT	Male Mouse•	C57BL/6	MWCNT	Purified MWCNT	3	1
					Control	3	
NanoGo-MSUa	IT	Male Mouse•	C57BL/6	MWCNT	Functionalized MWCNT	4	1
					Control	4	
NanoGo-MSU	IT	Male Mouse•	C57BL/6	MWCNT	Original MWCNT	4	1
					Control	4	
NanoGo-MSUa	IT	Male Mouse•	C57BL/6	MWCNT	Purified MWCNT	4	1
					Control	4	
NanoGo-NCSUb	IT	Male Mouse•	C57BL/6	MWCNT	Functionalized MWCNT	6	1
					Control	6	
NanoGo-NCSU	IT	Male Mouse•	C57BL/6	MWCNT	Original MWCNT	6	1
					Control	6	
NanoGo-NCSUb	IT	Male Mouse•	C57BL/6	MWCNT	Purified MWCNT	6	1
					Control	6	

NanoGo-UWc	IT	Male Mouse•	C57BL/6	MWCNT	Functionalized MWCNT	4	1
					Control	4	
NanoGo-UW	IT	Male Mouse•	C57BL/6	MWCNT	Original MWCNT	4	1
					Control	4	
NanoGo-UWc	IT	Male Mouse•	C57BL/6	MWCNT	Purified MWCNT	4	1
					Control	4	

*: Same control animals

**: Same control animals

†: Same control animals

‡: Same control animals

a: Same control animals

b: Same control animals

c: Same control animals

d: For the studies with 3 dose groups, they are 20, 70, and 200 ug. For the studies with 1 dose group, it is 40 ug.

•: 3 exposed groups used in the mouse studies, but only the highest dose group data was reported as the other two dose groups did not have responses statistically significantly different from control.

Table A-7: Updated Acute Inflammation Database Potency Estimates for BMR=Background+4% PMNs, 0-3 Days Post-Exposure, based on EPA BMDS 2.7 Modeling of NIOSH/ENPRA/CIIT and ATL/NIOSHTIC/OECD

Material	Material Type	Index	Cluster – Complete Linkage	Cluster – Ward's Method	BMD (ug/g lung)	BMDL (ug/g lung)
ZnO	Zno_fine	80	1	1	2.78E-03	2.42E-03
ZnO	Zno_fine	82	1	1	4.16E-03	2.36E-05
ZnO	Zno_Nano	84	1	1	4.52E-03	3.26E-03
ZnO	Zno_fine	79	1	1	5.66E-03	3.52E-03
ZnO	Zno_Nano	83	1	1	8.27E-03	6.30E-03
Silica	Silica	78	1	1	9.68E-03	7.72E-03
ZnO	Zno_fine	81	1	1	1.01E-02	8.47E-03
ZnO	Zno_Nano	85	1	1	1.48E-02	1.20E-02
Brass	Brass	75	1	1	1.51E-02	1.42E-02
ZnO	Zno_Nano	86	1	1	2.11E-02	1.90E-02

CeO2	NA	140	1	1	0.170121	0.131566
CeO2	NA	139	1	1	0.23381	0.232283
ZnO	NA	151	1	1	0.286346	0.259881
CeO_2	NA	142	1	1	0.372066	0.36939
ZnO	NA	153	1	1	0.434359	0.368279
ZnO	NA	152	1	1	0.514577	0.456355
TiO_2	TiO_2_Anatase	89	1	1	0.524778	1.17E-03
CeO_2	NA	141	1	1	0.570904	0.567336
TiO_2	Anatase_RL2	114	1	1	0.753529	2.15E-03
ZnO	NA	154	1	1	0.861645	0.804148
ZnO	ZnO 10% Fe	7	1	1	2.1	0.22
ZnO	ZnO pure	5	1	1	2.17	0.25
ZnO	ZnO 1% Fe	6	1	1	2.22	0.24
CeO^2	CeO_2	124	1	1	3.48397	2.64869
MWCNT	Original MWCNT	37	1	1	4.425345	1.57E-02
CeO_2	CeO_2_SiO_2	125	1	1	4.51773	3.57461
Silica	SiO_2	126	1	1	5.48215	4.03295
Aluminum	Aluminum	76	1	1	5.49272	4.09442
Fe_3O_4	Fe_3O_4 pure	4	1	1	7.3	0.57
ZnO	NA	134	1	1	8.919571	8.906
TiO_2	NB2	73	1	1	9.08	5.18
ZnO	NA	150	1	1	10.77434	6.820661
TiO_2	NB2	2	1	1	10.89	4.69
M5	M5_part	93	1	1	11.1529	8.9215
MWCNT	Functionalized MWCNT	39	1	1	11.17287	0.60831
CeO_2	NA	132	1	1	11.32078	2.60E-02
CNT	CNTsmall	105	1	1	11.7185	7.362857
CNF	CNF_ female	110	1	1	12.66636	11.96164
ZnO	NA	149	1	1	14.98412	10.99687
CeO_2	CeO_2-20Gd	122	1	1	18.6905	16.7475
TiO_2	Anatase/Rutile Nanospheres	48	1	1	21.39411	20.54749
CNT	MWCNT_O_RL1	117	1	1	21.6075	16.3397
TiO_2	NB1	1	1	1	25.36	14.23
TiO_2	Anatase Nanobelt	56	1	1	26.01996	0.460347
MWCNT	short	18	1	1	26.26	14.65
MWCNT	Original MWCNT	66	1	1	26.39101	21.5707
MWCNT	Original MWCNT	63	1	1	28.83192	17.03524
CNT	MWCNT_AP_Comp2	112	1	1	29.0127	20.5916
Silica	crystalline	12	1	1	29.68	3.73
Carbon	Printex90	74	1	1	30.5304	25.0193

MWCNT	Bare	10	1	1	32.07	23.96
MWCNT	Purified MWCNT	64	1	1	33.47429	18.09494
TiO_2	NB1	72	1	1	35.37	18.74
TiO_2	Anatase/Rutile Nanospheres	57	1	1	37.18729	22.01955
MWCNT	Purified MWCNT	67	1	1	40.16347	25.15848
TiO_2	Anatase Nanobelt	53	1	1	40.71477	26.00457
CNF	CNF_male	109	1	1	43.75519	37.80638
TiO_2	Anatase/Rutile Nanospheres	51	1	1	46.37419	26.30729
Carbon	ufCB_af	103	1	1	46.6377	39.8657
MWCNT	Original MWCNT	45	1	1	47.96727	43.6628
TiO_2	Anatase Nanobelt	50	1	1	51.48198	27.46147
CNT	MWCNT_P_RL1	119	1	1	51.5623	35.8148
MWCNT	Functionalized MWCNT	62	1	1	52.1596	46.48057
Graphene	Graphite	77	1	1	52.4907	49.185
MWCNT	Functionalized MWCNT	65	1	1	52.6213	22.76977
Graphene	Gr5	128	1	1	56.4505	41.0919
MWCNT	long	15	1	1	57.96	21.96
MWCNT	Purified MWCNT	38	1	1	58.2099	7.882537
Carbon	ufCB	102	1	1	59.4146	52.474
CNT	MWCNT_O_RL3	118	1	1	65.0521	52.1343
TiO_2	NA	148	1	1	65.05639	39.04495
TiO_2	TiO_2_nanorod	100	1	1	66.0566	39.8952
Graphene	Gr20	131	1	1	66.9411	41.8881
MWCNT	Purified MWCNT	61	1	1	67.54422	53.05456
CNT	MWCNT_P_RL3	120	1	1	72.1286	57.1132
MWCNT	Purified MWCNT	46	1	1	77.09749	57.19682
CNT	SWCNT_af	101	1	1	78.1518	69.4156
CNT	MWCNT_F_RL3	116	1	1	82.3309	77.5266
Graphene	Gr20	130	1	1	83.6657	59.8093
CNT	MWCNT_24PS	123	1	1	84.8604	54.3094
TiO_2	Anatase Nanobelt	44	1	2	93.10232	69.81431
Silica	crystalline	13	1	2	96.6	29.68
MWCNT	Functionalized MWCNT	47	1	2	98.36358	80.44119
TiO_2	NB_RL3	121	1	2	99.8324	97.0367
Graphene	Gr5	129	1	2	105.455	81.1492
Carbon	MicroC60	107	1	2	110.6656	102.1273
CNT	MWCNT_PC_Comp2	113	1	2	111.586	88.8327
CNT	MWCNT_F_RL1	115	1	2	115.253	72.8055
CNT	CNTlarge	106	1	2	118.0293	70.00429
MWCNT	Carboxylated	11	1	2	119.23	6.54

MWCNT	Functionalized MWCNT	71	1	2	121.4265	65.14559
TiO_2	NA	147	1	2	139.9034	105.9733
TiO_2	TiO_2_nanodot	99	1	2	140.598	112.575
Graphene	Gr1	127	1	2	143.345	101.931
MWCNT	Purified MWCNT	70	1	2	148.8371	96.13267
Silica	Silica_2dPE	92	1	2	165.169	82.1534
TiO_2	Anatase Nanobelt	59	1	2	167.5281	84.83356
TiO_2	TiO_2_uf3	95	1	2	175.313	140.968
TiO_2	TiO_2_fine	98	1	2	193.459	155.643
In_2O_3	In_2O_3	111	1	2	196.102	124.675
TiO2	Anatase Nanospheres	52	1	2	204.6802	139.2511
Silica	Silica_1dPE	91	1	2	211.301	62.6291
MWCNT	long	16	1	2	225.94	83.88
MWCNT	short	17	1	2	241.09	100.11
TiO_2	NA	146	2	3	361.1316	326.7409
TiO_2	TiO_2_1dPE	90	2	3	407.452	225.757
TiO_2	Ultrafine	35	2	3	440.3	365.33
TiO_2	TiO_2_fine	87	2	3	442.759	281.349
TiO_2	TiO_2_ufmeth	88	2	3	443.633	221.455
TiO_2	TiO_2_uf2	97	3	3	479.164	368.051
TiO_2	TiO_2_F1	94	3	3	479.236	197.864
TiO_2	TiO_2_uf1	96	3	3	533.019	235.931
TiO_2	TiO_2	104	3	3	620.691	411.847
Carbon	C60OHX	108	4	4	2375.814	2284.757
TiO_2	Fine	34	4	4	2489.55	2366.11

Table A-8: Materials and Data Sources

Material	Material Type	Index	Study Reference
ZnO	Zno_fine	80	D.B. Warheit, 2009
ZnO	Zno_fine	82	D.B. Warheit, 2009
ZnO	Zno_Nano	84	D.B. Warheit, 2009
ZnO	Zno_fine	79	D.B. Warheit, 2009
ZnO	Zno_Nano	83	D.B. Warheit, 2009
Silica	Silica	78	Christie M. Sayes, 2010
ZnO	Zno_fine	81	D.B. Warheit, 2009
ZnO	Zno_Nano	85	D.B. Warheit, 2009
Brass	Brass	75	SM Thomson, 1986
ZnO	Zno_Nano	86	D.B. Warheit, 2009
CeO_2	NA	140	Aalapati_2014
CeO_2	NA	139	Gosens_2014
ZnO	NA	151	Warheit_2009
CeO_2	NA	142	Keller_2014
ZnO	NA	153	Warheit_2009
ZnO	NA	152	Warheit_2009
TiO_2	TiO2_Anatase	89	Rona M. Silva, 2015
CeO_2	NA	141	Keller_2014
TiO_2	Anatase_RL2	114	Bonner_2013
ZnO	NA	154	Warheit_2009
ZnO	ZnO 10% Fe	7	Xia2011
ZnO	ZnO pure	5	Xia2011
ZnO	ZnO 1% Fe	6	Xia2011
CeO_2	CeO_2	124	Ma_2011
MWCNT	Original MWCNT	37	NanoGo-NIOSH
CeO_2	CeO_2_SiO_2	125	Ma_2015
Silica	SiO_2	126	Ma_2015
Aluminum	Aluminum	76	SM Thomson, 1986
Fe_3O_4	Fe_3O_4 pure	4	Xia2011
ZnO	NA	134	Jacobson_2015
TiO_2	NB2	73	Porter2013
ZnO	NA	150	Warheit_2009
TiO_2	NB2	2	Porter2013
M5	M5_part	93	David B. Warheit, 2006(B)
MWCNT	Functionalized MWCNT	39	NanoGo-NIOSH

CeO_2	NA	132	Morimoto_2015
CNT	CNTsmall	105	Poulsen_2014
CNF	CNF_female	110	DeLorme_2012
ZnO	NA	149	Warheit_2009
CeO_2	CeO_2-20Gd	122	Dunnick_2016
TiO_2	Anatase/Rutile Nanospheres	48	NanoGo-ECU
CNT	MWCNT_O_RL1	117	Bonner_2013
TiO_2	NB1	1	Porter2013
TiO_2	Anatase Nanobelt	56	NanoGo-NCSU
MWCNT	short	18	ENPRA-NRCWE
MWCNT	Original MWCNT	66	NanoGo-NCSU
MWCNT	Original MWCNT	63	NanoGo-MSU
CNT	MWCNT_AP_Comp2	112	Bishop_2017
Silica	crystalline	12	Porter1997
Carbon	Printex90	74	J. Gallagher, 2003
MWCNT	Bare	10	Sager2013
MWCNT	Purified MWCNT	64	NanoGo-MSU
TiO_2	NB1	72	Porter2013
TiO_2	Anatase/Rutile Nanospheres	57	NanoGo-UW
MWCNT	Purified MWCNT	67	NanoGo-NCSU
TiO_2	Anatase Nanobelt	53	NanoGo-MSU
CNF	CNF_male	109	DeLorme_2012
TiO_2	Anatase/Rutile Nanospheres	51	NanoGo-MSU
Carbon	ufCB_af	103	Haiyan Tong, 2009
MWCNT	Original MWCNT	45	NanoGo-UR
TiO_2	Anatase Nanobelt	50	NanoGo-ECU
CNT	MWCNT_P_RL1	119	Bonner_2013
MWCNT	Functionalized MWCNT	62	NanoGo-ECU
Graphene	Graphite	77	Robert S. Anderson, 1989
MWCNT	Functionalized MWCNT	65	NanoGo-MSU
Graphene	Gr5	128	Roberts_2016
MWCNT	long	15	ENPRA-NRCWE
MWCNT	Purified MWCNT	38	NanoGo-NIOSH
Carbon	ufCB	102	Haiyan Tong, 2009
CNT	MWCNT_O_RL3	118	Bonner_2013

TiO_2	NA	148	Warheit_2009
TiO_2	TiO2_nanorod	100	David B. Warheit, 2006
Graphene	Gr20	131	Roberts_2016
MWCNT	Purified MWCNT	61	NanoGo-ECU
CNT	MWCNT_P_RL3	120	Bonner_2013
MWCNT	Purified MWCNT	46	NanoGo-UR
CNT	SWCNT_af	101	Haiyan Tong, 2009
CNT	MWCNT_F_RL3	116	Bonner_2013
Graphene	Gr20	130	Roberts_2016
CNT	MWCNT_24PS	123	Hamilton_2018
TiO_2	Anatase Nanobelt	44	NanoGo-UR
Silica	crystalline	13	Porter1999
MWCNT	Functionalized MWCNT	47	NanoGo-UR
TiO_2	NB_RL3	121	Bonner_2013
Graphene	Gr5	129	Roberts_2016
Carbon	MicroC60	107	Sayers_2016
CNT	MWCNT_PC_Comp2	113	Bishop_2017
CNT	MWCNT_F_RL1	115	Bonner_2013
CNT	CNTlarge	106	Poulsen_2014
MWCNT	Carboxylated	11	Sager2013
MWCNT	Functionalized MWCNT	71	NanoGo-UW
TiO_2	NA	147	Warheit_2009
TiO_2	TiO_2_nanodot	99	David B. Warheit, 2006
Graphene	Gr1	127	Roberts_2016
MWCNT	Purified MWCNT	70	NanoGo-UW
Silica	Silica_2dPE	92	Donna D. Zhang, 2002
TiO_2	Anatase Nanobelt	59	NanoGo-UW
TiO_2	TiO_2_uf3	95	David B. Warheit, 2007
TiO2	TiO_2_fine	98	David B. Warheit, 2006
In_2O_3	In_2O_3	111	Badding_2016
TiO_2	Anatase Nanospheres	52	NanoGo-MSU
Silica	Silica_1dPE	91	Donna D. Zhang, 2002
MWCNT	long	16	ENPRA-NRCWE
MWCNT	short	17	ENPRA-NRCWE
TiO_2	NA	146	Warheit_2009
TiO_2	TiO2_1dPE	90	Donna D. Zhang, 2002
TiO_2	Ultrafine	35	Bermudez2004
TiO_2	TiO_2_fine	87	Doris Hohr, 2002

TiO_2	TiO_2_ufmeth	88	Doris Hohr, 2002
TiO_2	TiO_2_uf2	97	David B. Warheit, 2007
TiO_2	TiO_2_F1	94	David B. Warheit, 2007
TiO_2	TiO_2_uf1	96	David B. Warheit, 2007
TiO_2	TiO_2	104	David B. Warheit, 2010
Carbon	C60OHX	108	Xu_2009
TiO_2	Fine	34	Bermudez2002

Table A-9: Data Dictionary

Physicochemical Property Variable Name	Definition
Surface_reactivity	Description of the material's surface reactivity
Surface_modifications	Description of any modifications to the material's surface
Surface_Charge	Surface charge of particle
Median_Aerodynamic_Diameter	Point estimate of the median aerodynamic diameter, as reported
Aerodynamic_Diameter_GSD	Point estimate of the geometric standard deviation of the median aerodynamic diameter, as reported
Modification	Descriptor of any modifications (e.g. purification, functionalization, acid-wash) to the material
Purification_Type	Description of the type of purification applied to the material
Contaminant_Type	Descriptor of the contaminant(s) (more accurately impurity) present in the material
Contaminant_Amount	Description of the amounts, usually percentages, or contaminants (more accurately impurities) present in the material
Agglomerated_	Indicator of if the material is agglomerated
Functionalized_Type	Descriptor of the type of functionalization applied to the material
Solubility	Description of solubility properties of material
PP_size_nm	Primary particle diameter in nm as reported
Density	Density as reported
Zeta_Potential	Zeta potential as reported. Media may vary.
Crystal_Type	Descriptor of the crystal structure
Length	Length as reported
Crystal_Structure_	Indicator of if the material has a crystal structure (Y/N)
Contaminants_	Indicator of whether contaminants (more accurately impurities) are present (Y/N)
Structure	More detailed descriptor of the chemical composition of the material being studied (e.g. if material=TiO2, structure could be TiO2 85% rutile). AKA Material Type. Should not be included in models.
Scale	Descriptor of chemical's scale (e.g. nano, micro)
Diameter	Diameter as reported. Assay may vary (e.g. hydrodynamic)
Surface_Area	Specific surface area as reported
Structural_Form	Descriptor of the chemical's structure or shape (e.g. nanobelt)
material	Chemical composition of material being studied (e.g. TiO2)
Material_Category	Category of material being studed (e.g., Metal, Metal Oxide, etc.)
Material_Type	More detailed descriptor of the chemical composition of the material being studied (e.g. if material=TiO2, structure could be TiO2 85% rutile). Should not be included in models.

Table A-10: Summary of length across clusters assigned using hierarchical clustering with Ward's method for acute rodent pulmonary inflammation data from NIOSH/ENPRA/CIIT/NanoGo and Swiss-VCI/NIOSHTIC/ATL

		Cluster			
		1 (Most hazard)	**2**	**3**	**4 (Least hazard)**
Length (nm)	*Minimum*	800	670	-	-
	Q1	3000	4250	-	-
	Median	7250	7000	-	-
	Mean	6160	6917	-	-
	Q3	7500	7500	-	-
	Maximum	20000	20000	-	-
	n	80	24	9	2
	n missing	10	4	0	0
	n not applicable	40	10	9	2

Table A-11: Summary of crystal structures across clusters assigned using hierarchical clustering with Ward's method for acute rodent pulmonary inflammation data from NIOSH/ENPRA/CIIT/NanoGo and Swiss-VCI/NIOSHTIC/ATL

Cluster	Crystal Structure Indicator	Crystal Type	N
1	NA	NA	34
1	NR	NR	35
1	Y	Anatase	4
1	Y	Anatase 100%	3
1	Y	Anatase 81%; rutile 19%	3
1	Y	Crystalline Quartz	1
2	NA	NA	12
2	NR	NR	8
2	Y	Anatase 100%	3
2	Y	Crystalline Quartz	1
3	NR	NR	8
3	Y	Anatase	1
4	NA	NA	1
4	Y	Rutile	1

Table A-12: Summary of density across clusters assigned using hierarchical clustering with Ward's method for acute rodent pulmonary inflammation data from NIOSH/ENPRA/CIIT/NanoGo and Swiss-VCI/NIOSHTIC/ATL

		Cluster			
		1 (Most hazard)	**2**	**3**	**4 (Least hazard)**
Density (g/mL)	Minimum	0.01	0.10	3.9	4.25
	Q1	3.24	1.32	3.9	4.25
	Median	5.6	2.11	3.9	4.25
	Mean	4.54	2.87	3.9	4.25
	Q3	5.6	3.665	3.9	4.25
	Maximum	7.22	7.16	3.9	4.25
	n	80	24	9	2
	n missing	58	20	8	1

Table A-13: Summary of zeta potential across clusters assigned using hierarchical clustering with Ward's method for acute rodent pulmonary inflammation data from NIOSH/ENPRA/CIIT/NanoGo and Swiss-VCI/NIOSHTIC/ATL

		Cluster			
		1 (Most hazard)	**2**	**3**	**4 (Least hazard)**
Zeta Potential (mV)	*Minimum*	-48.4	-48.4	-	-
	Q1	-34.4	-39.55	-	-
	Median	-14.45	-30.3	-	-
	Mean	-23.4	-30.5	-	-
	Q3	-11.8	-22.05	-	-
	Maximum	-9.35	-11.8	-	-
	n	80	24	9	2
	n missing	52	17	9	2

Table A-14: Summary of primary particle size across clusters assigned using hierarchical clustering with Ward's method for acute rodent pulmonary inflammation data from NIOSH/ENPRA/CIIT/NanoGo and Swiss-VCI/NIOSHTIC/ATL

		Cluster			
		1 (Most hazard)	**2**	**3**	**4 (Least hazard)**
Primary Particle Size (nm)	*Minimum*	19	2691.7	25	-
	Q1	90	3268.8	240	-
	Median	111	3845.9	2144.3	-
	Mean	2959.8	3845.9	1529.6	-
	Q3	2130	4422.9	2583.6	-
	Maximum	20000	5000	2890.7	-
	n	80	24	9	2
	n missing	63	22	2	2

Appendix B: General Descriptive Results

Table B-1: All materials, assays, and endpoints

Analysis	Material	Assay	Exposure Duration	Endpoint	
NTP	Cobalt sulfate heptahydrate	in vivo	2 yr	Inflammation - Yes/No	Lung Cell Neoplasia - Y/N
NTP	Nickel sulfate hexahydrate	in vivo	2 yr	Inflammation - Yes/No	Lung Cell Neoplasia - Y/N
NTP	Ferrocene	in vivo	3 month	Inflammation - Yes/No	Lung Cell Neoplasia - Y/N
NTP	Nickel subsulfide	in vivo	2 yr	Inflammation - Yes/No	Lung Cell Neoplasia - Y/N
NTP	Gallium arsenide	in vivo	2 yr	Inflammation - Yes/No	Lung Cell Neoplasia - Y/N
NTP	Antimony trioxide	in vivo	2 wk; 2 yr	Inflammation - Yes/No	Lung Cell Neoplasia - Y/N
NTP	Molybdenum trioxide	in vivo	2 yr	Inflammation - Yes/No	Lung Cell Neoplasia - Y/N
NTP	Nickel (II) oxide	in vivo	2 yr	Inflammation - Yes/No	Lung Cell Neoplasia - Y/N
NTP	Vanadium pentoxide	in vivo	3 month; 2 yr	Inflammation - Yes/No	Lung Cell Neoplasia - Y/N

NTP	Calcium chromate	in vivo	2 yr	Inflammation - Yes/No	Lung Cell Neoplasia - Y/N
NTP	Talc	in vivo	2 yr	Inflammation - Yes/No	Lung Cell Neoplasia - Y/N
NTP	Indium phosphide	in vivo	3 month; 2 yr	Inflammation - Yes/No	Lung Cell Neoplasia - Y/N
NTP	o-Chlorobenzalmalononitrile (CS)	in vivo	2 yr	Inflammation - Yes/No	Lung Cell Neoplasia - Y/N
NTP	ortho-Phthalaldehyde	in vivo	3 month	Inflammation - Yes/No	Lung Cell Neoplasia - Y/N
NTP	Chromium	in vivo	2 yr	Inflammation - Yes/No	Lung Cell Neoplasia - Y/N
NTP	Cobalt	in vivo	2 wk; 3 month; 2 yr	Inflammation - Yes/No	Lung Cell Neoplasia - Y/N
NTP	Abrasive Blasting Agents: Blasting Sand	in vivo	2 wk; 39 wk	Inflammation - Yes/No	Lung Cell Neoplasia - Y/N
NTP	Abrasive blasting agents (coal slag)	in vivo	2 wk	Inflammation - Yes/No	Lung Cell Neoplasia - Y/N
NTP	Abrasive blasting agents (crushed glass)	in vivo	2 wk	Inflammation - Yes/No	Lung Cell Neoplasia - Y/N
NTP	Abrasive blasting agents (garnet)	in vivo	2 wk	Inflammation - Yes/No	Lung Cell Neoplasia - Y/N

NTP	Abrasive Blasting Agents: Specular Hematite	in vivo	39 wk	Inflammation - Yes/No	Lung Cell Neoplasia - Y/N
NTP	1020 Long Multiwalled Carbon Nanotube	in vivo	30 day	Inflammation - Yes/No	Lung Cell Neoplasia - Y/N
NTP	Wollastonite calcium silicates	in vivo	2 yr	Inflammation - Yes/No	Lung Cell Neoplasia - Y/N
NTP	TiO_2	in vivo	2 yr	N/A	Lung Cell Neoplasia - Y/N
NTP	TiO_2_P25	in vivo	2 yr	N/A	Lung Cell Neoplasia - Y/N
NTP	CB_Elft12	in vivo	2 yr	N/A	Lung Cell Neoplasia - Y/N
NTP	CB_P90	in vivo	2 yr	N/A	Lung Cell Neoplasia - Y/N
NTP	Toner	in vivo	2 yr	N/A	Lung Cell Neoplasia - Y/N
acute infl	TiO_2 NB1	in vivo	Single pharyngeal aspiration	Inflammation - PMN%	N/A
acute infl	TiO_2 NB2	in vivo	Single pharyngeal aspiration	Inflammation - PMN%	N/A
acute infl	TiO_2 NS	in vivo	Single pharyngeal aspiration	Inflammation - PMN%	N/A

acute infl	Fe_3O_4 pure	in vivo	Single intratracheal instillation	Inflammation - PMN%	N/A
acute infl	ZnO pure	in vivo	Single intratracheal instillation	Inflammation - PMN%	N/A
acute infl	ZnO 1% Fe	in vivo	Single intratracheal instillation	Inflammation - PMN%	N/A
acute infl	ZnO 10% Fe	in vivo	Single intratracheal instillation	Inflammation - PMN%	N/A
acute infl	Ag Silver Colloid	in vivo	5 hour inhalation	Inflammation - PMN%	N/A
acute infl	Ag Ionized MeSo Silver	in vivo	5 hour inhalation	Inflammation - PMN%	N/A
acute infl	MWCNT Bare	in vivo	Single pharyngeal aspiration	Inflammation - PMN%	N/A
acute infl	MWCNT Carboxylated	in vivo	Single pharyngeal aspiration	Inflammation - PMN%	N/A
acute infl	Silica crystalline	in vivo	Inhalation 6 hours/day, 5 days/week, 20-40-60-116 days	Inflammation - PMN%	N/A
acute infl	MWCNT long	in vivo	Single intratracheal instillation	Inflammation - PMN%	N/A
acute infl	MWCNT short	in vivo	Single intratracheal instillation	Inflammation - PMN%	N/A

acute infl	MWCNT entangled	in vivo	Single intratracheal instillation	Inflammation - PMN%	N/A
acute infl	ZnO coated	in vivo	Single intratracheal instillation	Inflammation - PMN%	N/A
acute infl	ZnO uncoated	in vivo	Single intratracheal instillation	Inflammation - PMN%	N/A
acute infl	TiO_2 neg_ch	in vivo	Single intratracheal instillation	Inflammation - PMN%	N/A
acute infl	TiO_2 pos_ch	in vivo	Single intratracheal instillation	Inflammation - PMN%	N/A
acute infl	TiO_2 anatase	in vivo	Single intratracheal instillation	Inflammation - PMN%	N/A
acute infl	TiO_2 rutile	in vivo	Single intratracheal instillation	Inflammation - PMN%	N/A
acute infl	TiO_2 Fine	in vivo	Inhalation 6 hours/day, 5 days/week, 13 weeks	Inflammation - PMN%	N/A
acute infl	TiO_2 Ultrafine	in vivo	Inhalation 6 hours/day, 5 days/week, 13 weeks	Inflammation - PMN%	N/A
acute infl	TiO2 Anatase Nanobelt	in vivo	Single intratracheal instillation	Inflammation - PMN%	N/A
acute infl	MWCNT Original MWCNT	in vivo	Single intratracheal instillation	Inflammation - PMN%	N/A

acute infl	MWCNT Purified MWCNT	in vivo	Single intratracheal instillation	Inflammation - PMN%	N/A
acute infl	MWCNT Functionalized MWCNT	in vivo	Single intratracheal instillation	Inflammation - PMN%	N/A
acute infl	TiO_2 Anatase Nanospheres	in vivo	Single intratracheal instillation	Inflammation - PMN%	N/A
acute infl	TiO_2 Anatase/Rutile Nanospheres	in vivo	Single intratracheal instillation	Inflammation - PMN%	N/A
	ZnO	in vitro	24h	THP-1 Cytotoxicity	N/A
	MW-O	in vitro	24h	THP-1 Cytotoxicity	N/A
	ZnO	in vitro	24h	THP-1 IL1-Beta Inflammation	N/A
	MW-O	in vitro	24h	THP-1 IL1-Beta Inflammation	N/A
	MW-P	in vitro	24h	THP-1 IL1-Beta Inflammation	N/A
	MW-F	in vitro	24h	THP-1 IL1-Beta Inflammation	N/A
	TNB	in vitro	24h	THP-1 IL1-Beta Inflammation	N/A

	SiO_2	in vitro	24h	THP-1 IL1-Beta Inflammation	N/A
zebrafish - OSU	Gold-MEE(1.5 nm)	Zebrafish	24h	Mortality - 24h	N/A
zebrafish - OSU	Gold-TMAT(0.8nm)	Zebrafish	24h	Mortality - 24h	N/A
zebrafish - OSU	Gold-MES(0.8 nm)	Zebrafish	24h	Mortality - 24h	N/A
zebrafish - OSU	Gold-MEE(0.8nm)	Zebrafish	24h	Mortality - 24h	N/A
zebrafish - OSU	Gold-TMAT(1.5nm)-ultrapure	Zebrafish	24h	Mortality - 24h	N/A
zebrafish - OSU	Gold-TMAT(1.5nm)-pure	Zebrafish	24h	Mortality - 24h	N/A
zebrafish - OSU	Gold-TMAT(1.5nm)-dirty	Zebrafish	24h	Mortality - 24h	N/A
zebrafish - OSU	Gold-MES(1.5nm)-ultrapure	Zebrafish	24h	Mortality - 24h	N/A
zebrafish - OSU	Gold-MES(1.5nm)-pure	Zebrafish	24h	Mortality - 24h	N/A
zebrafish - OSU	Gold-MES(1.5nm)-dirty	Zebrafish	24h	Mortality - 24h	N/A

zebrafish - OSU	Gold-TMAT(10nm)	Zebrafish	24h	Mortality - 24h	N/A
zebrafish - OSU	Gold-MHA(10nm)	Zebrafish	24h	Mortality - 24h	N/A
zebrafish - OSU	Gold-MEEE(0.8nm)	Zebrafish	24h	Mortality - 24h	N/A
zebrafish - OSU	Gold-MEEE(1.5 nm)	Zebrafish	24h	Mortality - 24h	N/A
zebrafish - OSU	Gold-MEEE(10nm)	Zebrafish	24h	Mortality - 24h	N/A
zebrafish - OSU	Gold-MEPA(1.5 nm)	Zebrafish	24h	Mortality - 24h	N/A
zebrafish - OSU	STARBURST (R) PAMAM Dendrimer DNT-104	Zebrafish	24h	Mortality - 24h	N/A
zebrafish - OSU	STARBURST (R) PAMAM Dendrimer DNT-105	Zebrafish	24h	Mortality - 24h	N/A
zebrafish - OSU	STARBURST (R) PAMAM Dendrimer DNT-106	Zebrafish	24h	Mortality - 24h	N/A
zebrafish - OSU	STARBURST (R) PAMAM Dendrimer DNT-107	Zebrafish	24h	Mortality - 24h	N/A
zebrafish - OSU	STARBURST (R) PAMAM Dendrimer DNT-174	Zebrafish	24h	Mortality - 24h	N/A

zebrafish - OSU	STARBURST (R) PAMAM Dendrimer DNT-189	Zebrafish	24h	Mortality - 24h	N/A
zebrafish - OSU	Aluminium Oxide Nanoparticles	Zebrafish	24h	Mortality - 24h	N/A
zebrafish - OSU	Titanium Dioxide Nanoparticles	Zebrafish	24h	Mortality - 24h	N/A
zebrafish - OSU	Zirconium Oxide Nanoparticles	Zebrafish	24h	Mortality - 24h	N/A
zebrafish - OSU	Cerium Oxide Nanoparticles	Zebrafish	24h	Mortality - 24h	N/A
zebrafish - OSU	Gadolinium Oxide Nanoparticles	Zebrafish	24h	Mortality - 24h	N/A
zebrafish - OSU	Dysprosium Oxide Nanoparticle	Zebrafish	24h	Mortality - 24h	N/A
zebrafish - OSU	Yttrium Oxide Nanoparticles	Zebrafish	24h	Mortality - 24h	N/A
zebrafish - OSU	Holmium Oxide Nanoparticles	Zebrafish	24h	Mortality - 24h	N/A
zebrafish - OSU	Samarium Oxide Nanoparticles	Zebrafish	24h	Mortality - 24h	N/A
zebrafish - OSU	alumina-doped silicon dioxide	Zebrafish	24h	Mortality - 24h	N/A

zebrafish - OSU	Erbium Oxide (III) Nanoparticles	Zebrafish	24h	Mortality - 24h	N/A
zebrafish - OSU	carboxylated FluoroSpheres	Zebrafish	24h	Mortality - 24h	N/A
zebrafish - OSU	sulfate FluoroSpheres	Zebrafish	24h	Mortality - 24h	N/A
zebrafish - OSU	aldehyde-sulfate FluoroSpheres	Zebrafish	24h	Mortality - 24h	N/A
zebrafish - OSU	gold nanorods (AuSoy95PC-1org1)	Zebrafish	24h	Mortality - 24h	N/A
zebrafish - OSU	gold nanorods (AuSoy95PC-1org2)	Zebrafish	24h	Mortality - 24h	N/A
zebrafish - OSU	gold nanorods (AuSoy95PC-3AQ)	Zebrafish	24h	Mortality - 24h	N/A
zebrafish - OSU	AuSoy95PC-2org1	Zebrafish	24h	Mortality - 24h	N/A
zebrafish - OSU	gold nanorods (AuSoy95PC-2org2)	Zebrafish	24h	Mortality - 24h	N/A
zebrafish - OSU	Carboxylated Nanocrystaline Cellulose	Zebrafish	24h	Mortality - 24h	N/A
zebrafish - OSU	Sulfonated Nanocrystaline Cellulose	Zebrafish	24h	Mortality - 24h	N/A

zebrafish - OSU	Aldrich ZnO+Oleic Acid (TLAD25A)	Zebrafish	24h	Mortality - 24h	N/A
zebrafish - OSU	Voxtel ZnO + Oleic Acid (TLAD25)	Zebrafish	24h	Mortality - 24h	N/A
zebrafish - OSU	Aldrich ZnO (TLAD24A)	Zebrafish	24h	Mortality - 24h	N/A
zebrafish - OSU	Voxtel ZnO (TLAD24)	Zebrafish	24h	Mortality - 24h	N/A
zebrafish - OSU	Aldrich ZnO + Octanoic Acid (TLAD27A)	Zebrafish	24h	Mortality - 24h	N/A
zebrafish - OSU	Voxtel ZnO + Octanoic Acid (TLAD27)	Zebrafish	24h	Mortality - 24h	N/A
zebrafish - OSU	Aldrich ZnO + para-Nitrobenzoic Acid (TLAD35A)	Zebrafish	24h	Mortality - 24h	N/A
zebrafish - OSU	Voxtel ZnO + para-Nitrobenzoic Acid (TLAD35)	Zebrafish	24h	Mortality - 24h	N/A
zebrafish - OSU	Aldrich ZnO + Cyclohexane Carboxilic Acid (TLAD31A)	Zebrafish	24h	Mortality - 24h	N/A
zebrafish - OSU	Voxtel ZnO + Cyclohexane Carboxilic Acid (TLAD31)	Zebrafish	24h	Mortality - 24h	N/A
zebrafish - OSU	Aldrich ZnO + Benzoic Acid (TLAD33A)	Zebrafish	24h	Mortality - 24h	N/A

zebrafish - OSU	Voxtel ZnO + Benzoic Acid (TLAD33)	Zebrafish	24h	Mortality - 24h	N/A
zebrafish - OSU	FITC Encapsulated SiO2 (W084)	Zebrafish	24h	Mortality - 24h	N/A
zebrafish - OSU	Silver - Nanocomposix BioPure (10nm)	Zebrafish	24h	Mortality - 24h	N/A
zebrafish - OSU	Nanocomposix BioPure (silver over gold - 20nm)	Zebrafish	24h	Mortality - 24h	N/A
zebrafish - OSU	Nanocomposix BioPure (silver over gold - 30nm)	Zebrafish	24h	Mortality - 24h	N/A
zebrafish - OSU	Nanocomposix BioPure (silver over gold - 40nm)	Zebrafish	24h	Mortality - 24h	N/A
zebrafish - OSU	Nanocomposix BioPure (silver over gold - 50nm)	Zebrafish	24h	Mortality - 24h	N/A
zebrafish - OSU	Nanocomposix BioPure (silver over gold - 60nm)	Zebrafish	24h	Mortality - 24h	N/A
zebrafish - OSU	Nanocomposix BioPure (silver over gold - 70nm)	Zebrafish	24h	Mortality - 24h	N/A
zebrafish - OSU	Nanocomposix BioPure (silver over gold - 80nm)	Zebrafish	24h	Mortality - 24h	N/A
zebrafish - OSU	Nanocomposix BioPure (silver over gold - 90nm)	Zebrafish	24h	Mortality - 24h	N/A

zebrafish - OSU	Nanocomposix BioPure (silver over gold - 100nm)	Zebrafish	24h	Mortality - 24h	N/A
zebrafish - OSU	Nanocomposix BioPure (silver over gold - 110nm)	Zebrafish	24h	Mortality - 24h	N/A
zebrafish - OSU	ZnO Prepared in EtOH (Q002)	Zebrafish	24h	Mortality - 24h	N/A
zebrafish - OSU	Iron Oxide Prepared in EtOH (Q009)	Zebrafish	24h	Mortality - 24h	N/A
zebrafish - OSU	ZnO Prepared in DEG (NM005)	Zebrafish	24h	Mortality - 24h	N/A
zebrafish - OSU	5% Fe Doped ZnO (Q007)	Zebrafish	24h	Mortality - 24h	N/A
zebrafish - OSU	Unoxidized Monothiol Capped Lead Sulfide Nanocrystals	Zebrafish	24h	Mortality - 24h	N/A
zebrafish - OSU	Oxidized Monothiol Capped Lead Sulfide Nanocrystals	Zebrafish	24h	Mortality - 24h	N/A
zebrafish - OSU	Unoxidized Dithiol Capped Lead Sulfide Nanocrystals	Zebrafish	24h	Mortality - 24h	N/A
zebrafish - OSU	Oxidized Dithiol Capped Lead Sulfide Nanocrystals	Zebrafish	24h	Mortality - 24h	N/A
zebrafish - OSU	ZnO I (NI001)	Zebrafish	24h	Mortality - 24h	N/A

zebrafish - OSU	ZnO I (NI002)	Zebrafish	24h	Mortality - 24h	N/A
zebrafish - OSU	ZnO I (NI003)	Zebrafish	24h	Mortality - 24h	N/A
zebrafish - OSU	ZnO I (NI005)	Zebrafish	24h	Mortality - 24h	N/A
zebrafish - OSU	ZnO II (QJ006)	Zebrafish	24h	Mortality - 24h	N/A
zebrafish - OSU	Cellulose Nanofibers by homogenization	Zebrafish	24h	Mortality - 24h	N/A
zebrafish - OSU	Cellulose Nanofibers by Sulfonation	Zebrafish	24h	Mortality - 24h	N/A
zebrafish - OSU	Cellulose Nanofibers by Tempo	Zebrafish	24h	Mortality - 24h	N/A
zebrafish - OSU	BioVision CNC BV3-2-11	Zebrafish	24h	Mortality - 24h	N/A
zebrafish - OSU	CNC_EDC-Taurine DW-1-23-4	Zebrafish	24h	Mortality - 24h	N/A
zebrafish - OSU	CNC_EDC-MEE DW-1-24-3	Zebrafish	24h	Mortality - 24h	N/A
zebrafish - OSU	CNC_EDC-Taurine DW-1-28-3	Zebrafish	24h	Mortality - 24h	N/A

zebrafish - OSU	CNC_EDC-MEE DW-1-38-4	Zebrafish	24h	Mortality - 24h	N/A
zebrafish - OSU	CNC_EDC-Taurine DW-1-40-1	Zebrafish	24h	Mortality - 24h	N/A
zebrafish - OSU	CNC_EDC-Ethlylenediamine MA-1-42-1	Zebrafish	24h	Mortality - 24h	N/A
zebrafish - OSU	CNC_EDC-Hexamethylethlylene diamine MA-1-62-1	Zebrafish	24h	Mortality - 24h	N/A
zebrafish - OSU	CNC_Carboxylated MA-1-77-1	Zebrafish	24h	Mortality - 24h	N/A
zebrafish - OSU	Gold Nanorods (10x34nm) #79-6000	Zebrafish	24h	Mortality - 24h	N/A
zebrafish - OSU	Gold Nanorods (10x73nm) #79-6015	Zebrafish	24h	Mortality - 24h	N/A
zebrafish - OSU	Gold Nanorods (10x29nm) #79-6020	Zebrafish	24h	Mortality - 24h	N/A
zebrafish - OSU	Holmium Oxide - Sonicated	Zebrafish	24h	Mortality - 24h	N/A
zebrafish - OSU	Holmium Oxide - vortexed	Zebrafish	24h	Mortality - 24h	N/A
zebrafish - OSU	1% Mn doped TiO_2	Zebrafish	24h	Mortality - 24h	N/A

zebrafish - OSU	3% Mn doped TiO_2	Zebrafish	24h	Mortality - 24h	N/A
zebrafish - OSU	TiO_2 - anatase	Zebrafish	24h	Mortality - 24h	N/A
zebrafish - OSU	Samarium Oxide - Sonicated	Zebrafish	24h	Mortality - 24h	N/A
zebrafish - OSU	Samarium Oxide - Vortexed	Zebrafish	24h	Mortality - 24h	N/A
zebrafish - OSU	Aerooxide® TiO_2 P 25	Zebrafish	24h	Mortality - 24h	N/A
zebrafish - OSU	Thiophosphoryl-PMMH-3 Dendrimer, Generation 0.5	Zebrafish	24h	Mortality - 24h	N/A
zebrafish - OSU	Thiophosphoryl-PMMH-6 Dendrimer, Generation 1.5	Zebrafish	24h	Mortality - 24h	N/A
zebrafish - OSU	Thiophosphoryl-PMMH-12 Dendrimer, Generation 2.5	Zebrafish	24h	Mortality - 24h	N/A
zebrafish - OSU	Thiophosphoryl-PMMH-24 Dendrimer, Generation 3.5	Zebrafish	24h	Mortality - 24h	N/A
zebrafish - OSU	Thiophosphoryl-PMMH-48 Dendrimer, Generation 5.0	Zebrafish	24h	Mortality - 24h	N/A
zebrafish - OSU	Aqueously Aged C60s	Zebrafish	24h	Mortality - 24h	N/A

zebrafish - OSU	Europium Oxide	Zebrafish	24h	Mortality - 24h	N/A
zebrafish - OSU	Platinum (3nm)	Zebrafish	24h	Mortality - 24h	N/A
zebrafish - OSU	Rhodamine NCC	Zebrafish	24h	Mortality - 24h	N/A
zebrafish - OSU	Sigma TiO_2	Zebrafish	24h	Mortality - 24h	N/A
zebrafish - OSU	PAMAM Succinamic Acid G5 Dendrimer	Zebrafish	24h	Mortality - 24h	N/A
zebrafish - OSU	Zinc nanoparticles doped with Aluminum oxide (AZO)	Zebrafish	24h	Mortality - 24h	N/A
zebrafish - OSU	Europium (III) Oxide	Zebrafish	24h	Mortality - 24h	N/A
zebrafish - OSU	Gold	Zebrafish	24h	Mortality - 24h	N/A
zebrafish - OSU	Neodymium (III) Oxide	Zebrafish	24h	Mortality - 24h	N/A
zebrafish - OSU	Silver 2 nm	Zebrafish	24h	Mortality - 24h	N/A
zebrafish - OSU	NanoGard ZnO	Zebrafish	24h	Mortality - 24h	N/A

zebrafish - OSU	Silica 12 nm	Zebrafish	24h	Mortality - 24h	N/A
zebrafish - OSU	Aluminum Oxide, 30nm alpha	Zebrafish	24h	Mortality - 24h	N/A
zebrafish - OSU	Aluminum Oxide, 10nm, gamma	Zebrafish	24h	Mortality - 24h	N/A
zebrafish - OSU	Aluminum Oxide, 30nm (gamma)	Zebrafish	24h	Mortality - 24h	N/A
zebrafish - OSU	Antimony (III) Oxide	Zebrafish	24h	Mortality - 24h	N/A
zebrafish - OSU	Cellulose Nanofibers 2.95%	Zebrafish	24h	Mortality - 24h	N/A
zebrafish - OSU	EDC-AEE CNC (DW 1-38-4 0.815%)	Zebrafish	24h	Mortality - 24h	N/A
zebrafish - OSU	CNC-GMAC	Zebrafish	24h	Mortality - 24h	N/A
zebrafish - OSU	Sigma Copper (II) Oxide	Zebrafish	24h	Mortality - 24h	N/A
zebrafish - OSU	Hydroxyl terminated Silica-coated Silver	Zebrafish	24h	Mortality - 24h	N/A
zebrafish - OSU	70nm Silica	Zebrafish	24h	Mortality - 24h	N/A

zebrafish - OSU	MWCNTs OD: 20-30nm	Zebrafish	24h	Mortality - 24h	N/A
zebrafish - OSU	MWCNTs OD: 5-15nm	Zebrafish	24h	Mortality - 24h	N/A
zebrafish - OSU	NanoTek Zinc Oxide	Zebrafish	24h	Mortality - 24h	N/A
zebrafish - OSU	SEF Amine-Terminated Silica coated Ag 70, 1/2x APTES	Zebrafish	24h	Mortality - 24h	N/A
zebrafish - OSU	SEF Amine-Terminated Silica coated Ag 70, 1x APTES	Zebrafish	24h	Mortality - 24h	N/A
zebrafish - OSU	SEF Amine-Terminated Silica coated Ag 70, 2x APTES	Zebrafish	24h	Mortality - 24h	N/A
zebrafish - OSU	Sigma MWCNTs OD=8nm ID=2-5nm Length= 0.5-200 um	Zebrafish	24h	Mortality - 24h	N/A
zebrafish - OSU	Terbium (III,IV) oxide	Zebrafish	24h	Mortality - 24h	N/A
zebrafish - OSU	ZnO NanoShield ZN-3008C	Zebrafish	24h	Mortality - 24h	N/A
zebrafish - OSU	Zinc Oxide Nanopowder	Zebrafish	24h	Mortality - 24h	N/A
zebrafish - OSU	Amine-Terminated Silica coated Ag 70, 1/2x APTES	Zebrafish	24h	Mortality - 24h	N/A

zebrafish - OSU	Amine-Terminated Silica coated Ag 70, 1x APTES	Zebrafish	24h	Mortality - 24h	N/A
zebrafish - OSU	Amine-Terminated Silica coated Ag 20, 1x APTES	Zebrafish	24h	Mortality - 24h	N/A
zebrafish - OSU	Amine-Terminated Silica coated Ag 70, 2x APTES	Zebrafish	24h	Mortality - 24h	N/A
zebrafish - OSU	70nm Amine Terminated Silica Coated Silver	Zebrafish	24h	Mortality - 24h	N/A
zebrafish - OSU	80nm Amine Terminated Silica	Zebrafish	24h	Mortality - 24h	N/A
zebrafish - OSU	SEF Amine-Terminated Silica coated Ag 20, 1x APTES	Zebrafish	24h	Mortality - 24h	N/A
zebrafish - Army	75_nm_Silver_Nanosphere_nanoComposix_Econix	Zebrafish	24h	Mortality - 24h	N/A
zebrafish - Army	US_Nano_Zinc_Oxide_30-40_nm	Zebrafish	24h	Mortality - 24h	N/A
zebrafish - Army	200_nm_Silica_Nanosphere_nanoComposix_NanoXact	Zebrafish	24h	Mortality - 24h	N/A
zebrafish - Army	US_Nano_Aluminum_Oxide_gamma_30_nm	Zebrafish	24h	Mortality - 24h	N/A
zebrafish - Army	US_Nano_Titanium_Dioxide_Rutile_5-15_nm	Zebrafish	24h	Mortality - 24h	N/A

zebrafish - Army	US_Nano_Titanium_Dioxide_Anatase_5-15_nm	Zebrafish	24h	Mortality - 24h	N/A
zebrafish - Army	US_Nano_Aluminum_Oxide_gamma_10_nm	Zebrafish	24h	Mortality - 24h	N/A
zebrafish - Army	US_Nano_Titanium_Dioxide_Rutile_30-50_nm	Zebrafish	24h	Mortality - 24h	N/A
zebrafish - Army	US_Nano_Titanium_Dioxide_Anatase_30-50_nm	Zebrafish	24h	Mortality - 24h	N/A
zebrafish - Army	US_Nano_Iron_Oxide_gamma_20_nm	Zebrafish	24h	Mortality - 24h	N/A
zebrafish - Army	50_nm_Silica_Nanosphere_nanoComposix_Nanoxact	Zebrafish	24h	Mortality - 24h	N/A
zebrafish - Army	100_nm_Silica_Nanosphere_nanoComposix_NanoXact	Zebrafish	24h	Mortality - 24h	N/A
zebrafish - Army	US_Nano_Aluminum_Oxide_alpha_30_nm	Zebrafish	24h	Mortality - 24h	N/A
zebrafish - Army	20nm_Silica_Nanosphere_nanoComposix_NanoXact	Zebrafish	24h	Mortality - 24h	N/A
zebrafish - Army	25_nm_Silver_Nanosphere_nanoComposix_Econix	Zebrafish	24h	Mortality - 24h	N/A
zebrafish - Army	US_Nano_Iron_Oxide_15-20_nm	Zebrafish	24h	Mortality - 24h	N/A

zebrafish - Army	NIST_PVP_Coated_Silver_Nanoparticles	Zebrafish	24h	Mortality - 24h	N/A
zebrafish - Army	400_nm_Silica_Nanosphere_nanoComposix_NanoXact	Zebrafish	24h	Mortality - 24h	N/A
zebrafish - Army	5_nm_Silver_Nanosphere_nanoComposix_Econix	Zebrafish	24h	Mortality - 24h	N/A
zebrafish - Army	Cerium_Oxide	Zebrafish	24h	Mortality - 24h	N/A
zebrafish - Army	US_Nano_Zinc_Oxide_50-80_nm	Zebrafish	24h	Mortality - 24h	N/A

Appendix C: In Vitro Inflammation and Cytotoxicity

Table C-1: BMD and BMDL estimates for NanoGo THP-1 IL-1 Beta dose-response relationships using Stochastic Kriging, BMR = γ+5%

Case	Material	BMD (μg/mL)	BMDL (μg/mL)
1	ZnO	N/A	N/A

2	ZnO	N/A	N/A
3	ZnO	Not Estimable	0.51
4	ZnO	N/A	N/A
6	ZnO	Not Estimable	Not Estimable
7	ZnO	Not Estimable	0.26
31	TNB	0.10	0.00
34	TNB	0.10	0.01
29	TNB	0.17	0.05
35	TNB	0.28	0.09
30	TNB	0.31	0.01
33	TNB	0.44	0.01
9	MW-O	0.59	0.01
39	SiO_2	0.78	0.02
13	MW-O	1.18	0.36
11	MW-O	1.21	0.03
37	SiO2	1.24	0.02
41	SiO2	1.62	0.46
14	MW-O	2.03	0.04
15	MW-P	2.12	0.05
20	MW-P	2.74	0.93
21	MW-P	3.17	0.06
8	MW-O	4.03	0.05
27	MW-F	11.14	2.14
36	SiO_2	16.19	4.45
28	MW-F	24.64	3.87
16	MW-P	N/A	N/A
18	MW-P	N/A	N/A
25	MW-F	N/A	N/A
32	TNB	N/A	N/A
42	SiO_2	N/A	N/A
5	ZnO	No Trend	No Trend
10	MW-O	No Trend	No Trend
12	MW-O	No Trend	No Trend
17	MW-P	No Trend	No Trend
19	MW-P	No Trend	No Trend
22	MW-F	No Trend	No Trend

23	MW-F	No Trend	No Trend
24	MW-F	No Trend	No Trend
26	MW-F	No Trend	No Trend
38	SiO_2	No Trend	No Trend
40	SiO_2	No Trend	No Trend

Table C-2: BMD and BMDL estimates for NanoGo THP-1 IL-1 Beta dose-response relationships using Stochastic Kriging, BMR = γ+1.1 standard deviations

Case	Material	BMD (μg/mL)	BMDL (μg/mL)
1	ZnO	N/A	N/A
2	ZnO	N/A	N/A
4	ZnO	N/A	N/A
3	ZnO	Not Estimable	Not Estimable
6	ZnO	Not Estimable	Not Estimable
7	ZnO	Not Estimable	Not Estimable
29	TNB	0.16	0.04
31	TNB	0.21	0.06
30	TNB	0.71	0.20
34	TNB	0.83	0.23
33	TNB	0.93	0.26
13	MW-O	1.12	0.30
9	MW-O	1.36	0.40
41	SiO_2	1.53	0.39
39	SiO_2	1.72	0.53
20	MW-P	2.59	0.77
11	MW-O	2.69	0.75
37	SiO_2	2.89	0.85
35	TNB	3.87	0.80
14	MW-O	4.27	1.10
21	MW-P	6.72	2.18
9827	MW-F	10.61	1.84
8	MW-O	12.06	5.14
15	MW-P	13.74	5.77
36	SiO_2	31.33	23.56
28	MW-F	32.55	25.13
16	MW-P	N/A	N/A
18	MW-P	N/A	N/A
25	MW-F	N/A	N/A
32	TNB	N/A	N/A
42	SiO_2	N/A	N/A
5	ZnO	No Trend	No Trend

10	MW-O	No Trend	No Trend
12	MW-O	No Trend	No Trend
17	MW-P	No Trend	No Trend
19	MW-P	No Trend	No Trend
22	MW-F	No Trend	No Trend
23	MW-F	No Trend	No Trend
24	MW-F	No Trend	No Trend
26	MW-F	No Trend	No Trend
38	SiO_2	No Trend	No Trend
40	SiO_2	No Trend	No Trend

Table C-3: In vitro Covariance Kernel choice for Stochastic Kriging modeling of the NanoGo data (both BMRs)

Case	Material	Kernel	Note		Case	Material	Kernel	Note
1	ZnO	None	non-monotonic		22	MW-F	None	non-monotonic
2	ZnO	None	non-monotonic		23	MW-F	None	non-monotonic
3	ZnO	Exp			24	MW-F	None	non-monotonic
4	ZnO	None	non-monotonic		25	MW-F	None	non-monotonic
5	ZnO	Gauss			26	MW-F	Exp	
6	ZnO	Exp			27	MW-F	Gauss	
7	ZnO	Exp			28	MW-F	Gauss	
8	MW-O	Gauss			29	TNB	Exp	
9	MW-O	Exp			30	TNB	Exp	
10	MW-O	Exp			31	TNB	Exp	
11	MW-O	Exp			32	TNB	None	non-monotonic
12	MW-O	Exp			33	TNB	Exp	
13	MW-O	Gauss			34	TNB	Exp	
14	MW-O	Exp			35	TNB	Gauss	
15	MW-P	Exp			36	SiO2	Gauss	
16	MW-P	None	non-monotonic		37	SiO2	Gauss	
17	MW-P	None	non-monotonic		38	SiO2	None	non-monotonic
18	MW-P	None	non-monotonic		39	SiO2	Exp	
19	MW-P	Gauss			40	SiO2	None	non-monotonic
20	MW-P	Gauss			41	SiO2	Exp	
21	MW-P	Exp			42	SiO2	None	non-monotonic

Figure C-1: Dose-response plots with Stochastic Kriging model fits for NanoGo

Best fitting models are shown below for each of the 42 cases. For those with a kernel selection of "None", meaning no model adequately fits typically due to non-monotonicity, the General Exponential plot is shown.

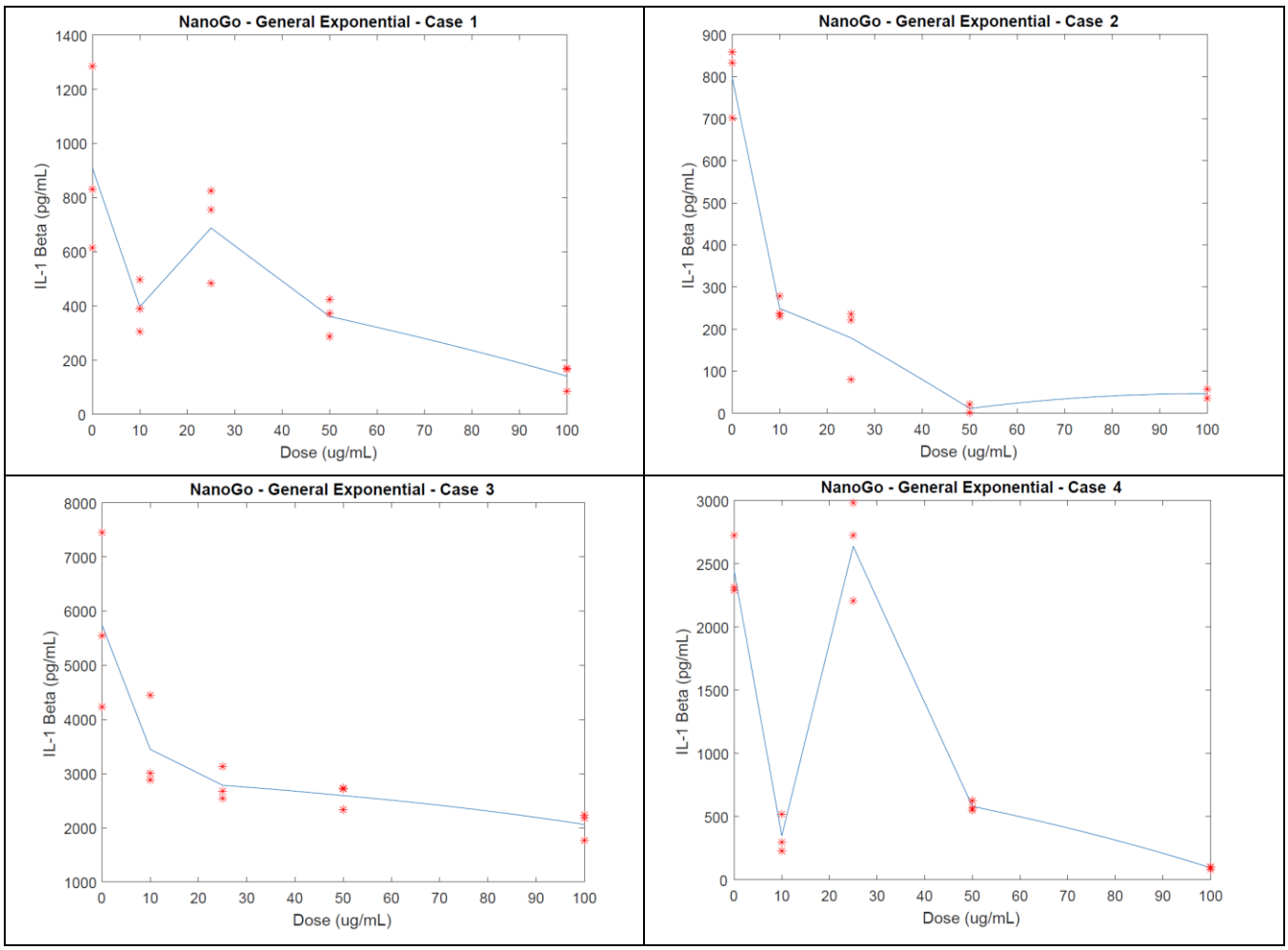

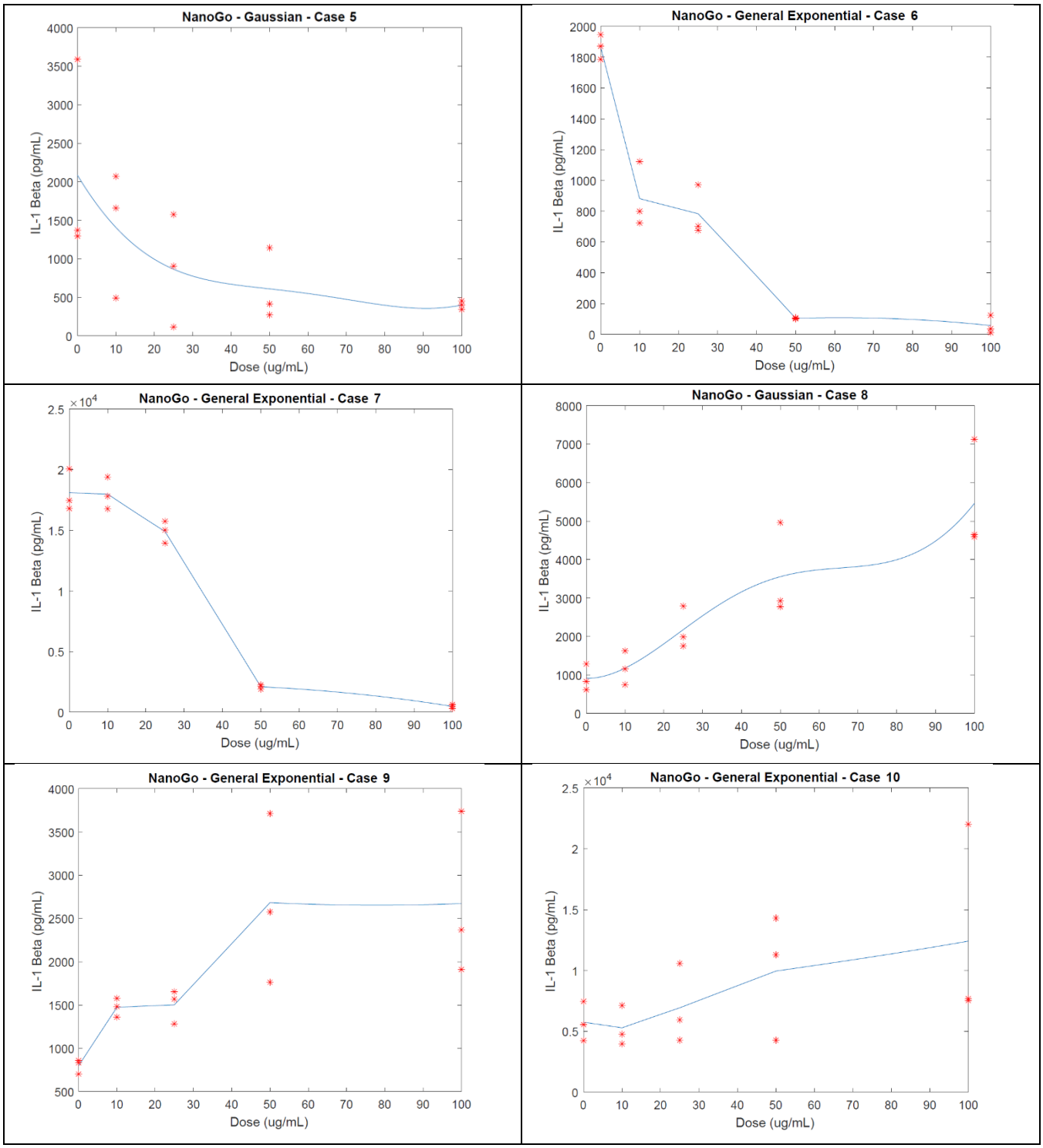

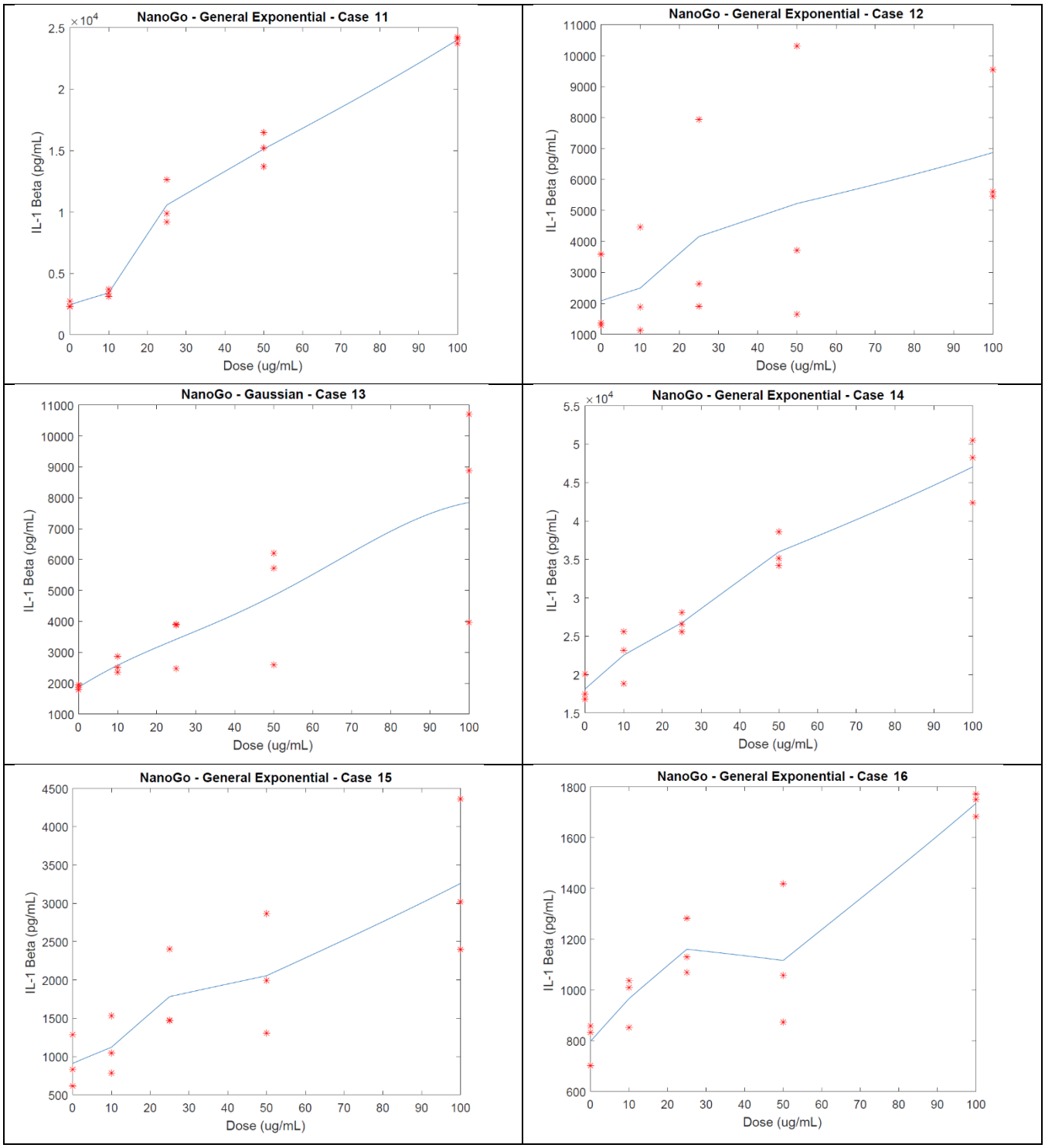

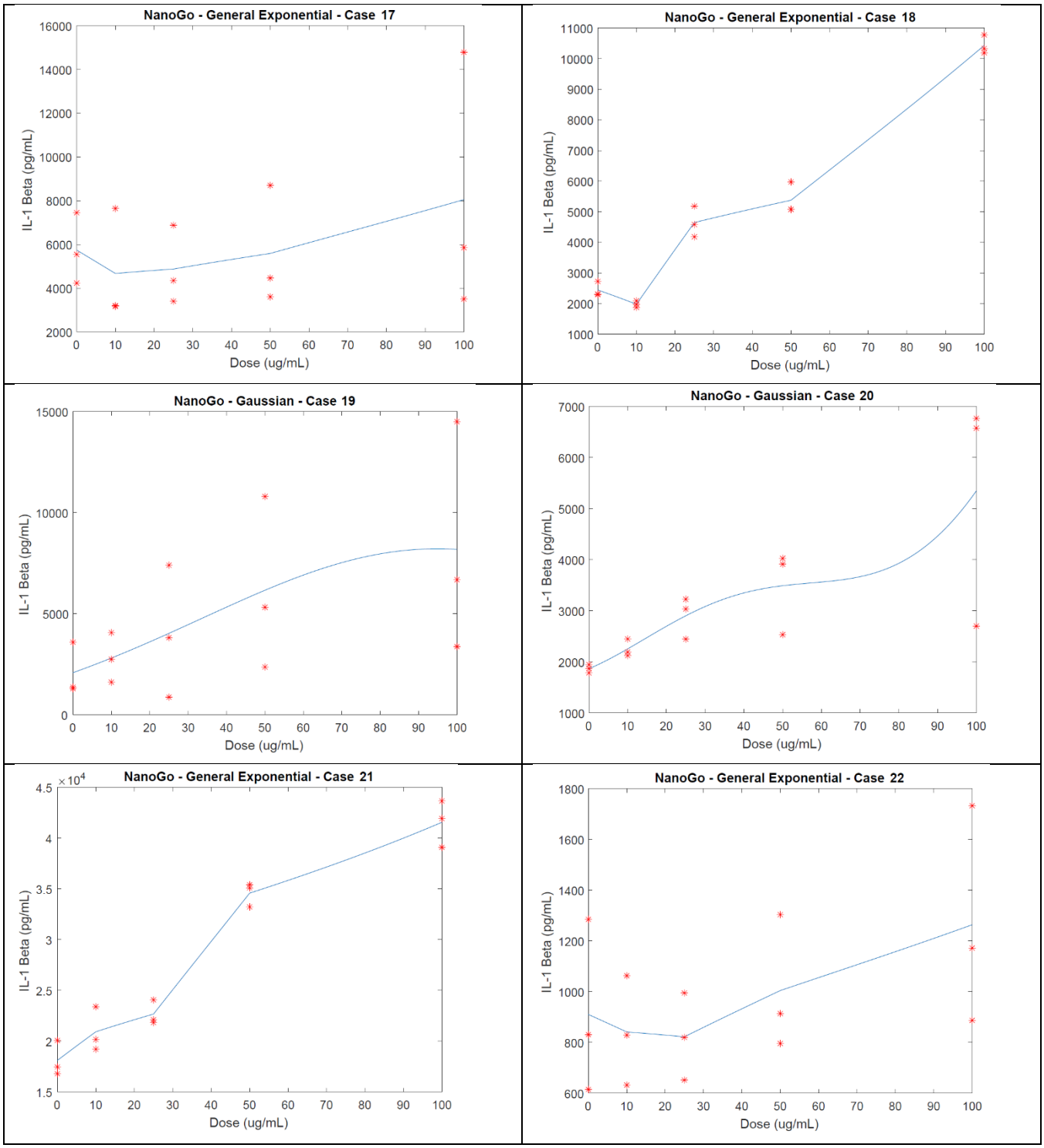

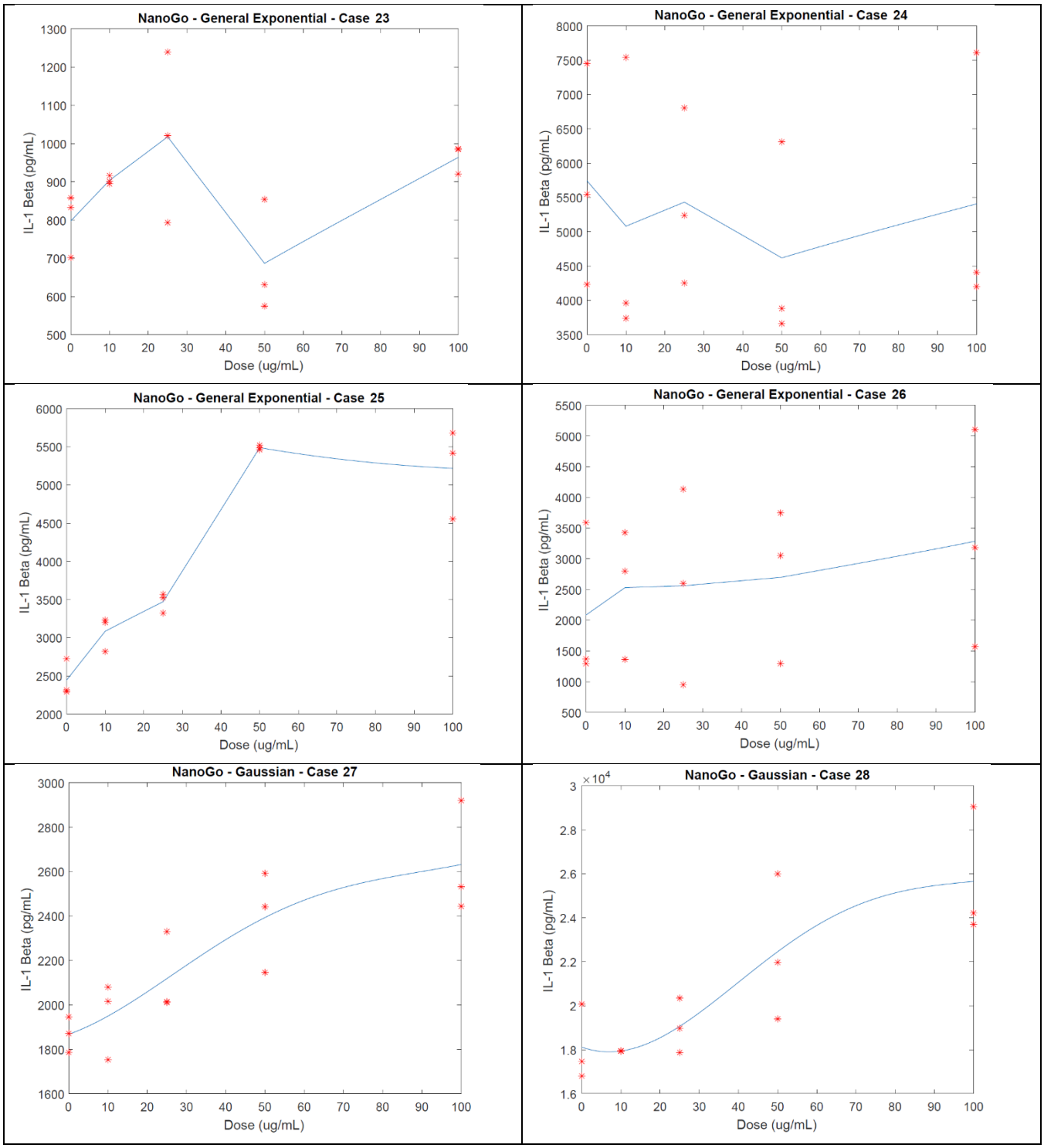

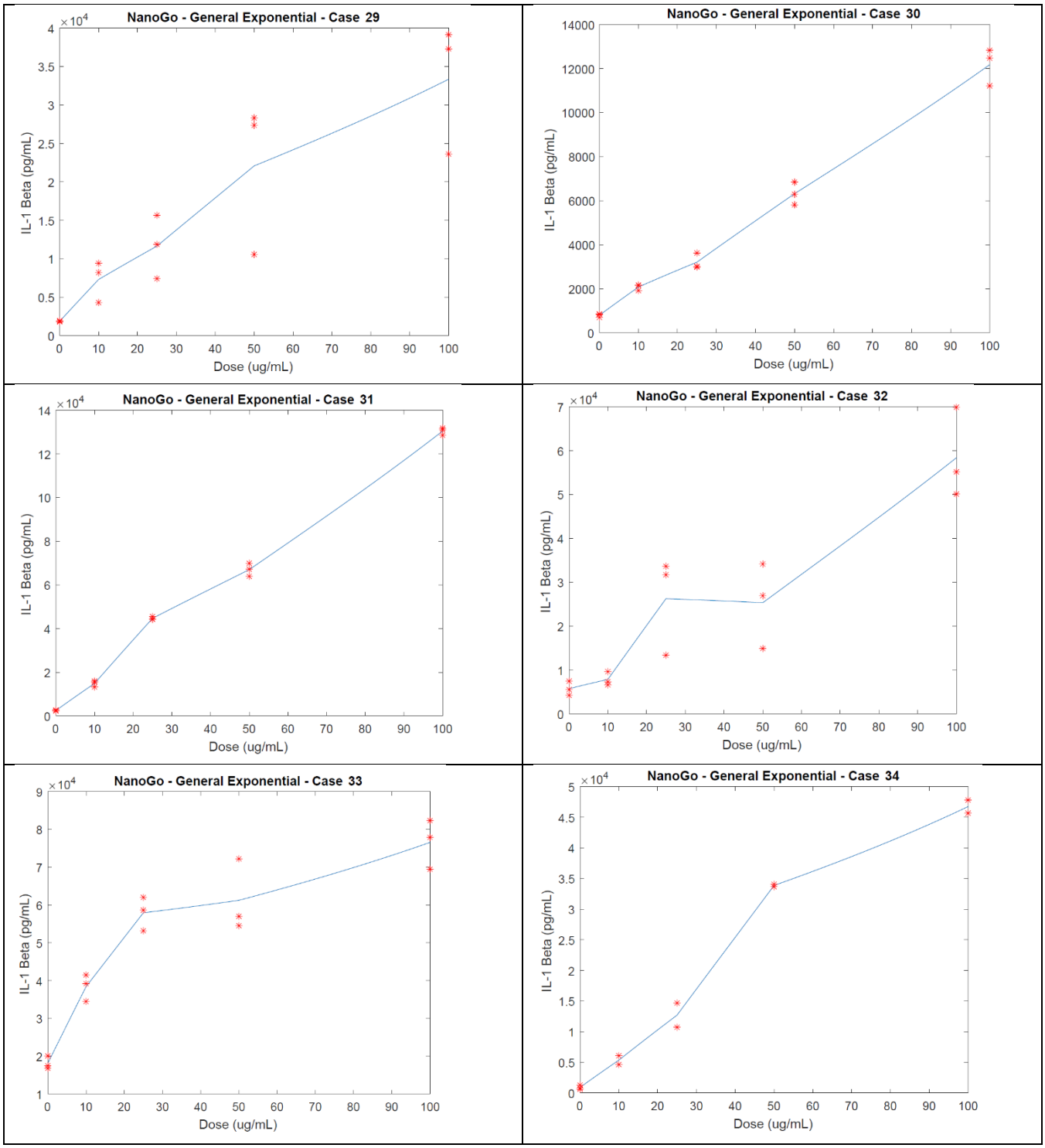

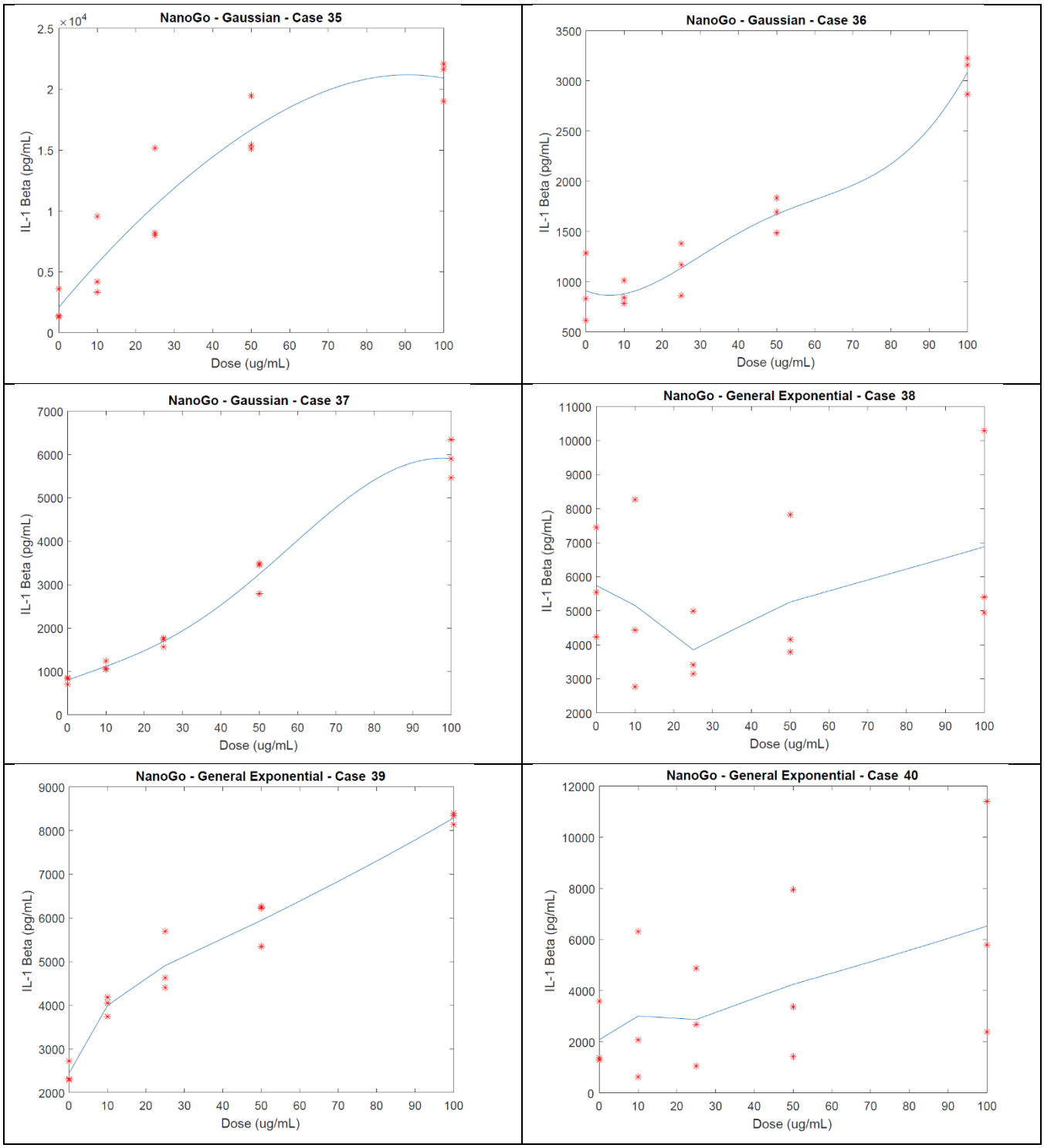

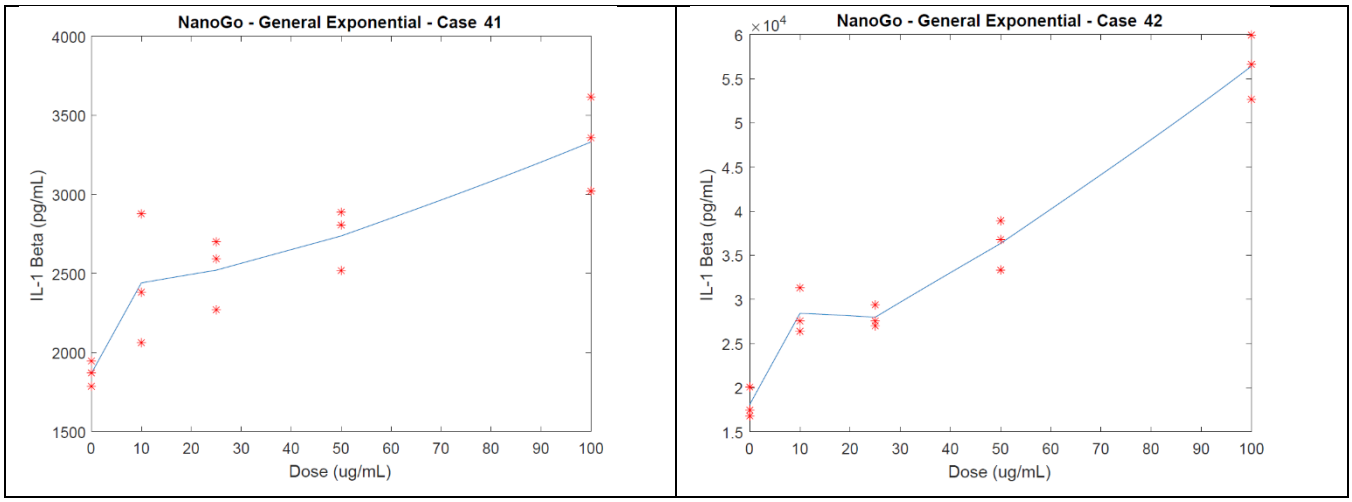

Cytotoxicity Methods and Results

Nine assays in the ENPRA database have cytotoxicity as the assigned Assay End Point, where the cell line is LA-4 (mouse respiratory epithelial cell). All nine assays were conducted by one laboratory, HelmHoltz – Muenchen. This cell line was chosen as it is a lung cell; other cell types were MH-S (Murine Alveolar Macrophage) and C3A (Human hepatocyte- subclone of the hepatoma-derived HepG2). Each assay tests a different ENPRA material:

1. NM110 – ZnO
2. NM111 – Silane-ZnO
3. NM400 – PC-MWCNT
4. NM402 – MWCNT
5. NRCWE001 – TiO_2 (Rutile/Anatase)
6. NRCWE002 – TiO_2+ (Positively Charged)
7. NRCWE003 – TiO_2- (Negatively Charged)
8. NRCWE004 – TiO_2 (Rutile)
9. NM101 – TiO_2 (Anatase/Rutile)

In each of these assays, the ENPRA protocol was to use seven concentrations (including control) in µg/cm2. Three post-exposure time points were used: 2, 6, and 24 hours. Because zebrafish mortality was measured at 24h post-exposure, this same time point will be analyzed. At each time point, there were three experiments, where each experiment was replicated three times. Thus, for any given material, there are seven concentrations with up to nine cytotoxicity observations per concentration. The raw data observations appear to be reporting the percentage of dead cells.

A dataset was constructed from the nine individual files for analysis, with a total of 567 rows. The cytotoxicity responses are treated as continuous and were modeled using SK. Each of the nine materials were modeled using both the Gaussian and General Exponential covariance functions. A visual check of fit

was used to pick the most appropriate covariance function. The BMD is the dose associated with a response of 50% cytotoxicity above the background level. The lower confidence of the BMD was found via bootstrapping, and as such is represented by the 5th percentile of bootstrapped BMD estimates.

For these data, only ZnO was adequately modeled and a BMD/BMDL estimate was found. For the other materials, which tended to be less potent, the BMR was not observed. Therefore, an estimate of the BMD would require extrapolation beyond the highest experimental dose. Silane-ZnO also has a noticeable association, however the BMR was not reached (average background response= 0.3729, largest average response from the model = 0.8222, BMR = 0.8729). At even the highest concentrations, the cytotoxicity observations were not much different from background for the other eight materials. The General Exponential covariance function was used for all nine dose-response relationships, as the Gaussian tended to wander unrealistically between the highest two doses. The BMD and BMDL estimates for each of the nine materials using each covariance function are shown in the Appendix (Table C-4). Dose-response plots are shown in the Appendix (Figure C-2), where the first column uses the Gaussian covariance function and the second column uses the General Exponential covariance function.

Table C-4: BMD and BMDL estimates for ENPRA Cytotoxicity, BMR=Background + 50%

Material	Type	Covariance	BMD	BMDL
NM110	ZnO	Gaussian	58.2747	12.27426
NM111	Silane-ZnO	Gaussian	36.12406	16.04347
NM400	PC-MWCNT	Gaussian	55.35114	32.23627
NM402	MWCNT	Gaussian	37.27649	32.43914
NRCWE001	TiO_2	Gaussian	37.57932	33.45411
NRCWE002	TiO_2 +	Gaussian	59.8922	59.59755
NRCWE003	TiO_2 -	Gaussian	34.00312	32.76126
NRCWE004	TiO_2	Gaussian	41.42327	33.76437
NM101	TiO_2	Gaussian	NaN	41.51826
NM110	ZnO	GenExp	14.30185	11.73017
NM111	Silane-ZnO	GenExp	NaN	23.58447
NM400	PC-MWCNT	GenExp	NaN	NaN
NM402	MWCNT	GenExp	NaN	NaN
NRCWE001	TiO_2	GenExp	NaN	NaN
NRCWE002	TiO_2 +	GenExp	NaN	NaN
NRCWE003	TiO_2 -	GenExp	NaN	NaN
NRCWE004	TiO_2	GenExp	NaN	NaN
NM101	TiO_2	GenExp	NaN	NaN

Figure C-2: Stochastic Kriging Dose-Response Plots for ENPRA Cytotoxicity of nine materials, BMR=Background+50%

Material	Gaussian Covariance Function Fit	General Exponential Covariance Function Fit
NM110 ZnO	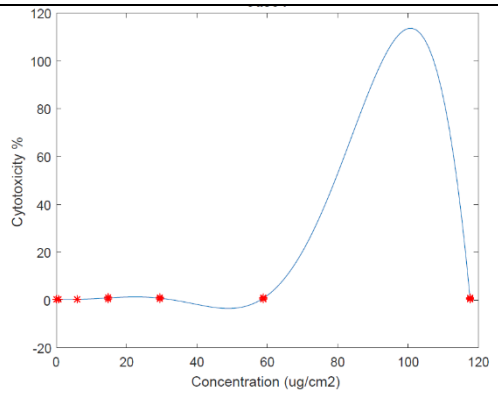	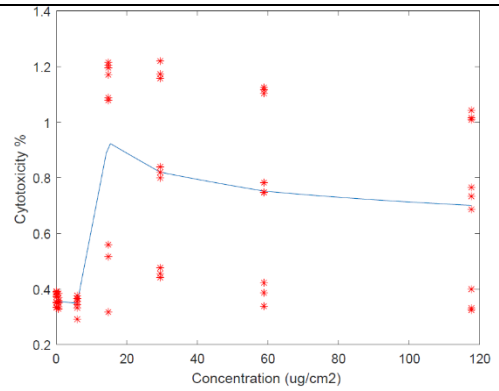
NM111 Silane-ZnO	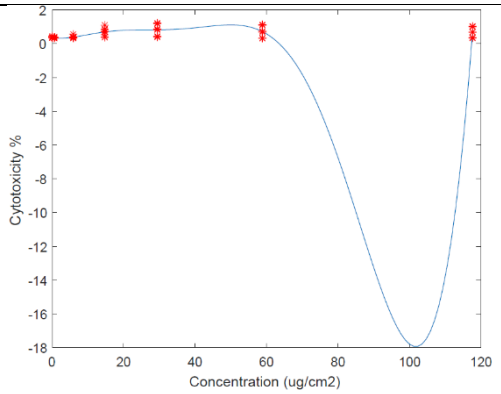	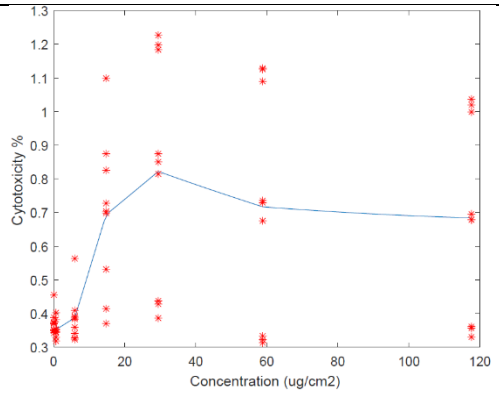
NM400 PC-MWCNT	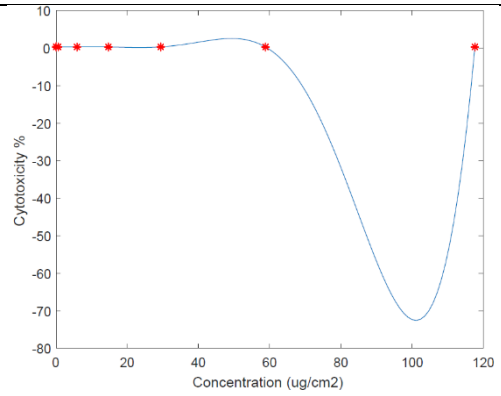	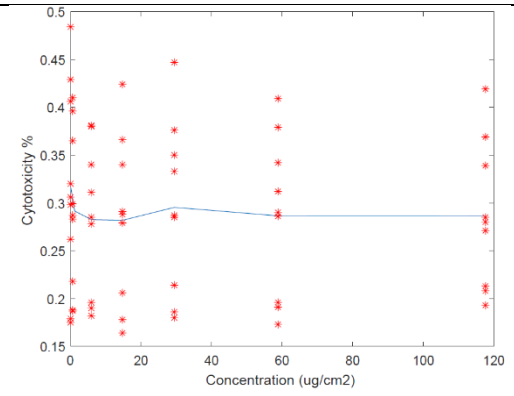

NM402 MWCNT	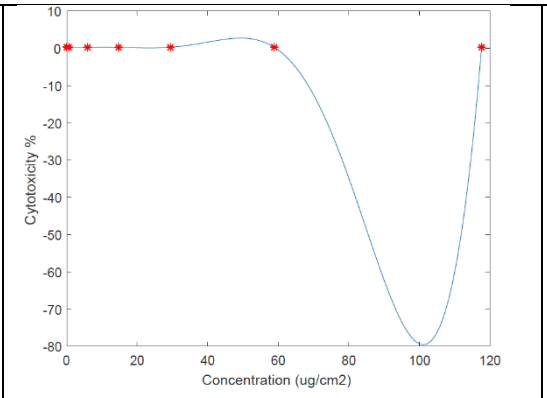	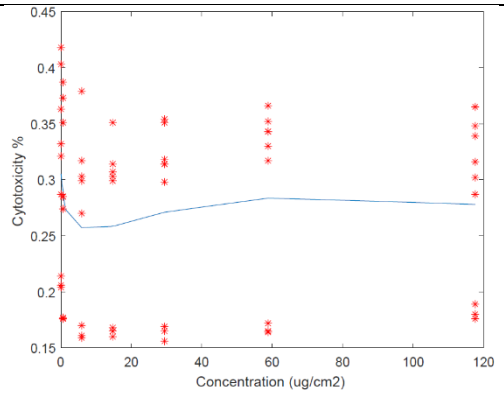
NRCWE001 TiO_2	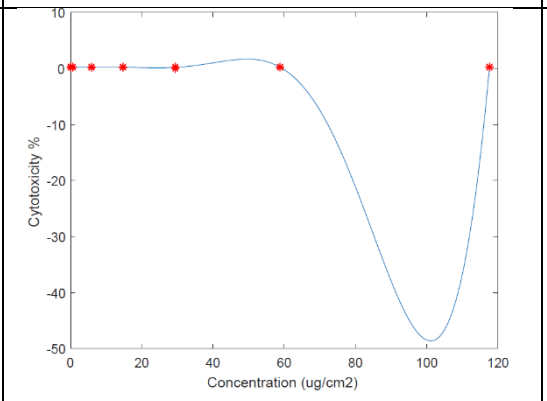	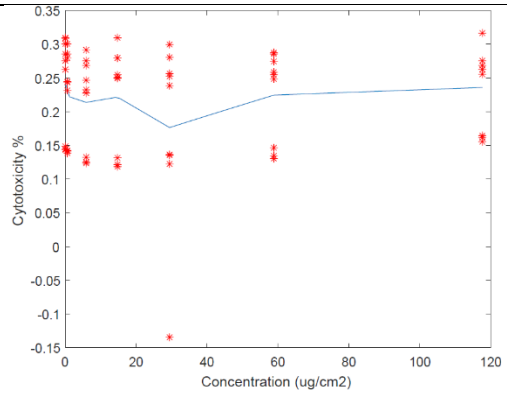
NRCWE002 TiO_2+	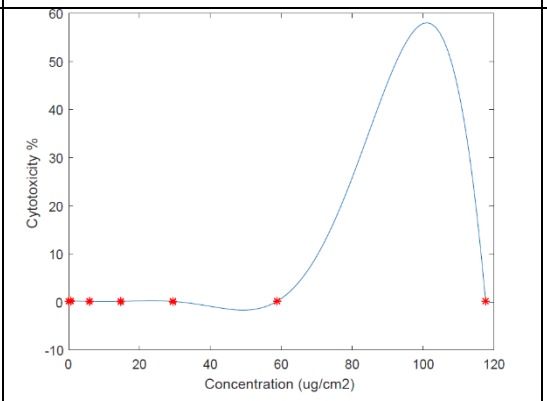	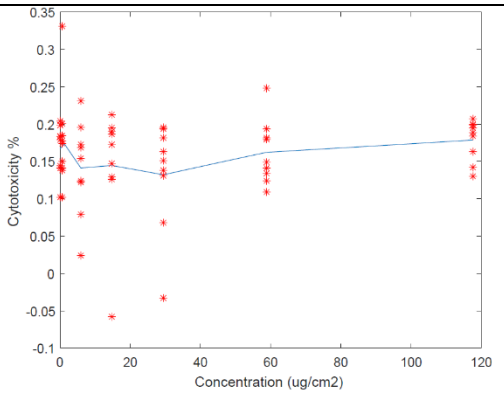
NRCWE003 TiO_2-	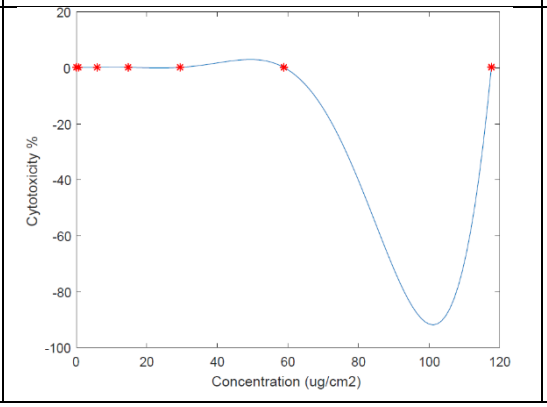	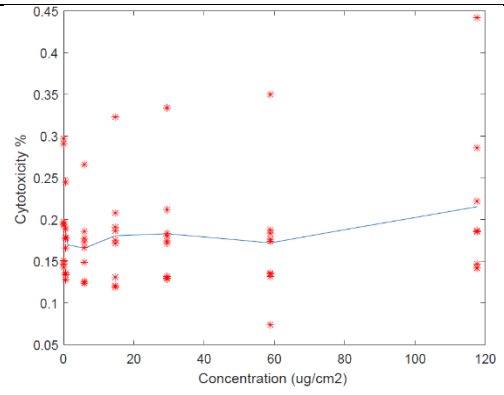

NRCWE004 TiO_2	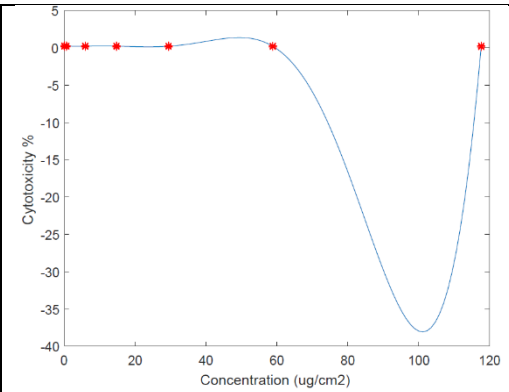	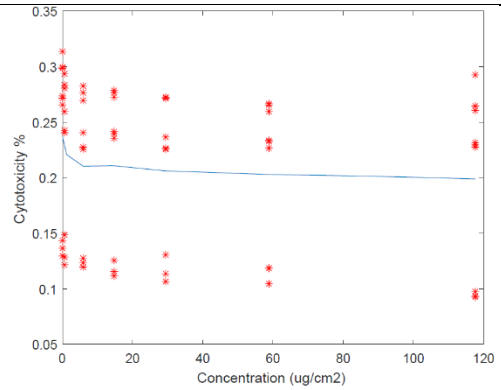
NM101 TiO_2	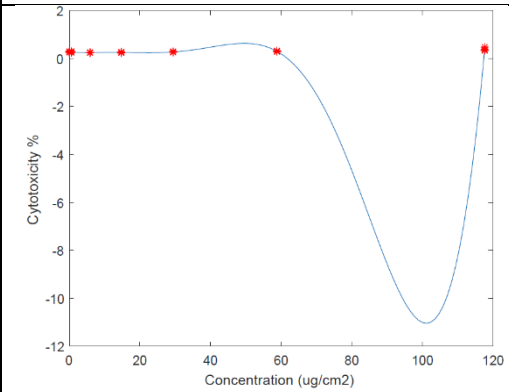	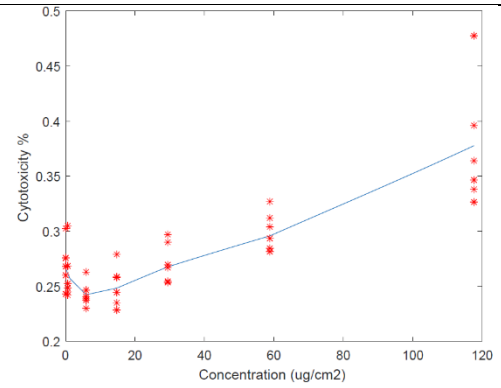

Out of the 650 *in vitro* assays in the ENPRA database, only nine used cytotoxicity as the endpoint. The assay results were variable and most did not have a clear association. ZnO and Silane-ZnO were the most potent and had associations that are more noticeable. A potency estimate could only be found for ZnO; positive associations were seen for Silane-ZnO and TiO_2 (NM101), but all responses were much lower than 50% above background. There appear to be no associations for the remaining six materials, but it may be assumed that their potency estimates lie somewhere above the maximum experimental concentration of 117 $\mu g/cm^2$. The choice of a lower BMR could permit more information (i.e., models can be fit to more associations than those for which a BMD can be found due to factors like extrapolation).

Due to the initially limited dataset and severely limited results, the NanoGo Cytotoxicity database may provide additional information for the relative ranking comparisons of nanomaterials between zebrafish mortality and *in vitro* cytotoxicity. These data are restricted in the sense that the observations are reported as "% Viable Cells Relative to Control", with no information about the actual observed Control response, thereby making it unable to

retrieve the original observed responses. This practice has resulted in a loss of information and complicates or frustrates BMR specification and BMD estimation.

For example, suppose the observed relative cytotoxicities (as would be seen in NanoGo) range from 0% to 97.7% (Table C-5). For a BMR of $\gamma + 50\%$, it would appear that the BMD is between 10 and 25, assuming that a BMR can be defined from the relative metric in this way. If we look at the original observed cytotoxicities (assuming 30% background cytotoxicity), however, the BMR of 0.8 falls beyond the highest dose and not between doses 10 and 25.

Table C-5: Example Data Comparing BMRs, Relative to Control vs. Observed

NanoGo Reporting Style			ENPRA Reporting Style	
Dose	% Cytotoxicity w.r.t Control		Dose	% Cytotoxicity
0	0		0	0.3
4	15.8		4	0.3474
10	15		10	0.345
25	87.7		25	0.5631
50	97.7		50	0.5931
BMD between 10 and 25			BMD above 50	

Appendix D: Zebrafish Mortality

A large dataset of zebrafish assay results was received from Oregon State University (OSU) researchers (Harper et al. 2015). This experiment tested the potency of a large number of ENMs across 21 toxicity endpoints, and various physicochemical properties were described for the nanomaterials. Thus, the data were appealing for further testing of the quantitative framework (Drew et al. 2017).

In addition, zebrafish assay results from the US Army Center for Environmental Health Research (CEHR) were also received. These files contain the zebrafish assay results and physicochemical properties of 22 materials of interest to the Army. There are only 21 materials in the toxicity data file and only 20 materials in the physicochemical data file. These materials are different from those used by OSU. All 21 toxicity endpoints are present in the toxicity data file, with the additional 120-hour endpoint of Notochord (curvy or otherwise abnormal).

In the US Army CEHR assays, exposure concentrations are given in μg/mL, whereas the OSU data are in ppm. Concentrations were converted to ppm (units conversion: μg/mL = ppm), and results are in ppm as that was the most common unit. In the US Army CEHR assays, 32 zebrafish were used per material per concentration. In the OSU design, between 12 and 72 zebrafish were used for each exposure.

A weighted embryonic zebrafish (EZ) metric score is provided, using the formula/weights presented in the Harper et al. [2015] paper and data file. Briefly, the EZ metric is a weighted average of various developmental measurements in the zebrafish. This metric was not used in the following analysis due to uncertainty of its applicability for comparison to other assays or endpoints. The difference is that 22 toxicity endpoints are considered versus the 21 in the OSU data; a 0.08 weight for 120h notochord is used. A 21-endpoint weighted EZ metric can be calculated to be commensurate with the OSU data. Additionally, the additive EZ metric can be calculated if needed, but is not already provided. The Harper et al. [2015] paper lists a weight of 0.02 for motility; however, that endpoint is not seen in the Army data nor the OSU data.

Various physicochemical properties (approximately 30) are reported. There is some overlap with the physicochemical properties reported in the OSU data, although many more properties were available in the OSU data (even though not all values are populated). For example, material name, particle size, zeta potential, and impurity information are available in both datasets.

Figure D-1: Heat map of correlations between physicochemical properties

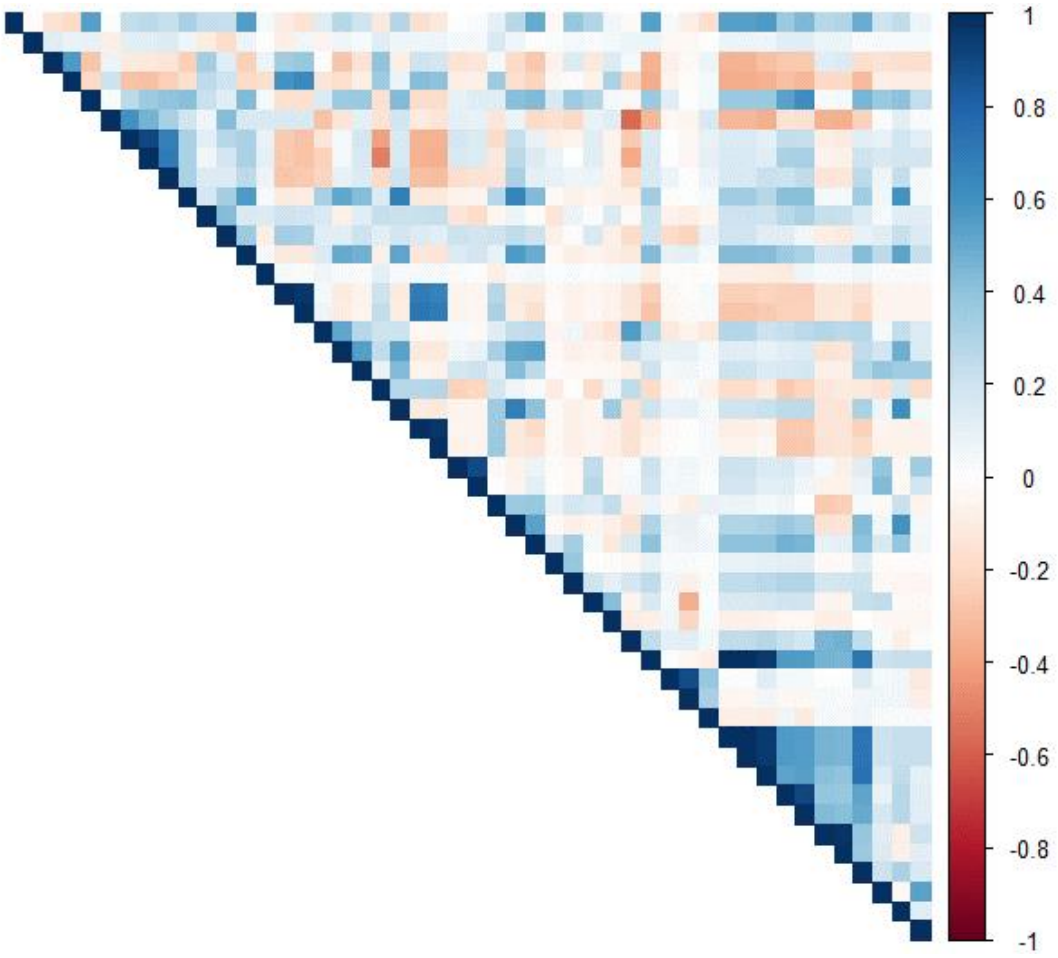

The endpoint of interest was mortality after 24 hours. Unfortunately, no endpoint was available which could be a closer analogue to the endpoints from other analyses, like inflammation or tumor. The one-sided Cochran-Armitage trend test was used to identify the subset of statistically significant relationships to be modeled from the initial set of 169, and a 5% level of significance was used. The EPA BMDS dichotomous model suite was used to estimate the potency for the 92 statistically significant dose-response relationships.

Concentration-response data on zebrafish mortality from two databases were used. The Army dataset has information on 21 ENMs; the OSU dataset covers 148 ENMs. Each dataset consisted of unique materials, so 169 distinct materials were available for analysis.

Mortality is a dichotomous outcome, so the Cochran-Armitage test for trend was performed and followed up by fitting traditional binomial dose-response models (i.e., BMDS model suite) of the data observed to have significant trends. These fitted models are used for estimating BMDs if they fit the data adequately and didn't require extrapolation. The BMR was chosen to be a response of 50% mortality above background.

Twelve of the 21 relationships of the Army dataset did not have a significant trend and were not modeled. The remaining nine were modeled using EPA BMDS. Results are summarized in the Appendix (Table D-1). Only four of the relationships had an estimable BMD, as the other five relationships did not observe mortality of at least 50% above the background rate, so the BMD estimate would require extrapolation (Figure D-2).

Table D-1: Benchmark Dose Modeling Results for Army Zebrafish Assays where a statistically significant trend was detected and no extrapolation was required, BMR=Added 50%, Endpoint=24h Mortality (µg/mL or ppm)

ID	Material	Trend	Extrapolation	Model	BMD	BMDL
N23901	US_Nano_Aluminum_Oxide_gamma_30_nm	Y	N	Log Probit	0.03	0.02
N44021	US_Nano_Titanium_Dioxide_Anatase_5-15_nm	Y	N	LogLogistic	0.07	0.05
N82750	25_nm_Silver_Nanosphere_nanoComposix_Econix	Y	N	LogLogistic	30.37	15.58
N98053	5_nm_Silver_Nanosphere_nanoComposix_Econix	Y	N	Probit	1.57	1.37

Figure D-2: Army Nanomaterial Data Waterfall – 24h Mortality, BMR=Added 50%

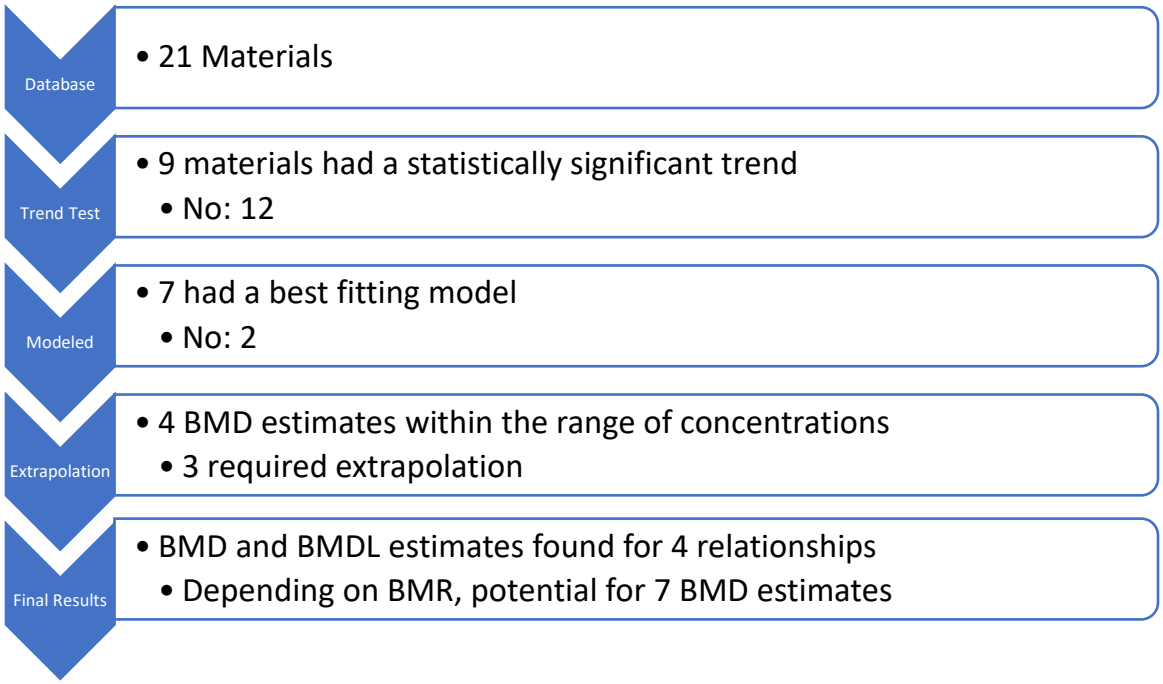

In the OSU dataset, 83 relationships were found to have significant trends. Like with the Army data subset, many of the dose-response relationships did not observe high rates of mortality, so no estimate of the BMD could be found without extrapolation (Figure D-3). A BMD was estimated for 35 of the relationships, with results shown in the Appendix (Table D-2).

Figure D-3: OSU Nanomaterial Data Waterfall – 24h Mortality, BMR = Added 50%

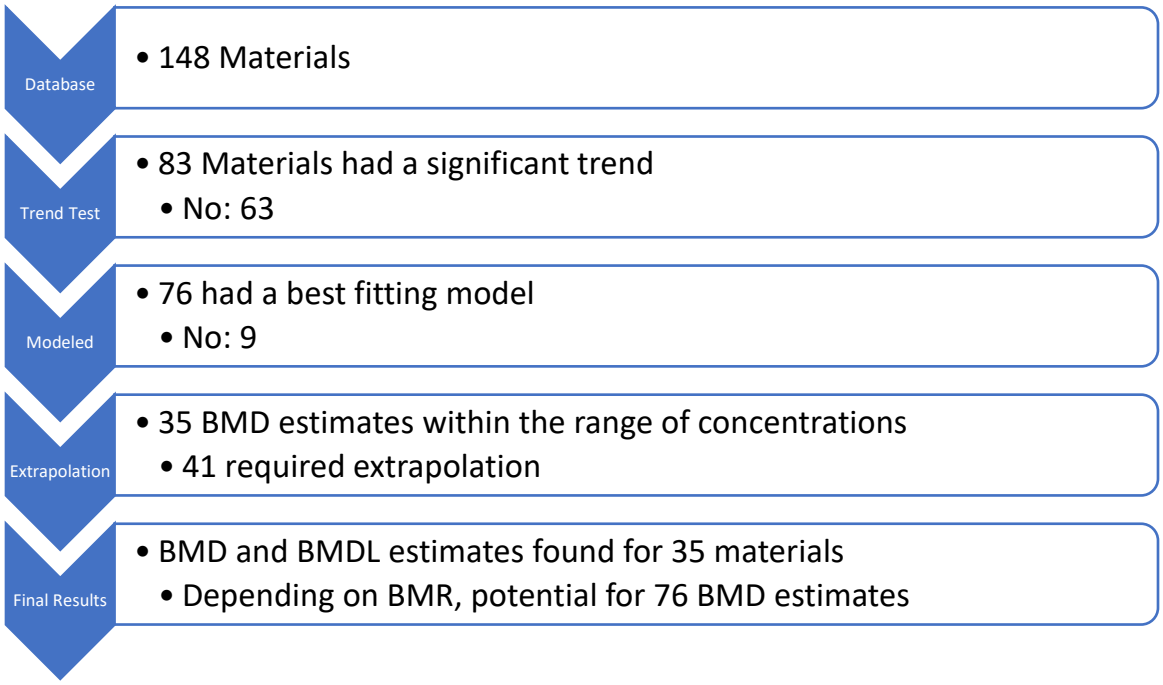

Table D-2: Benchmark Dose Modeling Results for OSU Zebrafish Assays where a statistically significant trend was detected and no extrapolation was required, BMR=Added 50%, Endpoint=24h Mortality (µg/mL or ppm)

ID	Material	Trend	Extrapolation	Model	BMD	BMDL
2	Gold-TMAT(0.8nm)	Y	N	LogProbit	3.46	2.04
5	Gold-TMAT(1.5nm)-ultrapure	Y	N	Gamma	33.87	23.53
6	Gold-TMAT(1.5nm)-pure	Y	N	Gamma	50.54	33.58
7	Gold-TMAT(1.5nm)-dirty	Y	N	LogProbit	1.51	0.88
8	Gold-MES(1.5nm)-ultrapure	Y	N	QuantalLinear	227.06	153.72
13	Gold-MHA(10nm)	Y	N	LogProbit	60.41	42.61
27	STARBURST (R) PAMAM Dendrimer DNT-104	Y	N	QuantalLinear	2.24	1.62
28	STARBURST (R) PAMAM Dendrimer DNT-105	Y	N	LogProbit	8.93	6.38
29	STARBURST (R) PAMAM Dendrimer DNT-106	Y	N	Logistic	8.90	5.73
30	STARBURST (R) PAMAM Dendrimer DNT-107	Y	N	Probit	17.41	12.02
72	gold nanorods (AuSoy95PC-1org1)	Y	N	Probit	88.89	63.28
73	gold nanorods (AuSoy95PC-1org2)	Y	N	Probit	110.65	74.96
74	gold nanorods (AuSoy95PC-3AQ)	Y	N	Gamma	17.26	12.66
75	AuSoy95PC-2org1	Y	N	LogLogistic	54.83	33.19
76	gold nanorods (AuSoy95PC-2org2)	Y	N	Gamma	123.87	86.73
105	Silver - Nanocomposix BioPure (10nm)	Y	N	QuantalLinear	55.07	33.74
106	Nanocomposix BioPure (silver over gold - 20nm)	Y	N	QuantalLinear	148.89	88.18

108	Nanocomposix BioPure (silver over gold - 40nm)	Y	N	Probit	211.96	165.13
110	Nanocomposix BioPure (silver over gold - 60nm)	Y	N	Gamma	52.81	33.35
111	Nanocomposix BioPure (silver over gold - 70nm)	Y	N	LogProbit	68.32	27.95
112	Nanocomposix BioPure (silver over gold - 80nm)	Y	N	Probit	155.12	121.33
113	Nanocomposix BioPure (silver over gold - 90nm)	Y	N	Gamma	37.55	24.54
114	Nanocomposix BioPure (silver over gold - 100nm)	Y	N	MS3	100.05	65.04
115	Nanocomposix BioPure (silver over gold - 110nm)	Y	N	MS3	106.36	66.35
133	Oxidized Monothiol Capped Lead Sulfide Nanocrystals	Y	N	MS3	44.21	37.75
147	Cellulose Nanofibers by homogenization	Y	N	Logistic	479.50	367.29
159	Gold Nanorods (10x34nm) #79-6000	Y	N	Logistic	2.37	1.47
161	Gold Nanorods (10x29nm) #79-6020	Y	N	LogLogistic	0.51	0.28
186	Silver 2 nm	Y	N	LogProbit	104.60	79.07
200	EDC-AEE CNC (DW 1-38-4 0.815%)	Y	N	LogLogistic	88.50	46.90
207	NanoTek Zinc Oxide	Y	N	Probit	173.33	147.52
214	ZnO NanoShield ZN-3008C	Y	N	Gamma	52.58	45.69
218	Amine-Terminated Silica coated Ag 20, 1x APTES	Y	N	MS3	19.01	15.93
221	80nm Amine Terminated Silica	Y	N	Gamma	88.72	81.16
222	SEF Amine-Terminated Silica coated Ag 20, 1x APTES	Y	N	LogProbit	24.37	17.12

The BMD estimates of the Army and OSU datasets were combined into a single group of 39, and Hierarchical Clustering was used to identify four groups of materials with similar mortality hazard. The 39 materials were also assigned to an Order of Magnitude group (<1, 1-10, 10-100, > 100) (Appendix Table D-3).

Table D-3: Hierarchical and Order of Magnitude Clusters for 39 Zebrafish BMD (µg/mL or PPM) Estimates, BMR=Added 50%, Endpoint=24h Mortality

index	Material	Name	BMD	BMDL	Cluster	Magnitude Group
1	N23901	US_Nano_Aluminum_Oxide_gamma_30_nm	0.0250367	0.0216831	1	1
2	N44021	US_Nano_Titanium_Dioxide_Anatase_5-15_nm	0.0655201	0.0536847	1	1
3	161	Gold Nanorods (10x29nm) #79-6020	0.512193	0.281566	1	1
4	7	Gold-TMAT(1.5nm)-dirty	1.50846	0.884504	1	2
5	N98053	5_nm_Silver_Nanosphere_nanoComposix_Econix	1.56613	1.36804	1	2
6	27	STARBURST (R) PAMAM Dendrimer DNT-104	2.24307	1.62023	1	2
7	159	Gold Nanorods (10x34nm) #79-6000	2.37263	1.47234	1	2
8	2	Gold-TMAT(0.8nm)	3.45795	2.04	1	2
9	29	STARBURST (R) PAMAM Dendrimer DNT-106	8.89561	5.72999	1	2
10	28	STARBURST (R) PAMAM Dendrimer DNT-105	8.92615	6.38441	1	2
11	74	gold nanorods (AuSoy95PC-3AQ)	17.2557	12.6589	1	3
12	30	STARBURST (R) PAMAM Dendrimer DNT-107	17.4103	12.0197	1	3
13	218	Amine-Terminated Silica coated Ag 20, 1x APTES	19.0077	15.9283	1	3
14	222	SEF Amine-Terminated Silica coated Ag 20, 1x APTES	24.3722	17.1212	1	3
15	N82750	25_nm_Silver_Nanosphere_nanoComposix_Econix	30.374	15.5758	1	3
16	5	Gold-TMAT(1.5nm)-ultrapure	33.8723	23.5254	1	3
17	113	Nanocomposix BioPure (silver over gold - 90nm)	37.5508	24.5368	1	3
18	133	Oxidized Monothiol Capped Lead Sulfide Nanocrystals	44.205	37.7541	1	3
19	6	Gold-TMAT(1.5nm)-pure	50.5363	33.5752	1	3
20	214	ZnO NanoShield ZN-3008C	52.5847	45.688	1	3
21	110	Nanocomposix BioPure (silver over gold - 60nm)	52.8109	33.3502	1	3
22	75	AuSoy95PC-2org1	54.8344	33.189	1	3
23	105	Silver - Nanocomposix BioPure (10nm)	55.0709	33.7419	1	3
24	13	Gold-MHA(10nm)	60.4106	42.6085	1	3
25	111	Nanocomposix BioPure (silver over gold - 70nm)	68.3194	27.9539	1	3
26	200	EDC-AEE CNC (DW 1-38-4 0.815%)	88.5018	46.8992	2	3
27	221	80nm Amine Terminated Silica	88.721	81.1627	2	3
28	72	gold nanorods (AuSoy95PC-1org1)	88.8857	63.2839	2	3
29	114	Nanocomposix BioPure (silver over gold - 100nm)	100.051	65.0391	2	4
30	186	Silver 2 nm	104.596	79.0685	2	4
31	115	Nanocomposix BioPure (silver over gold - 110nm)	106.355	66.3478	2	4
32	73	gold nanorods (AuSoy95PC-1org2)	110.651	74.9592	2	4
33	76	gold nanorods (AuSoy95PC-2org2)	123.868	86.725	2	4

34	106	Nanocomposix BioPure (silver over gold - 20nm)	148.888	88.1756	3	4
35	112	Nanocomposix BioPure (silver over gold - 80nm)	155.117	121.332	3	4
36	207	NanoTek Zinc Oxide	173.33	147.52	3	4
37	108	Nanocomposix BioPure (silver over gold - 40nm)	211.961	165.129	3	4
38	8	Gold-MES(1.5nm)-ultrapure	227.062	153.723	3	4
39	147	Cellulose Nanofibers by homogenization	479.502	367.285	4	4

Table D-4: List of available physicochemical/experimental properties in the Army and OSU files

Army PCHEM	**OSU PCHEM**
Nanoparticle	Description
Reference Number	Material Type
Vendor, Lot Number	Manufacture Date
Nominal Size	Manufacturer
Concentration	Synthesis Process
Sterility	Synthesis Precursors
Endotoxin	Purity
Particle Diameter by TEM	Types of Impurities
Hydrodynamic Diameter by Batch-mode DLS	Primary Particle Size: Avg. (nm)
Polydispersity Index by Batch-mode DLS	Primary Particle Size: Min. (nm)
Hydrodynamic Diameter by Flow-mode DLS	Primary Particle Size: Max (nm)
Total [ion] by ICP-MS	Method of Size Measurement
Total [Compound] by ICP-MS	Instrument Used for Size Measurement
Total [Compound] by TGA	Core Shape
Coating Detected	Core Structure
Coating Identity	Crystal Structure
Coating Concentration by TGA (mass coating per mass NP)	Core Atomic Composition
Zeta Potential	Number of Core Atoms
Metal Impurities by ICP- MS	Mass Core Atoms (ng)
Free [ions] by ICP-MS (1)	Shell Composition

Free [ions] by ICP-MS (2)	Shell Surface Shape
Free [ions] by ICP-MS (3)	Shell Linkage
	Functionalized
	Outermost Surface Functional Groups
	Surface Chemistry Linkage Group / Type
	Minimum Number of Ligands
	Maximum Number of Ligands
	Surface Area (Core + Shell + Ligands) (mm2)
	Method Used to Determine Surface Area
	Surface Charge: (positive, negative, neutral)
	Surface Charge: Value
	Solubility / Dispersity Medium
	Maximum Solubility Amount (ppm)
	Solubility Reference Temperature (Celsius)
	Hydrophilic
	Lipophilic
	Stability of Dispersions
	NBI Experiment ID
	NBI Material Identifier
	Exposure Metric / Assay
	Primary Exposure Route
	Primary Exposure Delivery
	Secondary Exposure Route
	Secondary Exposure Delivery
	Exposure Organism
	Exposure Organism Life stage
	Duration of Exposure (hours)
	Exposure Organism Gender
	Exposure Organism Average Weight (mg)
	Exposure Organism Initial Age (hours post-fertilization at start of exposure)
	Continuity of Exposure
	Exposure Temperature (Celsius)

	Exposure Media
	Media Composition
	Media pH
	Material Zeta Potential in Media (mV)
	Stable Average Agglomerate Size in Media (nm)
	Stable Agglomerate Size in Media Minimum (nm)
	Stable Agglomerate Size in Media Maximum (nm)
	Nanomaterial Preparation
	Experimental Notes
	LC50 (ppm)
	NOAEL (ppm)

Table D-5: Complete Results for Benchmark Dose Modeling of Army Zebrafish Assays, BMR=Added 50%, Endpoint=24h Mortality

Material	Test Statistic	p-value	Trend	Best Model	BMD	BMDL	GoF p-value	AIC	Extrapolation
N11697	5.753	<0.0001	Y						---
N17244	3.193	0.0007	Y	LogLogistic	372.659	101.946	0.4981	105.623	Y
N20458	-0.029	0.5115	N						N
N23901	8.216	<0.0001	Y	Log Probit	0.025037	0.021683	0.2407	135.717	N
N37701	2.771	0.0028	Y						---
N44021	7.573	<0.0001	Y	LogLogistic	0.06552	0.053685	0.6681	143.238	N
N50391	0.42	0.3372	N						N
N50810	3.321	0.0004	Y	Gamma	0.706833	0.633738	0.8994	116.838	Y
N58445	1.498	0.0671	N						N
N59938	-1.472	0.9295	N						N
N64731	1.285	0.0993	N						N
N73730	-0.756	0.775	N						N
N74948	3.063	0.0011	Y	LogLogistic	0.117209	0.112393	0.4056	109.277	Y
N79213	0.546	0.2924	N						N
N82750	5.266	<0.0001	Y	LogLogistic	30.374	15.5758	0.3895	230.802	N
N84505	-0.84	0.7995	N						N
N87223	0.218	0.4137	N						N
N96176	0.571	0.284	N						N
N98053	8.892	<0.0001	Y	Probit	1.56613	1.36804	0.2422	143.596	N
N98677	-0.52	0.6985	N						N
N99201	0.126	0.45	N						N

Table D-6: Full Results for Benchmark Dose Modeling of OSU Zebrafish Assays, BMR=Added 50%, Endpoint=24h Mortality

Material	Test Statistic	p-value	Trend	Best Model	BMD	BMDL	GoF p-value	AIC	Extrapolation
1	-1.38	0.084	N						N
2	-7.51	0.000	Y	LogProbit	3.46	2.04	0.581	142.0	N
3	-3.10	0.001	Y	Gamma	1668.29	519.103	0.998	24.8	Y
4	-1.67	0.047	Y	LogLogistic	55393700.00	280.25	0.911	53.6	Y
5	-10.02	0.000	Y	Gamma	33.87	23.5254	0.419	97.1	N
6	-9.06	0.000	Y	Gamma	50.54	33.5752	0.110	140.9	N
7	-6.81	0.000	Y	LogProbit	1.51	0.884504	0.982	140.8	N
8	-8.97	0.000	Y	QuantalLinear	227.06	153.723	0.391	68.7	N
9	-7.01	0.000	Y	Probit	280.27	229.728	0.177	72.5	Y
10	-2.16	0.015	Y	LogProbit	181279000.00	262.577	0.202	39.3	Y
12	-5.03	0.000	Y	LogProbit	809.88	268.974	0.969	73.1	Y
13	-10.33	0.000	Y	LogProbit	60.41	42.6085	0.424	78.0	N
15	-2.55	0.005	Y	MS3	644.25	418.539	1.000	10.4	Y
17	-1.41	0.079	N						N
27	-7.39	0.000	Y	QuantalLinear	2.24	1.62023	0.993	59.2	N
28	-9.15	0.000	Y	LogProbit	8.93	6.38441	1.000	34.6	N
29	-8.56	0.000	Y	Logistic	8.90	5.72999	1.000	10.3	N
30	-9.31	0.000	Y	Probit	17.41	12.0197	0.824	83.3	N
32	-3.43	0.000	Y	Gamma	982.01	497.929	0.728	39.0	Y
35	1.07	0.142	N						N
36	-3.56	0.000	Y	Gamma	664.03	367.746	0.137	64.0	Y
37	-0.85	0.196	N						N
38	-0.93	0.175	N						N
39	0.36	0.360	N						N
40	-5.82	0.000	Y	MS3	339.55	276.386	0.414	43.3	Y
41	-0.73	0.232	N						N
42	-3.82	0.000	Y	Probit	394.14	276.839	0.410	125.5	Y
43	-0.77	0.220	N						N
44	-3.78	0.000	Y	LogLogistic	4718.35	449.582	0.560	94.5	Y
45	0.99	0.161	N						N
47	-2.54	0.006	Y	LogProbit	6007.56	394.27	0.991	29.5	Y
48	-3.25	0.001	Y	LogProbit	1145.00	206.289	0.997	35.9	Y
72	-12.08	0.000	Y	Probit	88.89	63.2839	0.520	53.4	N
73	-12.37	0.000	Y	Probit	110.65	74.9592	0.372	46.1	N

74	-9.57	0.000	Y	Gamma	17.26	12.6589	0.954	82.3	N
75	-9.22	0.000	Y	LogLogistic	54.83	33.189	0.905	104.0	N
76	-8.55	0.000	Y	Gamma	123.87	86.725	0.652	116.7	N
77	0.81	0.210	N						N
78	0.23	0.408	N						N
85	0.79	0.215	N						N
86	-2.59	0.005	Y	LogLogistic	3792.96	183.419	0.240	204.1	Y
87	-0.99	0.162	N						N
88	-2.37	0.009	Y	Logistic	529.57	325.542	0.784	151.6	Y
89	-2.09	0.018	Y	LogProbit	79297.40	870.459	0.711	186.0	Y
90	-1.80	0.036	Y	LogLogistic	669652.00	1713.78	0.555	185.6	Y
91	0.14	0.445	N						N
92	0.36	0.360	N						N
93	-2.21	0.014	Y	LogProbit	9815.07	468.261	0.468	155.3	Y
94	-2.63	0.004	Y	MS3	459.82	339.461	0.183	52.2	Y
95	0.22	0.411	N						N
96	0.94	0.174	N						N
97	-0.96	0.168	N						N
105	-7.68	0.000	Y	QuantalLinear	55.07	33.7419	0.228	46.4	N
106	-5.41	0.000	Y	QuantalLinear	148.89	88.1756	0.543	74.7	N
107	-2.84	0.002	Y	MS3	326.65	247.645	0.527	57.3	Y
108	-6.05	0.000	Y	Probit	211.96	165.129	0.801	50.9	N
109	-5.84	0.000	Y						---
110	-7.69	0.000	Y	Gamma	52.81	33.3502	0.485	42.1	N
111	-4.65	0.000	Y	LogProbit	68.32	27.9539	0.980	58.8	N
112	-8.42	0.000	Y	Probit	155.12	121.332	0.585	28.4	N
113	-7.29	0.000	Y	Gamma	37.55	24.5368	0.792	42.4	N
114	-9.33	0.000	Y	MS3	100.05	65.0391	1.000	8.9	N
115	-8.91	0.000	Y	MS3	106.36	66.3478	0.533	21.4	N
127	1.19	0.118	N						N
128	-0.23	0.408	N						N
129	-1.47	0.071	N						N
130	0.60	0.275	N						N
132	-7.09	0.000	Y						---
133	-11.36	0.000	Y	MS3	44.21	37.7541	1.000	55.8	N
134	1.04	0.150	N						N
135	-1.72	0.043	Y	Gamma	759.14	340.184	0.682	36.1	Y
136	-3.05	0.001	Y						---

137	-0.46	0.322	N						N
138	0.15	0.442	N						N
139	-2.76	0.003	Y	Gamma	768.25	373.341	0.398	125.7	Y
140	1.65	0.050	Y	LogLogistic	25000.00	25000	0.273	98.4	Y
147	-19.54	0.000	Y	Logistic	479.50	367.285	0.653	69.7	N
148	-7.30	0.000	Y	LogProbit	44535.80	14507.2	0.565	162.4	Y
149	-8.83	0.000	Y	Gamma	9115.27	6492.95	0.674	185.3	Y
150	-9.01	0.000	Y	MS3	74415.50	65724.1	0.555	109.7	Y
151	-5.71	0.000	Y	Gamma	22398.70	6676.7	0.958	148.6	Y
152	1.41	0.080	N						N
153	0.48	0.315	N						N
154	-10.72	0.000	Y	Gamma	10476.20	7778.26	0.744	200.9	Y
155	-1.44	0.075	N						N
156	-5.01	0.000	Y	Gamma	9162.01	2504.07	0.269	140.9	Y
157	-6.75	0.000	Y	LogProbit	30884.00	7675.76	0.546	155.0	Y
158	-2.07	0.019	Y	Gamma	31452.10	2803.46	0.719	95.5	Y
159	-8.69	0.000	Y	Logistic	2.37	1.47234	0.854	36.2	N
160	-8.37	0.000	Y						---
161	-6.68	0.000	Y	LogLogistic	0.51	0.281566	0.731	14.5	N
162	0.85	0.198	N						N
163	-1.65	0.049	Y	LogLogistic	17000000000.00	283.619	0.892	59.1	Y
164	-1.93	0.027	Y	MS3	519.94	379.835	0.623	106.8	Y
165	-0.40	0.345	N						N
166	-2.73	0.003	Y	MS3	537.49	407.36	0.557	83.6	Y
167	-0.32	0.375	N						N
168	-5.59	0.000	Y	MS3	362.32	300.375	0.353	83.4	Y
169	-0.66	0.255	N						N
170	0.46	0.324	N						N
171	0.65	0.256	N						N
172	1.04	0.150	N						N
174	-0.84	0.199	N						N
177	1.20	0.116	N						N
178	1.20	0.116	N						N
179	1.20	0.116	N						N
181	1.00	0.159	N						N
182	0.82	0.205	N						N
184	0.48	0.315	N						N
186	-11.80	0.000	Y	LogProbit	104.60	79.0685	1.000	43.8	N

187	-2.74	0.003	Y	Weibull	281.80	266.235	0.419	30.0	Y
189	-0.96	0.169	N						N
194	-3.86	0.000	Y	MS3	358.12	285.746	0.432	82.9	Y
195	0.84	0.201	N						N
198	0.81	0.210	N						N
199	0.36	0.360	N						N
200	-8.39	0.000	Y	LogLogistic	88.50	46.8992	0.672	15.6	N
201	1.18	0.119	N						N
202	-4.30	0.000	Y	Gamma	452.15	263.145	0.635	116.9	Y
203	-8.78	0.000	Y						---
204	0.39	0.350	N						N
205	-3.19	0.001	Y	LogLogistic	49901.20	621.3	0.855	67.0	Y
206	-3.19	0.001	Y	LogLogistic	49901.20	621.3	0.855	67.0	Y
207	-10.91	0.000	Y	Probit	173.33	147.52	0.841	68.3	N
208	-1.52	0.064	N						N
209	-9.89	0.000	Y						---
211	-0.74	0.230	N						N
212	-5.02	0.000	Y						---
213	0.48	0.317	N						N
214	-12.02	0.000	Y	Gamma	52.58	45.688	1.000	34.6	N
215	0.23	0.410	N						N
216	-1.14	0.128	N						N
217	-9.12	0.000	Y						---
218	-11.47	0.000	Y	MS3	19.01	15.9283	0.894	73.1	N
219	-6.25	0.000	Y	LogLogistic	103.20	98.7582	0.536	57.5	Y
220	-10.52	0.000	Y						---
221	-10.80	0.000	Y	Gamma	88.72	81.1627	0.610	110.7	N
222	-9.14	0.000	Y	LogProbit	24.37	17.1212	0.109	149.5	N

As seen in earlier implementation of Hierarchical Clustering, a majority of materials tend to end up in the most potent group (Table D-7). This is due to the high amount of variability across all of the potency estimates, and the data-driven behavior of the clustering algorithm which is simply combining the potency estimates nearest together. The most potent materials have estimates that are closer to one another than to the least potent materials, which are often several orders of magnitude apart. The summary of the order of magnitude groups shows that a majority of the materials have potency estimates of at least 10 μg/mL, with only 10 materials being more potent (Table D-8).

Table D-7: Hierarchical Cluster Summary

Cluster	Number of Materials
1	25
2	5
3	8
4	1
TOTAL	39

Table D-8: Order of Magnitude Cluster Summary

Cluster	Number of Materials
1: <1	3
2: 1-10	7
3: 10-100	18
4: > 100	11
TOTAL	39

Cellulose nanofibers were the least potent by a large margin (2 times less potent than cluster 3; 4 times less potent than cluster 2; and 7 times less potent than cluster 1). The two most potent materials were Al_2O_3 (30 nm) and TiO_2 (5-15 nm).

Compared to the *in vivo* results, in which ZnO was the most potent in terms of pulmonary inflammation, ZnO is the 20th and 36th most potent material in terms of zebrafish mortality (24h).

Gold and Silver have varied potency estimates, depending on physical characteristics; gold nanorods and silver nanospheres are among the most potent, while ultrapure gold and BioPure silver over gold are among the least potent.

The BMD estimates for the 39 materials are shown in Figure D-4.

Figure D-4: Variability of Within-Material BMD estimates

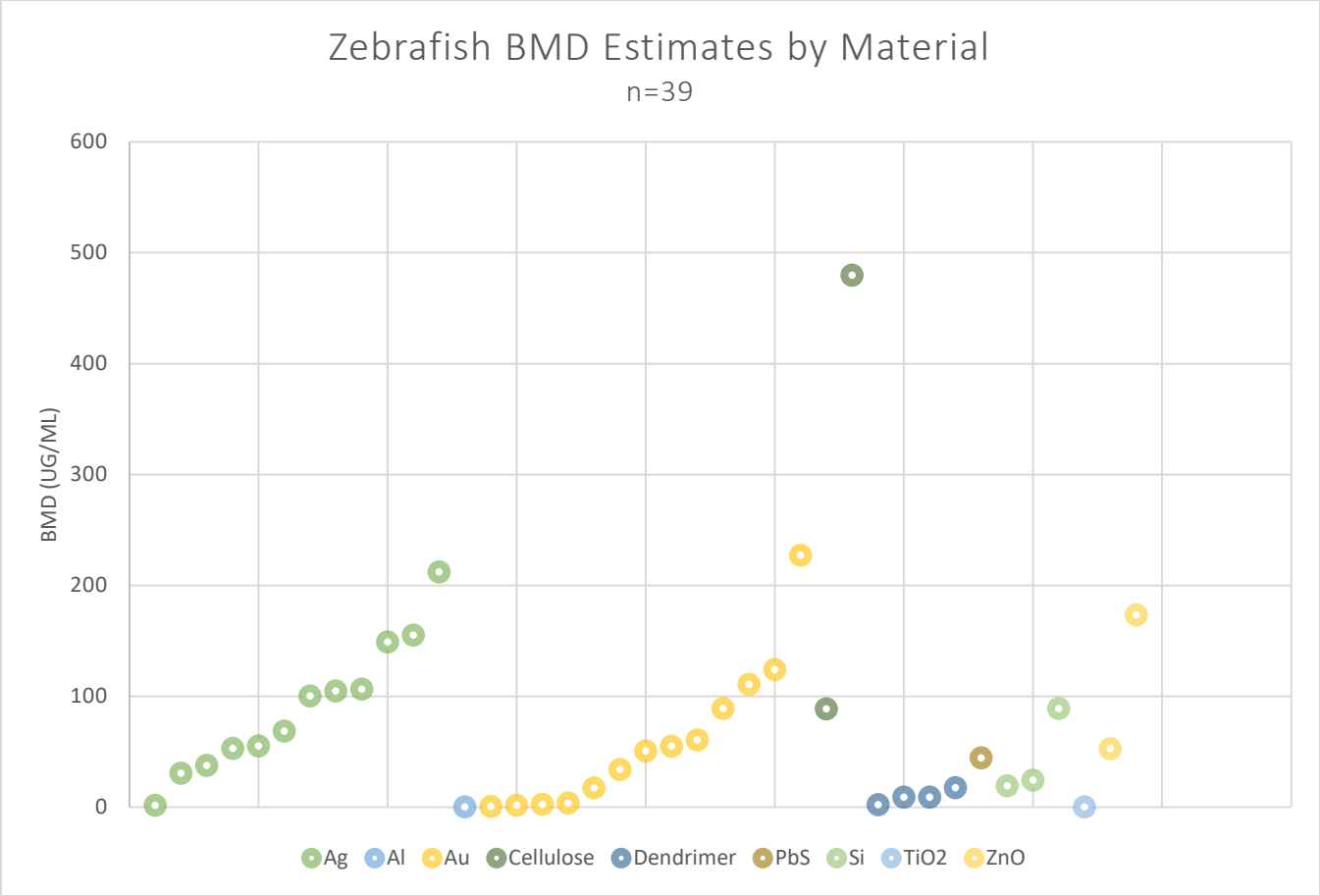

Materials containing Ag, aluminum oxide (Al), gold (Au), dendrimers, and TiO_2 were the most potent (i.e., smallest BMD estimates), followed by silica (SiO_2), lead sulfide (PbS), ZnO, and cellulose.

Ag potency estimates varied by a factor of 100; Au by 400; cellulose by 5; dendrimers by 8; SiO_2 by 4; ZnO by 3. Variability in the estimates may be due to factors such as size, shape (e.g., rod, sphere), or mixtures (e.g., silver over gold, silica coated silver) .

Further analysis into the potency estimates of Ag and Au were conducted as these two materials had the most potency estimates. The relationships of the physicochemical properties, particularly particle size, to the potency estimates were explored to understand why there were such large differences in the potencies (Figures D-5 and D-6)

Figure D-5: Exploring the Strength of the Association between Particle Size and Potency (BMD) for Silver Nanoparticles

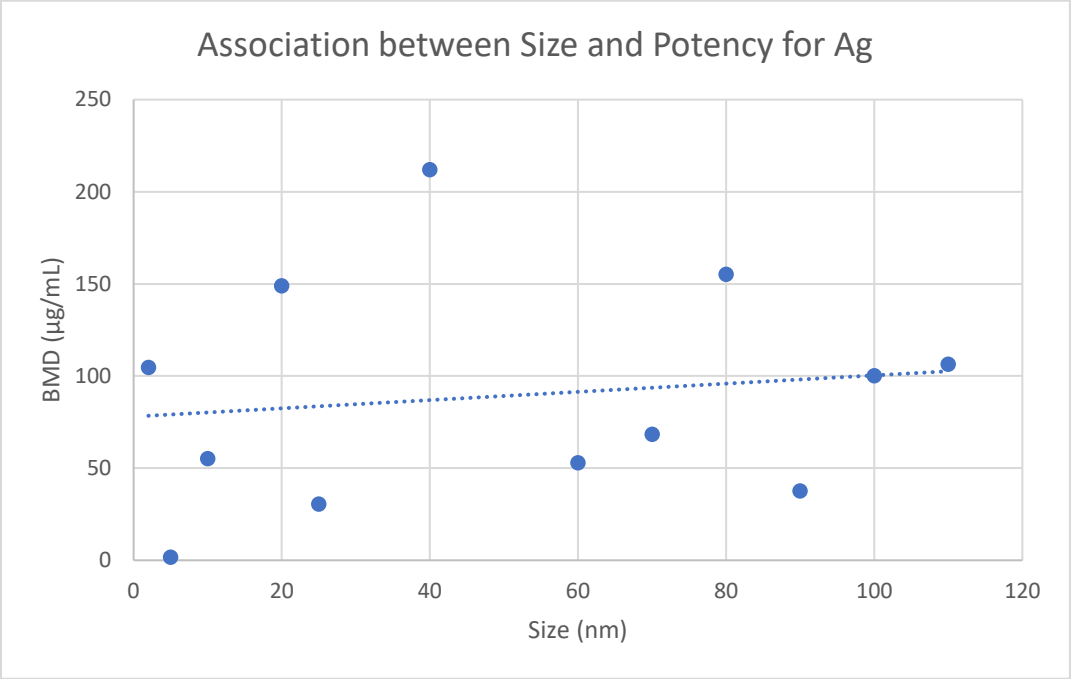

There is a very weak, positive linear association (r = 0.14) between material size (2 – 110 nm) and potency (1.6 – 212 µg/mL) for the Ag materials, where smaller materials tend to be slightly more potent. There is a large amount of variability ($\sqrt{MSE} = 63$) in the potency estimates around the regression line; the least potent material was at 40 nm, and the most potent was at 5 nm. The remaining variability may be due to other physicochemical properties, as the most potent materials are nanospheres, and the least potent are silver over gold mixtures.

Figure D-6: Exploring the Strength of the Association between Particle Size and Potency (BMD) for Gold Nanoparticles

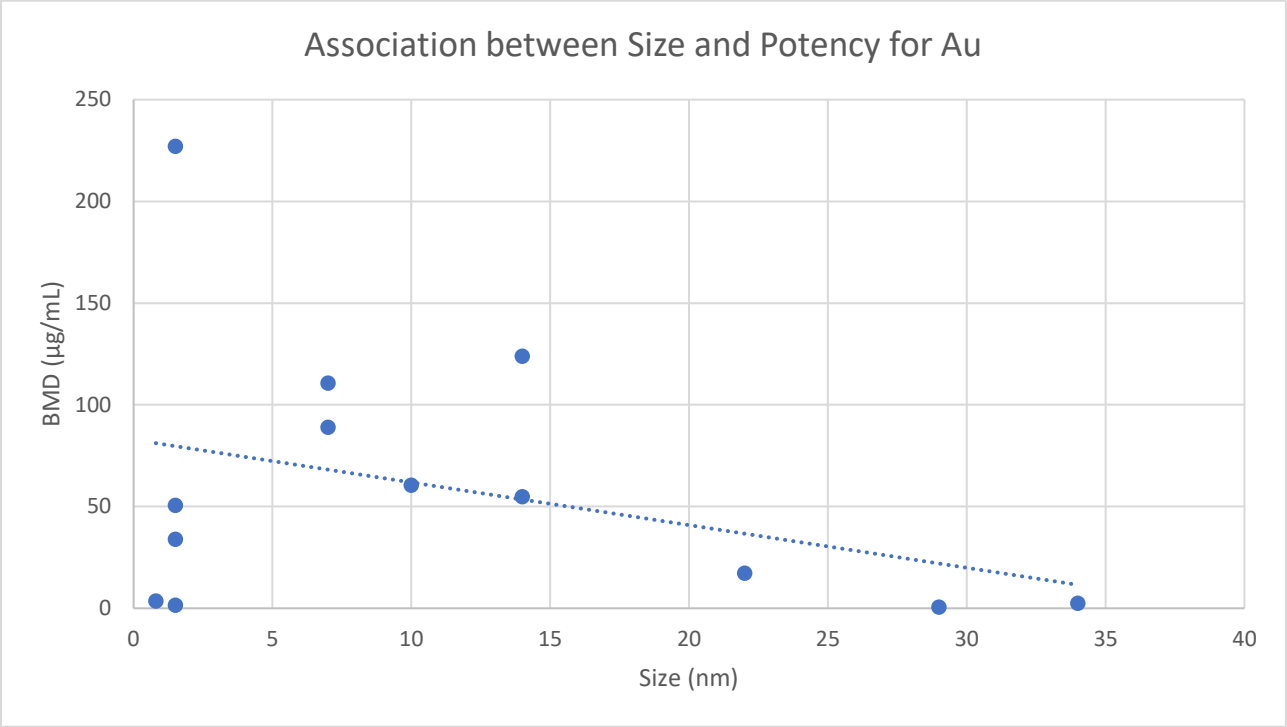

In the case of the Au materials, there is a weak negative linear association between size (0.8 – 34 nm) and potency (0.5 – 227 µg/mL), which suggests that larger gold-containing nanomaterials are more potent. Again, there is a large amount of variability in the potency estimates ($\sqrt{MSE} = 64$), so the association is not clear. The form of the association may be non-linear. The factors explaining the remaining variability are not clear. Physicochemical properties may be of help, but form does not seem to be useful as nanorods have potencies ranging from 0.5 to 124 µg/mL, purified forms range from 34 to 227 µg/mL, and others range from 1.5 to 60 µg/mL.

Appendix E: NTP Histopathologic Data on Inflammation, Fibrosis and Lung Cell Neoplasia

Table E-1: Inflammation Potencies for relationships with a Trend

CAS Number	Dose Unit	Species	Strain	Sex	Chemical Name	Duration	NOAEL	LOAEL	BMD	BMDL
10026-24-1	MG/M3	Rat	F 344/N	M	Cobalt sulfate heptahydrate	2 year		0.3	5.62E-11	
22398-80-7	MG/M3	Rat	F 344/N	F	Indium phosphide	2 year		0.03	1.67E-04	3.83E-05
1303-00-0	MG/M3	Rat	F 344/N	F	Gallium arsenide	2 year		0.01	1.90E-04	7.65E-05
22398-80-7	MG/M3	Rat	F 344/N	M	Indium phosphide	2 year		0.03	1.92E-04	3.15E-09
22398-80-7	MG/M3	Rat	F 344/N	M	Indium phosphide	3 month		1	1.94E-04	4.58E-07
22398-80-7	MG/M3	Rat	F 344/N	F	Indium phosphide	3 month		1	2.90E-04	5.29E-07
1303-00-0	MG/M3	Rat	F 344/N	M	Gallium arsenide	2 year		0.01	5.52E-04	4.03E-04
22398-80-7	MG/M3	Mouse	B6C3F1	F	Indium phosphide	3 month		1	8.53E-04	2.60E-04
7440-48-4	MG/M3	Rat	F 344/N	M	Cobalt	3 month		0.625	1.65E-03	8.62E-06
10026-24-1	MG/M3	Rat	F 344/N	F	Cobalt sulfate heptahydrate	2 year		0.3	2.31E-03	7.21E-04
7440-48-4	mg/m3	Rat	F344/N Tac	F	Cobalt	2 year		1.25	3.95E-03	8.49E-06
7440-48-4	mg/m3	Rat	F344/N Tac	M	Cobalt	2 year		1.25	3.96E-03	9.24E-06
7440-48-4	MG/M3	Rat	F 344/N	F	Cobalt	3 month		0.625	6.25E-03	6.03E-06
1313-99-1	MG/M3	Rat	F 344/N	M	Nickel (II) oxide	2 year		0.62	7.88E-03	
22398-80-7	MG/M3	Mouse	B6C3F1	M	Indium phosphide	3 month		1	1.02E-02	1.84E-03
12035-72-2	MG/M3	Mouse	B6C3F1	M	Nickel subsulfide	2 year		0.6	1.06E-02	6.17E-03
1309-64-4	mg/m3	Mouse	B6C3F1	F	Antimony trioxide	2 year		3	1.83E-02	
1309-64-4	mg/m3	Rat	Wistar Han	M	Antimony trioxide	2 year		3	2.74E-02	
1309-64-4	mg/m3	Rat	Wistar Han	F	Antimony trioxide	2 year		3	3.22E-02	
1314-62-1	MG/M3	Mouse	B6C3F1	M	Vanadium pentoxide	2 year		1	3.32E-02	1.99E-02

12035-72-2	MG/M3	Mouse	B6C3F1	F	Nickel subsulfide	2 year		0.6	4.22E-02	3.40E-02
BLASTING SAND	mg/m3	Rat	HSD	M	Abrasive Blasting Agents: Blasting Sand	39 week		15	9.67E-02	
1313-99-1	MG/M3	Mouse	B6C3F1	F	Nickel (II) oxide	2 year		1.25	0.100381	7.08E-02
L-MWNT-1020	mg/m3	Rat	HSD	F	1020 Long Multiwalled Carbon Nanotube	30 day	0.3	1	0.276428	1.91E-01
10101-97-0	MG/M3	Mouse	B6C3F1	F	Nickel sulfate hexahydrate	2 year		0.25	0.309902	2.67E-01
1303-00-0	MG/M3	Mouse	B6C3F1	F	Gallium arsenide	2 year	0.1	0.5	0.313561	2.47E-01
1313-99-1	MG/M3	Mouse	B6C3F1	M	Nickel (II) oxide	2 year		1.25	0.345576	2.94E-01
1303-00-0	MG/M3	Mouse	B6C3F1	M	Gallium arsenide	2 year	0.1	0.5	0.365734	3.07E-01
1314-62-1	MG/M3	Rat	F 344/N	M	Vanadium pentoxide	2 year	0.5	1	0.405075	3.46E-01
L-MWNT-1020	mg/m3	Rat	HSD	M	1020 Long Multiwalled Carbon Nanotube	30 day	0.3	1	0.446828	2.48E-01
1313-99-1	MG/M3	Rat	F 344/N	F	Nickel (II) oxide	2 year		0.62	0.464808	3.90E-04
10101-97-0	MG/M3	Mouse	B6C3F1	M	Nickel sulfate hexahydrate	2 year	0.5	1	0.473267	4.07E-01
1309-64-4	mg/m3	Mouse	B6C3F1	M	Antimony trioxide	2 year		3	0.493714	3.13E-01
14807-96-6	MG/M3	Mouse	B6C3F1	F	Talc	2 year		6	0.515589	3.48E-01
14807-96-6	MG/M3	Rat	F 344/N	F	Talc	2 year		6	0.882952	5.72E-01
L-MWNT-1020	mg/m3	Mouse	B6C3F1	M	1020 Long Multiwalled Carbon Nanotube	30 day		0.1	0.888737	2.80E-01
1314-62-1	MG/M3	Mouse	B6C3F1	F	Vanadium pentoxide	3 month	1	2	0.898818	2.82E-01
L-MWNT-1020	mg/m3	Mouse	B6C3F1	F	1020 Long Multiwalled Carbon Nanotube	30 day		0.1	0.905252	4.12E-01
1314-62-1	MG/M3	Mouse	B6C3F1	M	Vanadium pentoxide	3 month	2	4	0.90604	4.94E-01
1314-62-1	MG/M3	Rat	F 344/N	F	Vanadium pentoxide	2 year	1	2	0.935966	6.63E-01
643-79-8	ppm	Rat	HSD	M	ortho-Phthalaldehyde	3 month		0.44	1.0777	6.14E-01
643-79-8	ppm	Rat	HSD	F	ortho-Phthalaldehyde	3 month		0.44	1.10953	6.40E-01
14807-96-6	MG/M3	Mouse	B6C3F1	M	Talc	2 year		6	1.23089	9.68E-01
GARNET	mg/m3	Rat	F 344/N	M	Abrasive blasting agents (garnet)	2 week	3	15	1.36239	2.30E-01
1314-62-1	MG/M3	Rat	F 344/N	M	Vanadium pentoxide	3 month	16		1.56679	9.59E-01

643-79-8	ppm	Mouse	B6C3F1	F	ortho-Phthalaldehyde	3 month	1.75	3.5	1.99512	1.24E+00
643-79-8	ppm	Mouse	B6C3F1	M	ortho-Phthalaldehyde	3 month		0.44	2.49604	1.58E+00
1314-62-1	MG/M3	Rat	F 344/N	F	Vanadium pentoxide	3 month	16		2.6506	1.96E+00
7440-48-4	mg/m3	Mouse	B6C3F1	M	Cobalt	2 year	2.5	5	2.74034	2.29E+00
7440-48-4	MG/M3	Mouse	B6C3F1	F	Cobalt	2 week		2.5	2.78733	1.31E+00
7440-48-4	mg/m3	Mouse	B6C3F1	F	Cobalt	2 year	2.5	5	2.80554	1.87E+00
10026-24-1	MG/M3	Mouse	B6C3F1	M	Cobalt sulfate heptahydrate	2 year	3		5.00662	2.30E+00
HEMATITE SPEC	mg/m3	Rat	Harlan Sprague Dawley	M	Abrasive Blasting Agents: Specular Hematite	39 week		15	5.19575	3.27E+00
COALSLAG	mg/m3	Rat	F 344/N	M	Abrasive blasting agents (coal slag)	2 week		3	7.0232	3.07E+00
1313-27-5	MG/M3	Rat	F 344/N	M	Molybdenum trioxide	2 year	10	30	13.642	9.60E+00
7440-48-4	MG/M3	Rat	F 344/N	M	Cobalt	2 week		2.5	16.3897	8.00E+00
7440-48-4	MG/M3	Rat	F 344/N	F	Cobalt	2 week	20	40	18.105	9.46E+00
1309-64-4	mg/m3	Rat	Wistar Han	F	Antimony trioxide	2 week		3.75	19.9542	1.32E+01
1309-64-4	mg/m3	Rat	Wistar Han	M	Antimony trioxide	2 week		3.75	19.9542	1.32E+01
102-54-5	MG/M3	Rat	F 344/N	F	Ferrocene	3 month	30		30.0001	1.40E+01
7440-48-4	MG/M3	Mouse	B6C3F1	M	Cobalt	2 week	40		35.4711	1.45E+01
1309-64-4	mg/m3	Mouse	B6C3F1	F	Antimony trioxide	2 week		3.75	NA	
1309-64-4	mg/m3	Mouse	B6C3F1	M	Antimony trioxide	2 week		3.75	NA	
BLASTING SAND	mg/m3	Rat	F344/N Tac	M	Abrasive Blasting Agents: Blasting Sand	2 week		3	NA	
CRUSHED GLASS	mg/m3	Rat	F344/N Tac	M	NA	2 week	30		NA	
10026-24-1	MG/M3	Mouse	B6C3F1	F	Cobalt sulfate heptahydrate	2 year	3		NA	
1313-27-5	MG/M3	Mouse	B6C3F1	F	Molybdenum trioxide	2 year		10	NA	
1313-27-5	MG/M3	Mouse	B6C3F1	M	Molybdenum trioxide	2 year	100		NA	
13765-19-0	MG/M3	Rat	Sprague Dawley	M	Calcium chromate	2 year	20		NA	
13765-19-0	MG/M3	Hamster	Syrian Golden	M	Calcium chromate	2 year	20		NA	

13983-17-0	MG/M3	Rat	F 344/N	M	Wollastonite calcium silicates	2 year	10		NA	
2698-41-1	MG/M3	Mouse	B6C3F1	F	o-Chlorobenzalmalononitrile (CS)	2 year	1.5		NA	
2698-41-1	MG/M3	Mouse	B6C3F1	M	o-Chlorobenzalmalononitrile (CS)	2 year	1.5		NA	
2698-41-1	MG/M3	Rat	F 344/N	M	o-Chlorobenzalmalononitrile (CS)	2 year	0.75		NA	
102-54-5	MG/M3	Mouse	B6C3F1	F	Ferrocene	3 month	30		NA	
102-54-5	MG/M3	Mouse	B6C3F1	M	Ferrocene	3 month	30		NA	
102-54-5	MG/M3	Rat	F 344/N	M	Ferrocene	3 month	30		NA	
7440-48-4	mg/m3	Mouse	B6C3F1	F	Cobalt	3 month		0.625	NA	
7440-48-4	mg/m3	Mouse	B6C3F1	M	Cobalt	3 month		0.625	NA	
10101-97-0	MG/M3	Rat	F 344/N	F	Nickel sulfate hexahydrate	2 year	0.12	0.25	No adequate fits	
10101-97-0	MG/M3	Rat	F 344/N	M	Nickel sulfate hexahydrate	2 year	0.12	0.25	No adequate fits	
12035-72-2	MG/M3	Rat	F 344/N	F	Nickel subsulfide	2 year		0.15	No adequate fits	
12035-72-2	MG/M3	Rat	F 344/N	M	Nickel subsulfide	2 year		0.15	No adequate fits	
1313-27-5	MG/M3	Rat	F 344/N	F	Molybdenum trioxide	2 year	10	30	No adequate fits	
1314-62-1	MG/M3	Mouse	B6C3F1	F	Vanadium pentoxide	2 year		1	No adequate fits	
14807-96-6	MG/M3	Rat	F 344/N	M	Talc	2 year		6	No adequate fits	
22398-80-7	MG/M3	Mouse	B6C3F1	F	Indium phosphide	2 year		0.03	No adequate fits	
22398-80-7	MG/M3	Mouse	B6C3F1	M	Indium phosphide	2 year		0.03	No adequate fits	
2698-41-1	MG/M3	Rat	F 344/N	F	o-Chlorobenzalmalononitrile (CS)	2 year	0.25	0.75	No adequate fits	
7440-47-3	MG/M3	Rat	Sprague Dawley	M	Chromium	2 year		20	No adequate fits	
7440-47-3	MG/M3	Hamster	Syrian Golden	M	Chromium	2 year		20	No adequate fits	

Table E-2: Lung Fibrosis Potencies for relationships with a Trend

CAS Number	Dose Unit	Species	Strain	Sex	Material	Duration	NOAEL	LOAEL	BMD	BMDL
10026-24-1	mg/m³	Mouse	B6C3F1	F	Cobalt sulfate heptahydrate	2 year	NA	NA	NA	NA
10026-24-1	mg/m³	Mouse	B6C3F1	M	Cobalt sulfate heptahydrate	2 year	NA	NA	NA	NA
10026-24-1	mg/m³	Rat	F344/N	F	Cobalt sulfate heptahydrate	2 year	NA	0.3	0.002079	0.000654
10026-24-1	mg/m³	Rat	F344/N	M	Cobalt sulfate heptahydrate	2 year	NA	0.3	0.000507	5.33E-05
10101-97-0	mg/m³	Mouse	B6C3F1	M	Nickel sulfate hexahydrate	2 year	1	NA	NA	NA
10101-97-0	mg/m³	Mouse	B6C3F1	F	Nickel sulfate hexahydrate	2 year	NA	NA	NA	NA
10101-97-0	mg/m³	Rat	F344/N	F	Nickel sulfate hexahydrate	2 year	0.12	0.25	-99	-99
10101-97-0	mg/m³	Rat	F344/N	M	Nickel sulfate hexahydrate	2 year	0.12	0.25	-99	-99
102-54-5	mg/m³	Mouse	B6C3F1	F	Ferrocene	3 month	NA	NA	NA	NA
102-54-5	mg/m³	Mouse	B6C3F1	M	Ferrocene	3 month	NA	NA	NA	NA
102-54-5	mg/m³	Rat	F344/N	F	Ferrocene	3 month	NA	NA	NA	NA
102-54-5	mg/m³	Rat	F344/N	M	Ferrocene	3 month	NA	NA	NA	NA
12035-72-2	mg/m³	Mouse	B6C3F1	F	Nickel subsulfide	2 year	NA	0.6	0.571644	0.460027
12035-72-2	mg/m³	Mouse	B6C3F1	M	Nickel subsulfide	2 year	0.6	1.2	0.725894	0.5202
12035-72-2	mg/m³	Rat	F344/N	F	Nickel subsulfide	2 year	NA	0.15	-99	-99
12035-72-2	mg/m³	Rat	F344/N	M	Nickel subsulfide	2 year	NA	0.15	-99	-99
1303-00-0	mg/m³	Mouse	B6C3F1	F	Gallium arsenide	2 year	NA	NA	NA	NA
1303-00-0	mg/m³	Mouse	B6C3F1	M	Gallium arsenide	2 year	NA	NA	NA	NA
1303-00-0	mg/m³	Rat	F344/N	F	Gallium arsenide	2 year	NA	NA	NA	NA
1303-00-0	mg/m³	Rat	F344/N	M	Gallium arsenide	2 year	NA	NA	NA	NA
1309-64-4	mg/m³	Mouse	B6C3F1	F	Antimony trioxide	2 week	NA	NA	NA	NA
1309-64-4	mg/m³	Mouse	B6C3F1	M	Antimony trioxide	2 week	NA	NA	NA	NA
1309-64-4	mg/m³	Rat	Wistar	F	Antimony trioxide	2 week	NA	NA	NA	NA
1309-64-4	mg/m³	Rat	Wistar	M	Antimony trioxide	2 week	NA	NA	NA	NA
1309-64-4	mg/m³	Mouse	B6C3F1	F	Antimony trioxide	2 year	NA	3	0.91052	0.649451
1309-64-4	mg/m³	Mouse	B6C3F1	M	Antimony trioxide	2 year	NA	3	0.44513	0.337433
1309-64-4	mg/m³	Rat	Wistar	F	Antimony trioxide	2 year	NA	3	0.005028	0.000528
1309-64-4	mg/m³	Rat	Wistar	M	Antimony trioxide	2 year	NA	3	0.010638	0.002492
1313-27-5	mg/m³	Mouse	B6C3F1	F	Molybdenum trioxide	2 year	NA	NA	NA	NA

1313-27-5	mg/m³	Mouse	B6C3F1	M	Molybdenum trioxide	2 year	NA	NA	NA	NA
1313-27-5	mg/m³	Rat	F 344/N	F	Molybdenum trioxide	2 year	NA	NA	NA	NA
1313-27-5	mg/m³	Rat	F 344/N	M	Molybdenum trioxide	2 year	100	NA	NA	NA
1313-99-1	mg/m³	Mouse	B6C3F1	F	Nickel (II) oxide	2 year	5	NA	7.06505	4.8678
1313-99-1	mg/m³	Mouse	B6C3F1	M	Nickel (II) oxide	2 year	5	NA	NA	NA
1313-99-1	mg/m³	Rat	F 344/N	F	Nickel (II) oxide	2 year	2.5	NA	NA	NA
1313-99-1	mg/m³	Rat	F 344/N	M	Nickel (II) oxide	2 year	NA	NA	NA	NA
1314-62-1	mg/m³	Mouse	B6C3F1	F	Vanadium pentoxide	3 month	NA	NA	NA	NA
1314-62-1	mg/m³	Mouse	B6C3F1	M	Vanadium pentoxide	3 month	NA	NA	NA	NA
1314-62-1	mg/m³	Rat	F 344/N	M	Vanadium pentoxide	3 month	2	4	1.91189	1.44231
1314-62-1	mg/m³	Rat	F 344/N	F	Vanadium pentoxide	3 month	NA	4	2.6506	1.9557
1314-62-1	mg/m³	Mouse	B6C3F1	F	Vanadium pentoxide	2 year	2	4	2.66661	1.74444
1314-62-1	mg/m³	Mouse	B6C3F1	M	Vanadium pentoxide	2 year	1	2	1.35351	0.877877
1314-62-1	mg/m³	Rat	F 344/N	F	Vanadium pentoxide	2 year	1	2	-99	-99
1314-62-1	mg/m³	Rat	F 344/N	M	Vanadium pentoxide	2 year	0.5	1	0.623084	0.428107
13765-19-0	mg/m³	Rat	Sprague	M	Calcium chromate	2 year	20	NA	-99	-99
13765-19-0	mg/m³	Hamst	Syrian	M	Calcium chromate	2 year	20	NA	-99	-99
14807-96-6	mg/m³	Mouse	B6C3F1	F	Talc	2 year	NA	NA	NA	NA
14807-96-6	mg/m³	Mouse	B6C3F1	M	Talc	2 year	NA	NA	NA	NA
14807-96-6	mg/m³	Rat	F 344/N	F	Talc	2 year	NA	6	0.894807	0.711427
14807-96-6	mg/m³	Rat	F 344/N	M	Talc	2 year	NA	6	1.81249	1.40947
22398-80-7	mg/m³	Mouse	B6C3F1	F	Indium phosphide	3 month	NA	1	0.007928	0.000819
22398-80-7	mg/m³	Mouse	B6C3F1	M	Indium phosphide	3 month	NA	1	-99	-99
22398-80-7	mg/m³	Rat	F 344/N	F	Indium phosphide	3 month	NA	3	1.53302	0.966224
22398-80-7	mg/m³	Rat	F 344/N	M	Indium phosphide	3 month	NA	3	0.739796	0.273013
22398-80-7	mg/m³	Mouse	B6C3F1	F	Indium phosphide	2 year	NA	0.03	0.000199	7.58E-05
22398-80-7	mg/m³	Mouse	B6C3F1	M	Indium phosphide	2 year	NA	0.03	4.82E-05	5.07E-06
22398-80-7	mg/m³	Rat	F 344/N	F	Indium phosphide	2 year	NA	0.03	0.000148	4.73E-05
22398-80-7	mg/m³	Rat	F 344/N	M	Indium phosphide	2 year	NA	0.03	0.000808	0.000514
2698-41-1	mg/m³	Mouse	B6C3F1	F	o-Chlorobenzalmalononitrile (CS)	2 year	1.5	NA	NA	NA
2698-41-1	mg/m³	Mouse	B6C3F1	M	o-Chlorobenzalmalononitrile (CS)	2 year	NA	NA	NA	NA

2698-41-1	mg/m³	Rat	F 344/N	F	o-Chlorobenzalmalononitrile (CS)	2 year	NA	NA	NA	NA
2698-41-1	mg/m³	Rat	F 344/N	M	o-Chlorobenzalmalononitrile (CS)	2 year	NA	NA	NA	NA
643-79-8	ppm	Mouse	B6C3F 1	F	ortho-Phthalaldehyde	3 month	NA	NA	NA	NA
643-79-8	ppm	Mouse	B6C3F 1	M	ortho-Phthalaldehyde	3 month	NA	NA	NA	NA
643-79-8	ppm	Rat	HSD	F	ortho-Phthalaldehyde	3 month	7	NA	1.38959	0.73653
643-79-8	ppm	Rat	HSD	M	ortho-Phthalaldehyde	3 month	7	NA	NA	NA
7440-47-3	mg/m³	Rat	Sprague	M	Chromium	2 year	20	NA	NA	NA
7440-47-3	mg/m³	Hamst	Syrian	M	Chromium	2 year	20	NA	NA	NA
7440-48-4	mg/m³	Mouse	B6C3F 1	F	Cobalt	2 week	10	20	4.97597	3.06361
7440-48-4	mg/m³	Mouse	B6C3F 1	M	Cobalt	2 week	10	20	2.26083	1.38439
7440-48-4	mg/m³	Rat	F 344/N	F	Cobalt	2 week	5	10	NA	NA
7440-48-4	mg/m³	Rat	F 344/N	M	Cobalt	2 week	5	10	NA	NA
7440-48-4	mg/m³	Mouse	B6C3F 1	F	Cobalt	3 month	NA	NA	NA	NA
7440-48-4	mg/m³	Mouse	B6C3F 1	M	Cobalt	3 month	NA	NA	NA	NA
7440-48-4	mg/m³	Rat	F 344/N	F	Cobalt	3 month	NA	NA	NA	NA
7440-48-4	mg/m³	Rat	F 344/N	M	Cobalt	3 month	NA	NA	NA	NA
7440-48-4	mg/m³	Mouse	B6C3F 1	F	Cobalt	2 year	NA	NA	NA	NA
7440-48-4	mg/m³	Mouse	B6C3F 1	M	Cobalt	2 year	NA	NA	NA	NA
7440-48-4	mg/m³	Rat	F344/ N	F	Cobalt	2 year	5	NA	NA	NA
7440-48-4	mg/m³	Rat	F344/ N	M	Cobalt	2 year	NA	NA	NA	NA
BLASTINGSAND	mg/m³	Rat	F344/ N	M	Abrasive Blasting Agents: Blasting Sand	2 week	NA	NA	NA	NA
BLASTINGSAND	mg/m³	Rat	HSD	M	Abrasive Blasting Agents: Blasting Sand	39 week	NA	15	0.041955	NA
COALSLAG	mg/m³	Rat	F 344/N	M	Abrasive blasting agents (coal slag)	2 week	NA	NA	NA	NA
CRUSHEDGLASS	mg/m³	Rat	F344/ N	M	Abrasive blasting agents (crushed glass)	2 week	NA	NA	NA	NA
GARNET	mg/m³	Rat	F 344/N	M	Abrasive blasting agents (garnet)	2 week	NA	NA	NA	NA
HEMATITESPEC	mg/m³	Rat	HSD	M	Abrasive Blasting Agents: Specular Hematite	39 week	15	30	14.2652	9.34356
L-MWNT-1020	mg/m³	Mouse	B6C3F 1	F	1020 Long Multiwalled Carbon Nanotube	30 day	NA	NA	NA	NA
L-MWNT-1020	mg/m³	Mouse	B6C3F 1	M	1020 Long Multiwalled Carbon Nanotube	30 day	NA	NA	NA	NA
L-MWNT-1020	mg/m³	Rat	HSD	M	1020 Long Multiwalled Carbon Nanotube	30 day	NA	NA	NA	NA
L-MWNT-1020	mg/m³	Rat	HSD	F	1020 Long Multiwalled Carbon Nanotube	30 day	NA	NA	NA	NA
13983-17-0	mg/m³	Rat	F 344/N	M	Wollastonite calcium silicates	1 year	10	NA	NA	NA

13983-17-0	mg/m^3	Rat	F 344/N	M	Wollastonite calcium silicates	2 year	10	NA	NA	NA
13983-17-0	mg/m^3	Rat	F 344/N	M	Wollastonite calcium silicates	2 year	NA	10	-99	-99

Table E-3: Lung Cell Neoplasia Potencies for relationships with a Trend

CAS Number	Dose Unit	Species	Strain	Sex	Material	Duration	NOAEL	LOAEL	BMD	BMDL
22398-80-7	MG/M3	Rat	F 344/N	M	Indium phosphide	2 year		0.03	0.0121208	0.0075795
7440-48-4	mg/m3	Mouse	B6C3F1	M	Cobalt	2 year		1.25	0.0854971	0.0476235
1314-62-1	MG/M3	Mouse	B6C3F1	M	Vanadium pentoxide	2 year		1	0.158111	0.0789613
1303-00-0	MG/M3	Rat	F 344/N	F	Gallium arsenide	2 year	0.1	1	0.34188	0.212394
7440-48-4	mg/m3	Rat	F344/N Tac	M	Cobalt	2 year		1.25	0.367548	0.298966
7440-48-4	mg/m3	Mouse	B6C3F1	F	Cobalt	3 month		1.25	0.386928	0.298876
7440-48-4	mg/m3	Rat	F344/N Tac	F	Cobalt	2 year		1.25	0.418444	0.334535
10026-24-1	MG/M3	Mouse	B6C3F1	M	Cobalt sulfate heptahydrate	2 year	1	3	0.57379	0.3109
10026-24-1	MG/M3	Mouse	B6C3F1	F	Cobalt sulfate heptahydrate	2 year	0.3	1	0.753525	0.435314
12035-72-2	MG/M3	Rat	F 344/N	F	Nickel subsulfide	2 year	0.15	1	0.779124	0.347662
10026-24-1	MG/M3	Rat	F 344/N	M	Cobalt sulfate heptahydrate	2 year	1	3	2.65909	1.21528
1313-99-1	MG/M3	Rat	F 344/N	M	Nickel (II) oxide	2 year	2.5		2.91122	1.49506
Nik95	mg/m3	Rat	F 344/N	F	CB_Elft12	2 year		2.5	3.24535	2.72753
14807-96-6	MG/M3	Rat	F 344/N	F	Talc	2 year	6	18	15.1583	10.4784
1309-64-4	mg/m3	Rat	Wistar Han	F	Antimony trioxide	2 year	3	10	15.2881	9.27594
1309-64-4	mg/m3	Rat	Wistar Han	M	Antimony trioxide	2 year	30		25.9025	11.146
1313-27-5	MG/M3	Mouse	B6C3F1	F	Molybdenum trioxide	2 year	30	100	37.4835	22.7064
Lee85	mg/m3	Rat	SD	F	TiO2	2 year		10	199.333	153.741
Lee85	mg/m3	Rat	SD	M	TiO2	2 year	50	250	225.725	159.394
10026-24-1	MG/M3	Rat	F 344/N	F	Cobalt sulfate heptahydrate	2 year	0.3	1	NA	NA
12035-72-2	MG/M3	Rat	F 344/N	M	Nickel subsulfide	2 year		0.15	NA	NA
1309-64-4	mg/m3	Mouse	B6C3F1	M	Antimony trioxide	2 year		3	NA	NA
1313-99-1	MG/M3	Rat	F 344/N	F	Nickel (II) oxide	2 year	2.5		NA	NA
1314-62-1	MG/M3	Mouse	B6C3F1	F	Vanadium pentoxide	2 year		1	NA	NA
22398-80-7	MG/M3	Rat	F 344/N	F	Indium phosphide	2 year		0.03	NA	NA
Hein95	mg/m3	Rat	Wistar	F	TiO2_P25	2 year		9.3	NA	NA

Hein95	mg/m3	Rat	Wistar	F	CB_P90	2 year		11.4	NA	NA
22398-80-7	MG/M3	Mouse	B6C3F1	F	Indium phosphide	3 month		0.03	NA	NA
1309-64-4	mg/m3	Mouse	B6C3F1	F	Antimony trioxide	2 week	60			
1309-64-4	mg/m3	Mouse	B6C3F1	M	Antimony trioxide	2 week	60			
1309-64-4	mg/m3	Rat	Wistar Han	F	Antimony trioxide	2 week	60			
1309-64-4	mg/m3	Rat	Wistar Han	M	Antimony trioxide	2 week	60			
7440-48-4	MG/M3	Mouse	B6C3F1	M	Cobalt	2 week	40			
7440-48-4	MG/M3	Rat	F 344/N	F	Cobalt	2 week	40			
7440-48-4	MG/M3	Rat	F 344/N	M	Cobalt	2 week	40			
7440-48-4	mg/m3	Mouse	B6C3F1	F	Cobalt	2 week	10			
BLASTING SAND	mg/m3	Rat	HSD	M	Abrasive Blasting Agents: Blasting Sand	2 week		15		
CRUSHED GLASS	mg/m3	Rat	F344/N Tac	M	NA	2 week		3		
GARNET	mg/m3	Rat	F 344/N	M	Abrasive blasting agents (garnet)	2 week		3		
HEMATITE SPEC	mg/m3	Rat	Harlan Sprague Dawley	M	Abrasive Blasting Agents: Specular Hematite	2 week		15		
10101-97-0	MG/M3	Mouse	B6C3F1	M	Nickel sulfate hexahydrate	2 year	1			
10101-97-0	MG/M3	Mouse	B6C3F1	F	Nickel sulfate hexahydrate	2 year	1			
10101-97-0	MG/M3	Rat	F 344/N	F	Nickel sulfate hexahydrate	2 year	0.5			
10101-97-0	MG/M3	Rat	F 344/N	M	Nickel sulfate hexahydrate	2 year	0.5			
12035-72-2	MG/M3	Mouse	B6C3F1	F	Nickel subsulfide	2 year	1.2			
12035-72-2	MG/M3	Mouse	B6C3F1	M	Nickel subsulfide	2 year	1.2			
1303-00-0	MG/M3	Mouse	B6C3F1	F	Gallium arsenide	2 year	1			
1303-00-0	MG/M3	Mouse	B6C3F1	M	Gallium arsenide	2 year	1			
1303-00-0	MG/M3	Rat	F 344/N	M	Gallium arsenide	2 year	1			
1309-64-4	mg/m3	Mouse	B6C3F1	F	Antimony trioxide	2 year		3		
1313-27-5	MG/M3	Mouse	B6C3F1	M	Molybdenum trioxide	2 year		10		

1313-27-5	MG/M 3	Rat	F 344/N	F	Molybdenum trioxide	2 year	100			
1313-27-5	MG/M 3	Rat	F 344/N	M	Molybdenum trioxide	2 year	100			
1313-99-1	MG/M 3	Mouse	B6C3F1	F	Nickel (II) oxide	2 year		1.25		
1313-99-1	MG/M 3	Mouse	B6C3F1	M	Nickel (II) oxide	2 year	5			
1314-62-1	MG/M 3	Rat	F 344/N	F	Vanadium pentoxide	2 year	2			
1314-62-1	MG/M 3	Rat	F 344/N	M	Vanadium pentoxide	2 year	2			
13765-19-0	MG/M 3	Rat	Sprague Dawley	M	Calcium chromate	2 year	20			
13765-19-0	MG/M 3	Hamster	Syrian Golden	M	Calcium chromate	2 year	20			
14807-96-6	MG/M 3	Mouse	B6C3F1	F	Talc	2 year	18			
14807-96-6	MG/M 3	Mouse	B6C3F1	M	Talc	2 year	18			
14807-96-6	MG/M 3	Rat	F 344/N	M	Talc	2 year	18			
22398-80-7	MG/M 3	Mouse	B6C3F1	F	Indium phosphide	2 year	100			
22398-80-7	MG/M 3	Mouse	B6C3F1	M	Indium phosphide	2 year	0.3			
2698-41-1	MG/M 3	Mouse	B6C3F1	F	o-Chlorobenzalmalononitrile (CS)	2 year	1.5			
2698-41-1	MG/M 3	Mouse	B6C3F1	M	o-Chlorobenzalmalononitrile (CS)	2 year	1.5			
2698-41-1	MG/M 3	Rat	F 344/N	F	o-Chlorobenzalmalononitrile (CS)	2 year	0.75			
2698-41-1	MG/M 3	Rat	F 344/N	M	o-Chlorobenzalmalononitrile (CS)	2 year	0.75			
643-79-8	ppm	Mouse	B6C3F1	F	ortho-Phthalaldehyde	2 year	7			
7440-47-3	MG/M 3	Hamster	Syrian Golden	M	Chromium	2 year	20			
7440-48-4	MG/M 3	Mouse	B6C3F1	F	Cobalt	2 year	40			
BLASTING SAND	mg/m3	Rat	F344/N Tac	M	Abrasive Blasting Agents: Blasting Sand	2 year		3		
13983-17-0	MG/M 3	Rat	F 344/N	M	Wollastonite calcium silicates	2 year	10			
13983-17-0	MG/M 3	Rat	F 344/N	M	Wollastonite calcium silicates	2 year		10		
Nik95	mg/m3	Rat	F344/N	M	CB_Elft12	2 year	6.6			
Hein95	mg/m3	Rat	Wistar	F	CB_P90	2 year	5.4			
102-54-5	MG/M 3	Mouse	B6C3F1	F	Ferrocene	3 month	30			

102-54-5	MG/M3	Mouse	B6C3F1	M	Ferrocene	3 month	30			
102-54-5	MG/M3	Rat	F 344/N	F	Ferrocene	3 month	30			
102-54-5	MG/M3	Rat	F 344/N	M	Ferrocene	3 month	30			
1314-62-1	MG/M3	Mouse	B6C3F1	F	Vanadium pentoxide	3 month	16			
1314-62-1	MG/M3	Mouse	B6C3F1	M	Vanadium pentoxide	3 month	16			
1314-62-1	MG/M3	Rat	F 344/N	M	Vanadium pentoxide	3 month	16			
1314-62-1	MG/M3	Rat	F 344/N	F	Vanadium pentoxide	3 month	16			
22398-80-7	MG/M3	Mouse	B6C3F1	M	Indium phosphide	3 month	100			
22398-80-7	MG/M3	Rat	F 344/N	F	Indium phosphide	3 month	100			
22398-80-7	MG/M3	Rat	F 344/N	M	Indium phosphide	3 month	100			
643-79-8	ppm	Mouse	B6C3F1	M	ortho-Phthalaldehyde	3 month	7			
643-79-8	ppm	Rat	HSD	F	ortho-Phthalaldehyde	3 month	7			
643-79-8	ppm	Rat	HSD	M	ortho-Phthalaldehyde	3 month	7			
7440-47-3	MG/M3	Rat	Sprague Dawley	M	Chromium	3 month	20			
7440-48-4	mg/m3	Mouse	B6C3F1	M	Cobalt	3 month	10			
7440-48-4	MG/M3	Rat	F 344/N	F	Cobalt	3 month	5			
7440-48-4	MG/M3	Rat	F 344/N	M	Cobalt	3 month	5			
13983-17-0	MG/M3	Rat	F 344/N	M	Wollastonite calcium silicates	30 day	10			
L-MWNT-1020	mg/m3	Mouse	B6C3F1	M	1020 Long Multiwalled Carbon Nanotube	30 day		0.1		
L-MWNT-1020	mg/m3	Rat	HSD	M	1020 Long Multiwalled Carbon Nanotube	30 day		0.1		
L-MWNT-1020	mg/m3	Rat	HSD	F	1020 Long Multiwalled Carbon Nanotube	30 day		0.1		
COALSLAG	mg/m3	Rat	F 344/N	M	Abrasive blasting agents (coal slag)	39 week		3		
L-MWNT-1020	mg/m3	Mouse	B6C3F1	F	1020 Long Multiwalled Carbon Nanotube	39 week		0.1		

Table E-4: Lung Diagnoses and Lung Cell Neoplasia Certainty Grading by Ann Hubbs

Index	LUNG DIAGNOSIS [Neoplasia indicated by AFH in yellow highlight, n=100]	For Neoplasia Diagnosis, indicate if Lung Cell Neoplasia (Y/N) P-probably, U-unlikely, ? - not enough information
1		
2	Abscess	
3	Abscess, Chronic	
4	Abscess, Nos	
5	Accumulation, Hyaline Droplet	
6	Acinar-Cell Carcinoma, Metastatic	N
7	Adamantinoma Malignant	N
8	Adenoacanthoma	N
9	Adenocarcinoma	Y
10	Adenocarcinoma Nos Uncertain Primary/Metastatic	U
11	Adenocarcinoma, Nos	P
12	Adenocarcinoma, Nos, Metastatic	U
13	Adenocarcinoma/Squamous Metaplasia, Metastatic	U
14	Adenoma	Y
15	Adenoma, Nos	Y
16	Adenomatosis	
17	Adenomatous Polyp, Nos	
18	Adenosquamous Carcinoma	Y
19	Adenosquamous Carcinoma, Metastatic	U
20	Adhesion, Nos	
21	Alveolar Macrophages	

22	Alveolar/Bronchiolar Adenoma	Y
23	Alveolar/Bronchiolar Carcinoma	Y
24	Alveolar/Bronchiolar Carcinoma, Invasive	Y
25	Alveolar/Bronchiolar Carcinoma, Metastatic	Y
26	Amyloid Deposition	
27	Angiectasis	
28	Arteriosclerosis, Nos	
29	Aspiration, Foreign Body	
30	Atelectasis	
31	Atrophy	
32	Atypia, Nos	
33	Autolysis	
34	Bacterium	
35	Basal-Cell Carcinoma, Metastatic	N
36	Basal Cell Carcinoma	N
37	Basosquamous Tumor Malignant	U
38	Bile Duct Carcinoma, Metastatic	N
39	Bronchiectasis	
40	Bronchiolectasis	
41	Bronchiolization	
42	Bronchopneumonia Acute Suppurative	
43	Bronchopneumonia Chronic Suppurative	
44	Bronchopneumonia Diffuse	
45	Bronchopneumonia Necrotizing	
46	Bronchopneumonia Suppurative	
47	Bronchopneumonia, Acute	
48	Bronchopneumonia, Chronic	
49	Bronchopneumonia, Focal	

50	Bronchopneumonia, Nos	
51	C-Cell Carcinoma, Metastatic	N
52	Calcification, Focal	
53	Calcification, Metastatic	
54	Calcification, Nos	
55	Calculus, Unknown Gross Or Micro	
56	Carcinoma	P
57	Carcinoma, Nos	P
58	Carcinoma, Nos, Metastatic	U
59	Carcinosarcoma	P
60	Carcinosarcoma, Metastatic	U
61	Cell-Shape Alteration	
62	Cholangiocarcinoma	N
63	Chordoma	N
64	Chordoma, Metastatic	N
65	Choriocarcinoma	N
66	Cleft	
67	Collapse	
68	Congestion	
69	Congestion, Acute	
70	Congestion, Acute Passive	
71	Congestion, Nos	
72	Corpora Amylacea	
73	Cortical Carcinoma, Metastatic	N
74	Crystals	
75	Crystals, Nos	
76	Cyst	
77	Cyst, Multiple	

78	Cyst, Nos	
79	Cystadenocarcinoma	U
80	Cystic Keratinizing Epithelioma	Y
81	Cytomegaly	
82	Cytoplasmic Aggregate, Nos	
83	Cytoplasmic Change, Basophilic	
84	Cytoplasmic Change, Eosinophilic	
85	Cytoplasmic Change, Nos	
86	Cytoplasmic Vacuolization	
87	Degeneration	
88	Degeneration, Hyaline	
89	Degeneration, Mucoid	
90	Degeneration, Nos	
91	Desmoplasia	
92	Dilatation	
93	Dilatation, Ducts	
94	Dilatation, Nos	
95	Distention	
96	Dysplasia, Epithelial	
97	Ecchymosis	
98	Ectasia	
99	Edema	
100	Edema, Interstitial	
101	Edema, Nos	
102	Embolism, Nos	
103	Embolus	

104	Embolus Tumor	U - a tumor embolus could originate in any tissue but if the primary is in the lung, that would have been diagnosed in another section in most cases
105	Embolus, Septic	
106	Emphysema	
107	Emphysema, Alveolar	
108	Emphysema, Centrilobular	
109	Emphysema, Nos	
110	Empyema	
111	Endometrial Stromal Sarcoma, Metastatic	N
112	Epithelialization	
113	Epithelioma Benign	Y
114	Erosion	
115	Erythrophagocytosis	
116	Exudate	
117	Fibroma	Y
118	Fibrosarcoma	Y
119	Fibrosarcoma, Metastatic	U - a metastatic fibrosarcoma could originate in any tissue but if the primary is in the lung, that would have been diagnosed in another section in most cases
120	Fibrosis	
121	Fibrosis, Diffuse	
122	Fibrosis, Focal	
123	Fibrosis, Multifocal	
124	Fibrous Histiocytoma	U

125	Fibrous Histiocytoma, Metastatic	U
126	Foam-Cell	
127	Follicular-Cell Carcinoma, Metastatic	N
128	Foreign Body	
129	Foreign Body, Nos	
130	Foreign Material, Nos	
131	Giant-Cell, Multinucleate	
132	Giant Cell	
133	Granular Cell Tumor Malignant	U
134	Granulation Tissue	
135	Granuloma	
136	Granuloma, Eosinophilic	
137	Granuloma, Foreign Body	
138	Granuloma, Nos	
139	Granulosa-Cell Carcinoma, Metastatic	N
140	Granulosa-Theca Tumor Malignant	N
141	Granulosa Cell Tumor Malignant	N
142	Hemangioma	Y
143	Hemangiosarcoma	? Identifying the primary site of hemangiosarcoma is very difficult because it is a tumor of the blood vasculature, which is present in all tissues. It can also apparently begin at the same time in multiple tissues in rodents. However, it is described as a primary tumor type that can be chemically-induced in NTP studies.
144	Hemangiosarcoma, Metastatic	U
145	Hematoidin	

146	Hematopoiesis	
147	Hematopoietic Cell Proliferation	
148	Hemorrhage	
149	Hemosiderosis	
150	Hepatoblastoma	N
151	Hepatocellular Carcinoma	N
152	Hepatocellular Carcinoma, Metastatic	N
153	Hepatocholangiocarcinoma	N
154	Histiocytic Sarcoma	? Histiocytic sarcoma usually involves multiple tissue making identification as lung problematic
155	Histiocytosis	
156	Hyperkeratosis	
157	Hyperplasia	
158	Hyperplasia, Adenomatous	
159	Hyperplasia, Alveolar Epithelium	
160	Hyperplasia, Atypical	
161	Hyperplasia, Basal Cell	
162	Hyperplasia, Epithelial	
163	Hyperplasia, Focal	
164	Hyperplasia, Lymphoid	
165	Hyperplasia, Mesothelial	
166	Hyperplasia, Nos	
167	Hyperplasia, Papillary	
168	Hyperplasia, Plasma Cell	
169	Hyperplasia, Polypoid	
170	Hypertrophy	
171	Hypertrophy, Focal	

172	Hypertrophy, Nos	
173	Infarct	
174	Infarct, Acute	
175	Infarct, Nos	
176	Infection, Bacterial	
177	Infiltration Cellular	
178	Inflammation	
179	Inflammation, Acute	
180	Inflammation, Acute Diffuse	
181	Inflammation, Acute Fibrinous	
182	Inflammation, Acute Focal	
183	Inflammation, Acute Hemorrhagic	
184	Inflammation, Acute Suppurative	
185	Inflammation, Acute/Chronic	
186	Inflammation, Chronic	
187	Inflammation, Chronic Diffuse	
188	Inflammation, Chronic Focal	
189	Inflammation, Chronic Necrotizing	
190	Inflammation, Chronic Suppurative	
191	Inflammation, Diffuse	
192	Inflammation, Fibrinous	
193	Inflammation, Focal	
194	Inflammation, Granulomatous	
195	Inflammation, Granulomatous Focal	
196	Inflammation, Interstitial	
197	Inflammation, Multifocal	
198	Inflammation, Necrotizing	
199	Inflammation, Nos	

200	Inflammation, Obliterative	
201	Inflammation, Proliferative	
202	Inflammation, Pyogranulomatous	
203	Inflammation, Suppurative	
204	Inflammation, With Fibrosis	
205	Karyomegaly	
206	Keratin-Pearl Formation	
207	Leiomyosarcoma	P
208	Leiomyosarcoma, Metastatic	N
209	Leukemia	N
210	Leukemia Granulocytic	N
211	Leukemia Monocytic	N
212	Leukemia Mononuclear	N
213	Leukemia, Nos	N
214	Leukemoid Reaction	
215	Leukocytosis	
216	Leukocytosis, Neutrophilic	
217	Leukocytosis, Nos	
218	Liposarcoma	U
219	Liposarcoma, Metastatic	N
220	Lymphangiectasis	
221	Lymphocytic Inflammatory Infiltrate	
222	Lymphocytosis	
223	Lymphoma Malignant	N
224	Lymphoma Malignant Histiocytic	N
225	Lymphoma Malignant Lymphocytic	N
226	Lymphoma Malignant Mixed	N
227	Lymphoma Malignant Undifferentiated Cell Type	N

228	Lymphoma, Histiocytic-Malignant Type	N
229	Lymphoma, Lymphocytic-Malignant Type	N
230	Lymphoma, Mixed-Malignant Type	N
231	Lymphoma, Nos-Malignant	N
232	Lymphoma, Undifferentiated-Malignant Type	N
233	Mast Cell Tumor Malignant	Not translationally relevant - humans do not get these
234	Mast Cell Tumor Nos	Not translationally relevant - humans do not get these
235	Melanoma Malignant	N
236	Mesenchymal Tumor Malignant	P
237	Mesothelioma Benign	Y
238	Mesothelioma Malignant	Y -If not in a F344 rat. Mesothelioma is a common lesion of the lining of the testis in the F344 rat and can metastasize to the lung so a diagnosis of mesothelioma in the F344 rat lung could well be metastatic… In other species and strains, peritoneal mesothelioma can met to lung but chemicals inducing mesothelioma might be relevant to lung, even if originating in the peritonium because it is the same cell type of origin.

239	Mesothelioma Nos	Y -If not in a F344 rat. Mesothelioma is a common lesion of the lining of the testis in the F344 rat and can metastasize to the lung so a diagnosis of mesothelioma in the F344 rat lung could well be metastatic… In other species and strains, peritoneal mesothelioma can met to lung but chemicals inducing mesothelioma might be relevant to lung, even if originating in the peritonium because it is the same cell type of origin.
240	Mesothelioma, Malignant	Duplicative of 238 - should this be mesothelioma, malignant, metastatic?
241	Metaplasia	
242	Metaplasia, Atyp Squamous	
243	Metaplasia, Broncho-Alveolar	
244	Metaplasia, Cartilagenous	
245	Metaplasia, Nos	
246	Metaplasia, Osseous	
247	Metaplasia, Squamous	
248	Mineralization	
249	Mixed Tumor Malignant	P - mixed tumors of the lung have been described and if not noted to be metastatic, it is most likely primary
250	Monocytosis	

251	Mononuclear Giant-Cell	
252	Mucinous Adenocarcinoma	P
253	Mucocele	
254	Myxosarcoma	P
255	Necrosis	
256	Necrosis, Cytodegenerative	
257	Necrosis, Focal	
258	Necrosis, Nos	
259	Neoplasm Nos	P
260	Neoplasm, Malignant, Nos	P
261	Neoplasm, Nos, Metastatic	U
262	Nephroblastoma, Metastatic	N
263	Neural Crest Tumor	N
264	Neurilemoma, Metastatic	N
265	Neuroblastoma	N
266	Nodule	
267	Nuclear-Shape Alteration	
268	Obliteration, Fibrous	
269	Obstruction, Nos	
270	Organization	
271	Osteosarcoma	U - extraskeletal osteosarcomas have been described and foci of bone do occur in rodent lung. However, the translational relevance would be debatable.
272	Osteosarcoma, Metastatic	N
273	Papillary Adenoma	Y
274	Papillary Carcinoma	Y

275	Papilloma, Nos	Y
276	Parakeratosis	
277	Parasitism	
278	Periarteritis	
279	Perivascular Cuffing	
280	Perivasculitis	
281	Petechia	
282	Phagocytic Cell	
283	Pheochromocytoma Complex	N
284	Pheochromocytoma Malignant	N
285	Pheochromocytoma, Metastatic	N
286	Pigmentation	
287	Pigmentation, Nos	
288	Plasma-Cell Infiltrate	
289	Plasma Cell Tumor Malignant	N
290	Plasmacytosis	
291	Pneumonia, Aspiration	
292	Pneumonia, Chronic Murine	
293	Pneumonia, Giant-Cell	
294	Pneumonia, Interstitial Chronic	
295	Pneumonia, Lipid	
296	Pneumonia, Lobar Nos	
297	Polyarteritis	
298	Polyp Adenomatous	
299	Polyp, Inflammatory	
300	Polyp, Nos	
301	Proteinosis	
302	Proteinosis, Alveolar	

303	Psammoma Bodies	
304	Regeneration	
305	Rhabdomyosarcoma	N
306	Sarcoma	P
307	Sarcoma Stromal	P
308	Sarcoma, Nos	P
309	Sarcoma, Nos, Metastatic	U
310	Scar	
311	Schwannoma Malignant	P
312	Sclerosis	
313	Squamous Cell Carcinoma	Y
314	Squamous Cell Carcinoma, Invasive	Y
315	Squamous Cell Carcinoma, Metastatic	U
316	Stromal Nephroma	N
317	Teratoma Malignant	P
318	Thrombophlebitis	
319	Thrombosis	
320	Thrombosis, Nos	
321	Thrombus	
322	Thrombus, Fibrin	
323	Thymoma Malignant	N
324	Tubular-Cell Adenocarcinoma, Metastatic	U
325	Ulcer	
326	Ulcer, Nos	
327	Undifferentiated Carcinoma	P
328	Undifferentiated Carcinoma, Metastatic	U
329	Vacuolization Cytoplasmic	

Table E-5: Summary of Banding Results Across Materials, Endpoints, and Data Sources (Tables 4-2 to 4-4)

Material	Band	Health Endpoint	POD type	Duration of Exposure at POD	Source (CIB Table)
Ag	D	Lung Inflammation	NOAEL or LOAEL	90 days	4-4
Ag	E	Lung Inflammation	NOAEL or LOAEL	90 days	4-4
Antimony Trioxide	D	Lung Neoplasia	BMDL	2 years	4-3
Antimony Trioxide	D	Lung Inflammation	LOAEL	2 years	4-2
Au	E	Lung Inflammation	NOAEL or LOAEL	90 days	4-4
C60	D	Lung Inflammation	NOAEL or LOAEL	28 days	4-4
Calcium Chromate	B	Lung Inflammation	NOAEL	2 years	4-2
CB	D	Lung Neoplasia	BMDL	2 years	4-3
CB (HSCb)	E	Lung Inflammation	NOAEL or LOAEL	13 weeks	4-4
CB (Printex90)	D	Lung Inflammation	NOAEL or LOAEL	13 weeks	4-4
CeO_2	C	Lung Inflammation	NOAEL or LOAEL	90 days	4-4
CeO_2	C	Lung Inflammation	NOAEL or LOAEL	28 days	4-4
CeO_2	D	Lung Inflammation	NOAEL or LOAEL	90 days	4-4
CeO_2	D	Lung Inflammation	NOAEL or LOAEL	90 days	4-4
CeO_2	D	Lung Inflammation	NOAEL or LOAEL	90 days	4-4
Chromium	C	Lung Inflammation	LOAEL	2 years	4-2
Cobalt	D	Lung Neoplasia	BMDL	2 years	4-3
Cobalt	E	Lung Inflammation	BMDL	3 months, 2 years	4-2
Cobalt sulfate heptahydrate	D	Lung Neoplasia	BMDL	2 years	4-3
Cobalt sulfate heptahydrate	E	Lung Inflammation	BMDL	2 years	4-2
Fe_3O_4	D	Lung Inflammation	NOAEL or LOAEL	13 weeks	4-4
Fe_3O_4 (Magnetite)	E	Lung Inflammation	NOAEL or LOAEL	4 weeks	4-4
$FeCO_3$ (Siderite)	E	Lung Inflammation	NOAEL or LOAEL	4 weeks	4-4
Ferrocene	B	Lung Inflammation	BMDL	3 months	4-2
Gallium arsenide	D	Lung Neoplasia	BMDL	2 years	4-3

Gallium arsenide	E	Lung Inflammation	BMDL	2 years	4-2
Indium Phosphide	E	Lung Neoplasia	BMDL	2 years	4-3
Indium Phosphide	E	Lung Inflammation	BMDL	3 months, 2 years	4-2
Molybdenum Trioxide	B	Lung Inflammation	BMDL	2 years	4-2
MWCNT	B	Lung Inflammation	NOAEL or LOAEL	28 days	4-4
MWCNT	D	Lung Inflammation	NOAEL or LOAEL	24 months	4-4
MWCNT	D	Lung Inflammation	NOAEL or LOAEL	90 days	4-4
MWCNT	D	Lung Inflammation	NOAEL or LOAEL	28 days	4-4
MWCNT	D	Lung Inflammation	NOAEL or LOAEL	90 days	4-4
MWCNT	E	Lung Inflammation	NOAEL or LOAEL	60 days	4-4
MWCNT	E	Lung Inflammation	NOAEL or LOAEL	12 weeks	4-4
MWCNT	E	Lung Inflammation	NOAEL or LOAEL	30 days	4-4
MWCNT	D	Lung Inflammation	BMDL	30 days	4-2
Nickel (II) Oxide	D	Lung Neoplasia	BMDL	2 years	4-3
Nickel (II) Oxide	E	Lung Inflammation	BMDL	2 years	4-2
Nickel subsulfide	D	Lung Neoplasia	BMDL	2 years	4-3
Nickel subsulfide	E	Lung Inflammation	BMDL	2 years	4-2
Nickel Sulfate Hexahydrate	D	Lung Inflammation	BMDL	2 years	4-2
o-Chlorobenzalmalonitrile	D	Lung Inflammation	NOAEL	2 years	4-2
ortho-Phthalaldehyde	E	Lung Inflammation	BMDL	3 months	4-2
Abrasive Blasting Agent: Specular Hematite	B	Lung Inflammation	BMDL	39 weeks	4-2
Abrasive Blasting Agent: Crushed Glass	B	Lung Inflammation	NOAEL	2 weeks	4-2
Abrasive Blasting Agent: Coal Slag	C	Lung Inflammation	BMDL	2 weeks	4-2
Abrasive Blasting Agent: Garnet	D	Lung Inflammation	BMDL	2 weeks	4-2
Abrasive Blasting Agent: Blasting Sand	D	Lung Inflammation	LOAEL	2 weeks	4-2
SiO_2	C	Lung Inflammation	NOAEL or LOAEL	28 days	4-4
SiO_2	C	Lung Inflammation	NOAEL or LOAEL	28 days	4-4
SiO_2	C	Lung Inflammation	NOAEL or LOAEL	90 days	4-4

SWCNT	D	Lung Inflammation	NOAEL or LOAEL	28 days, 90 days	4-4
Talc	D	Lung Neoplasia	BMDL	2 years	4-3
Talc	C	Lung Inflammation	BMDL	2 years	4-2
TiO_2	C	Lung Inflammation	NOAEL or LOAEL	30 days	4-4
TiO_2	C	Lung Inflammation	NOAEL or LOAEL	28 days	4-4
TiO_2	C	Lung Inflammation	NOAEL or LOAEL	30 days	4-4
TiO_2	C	Lung Inflammation	NOAEL or LOAEL	28 days to 13.5 months	4-4
TiO_2	C	Lung Inflammation	NOAEL or LOAEL	90 days	4-4
TiO_2 (Micro)	C	Lung Neoplasia	BMDL	2 years	4-3
Vanadium Pentoxide	D	Lung Neoplasia	BMDL	2 years	4-3
Vanadium Pentoxide	C	Lung Inflammation	BMDL	3 months, 2 years	4-2
Wollastonite Calcium Silicates	B	Lung Inflammation	NOAEL	2 years	4-2
ZnO	C	Lung Inflammation	NOAEL or LOAEL	28 days	4-4

Table E-6: Summary of Band E results across endpoints where a hypothetical Band F may be required

endpoint	scale	material	material type	species	strain	sex	duration	original pod	original units	adjusted pod	pod type	pod unit	Band F? (<=3 ug/m3)
inflammation	nano	Ag	Nanosized silver	rat	Sprague-Dawley	m/f	28d	0.00348	mg/m3	1.16	NOAEL	ug/m3	Band F
inflammation	nano	Au	Nanosized gold	rat	Sprague-Dawley	m/f	90d	0.00038	mg/m3	0.38	NOAEL	ug/m3	Band F
inflammation	nano	MWCNT	MWCNT	rat	Wistar (Crl:WI)	m	90d	0.1	mg/m3	10	LOAEL	ug/m3	
inflammation	nano	MWCNT	Nanocyl NC 7000	rat	Wistar (Crl:WI)	f	90d	0.1	mg/m3	10	LOAEL	ug/m3	
inflammation	nano	MWCNT	MWCNT-7	rat	Fischer 344	m/f	90d	0.2	mg/m3	20	LOAEL	ug/m3	
inflammation	nano	HSCb		rat	F344	f	13w	0.01071	mg/m3	10.7128	BMDL	ug/m3	
inflammation	nano	Magnetite		rat	Wistar	m	28d	0.04255	mg/m3	14.18413333	BMDL	ug/m3	
inflammation	nano	Siderite		rat	Wistar	m	28d	0.03827	mg/m3	12.75553333	BMDL	ug/m3	
inflammation	micro	Cobalt sulfate heptahydrate		Rat	F 344/N	M	2 year	0.3	mg/m3	30	LOAEL	ug/m3	
inflammation	micro	Indium phosphide		Rat	F 344/N	F	2 year	3.8E-05	mg/m3	0.0382614	BMDL	ug/m3	Band F
inflammation	micro	Gallium arsenide		Rat	F 344/N	F	2 year	7.6E-05	mg/m3	0.0764569	BMDL	ug/m3	Band F
inflammation	micro	Indium phosphide		Rat	F 344/N	M	2 year	3.1E-09	mg/m3	3.14868E-06	BMDL	ug/m3	Band F
inflammation	micro	Indium phosphide		Rat	F 344/N	M	3 month	4.6E-07	mg/m3	0.000457508	BMDL	ug/m3	Band F
inflammation	micro	Indium phosphide		Rat	F 344/N	F	3 month	5.3E-07	mg/m3	0.00052947	BMDL	ug/m3	Band F
inflammation	micro	Gallium arsenide		Rat	F 344/N	M	2 year	0.0004	mg/m3	0.403491	BMDL	ug/m3	Band F
inflammation	micro	Indium phosphide		Mouse	B6C3F1	F	3 month	0.00026	mg/m3	0.260089	BMDL	ug/m3	Band F
inflammation	micro	Cobalt		Rat	F 344/N	M	3 month	8.6E-06	mg/m3	0.00861666	BMDL	ug/m3	Band F
inflammation	micro	Cobalt sulfate heptahydrate		Rat	F 344/N	F	2 year	0.00072	mg/m3	0.720818	BMDL	ug/m3	Band F
inflammation	micro	Cobalt		Rat	F344/N Tac	F	2 year	8.5E-06	mg/m3	0.0084923	BMDL	ug/m3	Band F
inflammation	micro	Cobalt		Rat	F344/N Tac	M	2 year	9.2E-06	mg/m3	0.00923732	BMDL	ug/m3	Band F
inflammation	micro	Cobalt		Rat	F 344/N	F	3 month	6E-06	mg/m3	0.0060286	BMDL	ug/m3	Band F
inflammation	micro	Indium phosphide		Mouse	B6C3F1	M	3 month	0.00184	mg/m3	1.8431	BMDL	ug/m3	Band F
inflammation	micro	Nickel subsulfide		Mouse	B6C3F1	M	2 year	0.00617	mg/m3	6.17418	BMDL	ug/m3	
inflammation	micro	Vanadium pentoxide		Mouse	B6C3F1	M	2 year	0.01985	mg/m3	19.8511	BMDL	ug/m3	
inflammation	micro	Nickel (II) oxide		Rat	F 344/N	F	2 year	0.00039	mg/m3	0.390229	BMDL	ug/m3	Band F
inflammation	micro	ortho-Phthalaldehyde		Rat	HSD	M	3 month	0.61374	ppm	0.613738	BMDL	ppm	Band F
inflammation	micro	ortho-Phthalaldehyde		Rat	HSD	F	3 month	0.64013	ppm	0.640126	BMDL	ppm	Band F
inflammation	micro	Talc		Mouse	B6C3F1	M	2 year	0.96841	mg/m3	0.968412	BMDL	ug/m3	Band F
inflammation	micro	ortho-Phthalaldehyde		Mouse	B6C3F1	F	3 month	1.24088	ppm	1.24088	BMDL	ppm	Band F
inflammation	micro	ortho-Phthalaldehyde		Mouse	B6C3F1	M	3 month	1.58349	ppm	1.58349	BMDL	ppm	Band F
inflammation	micro	Nickel subsulfide		Rat	F 344/N	F	2 year	0.15	mg/m3	15	LOAEL	ug/m3	
inflammation	micro	Nickel subsulfide		Rat	F 344/N	M	2 year	0.15	mg/m3	15	LOAEL	ug/m3	
inflammation	micro	Indium phosphide		Mouse	B6C3F1	F	2 year	0.03	mg/m3	3	LOAEL	ug/m3	Band F

inflammation	micro	Indium phosphide		Mouse	B6C3F1	M	2 year	0.03	mg/m3	3	LOAEL	ug/m3	Band F
neoplasia	micro	Indium phosphide		Rat	F 344/N	M	2 year	0.00758	mg/m3	7.5795	BMDL	ug/m3	
neoplasia	micro	Nickel subsulfide		Rat	F 344/N	M	2 year	0.15	mg/m3	15	LOAEL	ug/m3	
neoplasia	micro	Indium phosphide		Rat	F 344/N	F	2 year	0.03	mg/m3	3	LOAEL	ug/m3	
neoplasia	micro	Indium phosphide		Mouse	B6C3F1	F	3 month	0.03	mg/m3	3	LOAEL	ug/m3	
neoplasia	micro	ortho-Phthalaldehyde		Mouse	B6C3F1	F	3 month	7	ppm	7	NOAEL	ppm	
neoplasia	micro	ortho-Phthalaldehyde		Mouse	B6C3F1	M	3 month	7	ppm	7	NOAEL	ppm	
neoplasia	micro	ortho-Phthalaldehyde		Rat	HSD	F	3 month	7	ppm	7	NOAEL	ppm	
neoplasia	micro	ortho-Phthalaldehyde		Rat	HSD	M	3 month	7	ppm	7	NOAEL	ppm	
neoplasia	nano	1020 Long Multiwalled Carbon Nanotube		Mouse	B6C3F1	M	30 day	0.1	mg/m3	3.333333333	LOAEL	ug/m3	
neoplasia	nano	1020 Long Multiwalled Carbon Nanotube		Rat	HSD	M	30 day	0.1	mg/m3	3.333333333	LOAEL	ug/m3	
neoplasia	nano	1020 Long Multiwalled Carbon Nanotube		Rat	HSD	F	30 day	0.1	mg/m3	3.333333333	LOAEL	ug/m3	
neoplasia	nano	1020 Long Multiwalled Carbon Nanotube		Mouse	B6C3F1	F	39 week	0.1	mg/m3	10	LOAEL	ug/m3	
fibrosis	micro	Cobalt sulfate heptahydrate		Rat	F 344/N	F	2 year	0.00065	mg/m3	0.653828	BMDL	ug/m3	Band F
fibrosis	micro	Cobalt sulfate heptahydrate		Rat	F 344/N	M	2 year	5.3E-05	mg/m3	0.0532919	BMDL	ug/m3	Band F
fibrosis	micro	Nickel subsulfide		Rat	F 344/N	F	2 year	0.15	mg/m3	15	LOAEL	ug/m3	
fibrosis	micro	Nickel subsulfide		Rat	F 344/N	M	2 year	0.15	mg/m3	15	LOAEL	ug/m3	
fibrosis	micro	Antimony trioxide		Rat	Wistar	F	2 year	0.00053	mg/m3	0.528303	BMDL	ug/m3	Band F
fibrosis	micro	Antimony trioxide		Rat	Wistar	M	2 year	0.00249	mg/m3	2.49172	BMDL	ug/m3	Band F
fibrosis	micro	Indium phosphide		Mouse	B6C3F1	F	3 month	0.00082	mg/m3	0.818619	BMDL	ug/m3	Band F
fibrosis	micro	Indium phosphide		Mouse	B6C3F1	F	2 year	7.6E-05	mg/m3	0.0758423	BMDL	ug/m3	Band F
fibrosis	micro	Indium phosphide		Mouse	B6C3F1	M	2 year	5.1E-06	mg/m3	0.00506519	BMDL	ug/m3	Band F
fibrosis	micro	Indium phosphide		Rat	F 344/N	F	2 year	4.7E-05	mg/m3	0.0473448	BMDL	ug/m3	Band F
fibrosis	micro	Indium phosphide		Rat	F 344/N	M	2 year	0.00051	mg/m3	0.513937	BMDL	ug/m3	Band F

Appendix F: Other Data Sources for Future Analyses

A systematic literature review was designed by NIOSH and executed by ATL in order to develop a dataset of published toxicology studies of engineered nanomaterials (ENMs) or other airborne particles and fibers of the same or similar chemical composition. The searches were performed through February 2016 for all previous years. The goal of this review was to glean all high-quality and usable available inhalation exposure data from the literature to investigate the hazard of numerous ENMs. Previously available data typically cover a small subset of commonly studied materials such as TiO2, so a more varied material library was desired. Materials fell into 4 categories (Table F-1).

A wide net was cast for information that would be useful for exploring hazard, covering particle physicochemical properties, experimental design (animal species, sex, or strain, route of exposure, frequency of exposure, dose, cell type), and biological endpoints.

A total of 248 studies were chosen as they satisfied all literature selection criteria. The desired information was gleaned from each publication and entered into the database, but since a publication typically had a targeted focus (e.g. one endpoint and one material), many fields of the database were left empty. The data fields available from the in vivo and in vitro studies are shown in Tables F-2 and F-3, respectively.

The materials with in vivo lung inflammation response information reported as PMN measures were the first to be analyzed. After identifying and resolving issues in the database regarding formatting and entry, the dose-response data from a subset of 15 studies were modeled using benchmark dose modeling (Figure 1), resulting in 38 potency estimates (results not shown at this time). Another subset of 10 studies require manual calculation of the response of interest (% PMNs in BAL fluid) as they report the number of PMN cells and the total number of cells sampled from the BAL fluid. Potency estimates will then be generated for those studies and combined with the previous set of 38 potency estimates, followed by clustering the potency estimates to identify materials with similar hazard and exploration of the cluster characteristics. The selection of those studies for benchmark dose estimation is shown in Figure F-1.

Table F-1: Categories of nanomaterials included in ATL systematic literature search.

Carbon-containing	Metals	Metal Oxides	Inorganic
Boron carbide (B4C)	Aluminum (Al)	Antimony tin oxide (ATO)	Tungsten disulfide (WS2)
Calcium carbonate (CaCO3)	Gold (Au)	Aluminum oxide/Alumina (Al2O3)	Ceramics category, by type
Carbon black (C)	Brass	Barium titanate (BaTiO3)	Cadmium sulfide (CdS) quantum dots
Carbon aluminum composite	Cobalt (Co)	Cerium oxide (CeO2)	Cadmium selenide (CdSe) quantum dots
Clays	Copper (Cu)	Bismuth oxide (Bi2O3)	Cadmium telluride (CdTe)
Cellulose (C6H10O5)n	Iron (Fe)	Cuprous oxide (Cu2O)	Lead sulfide (PbS) quantum dots
Fullerene (C60)	Germanium (Ge)	Cupric oxide (CuO)	Lead selenide (PdSe) quantum dots
Graphene	Lithium aluminum silicate glass	Iron (II, III) oxides (Fe2O3, Fe3O4)	
Graphite	Nickel (Ni)	Magnesium hydroxide (Mg(OH2))	
Nylon	Palladium (Pd)	Silicon dioxide (SiO2)	
Polymer fibers	Platinum (Pt)	Titanium dioxide (TiO2), nanoparticles or nanowires	
	Silicon (Si)	Zinc oxide (ZnO)	
	Titanium (Ti)	Zirconium oxide (ZrO2)	
	Tungsten (W)		

Table F-2: In vivo database fields.

Particle Physicochemical Properties	Animals	Exposure	Lung Responses	Genotoxicity/Carcinogenicity	Responses in Other Organs	Effect Level

Chemical composition (purity/impurity)	Species	Route of administration	Cytotoxicity	Histopathological analysis of cancerous/pre-cancerous morphological changes in tissue (e.g., lung)	Hepatotoxicity	No observed adverse effect level
Cluster particle diameter and length (nm or µm)	Gender	pH of nanomaterial in suspension - specify media (if applicable)	Lung Function	DNA adduct formation	Cardiovascular effects	Lowest observed adverse effect level
Shape	Body weight, controls (beginning and end of exposure)	Measured tissue dose (if measured)	Inflammation	DNA damage assays (COMET, micronuclei) in tissue	Renal Toxicity	
Structure: crystallinity	Number of animals per group	Post-exposure duration	Oxidant Response/Oxidative Stress		Neurotoxicity	
Specific surface area (m2/kg, m2/m3, m2/g)	Strain	Aerosol generation technique (if applicable)	Fibrogenic Reponse		Immunotoxicity	

Surface charge - titration; the property surface charge density has SI units of C/m2.	Age	Exposure concentration (s) or dose groups				
Endotoxin (CFU) - Limulus Amebocyte Lysate Assay	Lung weight, controls (beginning and end of exposure)	Exposure duration(s) (hours per day, days per week, number of weeks)				
Zeta potential (V, mV) - measured as electrophoretic mobility in dilute aqueous salt solution and in vehicle						
Primary particle diameter and length (nm or μm)						
Aerodynamic diameter, mass and/or count median (and GSD)						
Bulk chemical composition [kg/kg or mol/mol (%)]						
Porosity (m3/m3, m3/kg, cm3/g)						

Surface reactivity (e.g., electron spin resonance, alterations following UV light exposure)						
Surface chemistry [mol/m2 (%)], including hydrophobicity/hydrophilicity						
Dissolution [mol/L, kg/kg, kg/m3 (%)] in water and delivery vehicle, at neutral and acidic pH of 7 and 4 to 5, and at room temperature and 37°C; rate of dissolution (mass per unit area per unit time)						
Generation method, catalyst						

Table F-3: In vitro database fields.

Particle Physicochemical Properties	Cell Type	Dose	Cytotoxicity	Inflammation	Oxidative Responses	Genotoxicity/Carcinogenicity	Fibrogenic Response	Effect Level
Chemical composition (purity/impurity)	Human Cells (small airway epithelial, immortalized, fibroblasts)	pH of nanomaterial in suspension - specify media	Membrane integrity - assay by vital and exclusion dyes, LDH assay, protease assay	Cytokine Production - using ELISA (IL-1b, IL-6, IL-8, IL-10, IL-12p70, IL-18, MCP-1, MIP-2, TNF-a)	Reactive oxygen species - Chemiluminescence, intracellular dyes (DCFH, DHE), OxyBurst Assay®	Cell transformation - Colony Forming Assay	Fibroblast proliferation - assayed using MMT, WST-1, CyQUANT, CellTiter 96, BrdU	No observed adverse effect level
Cluster particle diameter and length (nm or µm)	Rat or mouse alveolar epithelial cell culture line	Duration of exposure	ATP content - assay using a Luciferase Assay	Inflammatory Gene Expression Changes - measured using RNA-	Reactive nitrogen species - assayed using Greiss Reagent Assay, Peroxynitrite Assay	Apoptosis/necrosis - TUNEL Assay paired with alamar blue or BrdU	Tissue remodeling and collagen stimulating proteins - TGF-b, MMPs, TIMPs	Lowest observed adverse effect level (by endpoint)

				Analysis (Northern Blot), RT-PCR Array				
Shape		Exposure dose groups	Reduction enzyme activity - assay by MTT, WST-1	Cell Inflammatory Protein Content - measured using Western Blot	Antioxidant depletion - assayed using Total Antioxidant Assay	Chromosomal damage/abnormalities - In situ hybridization, FISH, COMET assay	Collagen production - Sircol Assay, Sirius Red Staining	
Structure: crystallinity		Post-exposure duration	Cell growth/proliferation - assay using BrdU, CyQUANT®, MTT, WST-1, CellTiter 96®		Free radical production - assay ESR	Cytokinesis - Cytokenisis block (CytoB)	Fibrotic gene expression analysis - RNA-Analysis, RT-PCR Array	

Specific surface area (m2/kg, m2/m3, m2/g)					Lipid peroxidation - assayed using LPO Assay	Metastatic potential - Cell migration/invasion		
Surface charge - titration; the property surface charge density has SI units of C/m2.					Oxidative stress gene expression changes - assayed using RNA-Analysis, RT-PCR Array	Mutagenesis - Micronucleus Assay (MNvit)		
Endotoxin (CFU) - Limulus Amebocyte Lysate Assay						Kinetichore morphometry - Immunolabeling mitotic spindle and motor proteins		
Zeta potential (V, mV) - measured as electrophoretic mobility in dilute aqueous salt solution and in vehicle						Cell cycle analysis - Cell Cycle Arrest Assay		
Primary particle diameter and length (nm or µm)								

Aerodynamic diameter, mass and/or count median (and GSD)								
Bulk chemical composition [kg/kg or mol/mol (%)]								
Porosity (m3/m3, m3/kg, cm3/g)								
Surface reactivity (e.g., electron spin resonance, alterations following UV light exposure)								
Surface chemistry [mol/m2 (%)], including hydrophobicity/hydrophillicity								
Dissolution [mol/L, kg/kg, kg/m3 (%)] in water and delivery vehicle, at neutral and acidic pH of 7 and 4 to 5, and at room temperature and 37°C; rate of dissolution (mass per unit area per unit time)								

Generation method, catalyst								

Figure F-1: Flowchart of PMN Study Identification and Eligibility for Benchmark Dose Modeling

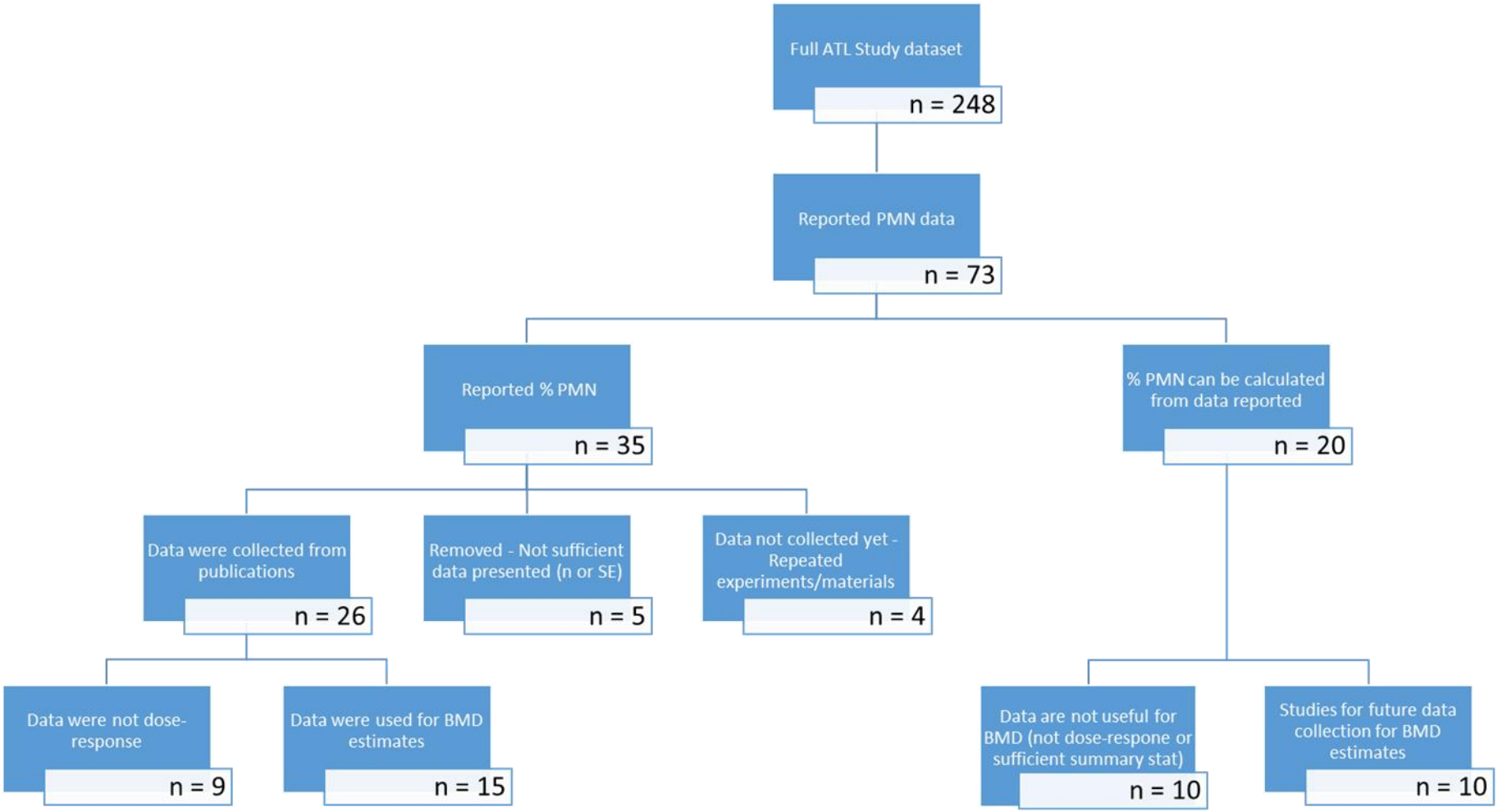

Other databases are in development, including a NIOSH nanotoxicology database, and are currently being evaluated to determine their utility for categorical occupational exposure limits. A database summarizing the published literature regarding the pulmonary inflammation adverse outcome pathway is being constructed by an OECD working group, with a focus on whether a significant response was identified. The database was an expert consolidation of broad descriptors of the presence of inflammation across assays. The database appears to be primarily qualitative, with some quantitative information such as NOAELs and LOAELs, but does not include the sufficient dose-response data or experimental design information for a quantitative risk assessment. The Gene Expression Omnibus (GEO) database is being used to conduct research into the utility of genotoxicity data of nanomaterials by identifying the relevant gene expressions associated with health endpoints of interest. GEO is a public repository of genomic data maintained by the National Institutes of Health (NIH). Researchers are typically required to submit their data to GEO, making the database a valuable resource for data analysis.